[redacted]

AFSWP-1100

THE NUCLEAR RADIATION HANDBOOK

CY333A

March 25, 1957

DNA1.941017.002

[redacted]

Declassified WITH DELETIONS by DNA,
Chief, IBTS
Date: 10/11/94

NUCLEAR DEVELOPMENT CORPORATION OF AMERICA
White Plains, New York

[redacted]

[redacted]

34305

TECHNICAL LIBRARY
APR 13 1959
of the
ARMED FORCES
SPECIAL WEAPONS PROJECT
426502

RECORD COPY

8415

[redacted]

ORO-JHU
LOG NO 7625

CY333A

[redacted]

AFSWP-1100

REPLACEMENT INSTRUCTION No. 1

9 December 1957

In accordance with the Letter of Promulgation found in the original document, AFSWP-1100 is changed as follows:

1. Insert pages ii.1 and ii.2.

2. Remove pages vii and viii and substitute revised page vii and page viii.

3. Remove pages xi and xii and substitute revised pages xi and xii.

4. Remove pages 173 through 178 and substitute revised pages 173 through 178, page 178a and page 178b.

[redacted]

[redacted]

ORO-JHU
LOG NO 9475

LETTER OF PROMULGATION

This handbook is being issued in order to present a compilation of nuclear radiation effects as a reference for those elements of the Armed Forces requiring a treatment in greater detail than is found in "Capabilities of Atomic Weapons."

An effort has been made to develop and present in a comprehensive treatment those aspects of nuclear effects which will be of most use. The information reflects weapons effects test data and analyses available early in 1956. It is intended that the material will be periodically revised in order to maintain a current status.

A. R. Luedecke

A. R. Luedecke
Major General, USAF
Chief, AFSWP

[redacted]

AFSWP-1100

THE NUCLEAR RADIATION HANDBOOK

CY333A

March 25, 1957

[redacted]

Work Performed under Contract DA 29-044-XZ-442
for the Armed Forces Special Weapons Project

NUCLEAR DEVELOPMENT CORPORATION OF AMERICA
White Plains, New York

[redacted]

[redacted]

CHANGE NO. 1 9 December 1957

LIST OF EFFECTIVE PAGES

Page Numbers	Effective Pages
i, ii	Original
ii.1, ii.2	Change 1
iii through vi	Original
vii, viii	Change 1
ix, x	Original
xi, xii	Change 1
1 through 172	Original
173 through 178	Change 1
178a, 178b	Change 1
179 through 218	Original

Page ii 2 is blank.

[redacted]

[redacted]

PREFACE

The status of our knowledge on the penetration of radiation from an atomic weapon through the atmosphere has undergone rapid change, and theoretical and experimental work have made great progress in the past several years. It was therefore felt desirable to take a snapshot of certain phases of this knowledge in order to provide a systematic account of these for military personnel who are required to use them and to assist research personnel by outlining the gaps in the current knowledge. Nuclear Development corporation of America (NDA) was assigned the task of preparing this handbook on nuclear radiation by the Armed Forces Special Weapons Project (AFSWP).

It is inevitable in the preparation of a handbook such as this in a field which is progressing so swiftly that all portions are not of equal timeliness. We have made every effort to include information reported formally or available to us up to the 1956 Weapons Tests as well as some limited information arising from those tests.

Since this is a handbook, information was gathered from many sources and it is not possible to acknowledge adequately all of them except by formal bibliographical references. We must, however, acknowledge the notable assistance rendered us by the following scientists, who gave their time and ideas freely and graciously when visited by NDA personnel for the purpose of securing advice and information: Dr. V. P. Bond (Brookhaven National Laboratory), Drs. Wendell Biggers, Payne S. Harris and John S. Malik (Los Alamos Scientific Laboratory), Dr. Marguerite Ehrlich (National Bureau of Standards), Dr. Donald K. Willet (Naval Research Laboratory), Dr. Robert Rapp (RAND Corporation), Dr. Richard D. Cadle (Stanford Research Institute) and Dr. Lester Machta (U. S. Weather Bureau).

The preparation of this handbook was the work of Messrs. Richard Bakal, Francis Clark, and Drs. Daniel Ekstein, Morton Fuchs, and Robert Liedtke, all of NDA, and Lt. Commander Nathaniel I. Berlin and his colleagues of AFSWP who prepared Chapter II. The quality of this document has been greatly improved as a result of comments and advice received from Major Thomas W. Connolly who acted as the Project Officer for AFSWP for most of the time that the work was being done.

J. Ernest Wilkins, Jr.
White Plains, N. Y.
March 22, 1957

Page iv is blank.

TABLE OF CONTENTS

		Page
CHAPTER 1 GENERAL CONSIDERATIONS		
1.1	Introduction	1
1.2	The Fission Reaction	2
1.3	The Fusion Reaction	4
1.4	Weapon Design and Construction	5
1.5	Cloud Dynamics	6
1.6	Flux-Distance Relations	7
1.7	Biological Considerations	9
1.8	Average Air Density	10
1.9	References	16
CHAPTER 2 BIOLOGICAL EFFECTS OF RADIATION		
2.1	Introduction	17
2.1.1	Sources of Data	17
2.1.2	Types of Hazard	18
2.1.3	Sources of Radiation	19
2.2	External Radiation	19
2.2.1	Introduction	19
2.2.2	Dosimetry	19
2.2.3	Units of Dose	19
2.2.4	Consideration of Depth Dose Curves and Correlation with Biological Effect	19
2.2.5	Dosimetric Methods	21
2.2.6	Significance of Air Dose, Skin Dose, and Mid-Line Dose from X-Ray Radiation	24
2.3	Concept of RBE (Relative Biological Effectiveness)	26
2.4	Acute Radiation Sickness	27
2.4.1	Symptomatology	27
2.4.2	Current Therapeutic Concepts	30
2.4.3	Problem of Partial Body Shielding	31
2.4.4	Description of Beta "Burn"	31
2.5	Long Term (Late) Effects	31
2.5.1	Shortening of Life Span	31
2.5.2	Cataracts	33
2.5.3	Fertility	33
2.6	Genetic Effects	34
2.7	Effect of Protraction and Fractionation	34
2.8	Internal Contamination	37
2.8.1	Source	37
2.8.2	Route of Entry into Man	38
2.8.3	Metabolic Fate	38
2.8.4	Biological Effects	39
2.8.5	Therapeutic Aspects	39
2.9	Combined Injuries	39

CONTENTS

2.10 Maximum Permissible Levels of Radiation 40
2.10.1 External Radiation 40
2.10.2 Internal Radiation 40
2.11 References 40

CHAPTER 3 INITIAL GAMMA RADIATION

3.1 Introduction 43
3.2 Dose-Distance Relations for Surface Bursts 45
3.2.1 Theoretical Considerations 45
3.2.2 Low and Intermediate Yield Weapons 53
3.2.3 High Yield Weapons 63
3.3 Dose-Distance Relations for Air Bursts 76
3.3.1 Low and Intermediate Yield Weapons 76
3.3.2 High Yield Weapons 77
3.4 Dose-Distance Relations for Underground Bursts 78
3.4.1 Low Yield Weapons 78
3.4.2 Intermediate and High Yield Weapons 81
3.5 Delivery Rate 81
3.6 Initial Gamma Ray Spectrum 84
3.6.1 Initial Gamma Ray Spectrum at the Source 85
3.6.2 Spectral Variation with Distance 87
3.7 Military Shielding 93
3.8 References 106

CHAPTER 4 NEUTRON RADIATION

4.1 Introduction 107
4.2 Theory of Neutron Generation 107
4.2.1 Influence of Weapon Design 107
4.2.2 Fission Weapons 108
4.2.3 Boosted Fission Weapons 109
4.2.4 Thermonuclear Weapons 109
4.3 Experimental Methods and Results 109
4.3.1 Physical Experimental Methods 109
4.3.2 Biological Experimental Methods 114
4.3.3 Experimental Results 115
4.4 Flux-Distance Relations 118
4.4.1 Non-Thermal Neutrons from Fission and Boosted Fission Weapons . 119
4.4.2 Non-Thermal Neutrons from Fusion Weapons 120
4.4.3 Thermal Neutrons from Fission and Boosted Fission Weapons . . 121
4.4.4 Effect of Variations in Atmospheric Density and Humidity 122
4.4.5 Scaling Relations for Variation of Average Quiescent Air Density and Weapon Yield 123
4.4.6 Major Deficiencies in Flux-Distance Relations 125
4.5 Dose-Distance Relations 125
4.5.1 Calculation of Total Neutron Dose 125
4.5.2 Discussion of Dose-Distance Relations 133
4.6 Relative Importance of Neutron Radiation 135
4.7 Neutron Energy Spectrum 137
4.8 Delivery Rates and the Hydrodynamic Effect 137
4.8.1 Prompt Neutrons 138
4.8.2 Delayed Neutrons 138
4.8.3 Experimental Results 139

[redacted]

CONTENTS

4.9 Military Shielding 141
4.10 References 143

CHAPTER 5 RESIDUAL GAMMA RADIATION

5.1 Introduction 145
5.2 Mechanism of Fallout 145
5.3 Computation Models 146
5.4 Decay of Activities 150
5.5 Isodose Rate Contours 156
5.6 Determination of Effective Wind Vectors, the Area of Fallout and the Time of Arrival 158
5.6.1 Determination of the Effective Wind Vector 160
5.6.2 Determination of the Fallout Area 164
5.6.3 Determination of Fallout Time Period 170
5.7 Delivery Rates 172
5.8 Scaling with Yield and Effective Wind Velocity 173
5.9 Scaling with Height of Burst 178
5.10 Energy Spectra of Fallout Gamma Radiation 179
5.11 Shielding from Residual Gamma Radiation 182
5.12 Variations Due to Environment 185
5.13 Neutron-Induced Activities 187
5.14 References 188

CHAPTER 6 RESIDUAL BETA RADIATION

6.1 Introduction 189
6.2 Radiation Source Characteristics 191
6.3 Beta-Gamma Dose Ratio at the Source 193
6.4 Beta Depth Dose Behavior 196
6.5 Beta-Gamma Biological Hazard 202
6.6 Miscellaneous Internal Effects 202
6.7 References 203

CHAPTER 7 THE ATOMIC CLOUD

7.1 Introduction 205
7.2 Cloud Dynamics 205
7.3 Cloud Heights and Dimensions 207
7.4 Cloud Characteristics for Calculation of Fallout and Initial Radiation 212
7.5 Cloud Characteristics for Calculation of Aircraft Penetration Dose 213
7.6 References 218

[redacted]

LIST OF TABLES

		Page
CHAPTER 1		
1.1:1	Charge and Mass of Nuclear Particles	3
CHAPTER 2		
2.2:1	LD_{50} Neutron Flux as a Function of Energy	23
2.4:1	Surface Doses (Rep) Required to Produce Recognizable Epidermal Injury	32
CHAPTER 3		
3.2:1	Summary of High Yield Test Data	64
3.2:2	Comparison of Gamma Doses and Mean Free Paths for Several Test Bursts	66
3.6:1	$4\pi R^2\phi$ for a Point Isotropic Source in Air with a Source Strength of One Gamma per Sec	88
3.6:2	Fraction of the Total Number of Gammas at the Source	89
3.7:1	Description of Shelters	96
3.7:2	Transmission Factors for Shelters	97
3.7:3	Description of Fortifications	98
3.7:4	Transmission Factors for Fortifications	99
3.7:5	Transmission Factors for Foxholes	100
3.7:6	Transmission Factors for Armored Vehicles	101
3.7:7	Transmission Factors for Vehicle Trenches	101
3.7:8	Transmission Factors for Standard Thicknesses of Five Common Shielding Materials as a Function of Gamma Ray Energy	104
CHAPTER 4		
4.3:1	Characteristics of Neutron Threshold Detectors	112
4.3:2	Neutron Flux-Dose Conversion Factors	116
4.5:1	Dose-Distance Relations as a Function of Weapon Type for Unboosted and Boosted Fission Weapons	128
4.5:2	Receiver Environment Factors for Dose-Distance Calculations	129
4.5:3	Probable Error Factor in Dose-Distance Calculations	129
4.5:4	Factors for Conversion of Sulphur Neutron Flux to Total Dose	130
4.6:1	Comparison of Critical Radii Due to Several Damage Mechanisms	136
4.7:1	Neutron Energy Spectra of Unboosted and Boosted Fission Weapons	137
4.8:1	Delayed Neutron Characteristics for U^{235}, U^{238}, and Pu^{239}	139
4.9:1	Neutron Flux Transmission Factors for Field Structures	142
CHAPTER 5		
5.6:1	Characteristics of Irregularly Shaped Falling Particles	161
5.6:2	Atomic Cloud Diameters for High-Yield Weapons at 10 min after Burst	165
5.11:1	Nominal Gamma Ray Transmission Factors for Common Materials	184

LIST OF FIGURES

		Page
CHAPTER 1		
1.8:1	Air Density ρ as a Function of Pressure and Temperature	11
1.8:2	Average Air Density $\bar{\rho}$ as a Function of the Difference in Pressure and Elevation between the Point of Burst and the Receiver	13
CHAPTER 2		
2.1:1	Neutron and Gamma Radiation as a Function of Distance Estimated for Bursts at Hiroshima and Nagasaki	18
2.2:1	The LD_{50} for Dogs for Bilateral Radiation as a Function of Energy	20
2.2:2	First Collision Neutron Rep Curve for Tissue	22
2.2:3	Theoretical Depth Dose Curves for Monoenergetic Beams Incident on a 30-Cm Slab of Tissue	23
2.2:4	Comparative Depth Doses in a Phantom Man of Initial Bomb Radiation and Radiation from a Field of Fission Products	25
2.2:5	Beta-Gamma Ratio at 1 Meter above Earth's Surface	26
2.4:1	Diagrammatic Representation of the Penetrating Radiation Syndrome in Man following Acute Exposure and the Stages at which Death Commonly Occurs	28
2.4:2	Diagrammatic Representation of Radiation Syndrome	28
2.4:3	Correlation between Human Mortality and White Blood Count	30
2.5:1	Predicted Shortening of Life Span from Chronic Radiation as a Function of Dose Rate for Rodents, with Extrapolation to Man	33
2.7:1	Comparison of the Various Equations Purporting to Calculate the Effective Dose for Chronic Radiation at 5 r per Day	36
2.7:2	The Ratio of the Physical Dose and the Effective Dose to H+1 Hr Dose Rate for a Fallout Field using the Blair Equations as Modified for a Changing Dose Rate	37
CHAPTER 3		
3.2:1	Idealized Shape of Hydrodynamic Scaling Factor Curve as a Function of Source-Receiver Distance and of Weapon Yield	49
3.2:2	Experimental Values of $D_\gamma R^2/W\ h_{eff}$ for Surface Bursts of Low and Intermediate Yield Weapons as a Function of Source-Receiver Distance	54
3.2:3	Comparison of Initial Gamma Dose-Distance Results from Several Sources for Surface Bursts of Low and Intermediate Yield Weapons	57
3.2:4	$W\ h_{eff}$ as a Function of Weapon Yield for Surface and Air Bursts of Low and Intermediate Yield Weapons	60
3.2:5	Initial Gamma Dose-Distance Results for Surface and Air Bursts of Low, Intermediate, and High Yield Weapons for Several Average Air Densities	61
3.2:6	Experimental Values of $D_\gamma R^2/W$ for Surface Bursts of High Yield Weapons as a Function of the Source-Receiver Distance	65
3.2:7	Effective Hydrodynamic Scaling Factors for Surface and Air Bursts of High Yield Weapons ($\bar{\rho} = 0.2$)	68
3.2:8	Effective Hydrodynamic Scaling Factors for Surface and Air Bursts of High Yield Weapons ($\bar{\rho} = 0.4$)	69

[redacted]

FIGURES

3.2:9 Effective Hydrodynamic Scaling Factors for Surface and Air Bursts of High Yield Weapons ($\bar{\rho} = 0.6$) 70
3.2:10 Effective Hydrodynamic Scaling Factors for Surface and Air Bursts of High Yield Weapons ($\bar{\rho} = 0.8$) 71
3.2:11 Effective Hydrodynamic Scaling Factors for Surface and Air Bursts of High Yield Weapons ($\bar{\rho} = 0.9$) 72
3.2:12 Effective Hydrodynamic Scaling Factors for Surface and Air Bursts of High Yield Weapons ($\bar{\rho} = 1.0$) 73
3.2:13 Effective Hydrodynamic Scaling Factors for Surface and Air Bursts of High Yield Weapons ($\bar{\rho} = 1.1$) 74
3.4:1 Initial Gamma Dose-Distance Results for Underground Bursts of Low Yield Weapons for Several Average Air Densities 80
3.5:1 Initial Gamma Radiation Delivery Rate for Buster Easy 82
3.5:2 Initial Gamma Radiation Delivery Rate for Jangle Underground 83
3.5:3 Initial Gamma Radiation Delivery Rate for Castle 4 (Union) 84
3.5:4 Percent of Initial Gamma Dose Accumulated as a Function of Time under Various Burst and Receiver Conditions 85
3.6:1 Initial Gamma Ray Spectrum at an Equivalent Point Source 86
3.6:2 Total Linear Attenuation Coefficient for Gamma Rays in Standard Density Air as a Function of Gamma Energy 89
3.6:3 Comparison of the Initial Gamma Ray Spectra at the Source and at a Receiver 2000 yd from the Source 94
3.7:1 Transmission Factors for Foxholes 102
3.7:2 Transmission Factors for Foxholes 103

CHAPTER 4

4.5:1 Neutron Dose as a Function of Distance for Fission and Boosted Fission Weapons 126
4.5:2 Neutron Dose as a Function of Distance for Fusion Weapons 127
4.8:1 Thermal Neutron Delivery Rates from Buster Baker and Tumbler-Snapper 140
4.9:1 Neutron Flux Transmission Factors for Two-Man Foxholes 141

CHAPTER 5

5.3:1 Wind Field and Fallout Pattern for Condition A 148
5.3:2 Wind Field and Fallout Pattern for Condition B 149
5.4:1 F (t) as a Function of Time after Burst 151
5.4:2 $D(H+1, t)/\dot{D}(H+1)$ as a Function of Time after Burst 151
5.4:3 Optimum Time for Evacuation of a Shelter within the Fallout Field as a Function of Transmission Factor Ratio T_V/T_S and Transit Time . . 154
5.5:1 Downwind Isodose Rate Pattern at H+1 Hr for 15-MT [redacted] Burst, 15-Knot Wind 157
5.5:2 Downwind Isodose Rate Pattern at H+1 Hr for 15-MT [redacted] Burst, 30-Knot Wind 157
5.5:3 Downwind Isodose Rate Pattern at H+1 Hr for 1.5-MT [redacted] Burst, 15-Knot Wind 158
5.5:4 Downwind Isodose Rate Pattern at H+1 Hr for 1.5-MT [redacted] Burst, 30-Knot Wind 158
5.5:5 Ground Zero Isodose Rate Pattern at H+1 Hr for 15-MT [redacted] Burst 159

[redacted]

[redacted]

FIGURES

5.6:1 Graphical Determination of Effective Wind Speed and Direction for Particles Falling from 80,000 ft 164
5.6:2 Total Particle Fall Time as a Function of Starting Altitude 166
5.6:3 Determination of Fallout Area (Method A) 169
5.6:4 Determination of Fallout Area (Method B) 169
5.10:1 Gamma Ray Energy Spectrum Histograms 180
5.11:1 Gamma Ray Transmission Factor for Soil as a Function of Time after Burst 184
5.11:2 Dose Rates Inside Structures without Basements 186
5.11:3 Dose Rates Inside Structures with Basements 187

CHAPTER 6

6.2:1 Beta-Gamma Activity Ratio, and Beta and Gamma Effective Energies at the Source as a Function of Time after Fission 192
6.4:1 Beta Depth Dose Curves for an Infinite Plane Isotropic Source given as a Percentage of the Dose at the Surface 197

CHAPTER 7

7.3:1 Experimental Measurements of the Equilibrium Heights of Top and Bottom of Cloud as a Function of Yield for Near-Surface Bursts 208
7.3:2 Height of Top of Cloud as a Function of Yield and Time after Burst for Near-Surface Bursts 209
7.3:3 Height of Bottom of Cloud as a Function of Yield and Time after Burst for Near-Surface Bursts 210
7.3:4 Height of Center of Cloud as a Function of Yield and Time after Burst for Near-Surface Bursts 210
7.3:5 Thickness of Cloud as a Function of Yield and Time after Burst for Near-Surface Bursts 211
7.3:6 Diameter of Cloud as a Function of Yield and Time after Burst for Near-Surface Bursts 211
7.4:1 Height of Center of Cloud for Short Times after Burst as a Function of Yield for Near-Surface Bursts 213
7.5:1 Total Dose Accumulated in Cloud as a Function of Time of Residence and Time of Entry 215
7.5:2 Diameter Reduction Factor 217

Page xii is blank.

[redacted]

Chapter 1

GENERAL CONSIDERATIONS

1.1 INTRODUCTION

In this manual an attempt will be made to summarize and correlate the quantitative information at present available on nuclear radiation produced by nuclear weapons. Specifically, it is desired to present methods of determining the values of dose from each of the several important kinds of bomb radiation as a function of distance (and in some cases direction) from the point of burst. It is also desired to know the energy distribution of the radiation making up the dose and the way in which the dose varies with time after burst. Ideally, these methods should be applicable to a wide variety of conditions, among others, bomb yields varying from 0.1 KT to 100 MT, burst heights varying from -1000 to 200,000 ft, air densities varying correspondingly, weapon types including pure fission, boosted, and thermonuclear, and bursts occurring over both earth and water and in the midst of a wide variety of meteorological conditions. In practice and with the present state of knowledge, it is possible to provide quantitative statements for only limited areas of these parameters. In other areas only qualitative statements can be made and sometimes even this is inadvisable.

Under these circumstances reliance must be placed on both experimental results and theoretical analyses. Measurements provide the most direct answers when available. Theoretical analyses are used to afford some understanding of the mechanisms involved, so that results can be predicted in areas where experiments are lacking, and so that experimental results can be applied to a variety of conditions. It should be noted that measurements bearing on important problems are often lacking; in addition, when they are available they are often in conflict. Similarly, the theoretical analyses are not always available; when they are available, they are, necessarily, based on simple models. Thus, the methods and results which follow are often subject to large and unknown errors. Where possible, an estimate of the magnitude of these errors accompanies the individual section or chapter.

Auxiliary to the discussion of the radiation doses themselves, information is presented on several related subjects such as the biological aspects of dose, shielding against the several types of radiation, and the dynamics of the atomic cloud.

The subject matter is divided into seven chapters, each of which is briefly outlined below. Chapter 1 (General Considerations) introduces the problems of nuclear radiation and covers those general areas which are necessary to a more detailed understanding of the subject. Since it is desirable and helpful to have a general knowledge of the nature and functional concepts of nuclear weapons, discussions of the fission and fusion reactions and of weapon design and construction are presented in Sections 1.2 through 1.4. Following these sections are introductory treatments of cloud dynamics (Section 1.5), the relationship between radiation flux and distance from the source point (Section 1.6), and terminology of biological dosage (Section 1.7). Finally, the calculation of the average air density, which applies to each of the later chapters, is covered in Section 1.8.

Chapter 2 presents a more detailed treatment of the biological effects of nuclear radiation. It reviews the sources of biological data, the pertinent units and definitions, and several of the measuring techniques. Radiation effects are considered, first due to sources external to the body and then due to

internal sources. Both the immediate reactions (which may include nausea, diarrhea, weight loss, fever, changes in blood count, death) and the longer-term effects (which may include reduction of life span, cataract formation, impairment of fertility, and genetic effects) are described. The dependence of these effects on the total dose and on its distribution in time is covered as thoroughly as our present understanding permits. Current values of tolerance levels for external and internal radiation are presented.

Chapters 3 through 6 discuss the four general categories of nuclear radiation which result from the explosion of a nuclear weapon.

Initial gamma radiation (Chapter 3) is radiation of electromagnetic waves similar to X-radiation except that the associated particles or photons possess much greater energy. (Photons, or gamma rays, are not particles in the technical sense that they do not possess a non-vanishing rest mass such as is possessed by electrons, protons, neutrons, etc. Nevertheless, they do possess other important properties of particles and it is more useful to think of them as particles for the purpose of the present work.) Initial gamma radiation is emitted during about the first 60 seconds after the time of burst. This time limit is somewhat arbitrary, being chosen for purely practical reasons. Actually, by far the greatest portion of this radiation is emitted during the first few seconds after burst. The source of the radiation is the material in the fireball which later becomes the atomic cloud. Initial gamma radiation usually refers to radiation effects at points external to the cloud.

Neutron radiation (Chapter 4) is also emitted during this same time interval. A neutron is an electrically uncharged particle whose mass is nearly the same as that of the nucleus of the hydrogen atom. There is reason to believe that most of the neutron radiation of biological importance is emitted nearly instantaneously at the time of burst. The sources of neutron radiation are also contained in the fireball, and neutron radiation also usually refers to radiation effects at points external to the cloud.

Residual gamma radiation (Chapter 5) is of importance at later times. It occurs when radioactive debris from the fission process is scavenged out of the atomic cloud, by large particles of earth for instance, and sifts back down to the ground under the influence of gravity and the local atmospheric conditions. The sources of residual gamma radiation, commonly called fallout, are then distributed upon the surface of the earth and irradiate the whole general environment.

Residual beta radiation (Chapter 6) also occurs as a consequence of fallout. The sources of residual beta radiation are, in the main, identical to the sources of initial gamma radiation. Beta particles are the smallest electrically charged particles known. Negatively charged beta particles are called electrons and positively charged beta particles are positrons. Under most circumstances residual beta radiation is of less importance than residual gamma radiation because the penetrating power of beta particles is much less than that of gamma rays. Beta radiation usually affects only the skin of an irradiated animal.

The most important properties of the several particles of concern in radiation processes, including protons and alpha particles in addition to the particles described above, are given in Table 1.1:1.

Chapter 7 presents a discussion of the atomic fireball and cloud. Attention is devoted to the dynamics of cloud formation and growth and to three of the problems upon which these dynamics have a strong influence: the cloud as source of most of the initial gamma and neutron radiation, as the generally accepted origin of the material carrying the residual radiation (fallout), and as a radioactive region of space which may be penetrated by aircraft.

1.2 THE FISSION REACTION

Nuclei of the elements uranium-235 (U^{235}), uranium-238 (U^{238}), and plutonium-239 (Pu^{239}) may, under favorable circumstances, break up into two parts when struck by a neutron of appropriate energy. (The symbols inside the brackets give the abbreviation for the element. The superscript on the right gives the mass number, which is the total number of protons and neutrons in the nucleus, for the element and isotope in question. Often the atomic number, which is the total number of elementary positively charged heavy particles or protons in the nucleus, is also given as a subscript to the left of the symbol.)

This fission reaction is accompanied by the release of an energy of approximately 200 Mev (1 Mev = 1 million electron volts = 1.603×10^{-6} ergs), which is the reason for the enormous destructive power of nuclear weapons. The fission products, i.e., the large two residual fragments, are not always of exactly the same size, or, equivalently, of the same atomic mass and number. There are, in fact, more than 50 different nuclides which may arise as a consequence of fission. These fission products are usually formed in highly excited states and must release additional energy before they become stable. This energy is released in the form of beta, gamma, and a very small amount of neutron, radiation. It accounts for a large portion of the radiation effects in which we are interested.

The fission process is accompanied by the emission of neutrons. There are an average of ν neutrons emitted per fission. The value of ν is between 2.5 and 4, depending on the type of material undergoing fission and the energy of the neutron causing the fission. A small fraction, approximately 0.73 percent for U^{235}, of these neutrons is somewhat delayed in time of emission[1] since it is emitted from the fission products, but the remainder of the neutrons accompany the fission process itself and are therefore emitted instantaneously. The delayed neutrons observed experimentally have not exceeded 0.7 Mev in energy.

TABLE 1.1:1

Charge and Mass of Nuclear Particles

Particle	Electric charge, coulombs	Rest Mass, gm	Comments
Electron	-1.6×10^{-19}	9.1×10^{-28}	Beta particle
Positron	1.6×10^{-19}	9.1×10^{-28}	Beta particle
Neutron	None	1.67×10^{-24}	
Proton	1.6×10^{-19}	1.67×10^{-24}	Nucleus of the hydrogen atom
Alpha	3.2×10^{-19}	6.64×10^{-24}	Nucleus of the helium atom
Photon	None	None	Gamma radiation

The reactions involved can be written as follows for fission in U^{235}, where ${}_0n^1$ is the symbol for a neutron. (Those for Pu^{239} and U^{238} are similar except that the neutron which causes fission in U^{236} must be greater than about 1.5 Mev in energy. Thermal neutrons, on the other hand, will induce fission in U^{235} and Pu^{239}.)

$$ {}_0n^1 \text{ (thermal energy)} + U^{235} \rightarrow 0.9927\ \nu\ {}_0n^1 + \text{excited fission fragments} + \text{gamma radiation} + \text{kinetic energy} $$

$$ \text{excited fission fragments} \rightarrow 0.0073\ \nu\ {}_0n^1 + \text{stable fission fragments} + \text{beta and gamma radiation} $$

U^{235} is present in only small amounts in natural uranium, and must be concentrated and purified for use in nuclear weapons.

Capture of a neutron by uranium does not always lead to fission. Instead, a heavier uranium isotope, which does not break up in this way, may be formed.

The energy release of nuclear weapons may be compared with the corresponding energy release from chemical explosives such as TNT. The energy released by the complete combustion of one thousand tons, or one kiloton, of TNT is 4.2×10^{19} ergs, 1.0×10^{12} calories, 3.1×10^{12} foot-pounds, or 2.62×10^{25} Mev. It can be seen, therefore, that insofar as energy release is concerned, about 1.3×10^{23} fissions are equivalent to one kiloton of TNT, assuming 200 Mev per fission.

The number of neutrons per kiloton of energy release is also of interest. Let α be the ratio of non-fission to fission neutron captures in the weapon, including non-fission captures in the fissionable material. Then for each fission there will be a net of $(\nu\text{-}1\text{-}\alpha)$ neutrons produced, since one neutron must be used to maintain the chain reaction. There will be then $(\nu\text{-}1\text{-}\alpha)\ 1.3 \times 10^{23}$ neutrons produced per equivalent kiloton of TNT. The value of $(\nu\text{-}1\text{-}\alpha)$ will usually be about 1.3, but may range from as low as 0.5 to as high as 2.0. Since the initial energy spectrum of fission neutrons is well known, it can be predicted that about 22 percent of these neutrons will initially be greater than 3 Mev in energy. The percentage emerging outside the weapon will, of course, be smaller because of energy degradation in penetrating the weapon casing.

The energy release of nuclear weapons, commonly called the yield, is usually measured in terms of kilotons (KT) or megatons (MT), meaning the equivalent number of thousand or million tons of TNT which, when completely burned, give the same energy release.

1.3 THE FUSION REACTION

As is now well known, the fission process is not the only way in which large amounts of energy can be released by nuclear reactions. Also of great importance is the fusion reaction utilized in thermonuclear weapons. In this reaction, several deuterium nuclei fuse together to form helium, tritium, and hydrogen nuclei with the release of a large amount of energy. A very high threshold energy is needed for this reaction to occur, however, so it is practical only at the high temperatures usually attained in fission weapons and a fission bomb is used, for this reason, to initiate the fusion reaction.

The fusion reaction is as follows, where ${}_1D^2$ stands for the deuterium nucleus, ${}_1H^1$ for the hydrogen nucleus, and ${}_1T^3$ for the tritium nucleus.

$$ {}_1D^2 + {}_1D^2 \rightarrow {}_1T^3 + {}_1H^1 + 4 \text{ Mev} $$

$$ {}_1D^2 + {}_1D^2 \rightarrow {}_2He^3 + {}_0n^1 + 3.2 \text{ Mev} $$

These two reactions are about equally likely to occur. The following reaction is about 50 times more probable and will usually go nearly to completion:

$$ {}_1D^2 + {}_1T^3 \rightarrow {}_2He^4 + {}_0n^1 + 17.6 \text{ Mev.} $$

The total effect of these three reactions is then obtained by summing, which gives

$$ 5\ {}_1D^2 \rightarrow {}_2He^4 + {}_2He^3 + {}_1H^1 + 2\ {}_0n^1 + 24.8 \text{ Mev.} $$

This is the fusion reaction for what is called <u>partial burn</u>. The following reaction is less probable, but may occur under favorable circumstances:

$$ {}_1D^2 + {}_2He^3 \rightarrow {}_2He^4 + {}_1H^1 + 18.4 \text{ Mev.} $$

Adding the last two reactions, we arrive at the reaction for what is called <u>complete burn:</u>

$$ 6\ {}_1D^2 \rightarrow 2\ {}_2He^4 + 2\ {}_1H^1 + 2\ {}_0n^1 + 43.2 \text{ Mev.} $$

Neutrons are generated in equal numbers by the DD and the DT reactions, as can be seen above. Neutrons from the former reaction are crudely comparable to fission neutrons in energy, but those from the latter are much more energetic -- possessing an energy of 14 Mev in fact. (The rest of the 17.6 Mev is taken up by the recoil of the $_2He^4$ nucleus.)

From the above reactions it is seen that there are emitted 1.05×10^{24} high energy (14 Mev) neutrons per kiloton fusion yield in the partial burn case, and an equal number of lower energy neutrons. There is also an average total of 16.1 neutrons emitted per 200 Mev, which may be compared with $(\nu\text{-}1\text{-}\alpha) \approx 1.3$ neutrons per fission characteristic of fission weapons. Thus, thermonuclear weapons generate many more neutrons for any given yield than fission weapons.

Corresponding figures for the complete burn case are 0.605×10^{24} high energy neutrons per kiloton, and an equal number of lower energy neutrons. Similarly, there is a total of 9.24 neutrons per 200 Mev.

In actual weapons, the true burn is intermediate between the partial and the complete burn cases, usually closer to the partial than the complete.

The total energy released in the explosion of a thermonuclear weapon is comprised of the energy yield from the fusion reaction plus a large yield from an associated fission reaction, which is not only that due to the initiating bomb. The 14 Mev neutrons generated in the fusion reaction are utilized to initiate additional fission in both U^{235} and U^{238}. (In this respect fusion neutrons differ from those produced in fission, which are not sufficiently energetic to fission U^{238} to any appreciable extent.) [redacted]

Boosted weapons are modified fission weapons to which a small amount of deuterium has been added. The fusion neutrons are utilized to augment the fission reaction in the uranium, thus giving an appreciably increased fission yield compared to that which would occur in the absence of the deuterium. The augmented fission yield is much greater than the direct fusion yield.

1.4 WEAPON DESIGN AND CONSTRUCTION

The characteristics of weapon radiation, particularly neutron radiation, are sensitive to the details of weapon design and construction.[2] The following discussion is confined to fission weapons. Thermonuclear weapons, for reasons of security classification in design, are beyond the scope of the present treatment.

Weapons are stockpiled with their fissionable materials in a subcritical state, signifying a configuration such that no nuclear reaction can occur. Criticality is reached when the configuration is altered in such a way that the nuclear reaction can just barely start. Further alterations of the same type result in supercriticality, which means that the nuclear reaction, when started, will proceed faster and much more vigorously.

It is important that there be no stray neutrons present while the system is going supercritical. If such neutrons are present, predetonation may occur. Predetonation occurs when the nuclear reaction commences before a condition of maximum supercriticality is reached. The result may be a fizzle, signifying the release of a much smaller amount of nuclear energy in the explosion than under optimum conditions. Under normal circumstances (no predetonation), at the precise moment that maximum supercriticality is reached, an artificial neutron source is activated, the fission reaction commences, and the explosion ensues.

Criticality is achieved from the initial subcritical condition in a number of ways. The most common is the spherical implosion system. A spherical high explosive shell surrounds the fissionable material. This is exploded at the proper time by detonators symmetrically placed on the outer surface. A spherical implosion shock wave progresses toward the center of the system, compressing the fissionable material abruptly into a highly supercritical state. At the last moment, the shock wave hits the center of the weapon where it activates an artificial neutron source; the weapon then explodes. This type of weapon is spherically symmetric. The neutron radiation is most strongly influenced by the

[redacted]

thickness of the high explosive shell. The high explosive contains hydrogen, which is very efficient in degrading the energy of neutrons by the process of elastic collision. Recent design has tended in the direction of making the high explosive shell thinner and thinner, resulting in less and less attenuation of the neutron dose by this hydrogenous material.

[redacted]

achieving criticality [redacted] does not depend on compression of the fissionable material. Instead, the fissionable material is divided into two parts which are subcritical when separated. The function of the high explosive at the ends of the apparatus in this case is merely to assemble the two parts quickly. Such weapons are called gun-type weapons. They are now used as artillery shells but are no longer popular as air-dropped weapons except when penetration of the ground surface is desired. [redacted]

Stockpiled weapon types are usually identified by a Mark number, which is abbreviated Mk-. When the models are still experimental, they are identified instead by a TX- number (i.e., Mk-35 or TX-35).

Weapons are boosted, when desired, by making minor modifications of the basic unboosted weapons. Boosted weapons fall into the same general classifications outlined above.

As previously noted, the weapon strength is called the yield and is given in terms of equivalent weights of TNT in kilotons (KT) or megatons (MT). The yield is controlled by the actual physical size of the weapon and by its detailed design characteristics. A change in physical size results, primarily, in a simple multiplication of the source strength of the radiation produced. A change in weapon design characteristics has much more complicated effects on the radiation. [redacted]

All weapons tested to date of up to about 100-KT yield have been pure fission weapons. In the range of 100 KT to about 1 MT the weapons are either pure fission or boosted fission weapons. In the boosted weapons, however, the yield is essentially all due to the fission reaction and the fusion contribution may be neglected. Above 1 MT the weapons are fusion. [redacted]

1.5 CLOUD DYNAMICS

For purposes of discussing initial and residual gamma radiation, some knowledge of cloud dynamics is required. Only the necessary definitions and a very crude description of the phenomena involved are presented here. A more detailed discussion will be found in Chapter 7.

Just after the time of burst, the weapon components are extremely hot. They expand rapidly, engulfing air from the atmosphere as they do so. In these early stages of expansion, we speak of this as the fireball. As the fireball continues to expand, it also rises because of the low density of the

[redacted]

material in its interior. Further expansion and rising is accompanied by cooling, and the edges of the fireball become somewhat less sharply defined. We then speak of the atomic cloud or just of the cloud. The cloud, except for very minor differences, is just the fireball at a later stage of development.

The cloud rise is slowed and, for sufficiently low-yield weapons, it is stopped at the elevation of the tropopause. The tropopause is the boundary between the troposphere and the stratosphere. The troposphere is the lower layer of the atmosphere in which nearly all vertical convection and turbulence occur. It is characterized by a general linear decrease of temperature with altitude, although localized temperature inversions at low altitudes occur frequently in some parts of the world. The stratosphere is that portion of the atmosphere above the troposphere and is characterized by a constant or slightly increasing temperature with altitude. As a consequence, the air in the stratosphere is quite stable with respect to vertical motion, and is therefore stratified into layers. The elevation of the tropopause depends mainly on the latitude and season of the year, although local weather disturbances may cause marked variations from the normal. The height of the tropopause in general varies from about 55,000 ft at the equator to about 30,000 ft at the poles. In middle latitudes, it varies from about 40,000 ft in summer to 33,000 ft in winter. Cloud dynamics, in turn, are markedly affected by the height of the tropopause. Strong local inversions at lower levels, likewise, can exert a damping effect on the cloud rise.

1.6 FLUX-DISTANCE RELATIONS

This section consists of a discussion of the relations between the flux of initial gamma or neutron radiation at points exterior to the fireball and the associated distance from the point of burst.

The flux of any type of radiation is the total number of particles (gamma ray photons, neutrons, electrons, positrons, etc.) per unit area and per unit time arriving at a particular point from all directions and at all energies. The unscattered flux is that portion of the total flux which arrives directly at the point in question from the source, without having suffered any previous collisions. The unscattered flux is monodirectional if the source of radiation is a point.

For the sake of conciseness, the time integral of the above is also often called the flux.

We are often interested in the flux due to particles (especially neutrons) within a prescribed range of energy ΔE, because the biological effect of the radiation is related in a complicated way to the particle energy.

The unscattered flux ϕ_u at a distance or slant range R from a point source of radiation of intensity S (total number of particles, or particles per unit time) in a uniform homogeneous medium is given by

$$\phi_u = \frac{S}{4\pi R^2} e^{-\mu_t R} \qquad (1.6:1)$$

$$\mu_t = \frac{1}{\lambda_t} = \rho\mu_{t0} = \frac{\rho}{\lambda_{t0}}$$

The symbol μ_t is the total linear attenuation coefficient, and λ_t is the total mean free path. The symbol ρ is the density of the medium measured in units of standard density. Quantities measured at the standard density are so designated by means of a zero subscript. Thus, μ_{t0} and λ_{t0} are the total attenuation coefficient and mean free path at the standard density. These equations show that μ_t and $1/\lambda_t$ are proportional to the air density ρ.

[redacted]

The total flux ϕ, however, also includes radiation which arrives at the point after scattering (and at a lower energy). We define the flux buildup factor $B(\mu_t R)$ such that

$$\phi = \phi_u B(\mu_t R). \tag{1.6:2}$$

$B(\mu_t R)$ itself is often crudely exponential in form

$$B(\mu_t R) \approx e^{k_1 \mu_t R} \tag{1.6:3}$$

where k_1 is a constant. Thus, ϕ is also still roughly exponential.

$$\phi \approx \frac{S}{4\pi R^2} e^{-\mu_t(1-k_1)R} = \frac{S}{4\pi R^2} e^{-\mu R} \tag{1.6:4}$$

$$\mu = \frac{1}{\lambda} = \rho\mu_\rho = \frac{\rho}{\lambda_\rho} = \mu_t(1-k_1)$$

where we call μ the apparent linear attenuation coefficient and λ the apparent mean free path. Most experiments have measured μ and λ rather than μ_t and λ_t. The biological effect of radiation is more closely related to μ than to μ_t.

The buildup factor concept can easily be generalized. One may define, for instance, buildup factors for flux due to radiation in a specific energy range, buildup factors for the energy transported rather than the number of particles, buildup factors for biological dose, etc.

Experimentally, it has usually been found that Eq. 1.6:4 remains a fair, although inexact, approximation even if the source of radiation is spread out over a broad band of energies. It also holds reasonably well for non-uniform media such as the atmosphere, whose density varies with elevation. In this case, however, it is necessary to calculate an average air density $\bar{\rho}$. Methods for doing this are described in Section 1.8.

Serious modification is required, however, because of perturbation of the medium by the blast. Eq. 1.6:4, even after defining the average air density $\bar{\rho}$, is still properly true only for an infinite homogeneous medium. At the time of the explosion, a blast wave spreads out from the point of burst. This blast wave is bounded at its outermost radius by a sharp discontinuity known as the shock front which separates the quiescent medium from the disturbed medium. Compression of the medium is maximum at the shock front. At sufficiently late times behind the shock front, there comes to exist a region of rarefied, low density hot air known as the rarefaction phase of the blast wave. Because of this rarefaction phase, the exponential term in Eq. 1.6:4 at times shortly after the time of burst can be much more than $e^{-\bar{\rho}\mu_\rho R}$. This enhancement of the radiation shortly after the burst by the shock wave has been called the hydrodynamic effect by its discoverer, J. Malik.[3]

The term time of arrival refers to the elapsed time required after the burst for an effect under discussion to arrive at a specified point. (The effect may be arrival of the shock front, contaminated material, etc.)

Several other terms which occur repeatedly in the literature should be understood.

Ground zero, or GZ is the vertical projection on the earth's surface of the burst point.

Burst height refers to the elevation of the point of burst, either above the ground surface -- or sometimes, above mean sea level.

[redacted]

[redacted]

Slant range R is the distance from the point of burst to that point at which the value of flux or dose is desired. If such a point is on the ground surface, R obviously satisfies the relation

$$R^2 = (\text{distance from ground zero to receiver})^2 + (\text{height of burst above the ground surface at the receiver})^2$$

We should understand, however, that neutron radiation and gamma radiation from the fission products emanate from a source which, to within a good approximation, is a point source of radiation at the center of the fireball. When the neutrons have been slowed down to thermal energy by successive collisions in the air, they are captured by nitrogen nuclei. About 6 percent of these excited nuclei then emit nitrogen capture gamma radiation, which is of quite high energy (an average of about 6 Mev). This radiation is part of the initial gamma radiation, but obviously its source is distributed over a much larger volume than the gamma radiation from fission products, and the point source treatment is a much poorer approximation. This is especially true at high altitudes.

1.7 BIOLOGICAL CONSIDERATIONS

The relation between radiation flux and biological damage is very complicated. It will be discussed in Chapters 2 and 4. In the present paragraphs only such definitions are included as are necessary to understand the terminology.

Dose is a general term used to signify some measure of the radiation absorbed by an organism. Dose is measured in several different kinds of units which are described below.

One roentgen or r represents that amount of gamma radiation which, when absorbed in one cubic centimeter of pure dry air at one atmosphere pressure and 0°C, will generate one e.s.u. of charge of either sign, that is 2.08×10^9 ion-pairs. (An ion-pair is the combination of a free electron plus a positively charged atom which is missing an electron.) Since one ion-pair requires the expenditure of an energy of 32.5 ev to form, this is equivalent to 0.1082 erg-cm^{-3} or 83.5 erg-gm^{-1} of air.

One roentgen equivalent physical or rep is defined as that amount of radiation of any type which, when absorbed in one gram of organic tissue, will deposit 93 ergs of energy. (This unit has also been defined in the literature as 84 erg-gm^{-1} of tissue, which has led to some confusion. The latter definition will not be used in the present work.)

One rad is defined as that amount of radiation of any type which, when absorbed in any material (not necessarily tissue), will deposit an energy of 100 erg-gm^{-1}.

One roentgen equivalent man (or mammal) or rem is defined as that amount of radiation which, when absorbed in mammalian tissue, will cause the same biological damage -- according to any definite but arbitrarily defined criterion -- as the absorption of one rep of 400 kev (1 kev = 1 thousand electron volts) gamma radiation.

The relative biological effectiveness or RBE is defined as the ratio of the dose in rem to the dose in rep. It is very close to unity for gamma rays above 400 kev, but is greater than unity and is dependent on energy for neutrons.

Neutron radiation dosages can be measured in rem, rad, or rep. It cannot be measured in roentgens. Gamma radiation, on the other hand, is most commonly measured in roentgens. This is identical to the dose in rep or rem for photons above 400 kev in energy.

The LD_{50} or 50 percent lethal dose is that dose of any type of radiation which will cause the death, within a certain period of time (usually 30 days), of 50 percent of the population of organisms irradiated.

Important simplifications in the relations between radiation flux and dose occur when

1. The shape of the flux energy spectrum is constant from point to point within a satisfactory degree of approximation. In this case, the dose in both rep and rem is simply proportional to the total flux in any specified energy range.

[redacted]

2. The RBE is constant with energy so that the doses in rem and rep are either identical or directly proportional to each other.

1.8 AVERAGE AIR DENSITY

The exponential term in Eq. 1.6:4 for the total (scattered and unscattered) radiation from a point source in a homogeneous medium is given as $e^{-\mu R}$ or $e^{-\rho\mu_0 R}$. For a non-homogeneous atmosphere, however, this exponential requires generalization. An approximation due to Weidler and Ward, [4] which is satisfactory for most applications, although not exact, replaces these terms as follows:

$$e^{-\mu R} = e^{-\int_0^R \mu dr} = e^{-\bar{\mu} R} \qquad (1.8:1)$$

$$e^{-\rho\mu_0 R} = e^{-\mu_0 \int_0^R \rho dr} = e^{-\bar{\rho}\mu_0 R}$$

where

$\bar{\mu}$ = average apparent linear attenuation coefficient between point of burst and receiver

$\bar{\rho}$ = average air density between point of burst and receiver, expressed in units of d_0

d_0 = density of pure dry air at 0°C and one atmosphere pressure, 1.293×10^{-3} gm-cm^{-3}

μ_0 = apparent linear attenuation coefficient for air at density d_0.

Since the exponential term will normally be expressed in terms of the apparent linear attenuation coefficient at standard conditions μ_0, it is therefore equal to $e^{-\rho\mu_0 R}$ for homogeneous atmospheres and $e^{-\bar{\rho}\mu_0 R}$ for non-homogeneous atmospheres. The required values of ρ or $\bar{\rho}$ are calculated as outlined below.

If the pressure and temperature of the atmosphere are uniform between the burst point and the receiver, the air density ρ may be calculated from the ideal gas laws and a knowledge of the air pressure and temperature.

$$\rho = \frac{1}{d_0} \frac{A_a}{G} \frac{p}{T} = 0.269 \frac{p}{T} \qquad (1.8:2)$$

where

ρ = air density between burst point and receiver, expressed in units of d_0

A_a = average molecular weight of air

G = gas constant

p = atmospheric pressure, millibars

T = atmospheric temperature, °K.

Eq. 1.8:2 is presented graphically in Fig. 1.8:1

If the pressure and temperature differences of the atmosphere between the burst point and the receiver are small, the average air density may be satisfactorily found by taking the average between

the density at the burst point ρ_B and at the receiver ρ_Z, these point densities in turn being calculated from Eq. 1.8:1

$$\bar{\rho} = \frac{1}{2}(\rho_B + \rho_Z) = \frac{0.269}{2}\left(\frac{p_B}{T_B} + \frac{p_Z}{T_Z}\right) \qquad (1.8:3)$$

If the pressure and temperature differences between the burst point and the receiver are not small, the average air density may be found most easily through a knowledge of the pressure and elevation of the two points.

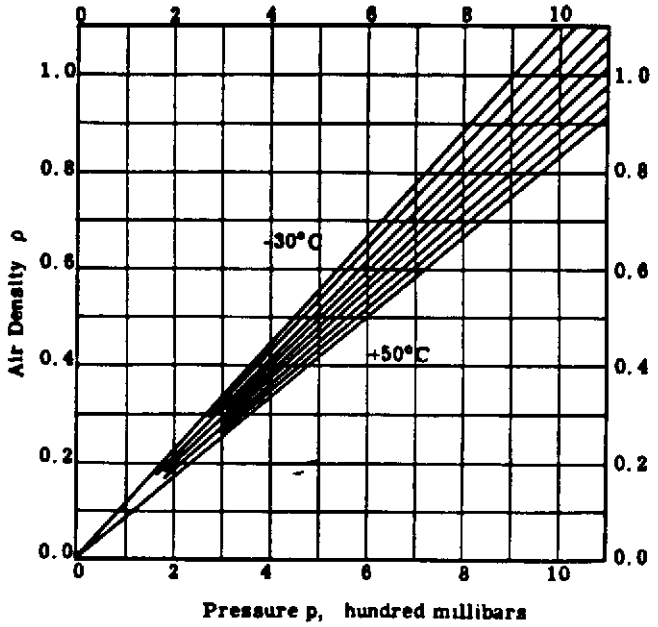

Figure 1.8:1 Air Density ρ (in units of 0.001293 gm-cm^{-3}) as a Function of Pressure and Temperature. The curves are spaced at 10° intervals going monotonically from -30°C to +50°C.

$$\rho = 0.269\,\frac{p}{T}$$

Eq. 1.8:1 defines the average air density $\bar{\rho}$ as follows:

$$\bar{\rho} = \frac{\int_0^R \rho dr}{R} \qquad (1.8:4)$$

If y represents the elevation, then dr is proportional to dy along the straight line connecting the point of burst and the receiver. Eq. 1.8:4 may then be written

$$\bar{\rho} = \frac{\int_{y_B}^{y_Z} \rho dy}{\Delta y} \qquad (1.8:5)$$

where

y_Z = elevation of the receiver

y_B = elevation of the burst point

$\Delta y = y_Z - y_B$

The relationship between change in pressure with elevation is

$$dp = -\rho g \, d_0 \, dy \tag{1.8:6}$$

where g = acceleration of gravity.

Substituting for ρdy in Eq. 1.8:5 yields

$$\bar{\rho} = \frac{-\int_{p_B}^{p_Z} dp}{d_0 g \, \Delta y} = \frac{1}{d_0 g} \left| \frac{\Delta p}{\Delta y} \right| \tag{1.8:7}$$

If Δp is expressed in millibars and y in feet, this becomes

$$\bar{\rho} = 25.8 \left| \frac{\Delta p}{\Delta y} \right| . \tag{1.8:8}$$

Eq. 1.8:8 is presented graphically in Fig. 1.8:2. Nearly all calculations of interest will be handled adequately by Eq. 1.8:2, 1.8:3, and 1.8:8, and the associated figures.

In addition to the three equations, presented above, there are other relationships which may be useful in special circumstances.

If as a low order approximation one assumes the temperature of the atmosphere to be uniform, it can easily be shown that

$$\bar{\rho} = \frac{\rho_B - \rho_Z}{2.303 \log_{10} \frac{\rho_B}{\rho_Z}} \tag{1.8:9}$$

As a matter of fact this is a better approximation than Eq. 1.8:3 and for small values of $(\rho_B/\rho_Z)-1$ reduces to Eq. 1.8:3. Because its accuracy is quite satisfactory for current uses and it is simpler to use, Eq. 1.8:3 is recommended, however.

A second alternative relation is derived if it is assumed that the temperature varies linearly with elevation, an assumption which is correct within the troposphere. Under this condition

$$\bar{\rho} = \frac{\rho_B \, G \, T_B}{A_a \, g \, \Delta y} \left[1 - \left(\frac{T_B}{T_Z} \right)^{\frac{A_a \, g \, \Delta y}{G \, \Delta T}} \right] \tag{1.8:10}$$

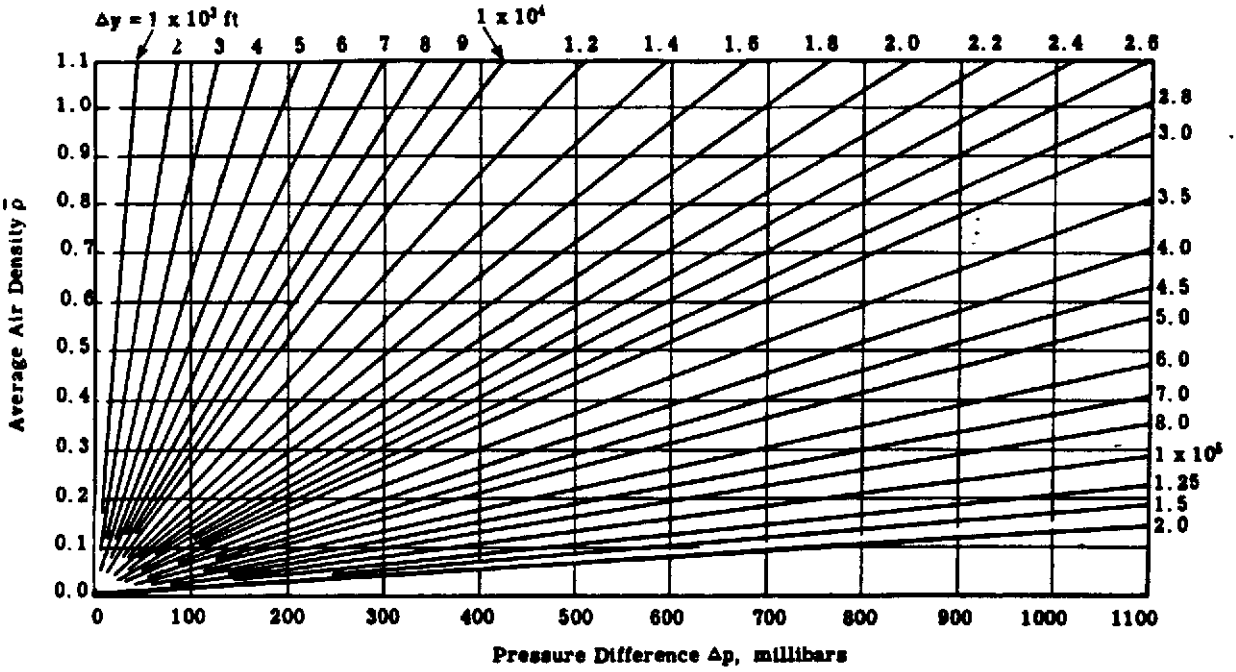

Figure 1.8:2 Average Air Density $\bar{\rho}$ (in units of 0.001293 gm-cm^{-3}) as a Function of the Difference in Pressure and Elevation Between the Point of Burst and the Receiver.

$$\bar{\rho} = 25.8 \left| \frac{\Delta p}{\Delta y} \right|$$

PROBLEM 1

The pressure and temperature at the point of burst are given. The air between the burst point and the receiver is at the same pressure and temperature. It is required to compute the average air density ρ between the two points, in units of d_0 (1.293 x 10^{-3} gram-cm^{-3}).

Solution

1. Convert the units of pressure to millibars and temperature to °K if the information has not been supplied in these units. (See the list of conversion factors after Problem 3.)
2. Either compute the air density at the point directly from the formula

$$\rho_B = 0.269 \frac{p_B}{T_B}$$

or read ρ_B from Fig. 1.8:1. Since the temperature and pressure are constant between the two points, the air density at the point of burst ρ_B, is equal to the desired air density ρ.

Example

The air pressure and temperature between the point of burst and a receiver point at a horizontal distance of 2000 yards are 950 millibars and 20°C. It is required to compute the air density in units of 1.293 x 10^{-3} gram-cm^{-3} between these two points.

1. We must convert the temperature to °K. Thus, $T = 273 + 20 = 293°K$.

2. The air density ρ is given by

$$\rho = 0.269 \frac{p}{T} = 0.269 \frac{950}{293} = 0.87,$$

which can also be read from Fig. 1.8:1 for p of 950 millibars and T equal to 20°C.

PROBLEM 2

The pressure and temperature at both the point of burst and an external point are given. The pressure, temperature and difference in elevation between the two points are not greatly different. It is required to find the average air density between the two points in units of 1.293×10^{-3} gram-cm^{-3}.

Solution

1. Convert the units of pressure to millibars and temperature to °K if the information has not been supplied in these units.

2. Compute the average air density directly from the formula

$$\bar{\rho} = \frac{1}{2}(\rho_B + \rho_Z) = \frac{0.269}{2}\left(\frac{p_B}{T_B} + \frac{p_Z}{T_Z}\right)$$

Example

At the point of burst the pressure is 950 millibars and the temperature 25°C. At the external point the corresponding figures are 900 millibars and 15°C. The difference in elevation is 1500 ft. It is required to find the average air density between the two points in units of 1.293×10^{-3} gram-cm^{-3}.

1. We must convert the temperatures to °K.

$$T_B = 273 + 25 = 298°K$$

$$T_Z = 273 + 15 = 288°K$$

2. The average air density $\bar{\rho}$ is given by

$$\bar{\rho} = \frac{0.269}{2}\left(\frac{950}{298} + \frac{900}{288}\right) = 0.85$$

PROBLEM 3

The pressure at both the point of burst and an external point are given. The difference in elevation is also given, and this may be large (more than 2500 ft). It is required to find the average air density between the two points in units of 1.293×10^{-3} gram-cm^{-3}.

Solution

1. Convert the units of pressure to millibars and difference of elevation to feet if the information was not supplied in these units.

2. Either compute the average air density $\bar{\rho}$ directly from the formula

$$\bar{\rho} = 25.8 \left| \frac{\Delta p}{\Delta y} \right|$$

or read $\bar{\rho}$ from Fig. 1.8:2

Example

The pressure at the point of burst is 1000 millibars. At a receiver of higher altitude the pressure is 700 millibars. The difference in elevation is 10,000 ft. It is required to find the average air density $\bar{\rho}$ between these points in units of 1.293×10^{-3} gram-cm^{-3}.

1. No changes of units are necessary.
2. The average air density $\bar{\rho}$ is given by

$$\bar{\rho} = 25.8 \left| \frac{\Delta p}{\Delta y} \right| = 25.8 \frac{1000-700}{10,000} = 0.77,$$

which can also be read directly from Fig. 1.8:2 for Δp of 300 millibars and Δy of 10,000 ft.

CONVERSION FACTORS

For convenience we include here some formulae and conversion factors for use when input data are supplied in units different from those illustrated.

Units of Pressure

1 standard atmosphere

= 29.92 in. of mercury at 0°C

= 76 cm of mercury at 0°C

= 33.9 ft of water at 4°C

= 1013.25 millibars

= 14.7 lb-in.$^{-2}$

= 2117 lb-ft^{-2}

1 millibar

= 1000 dyne-cm^{-2}

Units of Temperature

F = temperature in degrees Fahrenheit

C = temperature in degrees Centigrade

K = temperature in degrees Kelvin

C = 5/9 (F-32)

K = C + 273

Units of Length

1 meter
= 3.281 ft
= 1.094 yd
= 6.214×10^{-4} miles

1 in.
= 2.54 cm

1.9 REFERENCES

1. S. Glasstone and M. Edlund. Elements of Nuclear Reactor Theory. D. Van Nostrand Co. Inc. Nov. 1952. (Unclassified)
2. S. Glasstone. LA-1632. Jan. 1954. (Secret)
3. J. Malik. LA-1620. Jan. 1954. (Secret)
4. R.C. Weidler and E.N. Ward. SWR 54-4. May 1954. (Secret)

Chapter 2.

BIOLOGICAL EFFECTS OF RADIATION

2.1 INTRODUCTION

This chapter has been prepared to provide a review of the broad field of radiobiology as it applies to military problems.

There are some data available for man which are not particularly satisfactory. There is a large volume of data obtained from laboratory and weapons test studies in experimental animals. It is manifestly not possible to cover within the scope of this document the entire field of radiobiology. This chapter attempts to review the problems and to point out and evaluate areas of controversy. For details, it is suggested that the reader consult the general and specific references.

In many respects the data presented in other sections of this handbook have been collected for the purpose of evaluating the hazard of ionizing radiation to personnel. Except at very high dosages (10,000 r and greater), ionizing radiation is without effect on ordinary material other than radiation dosimeters and photographic film. The basic purpose of this chapter is to provide some guidance in the use of physical data for the estimation of personnel hazard. There will be some repetition of physical data detailed elsewhere in this handbook to provide continuity. In many, if not most, instances the needed correlation between exposure dose and clinical findings is lacking because of insufficient data.

2.1.1 SOURCES OF DATA

The primary sources of pertinent medical radiobiological information are:

1. the evaluation of the results of the Hiroshima and Nagasaki experience by the Atomic Bomb Casualty Commission (ABCC)[1],
2. the evaluation of the results of the accidental exposure of the Marshallese during Operation Castle[2],
3. accidents in atomic energy laboratories[3, 4], and
4. clinical radio-therapeutic experience.

In addition, there is a large volume of experimental animal data from which certain inferences regarding man may be drawn, but which cannot be directly applied.[5, 6, 7] In general, animal experiments indicate the pattern of response that may be anticipated in man, but are not an ideal source of information. Significant differences in details, particularly quantitative, preclude direct extrapolation to man. In fact, all sources lack certain pertinent critical information.

As an example, review of the problems associated with the calculation of radiation dosage at Hiroshima and Nagasaki results in the conclusion that at Hiroshima neutron effects might predominate while at Nagasaki, "nearly all the dosage is due to gamma rays." Aside from the difficulties associated

with estimating the flux and energy spectrum of neutrons and the gamma ray dose, Figure 2.1:1 illustrates the difficulty in assigning to a given location a number for dose because of the rapid decrease of the dose with ground distance, both for neutron and gamma rays.[8] This is without consideration of an estimate of shielding factors. As will be discussed later, the biological effectiveness of neutrons may be greater than gamma rays. Comparison of the results obtained at Hiroshima with those at Nagasaki should make some provision for this difference. But, in addition, the flux and spectrum for a given location are so poorly known that, in all probability, quantitative data purporting to relate lethality to dose are of dubious value.

The dosimetry problems associated with the exposure of the Marshallese make it difficult to determine precisely the gamma ray dose. The data were insufficient to permit even an attempt to be made to estimate the skin dose resulting from soft X-rays and beta radiation.[9] The many problems and uncertainties involved in the dosimetry of accidents in atomic energy laboratories are pointed out in a description of an accident at the Argonne National Laboratory.[4]

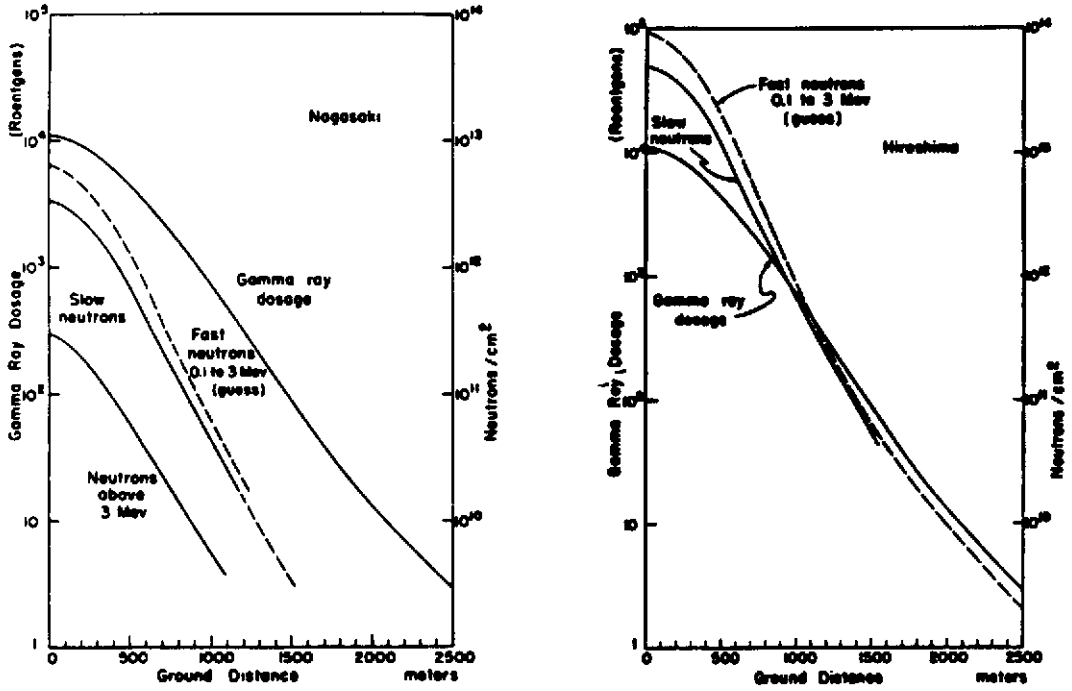

Figure 2.1:1 Neutron and Gamma Radiation as a Function of Distance Estimated for Bursts at Hiroshima and Nagasaki.[8] The gamma ray dosage in roentgens is plotted as a function of the distance along the ground from the point just below the bomb explosion. The number of neutrons-cm^{-2} is indicated in the scale at the right of each drawing. This scale applies for slow neutrons, namely those below 1 ev, and for fast neutrons as indicated. The fast neutron curve represents a really wild guess.

2.1.2 TYPES OF HAZARD

The personnel hazard may be divided into immediate and late considerations. The immediate hazard is that involved in the production of acute effects, principally lethality, acute radiation illness or skin lesions. The long term problem is that of the late effects; this involves both the individuals concerned and, through the genetic changes produced by radiation, their progeny for many generations.

2.1.3 SOURCES OF RADIATION

There are two separate sources of ionizing radiation to be considered. These are:

1. External gamma, beta, and neutron radiation. For residual radiation this is a combined beta and gamma radiation; for initial radiation, neutrons are an additional source of ionizing radiation.
2. Internally deposited radioactive materials. For military considerations, this is a problem associated with fallout.

2.2 EXTERNAL RADIATION

2.2.1 INTRODUCTION

External radiation constitutes a potential hazard to personnel from the moment of detonation of an atomic weapon. The initial radiation consists of gamma and neutron radiation, propagated for large distances in air. In addition, within the cloud there is beta radiation, but it is difficult to conceive of a situation where beta radiation will constitute a personnel hazard before fallout occurs. While falling and after completion of fallout, the external radiation consists of both beta and gamma radiation.

2.2.2 DOSIMETRY

From the standpoint of estimation of personnel hazard from external radiation, the basic necessary physical data are:

1. the type of radiation, whether it be gamma, beta, neutron, or some combination of these,
2. knowledge of the energy spectrum and flux, and
3. source geometry.

2.2.3 UNITS OF DOSE

There are several units of radiation dose currently employed.[10]

1. Roentgen - that quantity of X or gamma radiation which produces, in 1 cm^3 of pure dry air at STP conditions, 1 e.s.u. of charge of either sign, that is 2.08×10^9 ion-pairs. Since one ion-pair requires the expenditure of 32.5 ev to form, this is equivalent to 0.1082 ergs-cm^{-3} or 83.5 ergs-gm^{-1} of air.

2. Rep (roentgen equivalent physical) - that quantity of ionizing radiation which results in an absorbed dose in any material at the site of interest that is equivalent to that obtained from 1 r of gamma rays; this quantity is usually taken as 83.5 ergs for 1 gm of air; for soft tissue this is 93 ergs-gm^{-1} tissue. This unit is independent of the type of energy of the ionizing radiation.

3. Rad - that quantity of ionizing radiation which results in the transfer of 100 ergs-gm^{-1} to any material. This is a recently adopted unit. It can be seen that for soft tissue it is almost equivalent to the rep.

4. Rem - roentgen equivalent mammal (man) to be defined later (see Section 2.3).

From these definitions it is seen that the roentgen is a unit applicable only to X or gamma radiation, while the rep and rad are independent of the source type and energy.

2.2.4 CONSIDERATION OF DEPTH DOSE CURVES AND CORRELATION WITH BIOLOGICAL EFFECT

The effect of ionizing radiation is primarily dependent upon the dose absorbed in tissue, not the dose measured in air. The basic problem is a determination or a calculation of the absorbed dose in

tissue. This is probably best approached through the use of a depth dose curve. A depth dose curve is a graph of the relative amount of ionization produced at various depths in the body or some other absorber. Depth dose curves have had extensive application in radiation therapy and in radiobiological research. It is this experience which makes possible the quantitative prediction of biological effect from a depth dose curve.[11]

For the range of beta particle energies encountered in fission products maximum penetration into tissue is of the order of millimeters, while for X and gamma rays and neutrons the degree of penetration can vary from a few millimeters to those which traverse the entire body. As a consequence of the change in absorption coefficient with X-ray energy, penetration into the body varies with the energy. For example, at 50 KVP the dose delivered to tissues deeper than 2 cm is very small compared to that at the skin surface. The skin surface dose to produce in LD_{50} (lethal dose for 50 percent of the irradiated population) might reasonably be expected to be greater for 50-KVP X-rays than for 250-KVP X-rays since the 50-KVP X-rays may be considered to produce a skin "burn," while with 250-KVP X-rays a relatively uniform dose throughout the body is produced. Fig. 2.2:1 shows the variation in

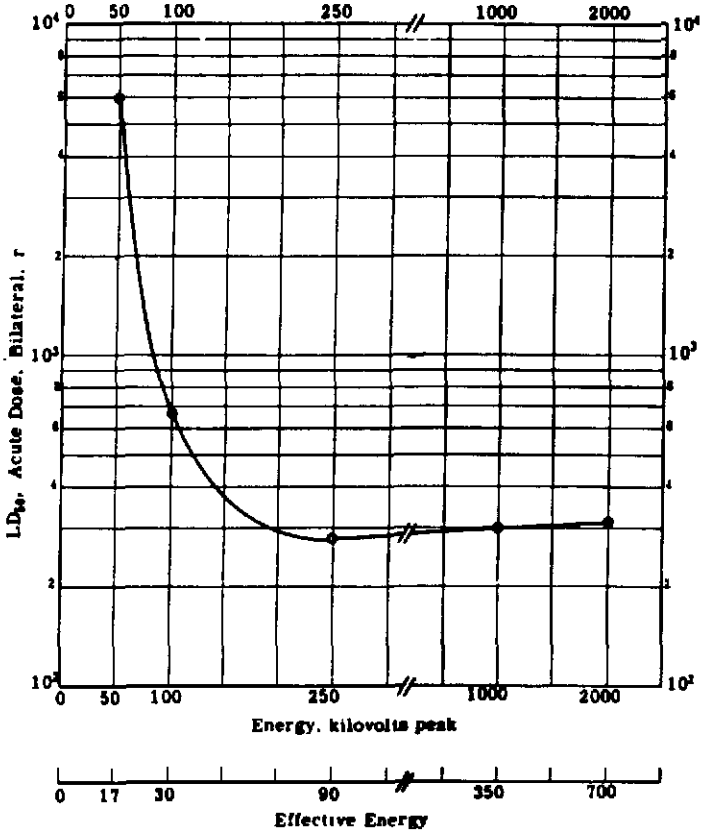

Figure 2.2:1 The LD_{50} for Dogs for Bilateral Radiation as a Function of Energy.[12]

LD_{50} for dogs for bilateral radiation as a function of energy.[12] (In this instance half of the total dose was delivered to each side of the animal.) This figure demonstrates that below 175 KVP the air exposure dose LD_{50} increases rapidly to 6000 r at 50 KVP. With the weaker X-rays, only the skin and subcutaneous tissues are irradiated. The dose to produce lethality increases with decreasing X-ray energy, since the deeper tissues are not irradiated. At 50 KVP the distribution of the dose in the tissue is comparable to that produced by external beta radiation in the range 2 to 3 Mev. This makes this energy (50 KVP) comparable to external beta radiation, and it would be anticipated that the dose to produce 50 percent lethality would be comparable to that required for external beta radiation.

The beta particles arising from fission products constitute a source of radiation only for the skin and, in sufficient quantity, produce a condition known as a "beta burn" which can be lethal. The two principal considerations in the evaluation of the hazard of beta radiation to the body are:

1. dose to skin, and
2. area of skin involved.

For example, it has been determined that the LD_{50}^{30} (lethal dose for 50 percent of the irradiated population in 30 days) for beta radiation to the entire body varies from 2200 rep (baby rat) to 17,000 rep (rabbit);[13] while the same dose range delivered to a small area of skin, e.g., 1 cm^2 will not result in death, but will produce only local changes in the skin. The relatively low LD_{50} for beta radiation for the baby rat is probably due to the fact that for such small animals there is significant ionization beneath the skin, and while this is not uniform total body irradiation, a considerably greater percentage of the tissues are irradiated than in larger animals.

The lethal dose for beta radiation of man is not known.[14] Animal studies indicate that the total integrated dose to produce 50 percent lethality may be directly proportional to the body mass. Extrapolation to man yields an LD_{50} for beta radiation of approximately 40,000 rep which is not in keeping with other data and should not be used for any personnel hazard calculations. On the other hand, from another line of approach, the beta radiation LD_{50} dose is calculated to be approximately 5000 rep. The latter appears to be a more acceptable value and is comparable to the LD_{50} for dogs for 50-KVP X-rays, but it is unestablished and must be considered only as an estimate of questionable value arrived at by extrapolation from animal data.

X-rays and neutrons of sufficient energy produce ionization throughout the body resulting, when applied in sufficient quantities, in acute radiation illness.

2.2.5 DOSIMETRIC METHODS

In general, and for most peacetime applications, film badges are the most common dosimeters in current use. Varying sensitivity to various types of ionizing radiations precludes their use for precise dose measurements in mixed radiation fields. In addition, at weapons tests, where mixed radiations make the physical measurement of dose difficult, biological dosimeters have been used. Generally, mice are placed at various distances from the point of detonation in suitable containers to protect against the effects of thermal radiation and blast. Then the effects of the ionizing radiation are measured by one or more biological endpoints. The biological endpoints used are:

1. mortality (30 day),
2. change in weight of the spleen and thymus,
3. depression of red cell formation, as measured by the incorporation of radioactive iron into red cells,
4. change in weight of the gastro-intestional tract, and
5. survival time (in the supralethal dose range).

The results are then compared with those obtained with X-rays in similar animals under laboratory conditions. The results are expressed not in terms of the mixed bomb ionizing radiation, but that at a particular station, the total effect of the ionizing radiations received is equivalent to a particular dose of X-rays.[15,16] The results may be expressed in rem (see Section 2.3 for definition of rem).

Chemical dosimeters have also been developed, but are less widely used than any other type of dosimeter. It is probable that because of their relative simplicity, chemical dosimeters will become more widely used.[17] Scintillation glass dosimeters have also been developed for wide distribution in the armed services.[18] Gamma radiation is generally best determined by some type of ionization chamber, although if suitably calibrated, photographic film may be used.

The measurement of neutrons is more complex. There are several methods; one is the measurement of flux and energy spectrum and calculation from this data of a depth dose curve. The flux and energy spectrum of neutrons can be determined through the use of the activation detector methods (see Chapter 4). Calculation of a depth dose curve for neutrons is not a simple matter. For small animals (mice), a first collision tissue dose calculation is adequate. Assuming a tissue equivalent medium, the mean energy absorbed is[19]

$$\overline{U} = 1.72 \times 10^{-32} E \sum_i \frac{2 A_i N_i \sigma_i}{(1 + A_i)^2} \quad \frac{\text{rep-cm}^2}{\text{neutron}} \qquad (2.2:1)$$

where

E = incident neutron energy, Mev

A_i = ratio of atomic mass of element i to neutron mass

N_i = concentration of element i, atoms-cm^{-3}

σ_i = scattering cross section of element i, barns (10^{-24} cm^2)

Fig. 2.2:2 shows a first collision neutron dose curve for tissue as a function of neutron energy.

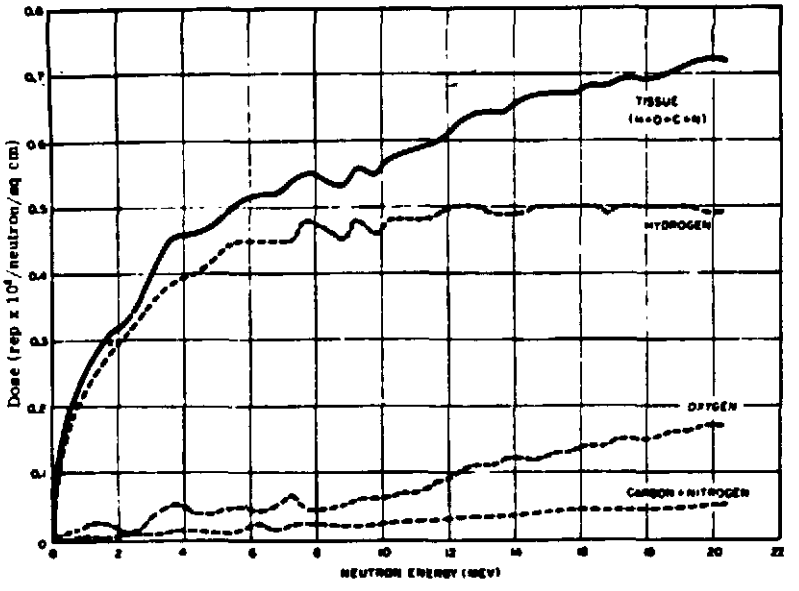

Figure 2.2:2 First Collision Neutron Rep Curve for Tissue[19]

For man it is necessary to consider subsequent collisions and to calculate a depth dose curve. Such depth dose curves have been calculated (see Fig. 2.2:3).[20] The use of suitable ionization chambers in a phantom permits a direct determination of the relative ionization as a function of depth.[19]

Table 2.2:1 shows the calculated flux to produce 50 percent lethality in man for neutrons from thermal energy to 3.0 Mev.[21] This table demonstrates that from 1 kev to 3.0 Mev there is approxi-

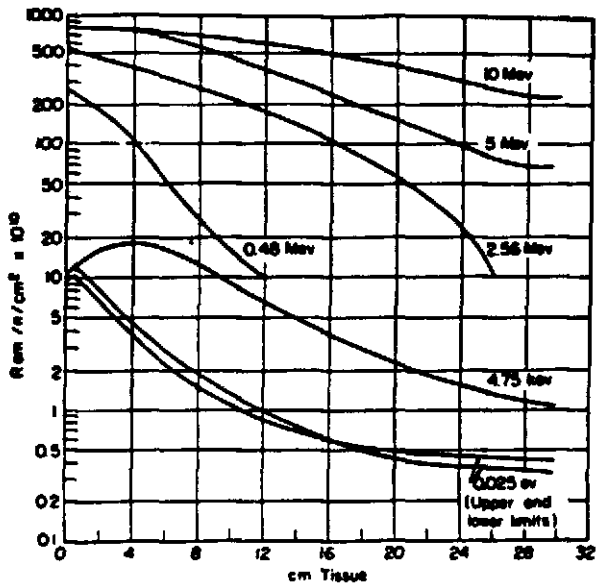

Figure 2.2:3 Theoretical Depth Dose Curves for Monoenergetic Beams Incident on a 30-cm Slab of Tissue.[20]

TABLE 2.2:1

LD_{50} Neutron Flux as a Function of Energy

	LD_{50} Flux, neutrons-cm^{-2}		
Neutron Energy	Ref.[21]	Ref.[22]	Ref.[23]
Thermal	1.6×10^{12} (1)	5×10^{12}	
1 kev	1.8×10^{12}		
3 kev	1.7×10^{12}		
10 kev	1.4×10^{12}		
30 kev	9.2×10^{11}		
100 kev	4.1×10^{11}		
300 kev	1.6×10^{11}		2.1×10^{11} (2)
1 Mev	5.0×10^{10}		14×10^{10}
3 Mev	1.7×10^{10}	6×10^{10}	9.1×10^{10}

(1) These are estimated values. It is suggested that the reader review the source reference[21] for a better appreciation of the methods used to calculate these numbers and their validity. It is probable that these numbers may be changed significantly in the future.

(2) Based on the values given in the source reference[23] for conversion from rep to neutron-cm^{-2} and values of the RBE and LD_{50} dose for neutrons of 1.3 and 450 rem, respectively.

mately a 94-fold decrease in the calculated flux to produce 50 percent lethality. Fast neutrons are slowed down in tissue by elastic collisions of which 85 to 95 percent occur with hydrogen and result in recoil protons. Because of this and because of the relatively high, compared to X-rays, linear energy transfer of protons, the biological effect produced is greater than would be predicted from a comparable absorbed dose (in erg-gm^{-1}) of X-rays (see Section 2.3).

For thermal neutrons, on the other hand, capture reactions predominate. These are the (n, p) reaction with N^{14}, resulting in the emission of a 0.66 Mev proton, and the (n, γ) reaction with hydrogen with subsequent emission of a 2.2 Mev gamma ray. It has been calculated that below 10 kev the latter reaction predominates.

Recently it has been observed that for five test weapons, within the ground range of interest, the bomb neutron spectrum is relatively constant. For these five weapons, a calculation of dose due to the entire bomb neutron spectrum can be carried out from the measurement of the flux of a single energy region. It has not been determined whether this will hold for other weapon types, although preliminary re-evaluation of previous weapons test biological data indicates that may be so.

The dose due to beta radiation is best determined by a suitable thin walled ionization chamber.

As will be discussed below, an important consideration is the source and receiver geometry.[24] Initial radiation can, to some extent, be considered to be unidirectional gamma and neutron irradiation, the departure from unidirectional being a result of multiple scattering in air, while for fallout radiation, the situation is different.

Beta radiation can be considered to arise from two sources:

1. beta particles emitted from fission products upon the surface of the ground, and
2. beta particles emitted from fission products that contaminate the skin or clothing.

In case one, the individual is in a field of beta radiation, and, aside from consideration of the protection due to clothing and the attenuation of the flux with height from the ground surface, may be considered to be in a field of uniform beta radiation. However, in case two, there is the beta radiation arising from "hot particles" contaminating the skin or clothing and producing a local area of intense irradiation which can result in a localized skin "burn."

Directly measured depth dose curves furnish the most satisfactory approach to the prediction of biological effect. The use of small ionization chambers in a phantom appears to be satisfactory.[25, 26] This type of measurement consists in the placing of small ionization chambers at various depths in a masonite phantom. After exposure, the readings of the ionization chambers are plotted as a function of the depth from the surface of the phantom. This is a directly determined depth dose curve for the particular source, source geometry and receiver. For neutron irradiation a first collision dose calculation with an estimate of the attenuation due to depth is a good approximation. Typical field test beta and gamma depth dose curves are shown in Fig. 2.2:4.

2.2.6 SIGNIFICANCE OF AIR DOSE, SKIN DOSE, AND MID-LINE DOSE FROM X-RAY RADIATION

1. Collimated beam source geometry

Considerable confusion has arisen from failure to stipulate how the dose was measured.[24] This is because from the same narrow collimated X-rays flux in air, the three quantities, air dose, skin dose, and mid-line dose, can and do differ significantly. Air exposure is the dose measured in free air, that is, without backscatter. Skin dose is the dose measured with backscatter, that is, the ionization chamber is placed at the surface of the body. Mid-line dose is the dose either measured in a phantom with size and radiation absorption characteristics similar to the biological object under consideration or calculated from a knowledge of the energy spectrum and absorption constants. The skin dose is higher than the air exposure dose due to backscatter. The increase due to backscatter varies with the energy and may amount to an increase of as much as 50 percent or more above the air dose.[27] The

mid-line dose is a function of the energy spectrum and body size and is usually less than the air dose and skin dose. The relationship between air dose and mid-line dose is dependent upon the source and receiver geometry and with low energy X-rays on the absorption coefficient. Since there is considerable variation with energy in the absorption coefficient, the ratio mid-line dose/air dose can vary considerably. For example, from weak X-rays (below 50 KVP), the mid-line dose may be negligible as compared to the skin dose, in which case the ratio mid-line dose/air dose will be very low while in the gamma ray region this ratio may approach one.

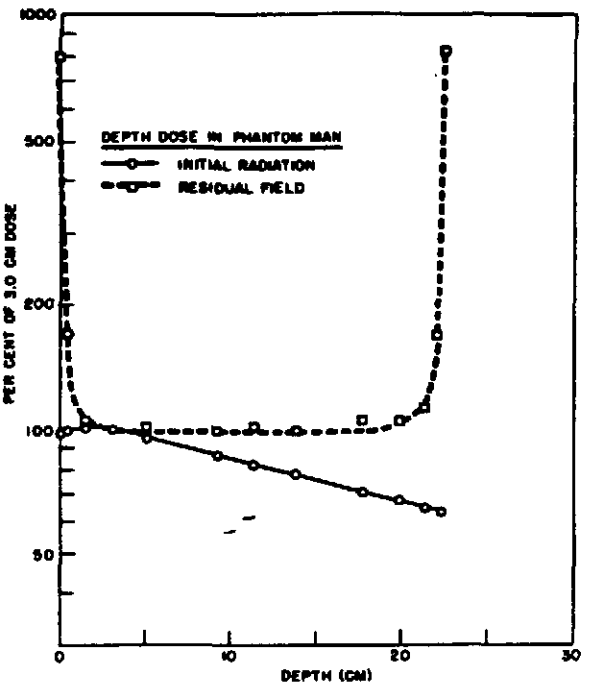

Figure 2.2:4 Comparative Depth Doses in a Phantom Man of Initial Atomic Bomb Radiation and Radiation from a Field of Fission Products.[2] (see also 25 and 26) The increase in dose at 20 cm for the residual radiation field is a result of exposure in an infinite plane source geometry of a finite-size phantom with measurement of dose throughout the phantom.

It can be readily seen that failure to stipulate the measurement conditions has led to considerable confusion.

2. *Infinite plane source geometry*

For the case of radiation in a fallout field, i.e., infinite plane source geometry, the relationship between air dose, skin dose, and mid-line dose is different. Direct observation of the hard gamma radiation component of a fallout field in a phantom masonite man indicates that within the error of measurement there is no appreciable change below 3 cm with depth, that is, the gamma radiation depth dose curve is relatively flat, and equal to the free air exposure in roentgens,[25, 26] as measured by a thick walled ionization chamber.

Which of these three measurements, air, skin or mid-line dose, is the most satisfactory? In all probability, there is no single measurement which will be satisfactory in all cases. For weak X-rays (below 50 KVP) certainly the mid-line dose is unsatisfactory, while the skin dose or air dose may be

misleading if it is not realized that this radiation is essentially body surface or skin radiation. The measurement to be used depends upon the biological endpoint under consideration. The mid-line dose is to be used when total body irradiation, acute radiation illness, and lethality are under consideration since it affords the best correlation between dose and effect. However, for consideration of the skin beta "burn" hazard, it is necessary to know the dose to the skin. It is then apparent that a single measurement or calculation is not satisfactory for all cases. For military operational purposes, it has not been determined if it is necessary to know both the skin and mid-line dose.

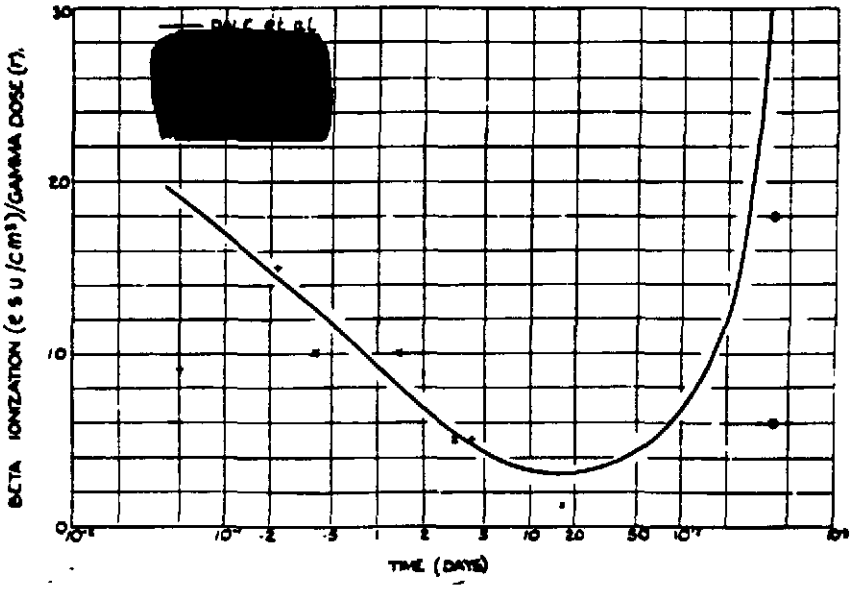

Figure 2.2:5 Beta-Gamma Ratio at 1 Meter Above Earth's Surface. The line represents theoretical values; the points represent observed values.

For the fallout field where there is a combination of both beta radiation X-rays, and gamma rays, the use of the phantom masonite man probably defines the problem most satisfactorily since the results permit an evaluation of the (1) dose to skin and (2) the whole body dose. The results may be expressed as a ratio, beta-gamma dose ratio. Experimentally this measurement has been carried out in a limited number of conditions. Values of the beta-gamma dose ratio varying between 2.5 and 28 have been observed at field tests.[26,28] Dale (cited by Kendall[28]) has worked out on a theoretical basis the variation with time of this ratio up to 400 days. Initially, the ratio surface dose/mid-line dose is high, approximately 15 to 20, decreasing to a minimum (approximately 2) at 10 to 20 days. (see Fig. 2.2:5).

2.3 CONCEPT OF RBE (RELATIVE BIOLOGICAL EFFECTIVENESS)[29,30,31,32]

With the availability of various types of ionizing radiation, it early became apparent that prediction of the effects of a given physical dose was inaccurate when the biological effects of heavy ionizing particles were compared to those of X-rays. This was particularly true for external neutron irradiation. Initially, neutron dosages were measured with a Victoreen ionization chamber and in units of n. One n is the neutron flux to produce a reading equivalent to 1 r in a 100 cm^2 Victoreen ionization chamber. Recently it has been confirmed that 1 n $\cong$ 2 rep.[33] However, the biological effect of 1 rep of neutrons is greater than would be anticipated from 1 rep of gamma radiation. To rationalize this discrepancy, the concept of relative biological effectiveness (RBE) was introduced. When compared to X-rays, and for equivalent biological effect, the dose required of any ionizing radiation is the product of the RBE and the dose delivered in rep. It should not be inferred that RBE is used only in connection

with neutrons. The RBE has been determined for alpha particles, protons, beta particles and within the spectrum of X and gamma rays. RBE is not a simple concept, it depends upon:

1. type and energy spectrum of ionizing radiation,
2. biological endpoint measured, and
3. dose and dose rate.[32]

It is particularly when different biological endpoints are considered that a large range of values for RBE are encountered. With the development of the concept of RBE, a new unit, the rem (roentgen equivalent mammal (man)), came into use. The rem is the product of the absorbed dose (in rep) and the RBE for the particular type of ionizing radiation used and biological endpoint measured.

An explanation for the fact that from a given physical dose the magnitude of the biological results varies is probably related to differences in linear energy transfer. Basically, it has been observed that, for the same physical dose, as the linear energy transfer (or the density of ionization per unit path length) increases, the magnitude of the biological effect goes through a maximum. A rigorous discussion of the mechanisms involved is not attempted here. Then, for the heavy charged particles (alpha particles and protons), the biological effect will generally be greater than for gamma rays. Since most of the energy transmitted to tissues from neutrons is through the ionization produced by recoil protons, it would be anticipated that for a given physical dose ($erg\text{-}gm^{-1}$) neutrons would produce a greater biological effect than gamma rays.

For military medical purposes, an important RBE, but not the only one desired, is the RBE for bomb neutrons for acute lethality, that is for the LD_{50}. This RBE has not been determined directly. An acute response which has been thoroughly studied is the spleen-thymus weight loss. Field tests indicate that this RBE is approximately 1.7 in mice.[34] Based on this value the spleen-thymus RBE for man has been estimated to be 1.3.[35] Until more definitive data become available, these values may be considered to apply for the LD_{50} RBE.

For 60-in. cyclotron fast neutrons with a different spectrum, the LD_{50} RBE in dogs is approximately one.[36] This indicates that the estimate of 1.3 may be high and that the RBE for acute lethality for man for bomb neutrons may be one or less.

2.4 ACUTE RADIATION SICKNESS

2.4.1 SYMPTOMATOLOGY

For military medical purposes the acute radiation syndrome should be considered from the following standpoints:

1. symptomatology and relationship of symptomatology to continued military effectiveness,
2. incidence and duration of symptoms as a function of dose, and
3. incidence of lethality as a function of dose.

For man the most useful sources of information are (1) the evaluation by the ABCC of the Hiroshima and Nagasaki experiences,[1] (2) experience derived from clinical radiation therapy, and (3) the evaluation of the Marshallese exposed in March 1954.[2] Unfortunately, all these sources of information contain basic uncertainties precluding good quantitative conclusions.

The Hiroshima and Nagasaki data are valuable for a description of disease, but cannot be closely correlated with dose because the dose is not known nor are estimates of the dose good. Clinical radiation therapy experience is complicated because most is partial body radiation, and in addition is complicated seriously by the underlying disease for which the patient is receiving therapy. Furthermore, many patients have imparted to them some degree of awareness of nausea and vomiting as possible complications of radiation therapy, making this symptom difficult to evaluate. The knowledge gained from the study and treatment of the Marshallese is also complicated by uncertainty as to the dose received and the effect of a changing dose rate.

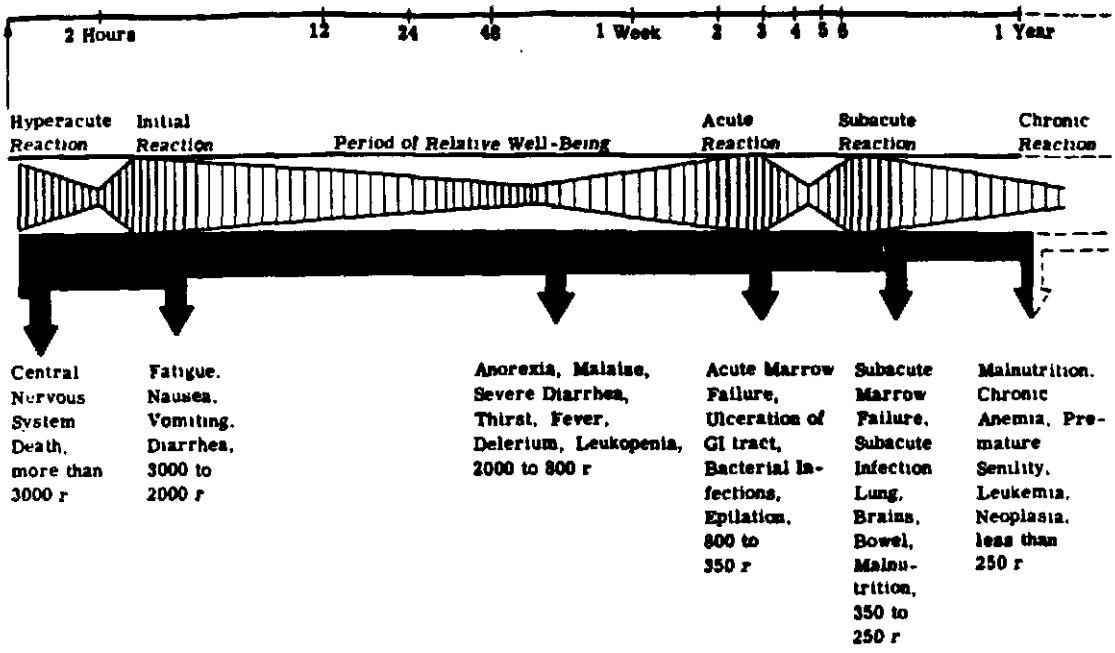

Figure 2. 4:1 Diagrammatic Representation of the Penetrating Radiation Syndrome in Man Following Acute Exposure and the Stages at Which Death Commonly Occurs.[37] The height of the vertical lines represents the severity, and the distance between the lines represents relative incidence of various conditions denoted at the bottom of the graph.

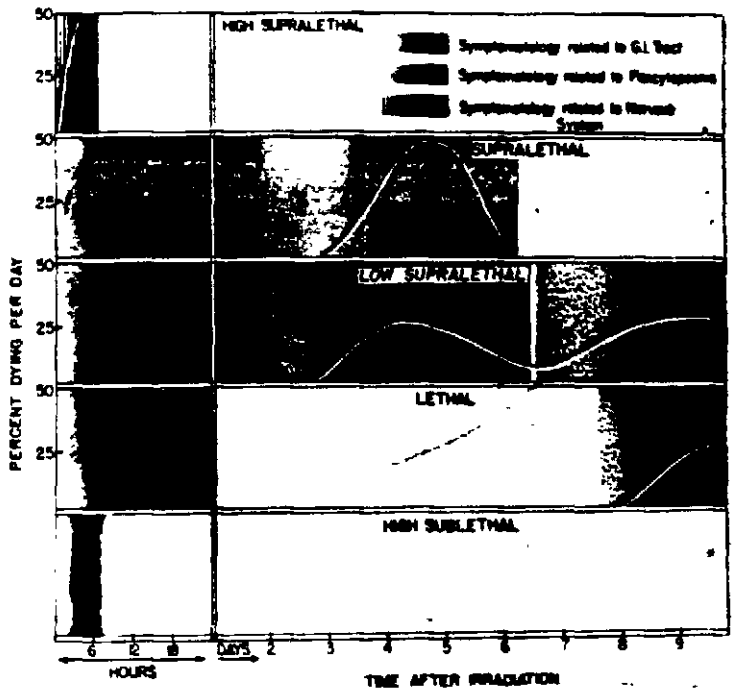

Figure 2. 4:2 Diagrammatic Representation of Radiation Syndrome.[38] The line represents the number of individuals dying per day. The degree of blackening represents the severity of the symptoms.

The situation is such that for the acute radiation syndrome, the symptoms encountered can be described. Evaluation in relation to dose, more importantly quantitative evaluation as to incidence, particularly in the range from no symptoms to 50 to 60 percent individuals symptomatically affected is not available. There is no information available for the case of protracted radiation.

The earliest symptoms are nausea and vomiting, generally occurring within 6 hours after a single acute whole body penetrating gamma ray exposure[37, 38] (see Figs. 2.4:1 and 2.4:2). Hereafter in the discussion, it is implied that the air dose figure mentioned does not include scattered soft gamma radiation. The incidence of nausea and vomiting as a function of dose is not well known. Probably below 50 to 100 r (air gamma exposure) there are no symptoms, and above 250 to 300 r there is a 100 percent involvement, but between no involvement and 100 percent involvement, the data are meager. The sickness dose for 50 percent of the population exposed is estimated as 150 r.[39] In a study of a small group (approximately 20 patients) treated with 200 r (skin dose) unilateral almost whole body radiation exposure, nausea and vomiting was noted in approximately 30 percent.[40] Of the Marshallese exposed to 175 r (air dose) over a period of approximately 46 hours, with 75 percent of the dose delivered in 36 hours, nausea was noted in two-thirds and vomiting and diarrhea in one-tenth. At doses below 200 r there are no additional symptoms. When both nausea and vomiting exist, it should be presumed that such individuals are not capable of satisfactorily performing a military task. There is no information on the capability of man to perform work following an exposure to radiation sufficient to induce these symptoms, nor is there adequate information as to the duration of these symptoms. Other clinical states involving nausea, vomiting and diarrhea are generally associated with malaise and lassitude sufficient to prevent the carrying out of useful physical work. In addition, the unevaluated and unknown degree to which individuals are motivated may play an important role. For the present the assumption of inability to perform a task is probably the best that can be made. The time required for recovery from these symptoms to full working or even partial working capability is not known: possibly a few days are sufficient.

At higher dose levels additional manifestations of radiation sickness appear, generally after a latent period of a few days. Because of the scarcity of data, it is difficult to describe the precise time course of the onset and extent of involvement, although various tables have been prepared in general, having their origin in the Hiroshima and Nagasaki experiences.

Following the initial nausea and vomiting, there is a latent period or asymptomatic period varying from approximately 1 to 3 weeks at 200 r to perhaps of the order of 1 week in the mid-lethal range (400-500 r). Following the asymptomatic period, at 2 to 4 weeks after exposure, malaise and loss of hair (epilation) occurs. Small hemorrhages (petechiae) in the skin and mouth appear. Ulcerations in the mouth with symptoms similar to that of a sore throat plus bleeding from the gums occur. Similar ulcerations in the bowel result in diarrhea. These complications are associated with alterations in the blood clotting mechanisms and a low white blood count. In the more heavily exposed (within the lethal range), anorexia, weight loss, and fever become the prominent symptoms. The red blood count decreases, and the symptoms become more pronounced, leading to death. Analysis of the Japanese experience indicates that percentage lethality can be correlated with lowest white blood count at particular times (see Fig. 2.4:3).[41] In the survivors there is a variable period during which recovery takes place. In the range of moderate to marked symptomatology, recovery to the point of being able to perform usual tasks may be of the order of 3 to 6 months or even longer.

At supralethal doses, 1500 r or greater, central nervous system alterations have been observed in monkeys. At very high doses (10,000 r or greater) delivered in less than an hour, death may supervene during the irradiation or within a few hours. In monkeys lethargy, convulsions, and other neurological manifestations occur.[42] No data are available for man in this dose range.

At present it is not possible to predict for a given air dose for either unilateral exposure or for infinite plane source geometry the percentage lethality. It is recognized that for unprotected exposure in a fallout field there is received a combined beta and gamma radiation. Consideration of the biological effect of this type of mixed radiation is not possible at present. Probably below 200 r air dose there will be no lethality, or at most, a few percent, while above 700 r there will be few survivors. Where in this range the LD_{50} falls is open to question. By convention it has been set at 400 to 450 r (with an unspecified source and source geometry), but this is not fixed. Furthermore, the shape of the

mortality vs dose curve is not known for man. In experimental animals, the shape of the mortality vs dose curve has been determined in a large number of experiments. A convenient method of expressing the result is the probit transformation, since this transformation results in a straight line.[43] However, it must be pointed out that these studies in animals, except for a few such as those carried out in mongrel dogs, have been conducted with pure bred laboratory animals of the same age. To postulate similar results from a probit transformation in man is not reasonable. In addition, the effect of changing the source geometry is not known for man, although it would be expected that a change from unilateral to bilateral exposure or to infinite plane source geometry would produce a significant decrease in air dose LD_{50} as it does in the pig.[44] The original analyses of the Hiroshima and Nagasaki data and speculation led to the adoption of 450 r as in LD_{50}. The experience gained from the Marshallese suggests a lowering below 450 r.

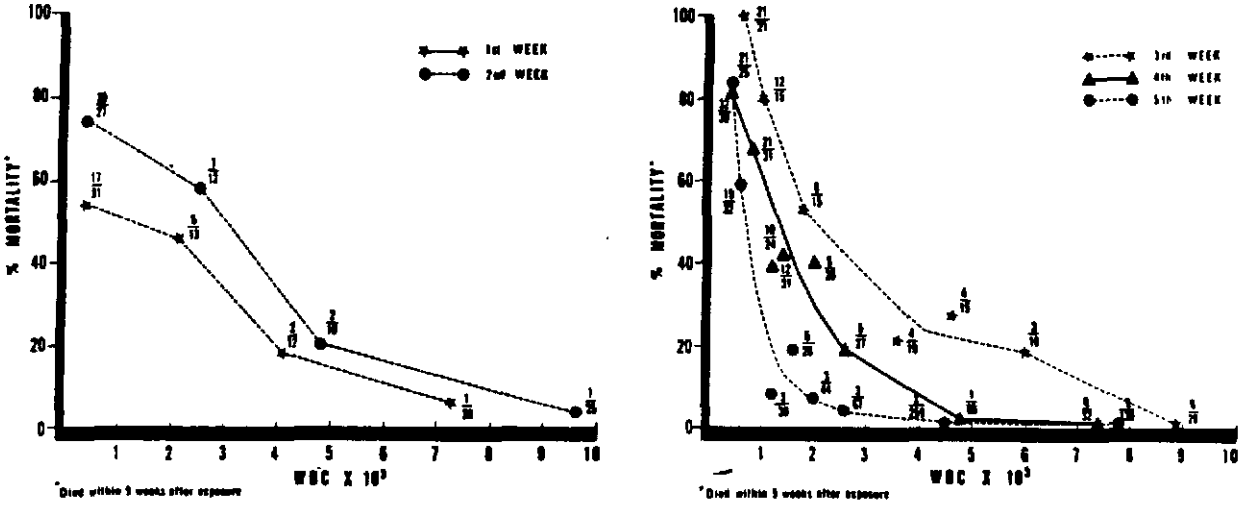

Figure 2.4:3 Correlation Between Human Mortality and White Blood Count.[41]

It should not be thought that these indicate basic differences: the original figures derived from the Japanese data are subject to considerable error with regard to dose and are for unilateral single short duration radiation, while the Marshallese data result from a more protracted radiation, with an infinite plane source geometry plus an unknown quantity and unknown effect of beta radiation to the skin, and from the opinion that the dose received was on the borderline of lethality (50 to 100 r more would produce some mortality). Recent review of the Japanese data in the light of newer weapons test data suggests an increase of the LD_{50} to approximately 650 r (air dose). Weapon yield, height of burst, air density, and shielding uncertainties for the Hiroshima and Nagasaki bombs are such as to cause this estimate to be questioned seriously. In fact, the error assigned is approximately $\pm$ 200 r.[35]

2.4.2 CURRENT THERAPEUTIC CONCEPTS[45]

As a basis for discussion, it must be presumed that at present there is no specific curative treatment for the acute radiation syndrome in man. For the experimental animal, there are a number of modalities used either before or after irradiation, leading to reduction in acute mortality. These are (1) radiation in the hypoxic state, (2) transfusion of bone marrow or spleen or homogenates of bone marrow or spleen, (3) various chemicals, e.g., cystein, (4) antibiotics, and (5) blood transfusions. Only the last two are, at present, to be considered applicable to man.

In clinical radiation therapy amelioration or reduction in the incidence of nausea and vomiting has been claimed for a number of diverse agents, e.g., (1) adrenal cortical hormones, (2) adrenocorticotrophic hormone, (3) various vitamin preparations, and (4) beta-mercaptoethylamine. All of

these are of somewhat dubious value. Lacking a specific therapeutic agent or regime, treatment has been symptomatic and supportive. Bed rest, fluids, antibiotics and transfusions have been used as indicated.

2.4.3 PROBLEM OF PARTIAL BODY SHIELDING

Clinical radiation therapy experience and extensive experimental animal research indicate that shielding part of the body is effective in reducing the magnitude of the actue radiation injury and is associated with an accelerated recovery, particularly of the bone marrow. It is probably this latter fact that accounts for the reduction in mortality. The value of such shielding in military situations is difficult to estimate. The degree to which this permits an individual to raise head and shoulders above ground level while in a foxhole or be exposed through an aperture in some other shielding and avoid the consequences of radiation injury is not known. An additional problem in shielding considerations is the fact that the more desirable types of shielding for neutrons are not the same as for gamma rays. It has been found that for shelters with about 3-1/2 ft or more overlay of earth, gamma radiation is the most important factor even when the outside neutron flux, as measured with a sulfur threshold detector, was 2.4×10^{11} neutrons-cm^{-2} or less[46], a flux which is approximately four times the LD_{50} (see Table 2.2:1).

2.4.4 DESCRIPTION OF BETA "BURN"

For localized beta radiation the best clinical description available is that of the results in the Marshallese. In these individuals the minimum time for development of skin lesions was 12 to 15 days. The first indication of the development of a skin lesion was an increase in skin pigment in localized areas. This was followed by scaly desquamation in the central portion of the lesion, leaving an area of pink depigmented skin. Gradually the pink area spreads out into the darker-pigmented area, with eventual complete healing. In other areas, presumably where the dose to the skin was greater, blisters developed which opened, leaving a raw, weeping area. This is comparable to a second degree thermal burn. New skin covered these areas in 7 to 10 days, and was followed by pigmentation. Unfortunately the dose to the skin could not be measured and cannot be calculated or estimated. Presumably lesions which developed blisters resulted from a dose to the skin, which, if the total body skin were involved, would be lethal. However, if lethality is comparable to that observed in thermal burns, involvement of less than 100 percent of the skin would result in lethality. For example, an untreated 33 percent body surface area second degree thermal burn is in the lethal range. Probably similar results would be obtained with beta radiation. Table 2.4:1 shows the surface dose required to produce recognizable epidermal injury for pigs, sheep, rabbits, rats, and mice for several different isotopes. Except for S^{35} this dose is from 1500-5000 rep. For S^{35} it is 20,000-30,000 rep. Higher doses are needed when S^{35} is used, since only a small fraction of the beta particles will penetrate to the sensitive layer of the skin. For other weak beta emitters similar considerations will apply. Calculation of the dose at the sensitive layer of the skin under these conditions is difficult and not reliable.

2.5 LONG TERM (LATE) EFFECTS

2.5.1 SHORTENING OF LIFE SPAN

The long term effects of irradiation can best be considered from the standpoint of reduction in life span.[47] Animal experimental data clearly indicate that one of the consequences of total body X-radiation is shortening of life span. This reduction in life span is conspicuous in the case of those who develop leukemia, but other tumors may have their origin in radiation. However, in many instances, there is no specific pathological change attributable to X-radiation but a general pattern of premature aging. For this reason, shortening of life span, which represents the end result of all the injury produced, is probably the most sensitive and satisfactory criterion for determination of the long-term hazard.

There are several different mathematical approaches to the study of this problem. These are the adaptation of the Gompertz formulation to radiation, the Sacher, and the Blair theories.[47]

From the available animal data, the life span shortening for a single acute dose is on the average 3 percent per 100 r. The relationship between reduction in remaining life span and dose is linear. For older animals, theory predicts that the percentage reduction of life span increases approximately threefold. Fig. 2.5:1 shows the predicted results for chronic radiation.

What can be said about man? At present, there is only one good potential opportunity for observation and that is the experience at Hiroshima and Nagasaki. It is hoped that in the near future the ABCC will publish their findings in this field. It is possible, but not probable, that some data regarding shortening of life span from a sublethal dose of radiation may become available from the continuing

TABLE 2.4:1

Surface Doses (rep) Required to Produce Recognizable Epidermal Injury[2]

Investigator	Animal	Isotope	Average Energy, Mev	Surface Dose, rep
Henshaw, et al.	Rats	P^{32}	0.5	1500-4000
Raper & Barnes	Rats	P^{32}	0.5	4000
Raper & Barnes	Mice	P^{32}	0.5	1500
Raper & Barnes	Rabbits	P^{32}	0.5	5000
Lushbaugh	Sheep	Sr^{90}	0.3	2500-5000
Moritz & Henriques	Pigs	S^{35}	0.05	20,000-30,000
Moritz & Henriques	Pigs	Co^{60}	0.1	4000-5000
Moritz & Henriques	Pigs	Cs^{137}	0.2	2000-3000
Moritz & Henriques	Pigs	Sr^{90}	0.3	1500-2000
Moritz & Henriques	Pigs	Y^{91}	0.5	1500-2000
Moritz & Henriques	Pigs	Y^{90}	0.7	1500-2000

study of the Marshallese. However, it has recently been reported that radiologists have an average life span of 5.2 years (approximately 12 percent) less than other physicians not exposed to radiation.[48] This reduction is compatible with the extrapolation of the animal results to man and estimates of the exposure of radiologists to radiation. Brues and Sacher have developed two postulates for the extrapolation from species to species. These are:

1. For the single acute dose - the percentage reduction in life span is the same.

2. For chronic irradiation - to produce the same percentage reduction remaining in life span, the dose rate to an individual of species 2 should be

$$\dot{D}_2 = \dot{D}_1 \Omega \qquad (2.5:1)$$

where

$$\Omega = \frac{\text{life span species 1}}{\text{life span species 2}}$$

$\dot{D}_1$ = chronic dose rate to species 1

$\dot{D}_2$ = chronic dose rate to species 2

Thus, for man, the dose rate to produce the same percentage decrease in life span should be approximately 1/18 that observed in the rodent.

There are two features of Blair's theory and method of analysis that require further explanation. The Blair theory predicts that the acute dose LD_{50} decreases with age and that this decrease is linear. This has been tested in only a very limited way, and indeed the acute LD_{50} dose does decrease with age in rats, but the data are not sufficient to determine the rate of decrease of LD_{50} with age. Because of certain pulmonary complications observed in older rats, extension of this observation to other species may not be warranted. The Gompertz function type of analysis also predicts that the LD_{50} should decrease with age. Since aging and irradiation injury are additive, older animals will require less additional injury, whatever the source, to produce death if the injury produced is comparable to normal aging. For man, there is no information available on this aspect.

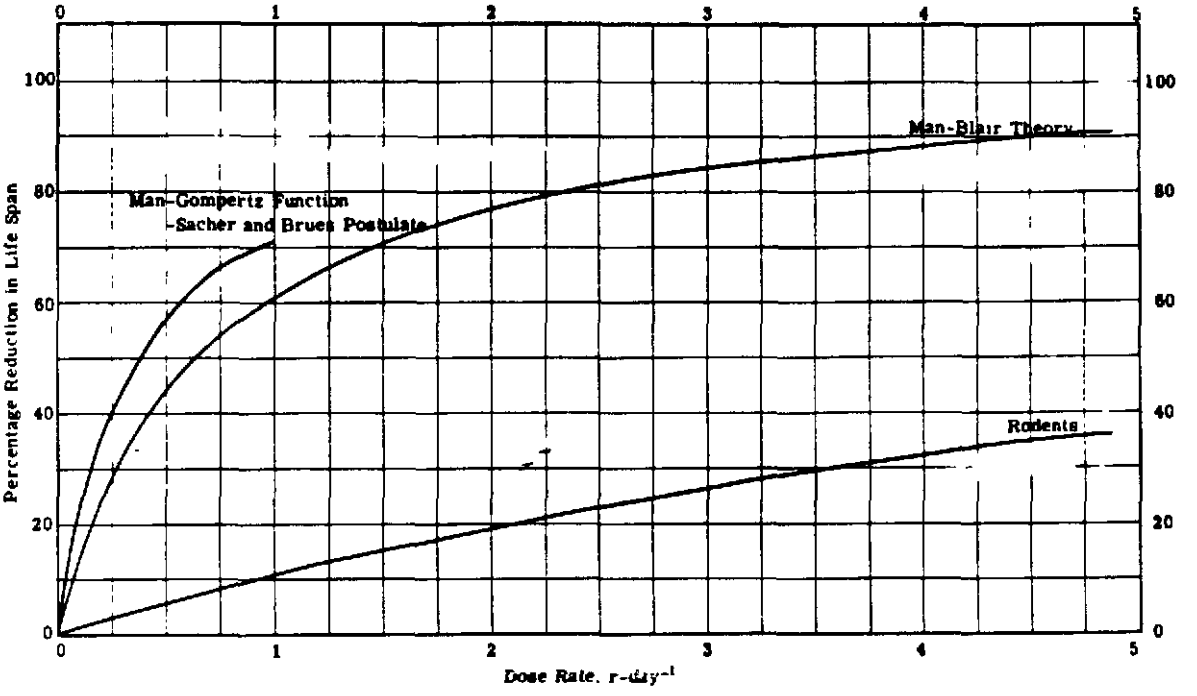

Figure 2.5:1 Predicted Shortening of Life Span from Chronic Radiation as a Function of Dose Rate for Rodents, with Extrapolation to Man. Extrapolated results for man are given based on the Blair Theory, the Gompertz Function, and the Sacher and Brues Postulate. The results of the Sacher and Brues Postulate are almost identical to those obtained and plotted from the Gompertz Function.

2.5.2 CATARACTS[49]

Cataracts are changes in the lens of the eye which can impair vision. The dose to produce cataracts in man is not known with any degree of certainty. It is probably relatively low for X-rays, in the range of the LD_{50}, and considerably lower (estimated at 50 n or approximately 100 rep) for neutrons. Cataracts are a particularly serious potential complication of neutron radiation. The RBE for cataract formation from neutrons is approximately 10 to 20.

2.5.3 FERTILITY[48]

Fertility is difficult to evaluate quantitatively. Depending upon the dose, there can be anything from a mild depression of sperm formation up to permanent sterilization. The dose for permanent sterilization is in the range of slightly larger than the lethal dose. In males a single sublethal dose re-

sults in a decrease in sperm count that can be considered as relative sterility. Recovery is a slow process, taking up to one year.[4] For the female, doses of 125-150 r produce amenorrhea, and 170 r produces sterility of 12 to 36 months duration. Parenthetically, it is of interest to note that survivors of serious radiation accidents have produced children.

2.6 GENETIC EFFECTS[48]

That radiation results in genetic changes is unquestioned. While much work has been done on the genetic changes induced in lower organisms, particularly the fruit fly, there is little mammalian experimental data and that almost entirely in the mouse. The great uncertainty for man is the relationship between dose and number of mutations produced and their manner of expression. In general, it is assumed that radiation-induced mutations are deleterious. Genetic changes are a problem for the survival of mankind when the whole population or a large fraction of the population is heavily exposed; radiation of small groups is more a problem in the concern of the individual for the welfare of his progeny than for the survival of mankind but cannot be neglected. With the increasing development and use of various radioactive isotopes for nonmedical purposes and the use of reactors for propulsion and power systems, large numbers of people may be exposed to radiation. Thus, the small groups may become considerably larger in the near future.

There are several observations regarding the genetic changes induced by radiation which may be summarized as follows:

1. Radiation induced mutations are deleterious--if not all, most are.
2. There is no recovery from radiation-induced injury as it concerns genetic changes.
3. The amount of injury produced is directly proportional to the total dose.

From experimental observations in fruit flies and mice, it is suggested that a dose of 30-80 r to the entire population will double the mutation rate. The consequences of this are difficult to estimate. Particularly so since the manner of expression of many of these genetic changes is not completely understood; in fact, is but little understood. These changes could find expression in terms of various constitutional deficiencies, varying from those which result in a shortening of life span to those involving the capacity to perform mental tasks. It is entirely possible that doubling the mutation rate could be a serious burden, economically and medically.[39] It has been recommended that the average dose for the reproductive period be kept below 10 r above background. For some individuals, this may be exceeded but should be limited to a total dose of 100 r, of which no more than 50 r should be accumulated before age 30.[48]

2.7 EFFECT OF PROTRACTION AND FRACTIONATION[47]

Both animal experimental evidence and clinical radiation therapy experience clearly indicate that protraction of the delivery of the dose for days, weeks or months, or fractionation of the dose over similar periods of time results in a smaller biological effect, generally a lower incidence of lethality that does a single dose of the same magnitude delivered over a period of minutes. This does not include genetic effects.

This implies recovery from the injury produced by radiation. The rate of recovery may be measured by administering a sublethal dose, generally 1/2 LD_{50}, and then at various later time intervals determining the additional dose required to produce 50 percent lethality. Such experiments show that the amount of the second dose to produce 50 percent lethality increases with time. If the logarithm of the difference between the single dose LD_{50} and the second dose to produce 50 percent lethality is plotted as a function of time, a straight line is obtained for short times, implying that recovery is a first order process. (LD_{50} - Second Dose) = (First Dose) $e^{-\theta t}$. However, experimental studies show that recovery is not complete; the irreparable component amounts to about 10 to 20 percent of the injury produced.

In the mouse the recovery rate is from 10 to 20 percent-day^{-1}, in the rat 7 to 10 percent-day^{-1}, in the dog about 4 to 5 percent-day^{-1}, and in the monkey 14 percent-day^{-1}. The recovery rate for man

is not known. Studies of the recovery rate for erythema (reddening of the skin) in man indicate much larger recovery rates; however, this is not the recovery rate desired for military medical purposes. Actually, the recovery measured in lethality experiments is not a single physiological process; it represents the net recovery of all the physiological processes necessary for the maintenance of life, and with each weighted according to its significance in the maintenance of life.

The effective dose is defined in terms of the results of a single acute dose, and is best illustrated by an example. If the acute dose to produce 50 percent lethality within 30 days is 400 r, then the effective dose of any system of fractionation or protraction that produces 50 percent mortality in 30 day is 400 r, although the physical dose may be much greater than 400 r.

From the Blair theory, for the particular case that the animals are young, that each dose is administered within a short period of time, and that death occurs in a few weeks

$$D_{eff} = \left[nf + (1-f) \frac{(e^{-n\Theta\Delta t} - 1)}{(e^{-\Theta\Delta t} - 1)} \right] D \qquad (2.7:1)$$

where

f = fraction of injury, irreparable

D = single dose

n = number of single doses D

Θ = rate of recovery, day^{-1}

Δt = interval between single doses, days.

For man it is recommended that $\Theta = 0.05\ day^{-1}$ be used rather than the more commonly quoted $\Theta = 0.29\ day^{-1}$, which is based on animal data and a limited interpretation of animal data. It is recommended that a value of f between 0.10 and 0.20 be used, although there is no evidence to support this recommendation. Other relationships proposed for calculation of the effective dose are those of Loutit, that in the French EAW, and that of Hoffman and Reinhard.

Loutit proposes that

$$D_{eff} = t^{k_2} \dot{D}(0) \qquad (2.7:2)$$

where

$\dot{D}(0)$ = constant dose rate, $r\text{-}day^{-1}$

k_2 = constant = 0.64

t = time of irradiation, days.

The French EAW proposed that

$$D_{eff} = \frac{\dot{D}(0)}{k_3} \left[1 - (1-k_3)^t \right] \qquad (2.7:3)$$

where k_3 = constant = 0.36.

Hoffman and Reinhard propose that

$$D_{eff} = \dot{D}(0)\left[\frac{1-k_4^{\,t}}{1-k_4}\right] \qquad (2.7:4)$$

where k_4 = constant = 0.96.

These latter three equations are concerned with one parameter, that relating to recovery, and make no provision for the accumulation of an irreversible injury. Fig. 2.7:1 shows that there is considerable disagreement between the results predicted by these equations. In the absence of data, no one can be selected as being applicable to man.

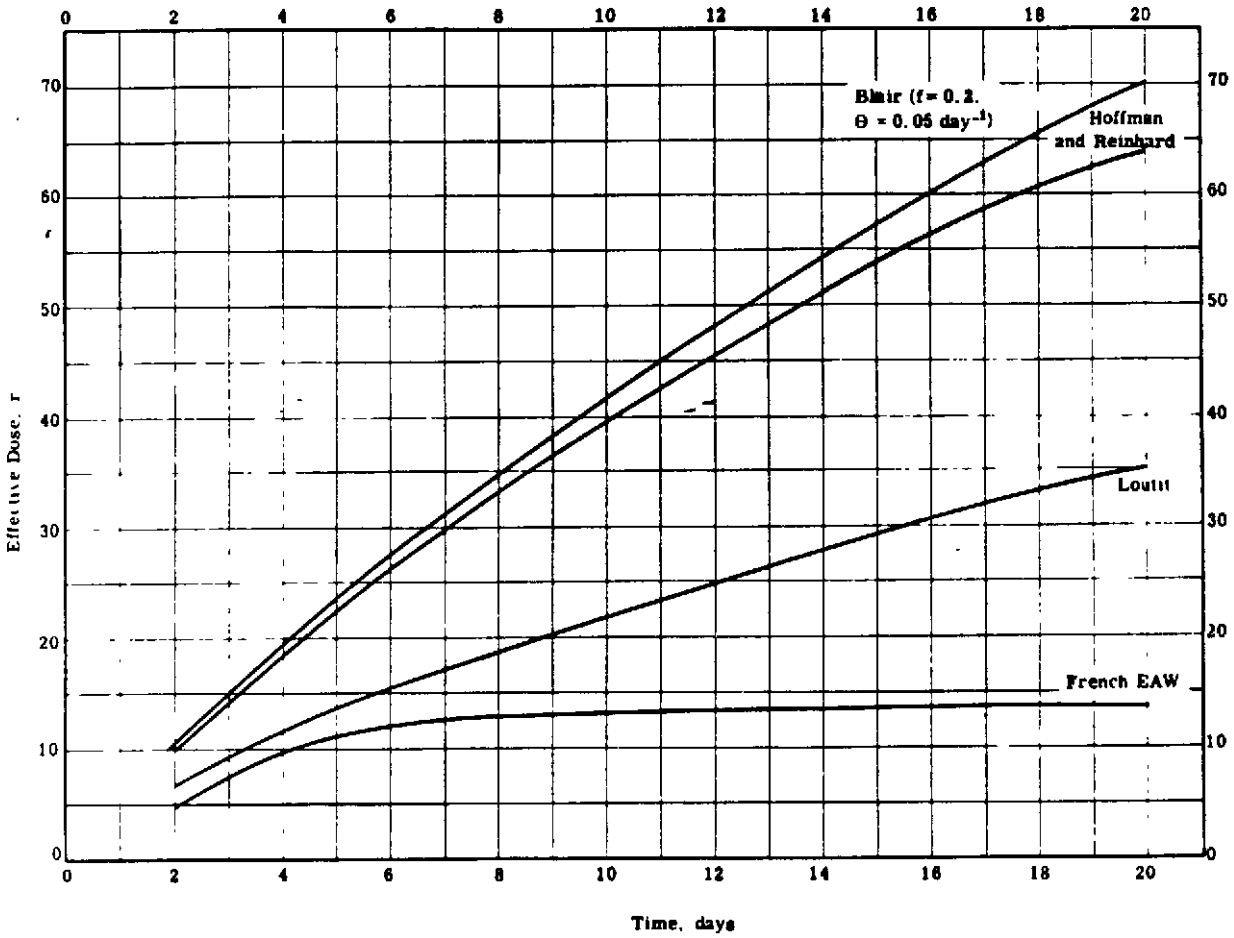

Figure 2.7:1 Comparison of the Various Equations Purporting to Calculate the Effective Dose for Chronic Radiation at 5 r per Day.

In terms of the Blair theory, it may be shown that for a fallout field the effective dose rate is

$$D_{eff} = \dot{D}(H+1)\left[5f(t_{en}^{-0.2} - t_{ex}^{-0.2}) + (1-f)\,e^{-\Theta t_{ex}}\int_{t_{en}}^{t_{ex}} e^{\Theta t}\,t^{-1.2}\,dt\right] \qquad (2.7:5)$$

where

$\dot{D}(H+1)$ = dose rate at H + 1 hr

t_{en} = time of entry into fallout field (units of time after detonation).

t_{ex} = time of exit from fallout field (units of time after detonation).

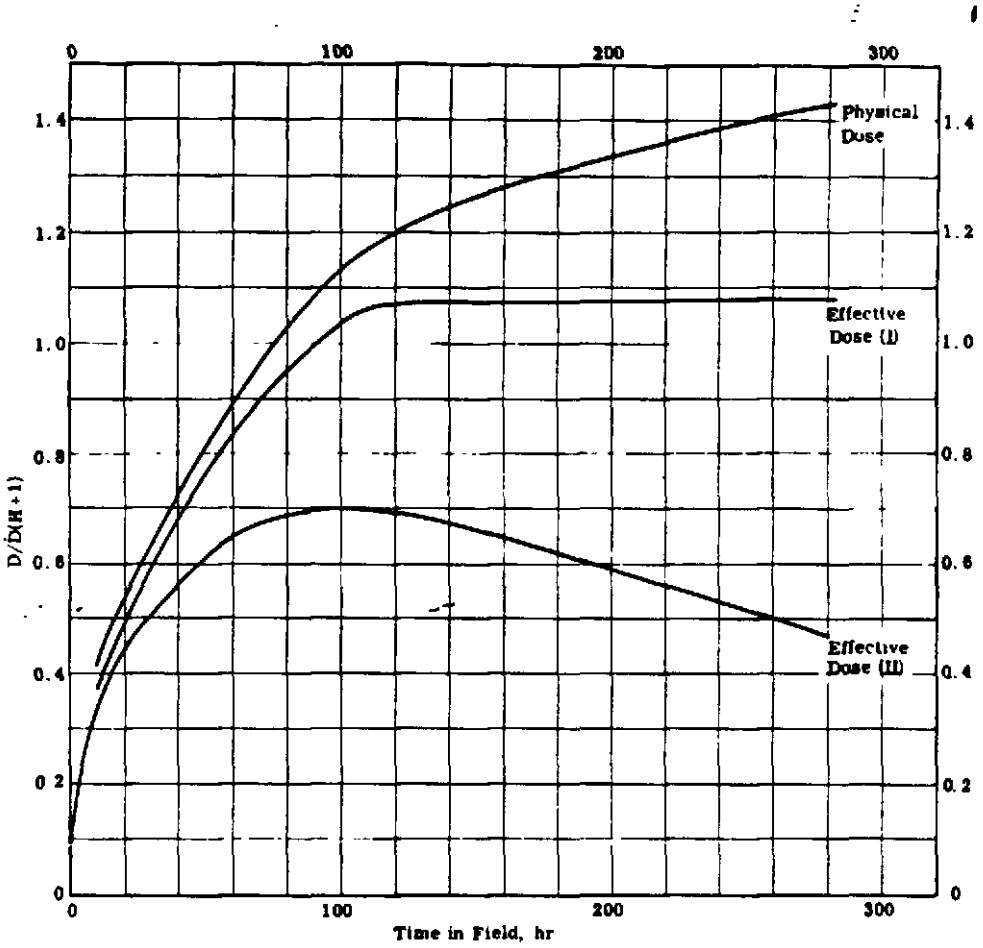

Figure 2.7:2 The Ratio of the Physical Dose and the Effective Dose to H+1 Hour Dose Rate for a Fallout Field Using the Blair Equations as Modified for a Changing Dose Rate. Time of entry into fallout field is H+12 hr. Curve I shows the predicted effective dose for the condition that $f = 0.2$ and $\theta = 0.04$ day^{-1}. Curve II shows the predicted effective dose for the conditions that $f = 0.2$ and $\theta = 0.24$ day^{-1}.

Fig. 2.7:2 shows examples of the calculations that may be carried out. Particularly of interest is the effect of variation of Θ.

2.8 INTERNAL CONTAMINATION

2.8.1 SOURCE

The radioactive isotopes produced in the process of fissioning of uranium and plutonium in an atomic explosion are widely distributed over the entire world by the winds. There is a slow settling of

these particles from the atmosphere, the rate of descent being governed by particle size and shape, and the location of the fallout being dependent upon the rate of descent and wind patterns. There are a number of variables involved, none of which is completely understood.[50] The quantity of material in the stratosphere and the rate of movement from the stratosphere to the troposphere have been estimated, the latter having a half-time of approximately 10 years and the former has been estimated as varying upwards from a few percent to over 50 percent for a land burst.

2.8.2 ROUTE OF ENTRY INTO MAN

There are three routes of entry: inhalation, ingestion, and open wounds.

1. Inhalation

During the period when radioactive particles are falling out, inhalation is a route of entry into the body. After settling on the ground, these particles can become airborne again and thus available for inhalation. The distribution within the respiratory passage of radioactive particles inhaled is strongly dependent upon particle size.[51] In general,

a. Particles less than 0.1 micron are inhaled and then exhaled.

b. Particles 0.1 to 3.0 microns reach the lungs and are deposited in the alveoli.

c. From 3.0 to 10 microns particles reach and deposit themselves upon the walls of the trachea, bronchi, and bronchioles, and are worked up to the larynx and ultimately swallowed.

d. Above 10 microns particles are filtered out in the nose. Rainfall occurring at the time of passage of the atomic cloud has been shown to result in an increase in the urinary Sr^{90} and I^{131} content of man, strongly implicating inhalation as a significant route of entry.[52]

2. Ingestion

Radioactive materials settling upon the ground may be incorporated into or coat the surface of plants which are subsequently eaten by man or by livestock which later are eaten by man. Evaluation of the importance of this route of entry and the hazard involved is complex. Movement of fission products through the soil, uptake by plants, use of plants for animal fodder, and subsequent ingestion by man all are important and not well documented factors. The presence and amount of Sr^{90} in dairy products is well documented, although the details, particularly quantitative, of the movement of this Sr^{90} through the biosphere are lacking.[53]

The relative significance of these two routes of entry is still to be determined.

Water does not appear to be a significant route of entry of fission products into man.[53] However, this may not be applicable for local fallout.

3. Open wounds

Open wounds do not appear to be a significant route of entry into man except in unusual circumstances.

2.8.3 METABOLIC FATE

The metabolic fate of the fission products is dependent upon a number of factors. For each element it is different, and for each element and chemical species of a given element it may be different. For example, particles inhaled and reaching the alveoli, if they are soluble in body fluids, are absorbed, reaching the blood stream, and are subsequently distributed throughout the body in accordance with the manner in which the body treats that particular compound, while if insoluble, the particles may be concentrated in the lymphatic system of the lung and remain within the lungs and lymph nodes draining the lungs for that individual's lifetime, constituting local areas of intense radiation. The considerations of particle size and chemistry must be applied to all of the fission products.

Within the gastro-intestinal tract, similar considerations apply. For materials that are absorbed, the distribution in the body varies. For example, iodine, as iodide, is taken up by the thyroid gland and subsequently released to the blood stream as organically bound iodine.

Probably most important is the fact that many of the fission products that reach the blood stream are taken up and retained for long periods of time by bone. Animal experimentation and the history of the radium dial workers indicate that this is a serious problem leading to serious complications, such as malignant bone tumors, although other less serious pathology can and does occur. In fact, in animal experiments it can be shown that such bone deposition can lead to shortening of life span in the absence of specific pathological changes in the bone.[54]

2.8.4 BIOLOGICAL EFFECTS

The quantities of most materials that can gain entry into the body are such that if they are not normal metabolites, the quantity present is not sufficient to be toxic merely by virtue of their chemistry; the injury produced is that of irradiation of the tissues. Depending upon the tissue involved, time factors, and the dose and dose rate, a wide range of pathological changes may occur. These will vary from no discernible anatomical change, but with subtle physiological changes for low doses, to the production of malignant tumors at higher doses. The latent period for these changes may, as in the case of radium dial workers, be up to 10 to 20 years or more.

2.8.5 THERAPEUTIC ASPECTS

The therapeutic problem is largely concerned with a particular class of isotopes, namely, those associated with deposition in the bone and commonly called "bone seekers." Unfortunately, therapeutic measures now under investigation, principally removal by chemical agents, are not particularly promising.[55] Therapy of the radiation injury produced by internally deposited radioactive isotopes is as unsatisfactory as for external radiation; there is no good means of treatment.

Analysis of the biological properties of the fission products has indicated that the long-lived isotope of strontium, Sr^{90}, is the greatest hazard, although it is not the only long-lived isotope that may be hazardous. Project Sunshine has reviewed the biological properties of strontium, the worldwide distribution, in particular in food and water, and the present levels of body burden of Sr^{90}.[53] The fact is that Sr^{90} is now present in human bone and is thought to be derived from food, principally dairy products. At present the quantity of Sr^{90} present in man is low compared to the estimated toxic levels. However, the change in bone Sr^{90} content with time is not known; a good evaluation of the tolerance level is lacking and recent work implicates an inhalation route of entry as at least partially responsible for the present body burden. While considerable attention has been directed towards Sr^{90}, other fission products can and do gain entrance to the body.[52, 56] It is the bone deposition of Sr^{90} that gives rise to concern; the majority of the other fission products are either produced in small quantities compared to strontium, are relatively rapidly excreted or have short physical half-lives. In the latter class fall the iodine isotopes. Nevertheless, they will contribute to the injury produced and should not be ignored.

2.9 COMBINED INJURIES[57, 58, 59]

Experiments in swine, dogs, and in rats indicate that the lethality of combined nuclear radiation damage and thermal injury is greater than would be expected. These studies have been carried out by determining the lethality produced by thermal injury alone, by radiation injury alone, and by combined injuries. For example, thermal burns and radiation exposures that, by themselves, would result in no mortality give rise to significant mortality when combined. Also thermal burns or radiation injury at levels that result in low mortality when combined lead to considerably greater lethality than expected. Quantitative translation of this data to man is not possible at this time. Nevertheless, it should be anticipated that in man the same findings will occur; namely, that these effects are not simply additive.

It is also probable that similar results will be obtained when radiation is combined with other forms of traumatic injury. A calculation of the magnitude of this effect is not possible. The variety of types of traumatic injury is such that any calculation would be of little value.

2.10 MAXIMUM PERMISSIBLE LEVELS OF RADIATION

As a fundamental premise it must be considered that all radiation is deleterious. However, radiation and certain radioisotopes have come to play important roles. For example, great strides have been made in medicine since the introduction of X-rays for diagnostic purposes; radioactive isotopes have proven to be a potent tool in medical research, and to have therapeutic value in certain diseases; the industrial uses of X-rays and radioactive isotopes are increasing rapidly; and finally, reactors are being used for the production of power. With all these beneficial uses, there comes the hazard involved.

2.10.1 EXTERNAL RADIATION

Since the introduction of X-rays, as more data on the late effects of irradiation became available, there has been a progressive reduction in what has been considered to be a "safe" maximum level of exposure.

Handbook No. 59 (National Bureau of Standards) reviews the present "tolerance" levels. In general, it is recommended that for continuous total body X or gamma radiation, the maximum permissible exposure be 0.3r-week^{-1}. However, it should be mentioned that this number is being reviewed, and that probably some reduction will be made.[1]

2.10.2 INTERNAL RADIATION

The maximum allowable concentration of radioactive isotopes in the body is largely based upon the assumption that the dose rate to the critical organ be no greater than 0.3r-week^{-1}. Because of varying biological properties, the critical organs vary with different isotopes. In general, bone and bone marrow are the critical organs, although not for all isotopes. Handbook No. 52 (National Bureau of Standards) lists values of the maximum permissible amount for a number of isotopes. Calculation of these quantities is complex, and depends upon the distribution within the body, the radiations emitted, the biological turnover time, and for alpha emitters an estimate of RBE or comparison with radium. There are many uncertainties involved, and like the limits set for external radiation, they are being reviewed.

2.11 REFERENCES

1. A.W. Oughterson et al. USAEC NP-3036 through 3041. 1951. (Unclassified)
2. E.P. Cronkite et al. WT-923. Oct. 1954. (Confidential)
3. L.H. Hemplemann et al. Ann. Inst. Med. 36. 279. 1952. (Unclassified)
4. R.J. Hasterlik and E.D. Marinelli. Proc. Int. Conference on the Peaceful Uses of Atomic Energy. Vol. XI. 1956. (Unclassified)
5. A. Hollaender. Radiation Biology. McGraw-Hill Book Co. 1954-55. (Unclassified)
6. Z.M. Bacq and P. Alexander. Fundamentals of Radiobiology. Academic Press. 1955. (Unclassified)
7. D.E. Lea. Action of Radiations of Living Cells. 2nd ed. Macmillan Co. 1954. (Unclassified)
8. R.W. Wilson. Radiation Research 4. 349. 1956. (Unclassified)
9. C.A. Sondhaus and V.P. Bond. WT-939. Dec. 1955. (Secret)

(1) The results of this review were unofficially announced at the time of publication of this handbook. The revised value of the maximum permissible exposure for external and continuous total body X or gamma radiation is 5 r-yr^{-1} or an average of 0.1 r-week^{-1}. Somewhat higher dose rates are allowed for shorter time periods.

10. Permissible Dose From External Sources of Radiation. NBS Handbook 59. Sept. 1954. (Unclassified)

11. O. Glasser et al. Physical Foundation of Radiology. 2nd ed. P. B. Hoeber, Inc. 1952. (Unclassified)

12. E. L. Alpen and V. P. Bond. USNRDL. Private Communication.

13. J. R. Raper et al. Comparative Lethal Effects of External Beta Radiation; from R. E. Zirkle. Effects of External Beta Radiation. NNES. Div. IV. Vol. 22E. McGraw-Hill Book Co. 1951. (Unclassified)

14. A. Broido and J. D. Teresi. USNRDL. Tech. Memo. No. 4. 1954. (Unclassified)

15. Scientific Director's Report of Atomic Weapons Tests at Eniwetok. WT-18. 1951. (Secret)

16. Scientific Director's Report of Atomic Weapons Tests at Eniwetok. Wt-43. 1951. (Secret)

17. G. V. Taplen. Chemical and Colorimetric Indicators; from G. J. Hine and G. L. Brownell. Radiation Dosimetry. Academic Press. 1956. (Unclassified)

18. J. H. Schulman et al. Nucleonics 11. 10. 1953. (Unclassified)

19. E. Tochilin et al. Radiation Research 4. 158. 1956. (Unclassified)

20. H. H. Rossi. Neutron and Mixed Radiation; from G. H. Hine and G. L. Brownell. Radiation Dosimetry. Academic Press. 1956. (Unclassified)

21. L. Cave. FWE-16. Dec. 1951. (Confidential)

22. V. P. Bond. USNRDL. Private Communication. Aug. 1956.

23. J. S. Cheka. Nucleonics 12. 6. 1954. (Unclassified)

24. V. P. Bond et al. BNL and NMRI. The Effect of Exposure Geometry and Beam Spectrum on the Lethal Dose of Penetrating Ionizing Radiation for Large Mammals and Man. To be published. (Unclassified)

25. F. W. Chambers et al. WT-719. Dec. 1955. (Secret)

26. G. W. Imiri, Jr. and R. Sharp. ITR-1120. May 1955. (Confidential)

27. H. E. Johns. X-Rays and Telisotope Gamma Rays; from G. J. Hine and G. L. Brownell. Radiation Dosimetry. Academic Press. 1956. (Unclassified)

28. R. A. Kendall. FWE-74. May 1956. (Confidential)

29. J. W. Boag. NBS-2946. Dec. 1953. (Unclassified)

30. J. Furchner. LA-1849. March 1954. (Unclassified)

31. R. E. Zirkle. The Radiobiological Importance of Linear Energy Transfer; from A. Hollaender. Radiation Biology. Vol. 1. McGraw-Hill Book Co. 1954. (Unclassified)

32. J. B. Storer et al. Biological Effectiveness of Varying Radiations in Mammalian Systems. To be published in Radiation Research. 1956. (Unclassified)

33. H. H. Rossi. Radiology 61. 93. 1953. (Unclassified)

34. P. S. Harris et al. ITR-1167. May 1955. (Secret)

35. P. S. Harris. Proc. Tripartite Conference on Weapons Effects. Nov. 1955. (Secret)

36. V. P. Bond et al. Radiation Research 4. 139. 1956. (Unclassified)

37. W. M. Court-Brown. British Med. J. April 1953. (Unclassified)

38. R. A. Conard. Radiation Research 5. 167. 1956. (Unclassified)

39. United Kingdom Medical Research Council. The Hazards to Man of Nuclear and Allied Radiations. Her Majesty's Stationery Office. June 1956. (Unclassified)

40. V. P. Collins et al. AFSWP-809. Jan. 1956. (Unclassified)

41. E. P. Cronkite et al. NMRI. Private Communication.

42. J. E. Pickering et al. School of Aviation Medicine. Report No. 55-77. March 1956. (Secret)

43. D. J. Finney. Probit Analysis. 2nd ed. Cambridge Univ. Press. 1952. (Unclassified)

44. J. L. Tullis et al. Amer. J. of Roentgenology 67. 620. 1952. (Unclassified)

45. E. P. Cronkite. Military Medicine 118. 328. 1956. (Unclassified)

46. V. P. Bond. WT-793. Sept. 1953. (Secret)

47. N. I. Berlin and F. L. Dimaggio. AFSWP-608. June 1956. (Unclassified)

48. National Research Council. The Biological Effects of Atomic Radiation, Summary Reports. 1956. (Unclassified)

49. W. T. Hamm, Jr. Arch. Opthal. 50. 618. 1953. (Unclassified)

50. R. D. Maxwell et al. AFSWP-978. Sept. 1956. (Secret)

51. J. H. Brown et al. Amer. J. Pub. Health 40. 450. 1950. (Unclassified)

52. J. B. Hartgering et al. AFSWP-893. Nov. 1955. (Secret)

53. W. F. Libby. WASH-406. July 1956. (Secret)

54. H. A. Blair. UR-274. Sept. 1953. (Unclassified)

55. H. Foreman. J. Amer. Pharm. Assoc. 42. 629. 1953. (Unclassified)

56. C. E. Miller and L. D. Martinelli. *Amer. Assn. for the Advancement of Science.* Vol. 124. No. 3212. June 1956. (Unclassified)

57. H. Baxter et al. Ann. Surg. 137. 450. 1953. (Unclassified)

58. J. W. Brooks et al. Ann. Surg. 136. 533. 1952. (Unclassified)

59. E. L. Alpen and G. E. Sheline. USNRDL-402. May 1953. (Unclassified)

GENERAL REFERENCES

a. A. Hollaender. Radiation Biology. McGraw-Hill Book Co. 1954-55. (Unclassified)

b. Z. M. Bacq and P. Alexander. Fundamentals of Radiobiology. Academic Press. 1955. (Unclassified)

c. A. Haddow. *Biological Hazards of Atomic Energy.* Oxford Univ. Press. 1952. (Unclassified)

d. D. E. Lea. Action of Radiation on Living Cells. 2nd ed. MacMillan Co. 1954. (Unclassified)

e. O. Glasser et al. Physical Foundation of Radiology. 2nd ed. P. B. Hoeber, Inc. 1952. (Unclassified)

f. E. P. Cronkite and V. P. Bond. Effects of Radiation on Mammals. Annual Review of Physiology 18. 483. 1956. (Unclassified)

g. G. J. Hine and G. L. Brownell. Radiation Dosimetry. Academic Press. 1956. (Unclassified)

h. National Research Council. Pathologic Effects of Atomic Radiation. Publication 452. (Unclassified)

i. United Kingdom Medical Research Council. The Hazards to Man of Nuclear and Allied Radiations. Her Majesty's Stationery Office. June 1956. (Unclassified)

j. E. Tochilin et al. Cyclotron Neutron and Gamma Ray Dosimetry for Animal Irradiation Studies. Radiation Research 4. 158. 1956. (Unclassified)

k. A. Oughterson and S. Warren. Medical Effects of the Atomic Bomb in Japan. NNES. Div. VIII. Vol. 8. McGraw-Hill Book Co. 1956. (Unclassified)

[redacted]

Chapter 3

INITIAL GAMMA RADIATION

3.1 INTRODUCTION

Initial gamma radiation is here taken to be the gamma radiation emitted during the first 60 seconds after the detonation of a nuclear weapon. The initial gammas are accompanied by neutron emission (see Chapter 4) but in most operational situations (except for short distances from the point of burst, for thin casing weapons and/or high altitude, low atmospheric density bursts) the initial gamma contribution to the total dose[1] (for unshielded receivers) is much greater than that from neutrons. About 5 percent of the fission energy appears in the form of gamma radiation (both initial and residual). This figure does not include gammas produced as a result of neutron capture.

The gamma radiations can stem from several processes but only two processes account for essentially all of the initial gamma dose. The first of these is the gamma radiation produced as a result of capture of bomb neutrons in atmospheric nitrogen.[2] About 11 Mev of gamma energy are released per neutron capture in nitrogen and the gammas produced are primarily in the energy range of 4.5 to 11 Mev. The second source is the gammas emitted by decaying fission products and a total, over all time, of about 5 Mev of gamma energy is produced per fission. The energy of these fission product gammas is much lower than that of the nitrogen capture gammas, their average energy being about 1 Mev. This chapter deals with the doses resulting from these two sources. (A third and relatively unimportant gamma source, which we do not consider, is the gammas which are emitted during the fission process rather than from fission products. Most of the prompt fission gammas are thought to be absorbed in the weapon components.)

It is convenient for our present purposes to classify weapons in terms of low, intermediate, and high yield. Low yield weapons will be defined as those below 10 KT, intermediate yield weapons those from 10 to 100 KT, and high yield weapons those above 100 KT. These divisions are appropriate for the phenomenology involved and facilitate the presentation of results.

In addition, the gamma radiation from all fission and boosted fission weapons, independent of yield, will be taken as resulting entirely from the fission reaction. (The small contribution of gamma rays due to the fusion reaction in boosted weapons will be neglected.) The gamma radiation from thermonuclear weapons results from both fission and fusion reactions. [redacted]

The gamma dose received at a point is dependent on

1. the characteristics of the source, i.e., its strength and distribution in space and energy, and
2. the characteristics of the medium between source and receiver, i.e., the distance and materials traversed by the gammas.

The gamma source strength and distribution are determined by the bomb yield and design.

[redacted]

For a given design the source strength always varies linearly with the yield. The yield affects the gamma dose at the receiver in a second important manner, however. As the bomb yield increases above about 10 KT, the shock effects become increasingly important. The shock wave tends to reduce seriously the attenuating properties of the atmosphere around the burst point and therefore to increase the amount of radiation arriving at the receiver. The design of the bomb affects both the source strength and its distribution in space and in energy. That portion of the gamma dose arising from the (n, γ) reaction in N^{14} will obviously be affected by the spatial distribution of captures in nitrogen. This spatial distribution may be changed by modifications in the bomb design which alter the number of neutrons escaping into the air and/or their spectrum.

The distance between source and receiver reduces the dose, due to a purely geometrical factor. For a point source which, in most cases, fairly well approximates the initial gamma radiation source, the decrease of dose with distance follows the inverse square law.

The media between the source and the receiver attenuate the gamma radiation by the processes of absorption and scattering. Absorption completely eliminates the gamma ray while scattering reduces its energy and changes its direction. The gammas that arrive at any given receiver may do so with or without having experienced scattering during their flight from the source. The fraction that arrives directly from the source without scattering may be represented by an exponential function whose argument depends upon distance, upon the physical properties of the medium, and upon the energy of radiation. Determination of the scattered fraction is much more complex. For relatively simple geometries, scattering can be treated accurately through the use of a function known as the buildup factor.[3] Calculations of the buildup factor have been made for only certain of the situations of interest. For more complicated and realistic geometries, determination of the scattered radiation is quite difficult and up to the present such calculations have not been done. Thus, should the straight line path between source and receiver lie in one medium whose density varies sharply along the path, or in two different media, or should the path lie close to the boundary between two media, it is not possible at present to rely upon previously calculated results to compute theoretically the scattered dose.

The medium usually traversed by the gamma rays is air, although other materials in the vicinity of the burst point or receiver may also be of importance. The presence of water in the air, as vapor or liquid, does not appreciably alter its properties for the purposes of gamma ray transmission. On the other hand, changes of air density resulting from changes in temperature or pressure do affect gamma ray transmission characteristics in air. In particular, as noted previously, changes in air density due to the shock effect of intermediate and high yield weapons, have a very marked influence on the attenuation provided by the atmosphere and therefore on the gamma dose at the receiver.

There are a number of uncertainties in our knowledge of the source and attenuating media characteristics described above. Among the most important of these are:

Uncertainties in source characteristics

1. Only limited information is available on the spectrum of fission product gammas.[4]
2. The importance of gamma rays produced as a result of neutrons interacting with weapon materials is not well known. Not all of these neutron reactions are understood and the number of neutrons interacting will vary depending upon the bomb design. (It is thought, however, that in most cases this gamma source is probably small compared to the nitrogen capture and fission product gammas.)
3. The spatial distribution of fission products, bomb and blast debris within the fireball and the rise of the fireball with time during the initial gamma period are not well known. This has led to considerable uncertainty in the dose at small distances.

Uncertainties in attenuating media characteristics

1. The influence of the blast on the medium is difficult to calculate accurately.

2. Computations of buildup factors for scattered radiation in the atmosphere (which has constant composition but a density which varies exponentially with elevation) are not available. The use of buildup factors based on average quiescent air density between the point of burst and the receiver, as described in Chapter 1, may not be an entirely adequate treatment.

3. The effects of the two-medium geometry and of the complications introduced in the scattered dose by the air-earth boundary have not been adequately evaluated.

4. The extension of the fireball into the two media, as sometimes occurs, requires a more elaborate treatment of both direct and scattered doses.

In spite of the above uncertainites it is possible to get usable results for a number of situations of interest. These results are primarily based on experimental data and simple theoretical models. In some cases, for example surface bursts for low and intermediate yield weapons, the data are plentiful; in others very few or no adequate measurements have been made. Transformations of results from one situation to another have been made when possible and appropriate.

The following sections of this chapter treat in turn the dose-distance relations for surface bursts (Section 3.2), air bursts (Section 3.3) and underground bursts (Section 3.4). In each of these sections the discussion is presented on the basis of bomb yield, the dose results being strongly dependent on this parameter. Section 3.5 presents a summary of information currently available on the delivery rate of the initial gamma dose and Section 3.6 discusses the distribution in energy of these gammas, both at the source point and at varying distances from the source. Finally, Section 3.7 treats the problem of military shielding against initial gamma radiation.

3.2 DOSE-DISTANCE RELATIONS FOR SURFACE BURSTS

A surface burst is one which occurs on the earth's surface. A near-surface burst is one which occurs above the earth's surface but sufficiently close so that some portion of the fireball intersects the earth (either at the time of burst or within a few seconds thereafter). While some variation in dose-distance relations is to be expected with variation in burst altitude, surface and near-surface bursts will not be distinguished in this treatment but will be lumped under the single classification. Any error so introduced will be quite negligible compared to other errors which must be accepted.

3.2.1 THEORETICAL CONSIDERATIONS

The results presented for surface bursts are based on curves fitted to experimental data. These data are examined and correlated empirically with theoretical considerations which are developed in the following paragraphs.

The model upon which the theoretical formulations are based is that of a point source of radiation in a single, infinite, and homogeneous medium and separated from a given receiver point by a fixed distance. The physical situation is, of course, considerably more complicated.

First, the total gamma source, and particularly that portion of the source due to nitrogen capture, is actually distributed within some volume rather than being concentrated at a point. The boundaries of the volume source of fission product gammas are rather well defined by the boundaries of the fireball, while the volume source of nitrogen capture gammas extends beyond the fireball and is without sharp definition.[2] The total initial gamma source is sufficiently well localized, however, so that at reasonable distances at sea level (say 1000 yd or more) it can be regarded to a good approximation as a point source.[5, 6, 7, 8, 9, 10] The validity of this approximation at medium and large distances has been established in every test where dose-distance measurements have been made. At distances less than 1000 yd, the point source approximation grows progressively worse.

Second, the initial gamma radiation leaving the source sees at least two different media, earth (or water) and air, neither of which is necessarily homogeneous. The non-homogeneity of the atmosphere is of primary importance while non-homogeneity of the second medium, earth or water, is only of minor interest. Non-homogeneity of the atmosphere is the result of two separate causes, the

shock wave effect and the normal variations in atmospheric temperature and pressure. At least partial correction for each of these effects is possible. Thus, the effect of the bomb shock wave on the air density between source and receiver is treated through the use of the hydrodynamic scaling factor. The effect of variations in the quiescent air density due to normal fluctuations in ambient temperature and pressure is handled through the use of the average quiescent air density (see Chapter 1). At the present time we are unable, however, to treat properly the presence of two attenuating media. This problem is additionally complicated by the fact that the position of the source volume changes with respect to the two media during the 60-sec initial gamma period. During the first few seconds after the burst, part of the source volume may be within each of the two media. As the fireball rises, the source region emerges completely into the air so that the unscattered dose becomes independent of the effect of the earth. The effect on the scattered radiation decreases with time until at some height the effect of the earth on the scattered dose becomes unimportant.

Third, the distance between the source and the receiver is not constant with time since the center of the fireball rises from 10,000 to 40,000 ft in the first minute after the burst, depending on the bomb yield. A correction for cloud rise is not made in the present treatment.

Derivation of Dose Equation

Within the inherent limitations of the model established, the equation for the initial gamma dose may be derived.

For a point source of gamma rays in a single infinite homogeneous medium whose energy spectrum is continuous over an energy range from E_{min} to E_{max}, the dose at a point (integrated over all time) is given by

$$D = \int_{E_{min}}^{E_{max}} \frac{C(E)\, S_\gamma(E)\, e^{-\mu_t(E)R}\, B[\mu_t(E)R]}{4\pi R^2}\, dE \qquad (3.2:1)$$

where

D = dose measured at the receiver

$C(E)$ = conversion factor which determines the dose units

$S_\gamma(E)$ = gamma source strength per unit energy interval and integrated over all time

$\mu_t(E)$ = total linear attenuation coefficient for gamma rays of energy E

$B[\mu_t(E)R]$ = dose buildup factor applying to gamma rays of initial energy E which have penetrated $\mu_t(E)R$ mean free paths

R = source-receiver distance

A useful approximation to Eq. 3.2:1 for the dose from a single source has been found to hold in most experimental situations. Thus

$$D = \frac{C\, S_\gamma\, e^{-\mu R}}{4\pi R^2} \qquad (3.2:2)$$

where

C = conversion factor averaged over energy

S_γ = total gamma source strength integrated over all time and energy

μ = apparent linear attenuation coefficient.

Both the buildup factor and the integration over energy are now included in the apparent linear attenuation coefficient characteristic of the actual energy spectrum. This lumping of factors into μ decreases the accuracy of the resulting expression but it remains useful for many circumstances.

It is customary to characterize particular bomb bursts by the yield W. Since for a given weapon design the source strength S_γ is always directly proportional to the yield, W will be substituted for S_γ in all further equations. The required proportionality constant between S_γ and W is now included in C, the averaged conversion factor. It should be carefully noted, however, that changes in weapon design (which usually accompany large changes in yield) may strongly affect the energy distribution of the source and the proportionality constant between source strength and yield. Both C and μ may therefore be expected to vary to some as yet unknown degree with weapon design.

The initial gamma dose D_γ results primarily from two separate sources, fission product gammas and nitrogen capture gammas. Thus

$$D_\gamma = W\left[D_{fp} + D_{nc}\right] \tag{3.2:3}$$

where D_{fp} and D_{nc} are the doses due to fission product and nitrogen capture gammas from a bomb of unit yield.

Each of the two components of the dose may be expressed by Eq. 3.2:2.

$$D_\gamma = W\left[\frac{C_{fp}\, e^{-\mu_{fp}R}}{4\pi R^2} + \frac{C_{nc}\, e^{-\mu_{nc}R}}{4\pi R^2}\right] \tag{3.2:4}$$

The apparent linear attenuation coefficient may be expressed in terms of the quiescent air density ρ, the apparent linear attenuation coefficient in standard density air μ_0, and the corresponding apparent mean free paths in air λ and λ_0. The quiescent air density ρ is defined in units of d_0, the density of pure dry air at standard conditions ($d_0 = 1.293 \times 10^{-3}$ gm-cm^{-3}). Thus ρ is equal to the ratio of the actual air density to the standard air density d_0.

$$\mu = \rho\mu_0 = \frac{1}{\lambda} = \frac{\rho}{\lambda_0} \tag{3.2:5}$$

Thus the initial gamma dose is

$$D_\gamma = W\left[\frac{C_{fp}\, e^{-\frac{\rho R}{\lambda_{fp0}}}}{4\pi R^2} + \frac{C_{nc}\, e^{-\frac{\rho R}{\lambda_{nc0}}}}{4\pi R^2}\right] \tag{3.2:6}$$

We may now make the approximate correction for variations in the quiescent air density between source and receiver due to normal and relatively small changes in air temperature and pressure. The average quiescent air density $\bar{\rho}$ has been defined in Chapter 1 and the method of calculation presented. Substituting $\bar{\rho}$ for ρ Eq. 3.2:6 becomes

$$D_\gamma = W\left[\frac{C_{fp}\, e^{-\frac{\bar{\rho}R}{\lambda_{fp0}}}}{4\pi R^2} \bullet \frac{C_{nc}\, e^{-\frac{\bar{\rho}R}{\lambda_{nc0}}}}{4\pi R^2}\right] \tag{3.2:7}$$

Finally a correction must be made for the variation in air density due to blast wave perturbation of the attenuating atmosphere between point of burst and receiver. This is accomplished by means of a hydrodynamic scaling factor h, which is a function of the bomb yield, the average quiescent air density, the distance from point of burst, and the type of radiation. Thus

$$D_\gamma = W\left[h_{fp} D_{fp} + h_{nc} D_{nc}\right] = W\left[h_{fp} C_{fp} \frac{e^{-\frac{\bar{\rho}R}{\lambda_{fp0}}}}{4\pi R^2} + h_{nc} C_{nc} \frac{e^{-\frac{\bar{\rho}R}{\lambda_{nc0}}}}{4\pi R^2}\right] \tag{3.2:8}$$

The reason for the existence of the hydrodynamic scaling factor can easily be understood. The attenuation of any radiation between source and receiver is dependent upon the number of mean free paths between these two points. The number of mean free paths is directly proportional to

$$\int_0^R \rho(x)dx$$

In a quiescent atmosphere with given uniform density ρ_1 the value of the integral is obviously $\rho_1 R$. Now suppose that all the atmosphere inside a sphere of radius R is compressed into a very thin spherical shell just inside radius R. Applying the law of conservation of mass, it can easily be shown that the value of the integral is in this case equal to $\rho_1 R/3$ so that the number of mean free paths has been decreased to 1/3 of the unperturbed value. Since the blast wave is travelling outward from the point of burst, it is evident that the number of mean free paths to a point at radius R changes as a function of time. When the thin shell moves past the point at R, the number of mean free paths may become much less than 1/3 of the unperturbed value over some period of time.

The phenomena which occur in the propagation of the blast wave due to the explosion at a point are in reality much more complicated than the simple picture presented above. Certain properties of the real hydrodynamic scaling factor, however, are clear from the following physical considerations.

1. For yields sufficiently low the value of h is unity, i.e., there is no appreciable compression effect on the atmosphere.

2. For any given yield and quiescent air density, h will become constant with distance at a sufficiently large value of R. This is because the blast wave will have disappeared before reaching the distant point. The attenuation of radiation in penetrating to greater distances does not therefore depend upon the blast wave but only upon the quiescent atmosphere at those distances.

3. The value of h for a particular kind of radiation can never exceed $e^{+\bar{\rho}R/\lambda_0}$, where λ_0 is the mean free path for that radiation in standard density air. This is the value which the hydrodynamic scaling factor would have for the case of infinite yield, in which case all of the attenuating medium would be permanently removed between the point of burst and the receiver. This factor is just sufficient to cancel the exponential factor in the dose equations and its use is equivalent to specifying that in this case attenuation is only by geometrical and not by material means.

4. For sufficiently small distance from the point of burst R, any explosion will tend to appear somewhat like an infinite explosion, at least for a short time. In this period all of the intervening atmosphere will be blasted away from between the point of burst and the receiver. Under such conditions h will also be given by $e^{+\bar{\rho}R/\lambda_0}$. This statement is true to the extent that one can neglect the return of the atmosphere to its equilibrium condition while the radiation source intensity remains high. Naturally, for small yields this last condition is bound to be violated.

From these considerations it is possible to immediately draw the general shape of the hydrodynamic scaling factor curve as a function of distance for some chosen air density and yield. The curve should begin at the origin (h = 1, R = 0) with a slope determined by the infinite yield value for $h = e^{+\bar{\rho}R/\lambda_\phi}$. The slope should gradually decrease with distances, at large distances reaching a constant value. An idealized plot of h as a function of R is shown in Fig. 3.2:1 for constant quiescent air density, and with yield as a parameter.

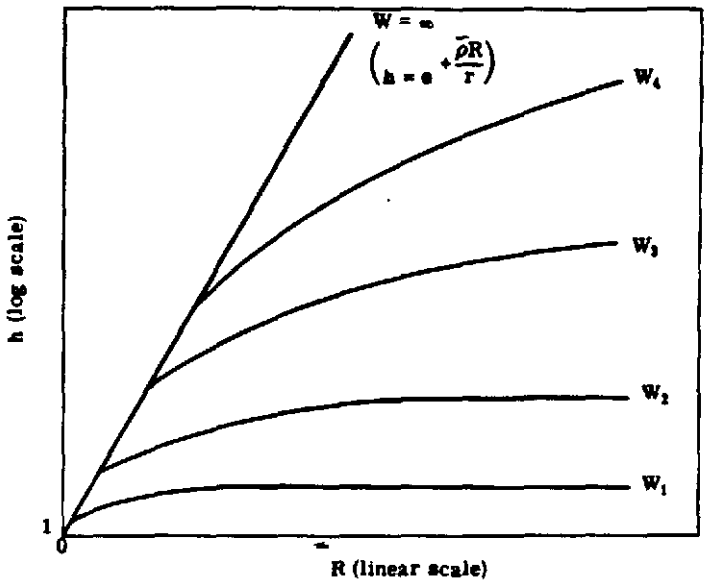

Fig. 3.2:1 Idealized Shape of Hydrodynamic Scaling Factor Curve as a Function of Source-Receiver Distance R, and of Weapon Yield W.

Simplification of Dose Equation

The general equation for the initial gamma dose which applies for all ranges of weapon yields and designs has been derived.

$$D_\gamma = W\left[h_{fp}\, D_{fp} + h_{nc}\, D_{nc}\right] \qquad (3.2{:}8)$$

This equation shows the dependence of the initial gamma dose on two separate gamma sources and on the corresponding hydrodynamic scaling factors. As will be shown below, the component doses (D_{fp} and D_{nc}) do not scale with variations in air density in the same manner as do the hydrodynamic scaling factors (h_{fp} and h_{nc}). It is therefore necessary to be able, in some manner, to determine the component doses separately from the hydrodynamic factors if we are to attempt to extend the limited data available over the wide range of air densities of importance.

To achieve this separation we necessarily resort to simplification of Eq. 3.2:8 since with our present knowledge it is not possible to use this relation directly. Two possible approaches to such simplification have been considered and are briefly discussed below.

The first method attempts to use the little insight we have on the interrelationships of the time of emission of fission product and nitrogen capture gammas, the yield, and the hydrodynamic effect. The emission times for fission product and nitrogen capture gamma radiation are quite different.

Thus, the neutrons which generate nitrogen capture gammas are emitted very quickly during the fission reaction and escape into the atmosphere where they are slowed down and finally captured. The mean lifetime in air at sea level of a neutron of any initial energy is about 0.07 sec. Thus, the gamma radiation produced from neutron capture in nitrogen should be most intense at early times, of the order of 0.1 sec. Fission product gamma radiation, on the other hand, is emitted mostly after the nuclear reaction is over and this source remains intense over a much greater time interval. Because of the early birth of nitrogen capture gammas, it is to be expected that they should arrive at the receiver before the blast wave and thus escape most or all of the resulting multiplication of dose. To a low order approximation one would expect therefore that $h_{nc} \approx 1.0$ and that this approximation holds equally well for low, intermediate, and high yields. The blast effect would then act only on the fission product gamma rays and the determination of h_{fp} is what is required. Further simplification can be obtained by consideration of the variation of the hydrodynamic effect with bomb yield. For low yields (less than 10 KT) the hydrodynamic effect has been shown to be unimportant and h is essentially 1, while for high yields (above 100 KT) it is of dominant importance and h may be as high as 10^4 in the MT region. We may now consider the modifications of Eq. 3.2:8 for the three ranges of weapon yield.

Low Yield (less than 10 KT). Both h_{fp} and h_{nc} are approximately equal to 1. Thus,

$$D_\gamma = W\left[D_{fp} + D_{nc}\right] \tag{3.2:9}$$

Intermediate Yield (10 to 100 KT). In this yield range h_{nc} is still approximately equal to 1 but this *may no longer be true of* h_{fp}. Thus

$$D_\gamma = W\left[h_{fp}D_{fp} + D_{nc}\right] \tag{3.2:10}$$

High Yield (above 100 KT). The equation shown for intermediate yields can also be applied to high yield weapons. Thus

$$D_\gamma = W\left[h_{fp}D_{fp} + D_{nc}\right] \tag{3.2:11}$$

In the very high yield range where h_{fp} is quite large, D_{nc} may be small in comparison to $h_{fp}D_{fp}$ and therefore

$$D_\gamma = W\, h_{fp}D_{fp} \tag{3.2:12}$$

The second method of simplifying Eq. 3.2:8 does not attempt to explore the separate fission product and nitrogen capture gamma doses but rather defines an effective hydrodynamic scaling factor which applies to the sum of the two. Thus the effective hydrodynamic scaling factor is

$$h_{eff} = \frac{h_{fp}D_{fp} + h_{nc}D_{nc}}{D_{fp} + D_{nc}} \tag{3.2:13}$$

The initial gamma dose is now given as

$$D_\gamma = W\, h_{eff}\left[D_{fp} + D_{nc}\right] \tag{3.2:14}$$

We have chosen the second method of simplification and accordingly the presentation of initial gamma dose results and the correlation of experimental measurements will use Eq. 3.2:14. The analysis of experimental results will yield values of h_{eff} rather than either h_{fp} or h_{nc}. This choice was based on several factors but primarily because the second approach appears to yield results more reasonably consistent with the limited amount of high and intermediate yield experimental data

available at present. Further, it does so in a considerably simpler fashion and has the added advantage that the single equation can be applied to all yield ranges.

Scaling for Variations in Average Quiescent Air Density

Values of the initial gamma dose D_γ and the hydrodynamic scaling factor h_{eff} are required over a wide range of conditions. While measured values of the dose (and consequently of h_{eff}, which is determined from dose measurements) are available over most of the range of interest for two of the important variables R and W, this is not true of the third, the average quiescent air density $\bar{\rho}$. Almost all dose measurements for surface bursts have been made while $\bar{\rho}$ was in the range 0.8 to 0.9. Consequently, it is necessary to formulate scaling relations to allow extension of the measured values of D_γ and of the derived values of h_{eff} to other average air densities.

Since a theoretical equation has been constructed for D_γ, scaling can be done simply and exactly within the accuracy of the theoretical model. However, since the relationship between h_{eff} and $\bar{\rho}$ is not known, scaling of h_{eff} requires the use of additional approximations and is therefore subject to greater uncertainties.

Scaling the initial gamma dose can be done in several ways, the most convenient approach being used here. The dose equation is

$$D_\gamma = W h_{eff}\left[\frac{C_{fp}}{4\pi R^2} e^{-\frac{\bar{\rho}R}{\lambda_{fp\bullet}}} + \frac{C_{nc}}{4\pi R^2} e^{-\frac{\bar{\rho}R}{\lambda_{nc\bullet}}}\right] \qquad (3.2{:}15)$$

Transposing,

$$\frac{D_\gamma R^2}{W h_{eff}} = \frac{C_{fp}}{4\pi} e^{-\frac{\bar{\rho}R}{\lambda_{fp\bullet}}} + \frac{C_{nc}}{4\pi} e^{-\frac{\bar{\rho}R}{\lambda_{nc\bullet}}} \qquad (3.2{:}15)$$

Since $\bar{\rho}$ and R are the only variables on the right side of the equation and they appear only as a product $\bar{\rho}R$,

$$\frac{D_\gamma R^2}{W h_{eff}} = f(\bar{\rho}R) \qquad (3.2{:}16)$$

Therefore, if the quantity $D_\gamma R^2/W h_{eff}$ is known for some distance R_1 and average density $\bar{\rho}_1$, then the same value of $D_\gamma R^2/W h_{eff}$ holds for any other density $\bar{\rho}_2$ and distance R_2, chosen such that

$$\bar{\rho}_1 R_1 = \bar{\rho}_2 R_2$$

or

$$R_2 = \left(\frac{\bar{\rho}_1}{\bar{\rho}_2}\right) R_1 \qquad (3.2{:}17)$$

The same relation restated is

$$\frac{D_1 R_1^2}{W_1 h_1}(\bar{\rho}_1 R_1) = f(\bar{\rho}_1 R_1) = f(\bar{\rho}_2 R_2) = \frac{D_2 R_2^2}{W_2 h_2}(\bar{\rho}_2 R_2). \qquad (3.2{:}18)$$

Eq. 3.2:17 and 3.2:18 are then the scaling relations required for transferring, not the dose, but rather the quantity $D_\gamma R^2/W h_{eff}$ to other air densities.

Scaling of the hydrodynamic scaling factor for different air densities requires analytical examination of h_{eff}, albeit a very crude one.

It is assumed that the energy spectrum of fission product and nitrogen capture gammas can be represented by a single effective energy and further that this effective energy does not change with time. The expression for the total initial gamma ray dose received at point R, with average quiescent air density $\bar{\rho}$, yield W, and with the hydrodynamic effect included is

$$D(R, \bar{\rho}, W) = \frac{CW}{4\pi R^2} \int_0^{t_\gamma} \frac{S_\gamma(t)}{W} e^{-\mu(R, \bar{\rho}, W, t)R} B[\mu(R, \bar{\rho}, W, t)R]\, dt. \qquad (3.2{:}19)$$

If there were no hydrodynamic effect to be considered, the dose would be

$$D_q(R, \bar{\rho}, W) = \frac{CW}{4\pi R^2} e^{-\mu(\bar{\rho})R} B[\mu(\bar{\rho})R] \int_0^{t_\gamma} \frac{S_\gamma(t)}{W} dt \qquad (3.2{:}20)$$

where

$D(R, \bar{\rho}, W)$ = dose received with the hydrodynamic effect included

$D_q(R, \bar{\rho}, W)$ = dose received with the hydrodynamic effect ignored

C = conversion factor which determines the dose units

W = yield

$S_\gamma(t)/W$ = rate of emission of gamma rays per-unit yield

$\mu(R, \bar{\rho}, W, t)$ = total linear attenuation coefficient under shock conditions

$\mu(\bar{\rho})$ = total linear attenuation coefficient under ambient conditions

$B[\mu(R, \bar{\rho}, W, t)R]$ = buildup factor under shock conditions

$B[\mu(\bar{\rho})R]$ = buildup factor under ambient conditions

t_γ = time chosen as the end of initial gamma dose period

The ratio of D/D_q is the hydrodynamic scaling factor h, which is then given by

$$h = \frac{D}{D_q} = \frac{\int_0^{t_\gamma} \frac{S_\gamma(t)}{W} e^{-\mu(R, \bar{\rho}, W, t)R} B[\mu(R, \bar{\rho}, W, t)R]\, dt}{e^{-\mu(\bar{\rho})R} B[\mu(\bar{\rho})R] \int_0^{t_\gamma} \frac{S_\gamma(t)}{W} dt} \qquad (3.2{:}21)$$

Using the mean value theorem

$$h = \frac{t_\gamma \frac{S_\gamma(t_1)}{W} e^{-\mu(R, \bar{\rho}, W, t_1)R} B[\mu(R, \bar{\rho}, W, t_1)R]}{t_\gamma \frac{S_\gamma(t_1)}{W} e^{-\mu(\bar{\rho})R} B[\mu(\bar{\rho})R]} \qquad (3.2{:}22)$$

where t_1 is a time between 0 and t_γ.

If we now make the following assumptions:

1. $B(\mu R) \quad e^{k_1 \mu R}$
2. $\mu(R, \bar{\rho}, W, t_i) = \bar{\rho}\ \mu_0(R, W, t_i)$

   $\mu(\bar{\rho}) = \bar{\rho}\mu_0$
3. t_i is not a function of ρ

$$h = \frac{e^{(k_1 - 1)\ \bar{\rho}\ \mu_0(R, W, t_i)R}}{e^{(k_1 - 1)\ \bar{\rho}\ \mu_0 R}} = \frac{\left[e^{(k_1 - 1)\ \mu_0(R, W, t_i)R}\right]^{\bar{\rho}}}{\left[e^{(k_1 - 1)\ \mu_0 R}\right]^{\bar{\rho}}} \tag{3.2:23}$$

$$= [F(R, W, t_i)]^{\bar{\rho}}$$

where F is some unspecified function of R, W, and t_i. Consequently if the hydrodynamic scaling factor is known for some quiescent air density $\bar{\rho}_1$ and it is desired to transform h_{eff} to a different density $\bar{\rho}_2$, the scaling law (using the listed assumptions) is

$$h(\bar{\rho}_2) = [h(\bar{\rho}_1)]^{\frac{\bar{\rho}_2}{\bar{\rho}_1}} \tag{3.2:24}$$

It should be observed that while assumption 1 above is probably not bad, the remaining assumptions taken together are subject to serious question.

3.2.2 LOW AND INTERMEDIATE YIELD WEAPONS

The results presented for low and intermediate yield weapons are based on experimental film badge measurements reported by Los Alamos[6, 8, 9] and the Evans Signal Laboratory.[7, 11] These measurements, despite some discrepancies, provide a reasonably consistent and accurate picture of the dose-distance relations for low altitude bursts and low to intermediate yields, this area of nuclear radiation effects being one of the best known. The experimental data underlying even these results are, however, by no means complete; data for very long and very short distances and for yields between 50 and 100 KT are still inadequate.

From the curves included in this section it is possible to calculate the initial gamma dose for fission and boosted fission weapon yields of up to 100 KT, average quiescent air densities ranging from 0.2 to 1.1, and source-receiver distances of between 500 and 6000 yd. These results are estimated to be accurate to within a factor of two.

The dose-distance curve derived from the film badge measurements is compared below with results from two other sources. An analysis by Malik[2] using both theoretical considerations and experimental results permits calculation of the initial gamma dose by separation into its two major components. Harris and Vortman[12] give a simple equation for the initial gamma dose based on fitting the point source formula to experimental results.

Dose Measurements and Analysis (Film Badge Readings)

Fig. 3.2:2 is a plot of experimental values of $D_\gamma R^2/W\ h_{eff}$ as a function of distance R. All of the experimental data have been adjusted to an average air density $\bar{\rho} = 0.9$ and to $W\ h_{eff}$ rather than to the yield W. The methods of adjustment are described in Section 3.2:1 and below, respectively. The representative experimental data were selected from Teapot (Shots 1 through 12)[11] and Tumbler-Snapper (Shots 2 through 8),[7] both instrumented by Evans Signal Laboratory, and from Tumbler-Snapper (Shots 2 through 8),[6] Buster (Baker, Charlie, Dog, Easy),[6] and Ranger (A, B_1, B_2, E, F),[9]

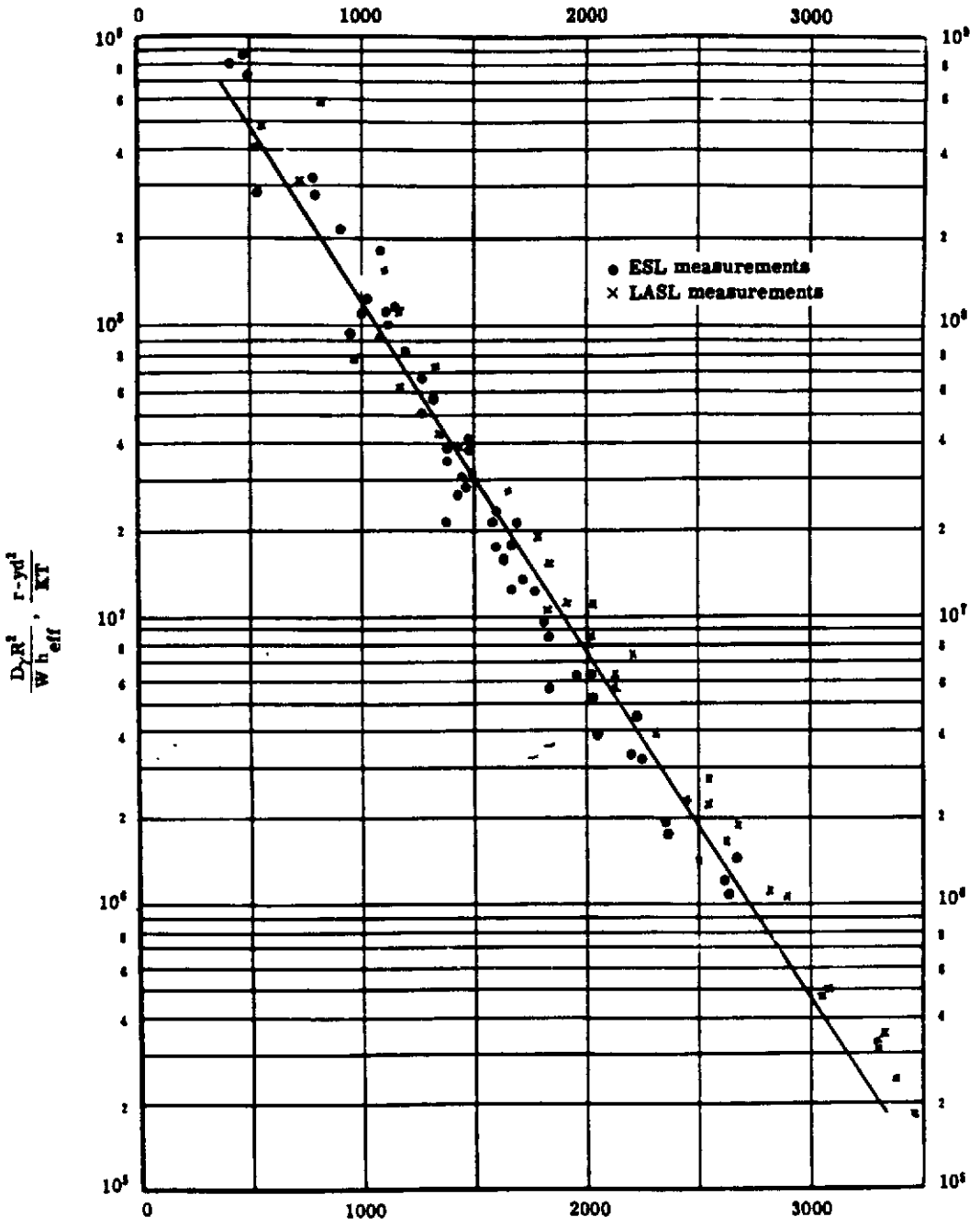

Fig. 3.2:2 Experimental Values of $D_\gamma R^2/W\ h_{eff}$ for Surface Bursts of Low and Intermediate Yield Weapons as a Function of Source-Receiver Distance R ($\overline{\rho} = 0.9$).

all instrumented by Los Alamos Scientific Laboratory. Points determined by ESL are plotted as dots while those determined by LASL are plotted as crosses. Inspection of Fig. 3.2:2 shows two significant differences between the Los Alamos and Evans data – the LASL data is above the ESL data and the apparent mean free path of the LASL data appears slightly longer than the corresponding mean free path for ESL. The reasons for these differences are thought to lie in the differing sensitivities of the two types of film detectors used by ESL and LASL, and in the change of initial gamma spectrum with distance. A firm explanation is not possible at this time because the measured results are at least partially inconsistent with what would be expected on the basis of what is known about the detector sensitivities and the spectral change.

The ESL film detectors have a reasonably flat response to gammas except at the high energy end of the spectrum. At low energies, however, there is a cutoff at 80 kev with only a slight hump in the response curve immediately above this energy. The ESL results therefore can be expected to underreport the effects of low energy gammas. The LASL film detectors cut off at a threshold of 40 kev but are extremely sensitive to that part of the spectrum between 40 and 100 kev, and should therefore overstate the effects of the soft gammas. The conclusion would seem to be that for a spectrum where the low energy component is appreciable the LASL dose should lie above the ESL value.

Theoretical calculations by Borg and Eisenhauer[4] of the initial gamma ray energy spectrum as a function of distance have indicated that an appreciable hardening of the energy spectrum or shift in the high energy direction occurs as the distance from the point of burst increases. Thus the importance of the low energy component decreases with distance and one would expect that the dose reading would drop faster for the low energy sensitive detector, i.e., this detector would have the shorter apparent mean free path. While the LASL data lie above the ESL data, which from the arguments given above might be expected, the relative values of the observed apparent mean free paths are the reverse of expected. Further effort is required to resolve this conflict. It is conceivable that further differences in the high energy sensitivities of the two detectors may be at least partially responsible.

A straight line of best fit is drawn for the data shown in Fig. 3.2:2 but the line is adjusted preferentially in favor of the ESL detector on the basis of estimates that its over-all response yields results closer to the true dose than the LASL detector.[13,14]

The equation describing the straight line fit of Fig. 3.2:2 is

$$\frac{D_\gamma R^2}{W\, h_{eff}} = 1.93 \times 10^9\, e^{-\frac{\bar{\rho} R}{324}} \qquad (3.2{:}25)$$

where

D_γ = total initial gamma dose, r

R = distance between source and receiver, yd

W = weapon yield, KT

h_{eff} = effective hydrodynamic scaling factor.

For present purposes this equation will be used as the basis of dose calculations for low and intermediate yield, low altitude bursts. The apparent mean free path in standard density air is indicated to be 324 yd for R between 500 and 3500 yd and this value should be interpreted as an average for fission product and nitrogen capture gamma radiation.

Not only does the composite data permit such a straight line fit but the values of $D_\gamma R^2/W\, h_{eff}$ as a function of R for any one individual shot also plot as a straight line within the limits of experimental error and over the distances at which measurements were made. This is somewhat surprising since the apparent mean free path for neutron capture gammas should be considerably longer than that for fission product gammas. Such a difference would lead us to expect a mean free path which increases with increasing distance from the source and therefore a somewhat curved rather than a

straight line. If the experimental film badge data plotted as in Fig. 3.2:2 did show some deviation from a straight line, it would be possible in principle and to a low order of accuracy to make a separation of the total dose into its components, i.e., into fission product and nitrogen capture gamma doses. Since film badge detectors record only the total dose integrated over all time, they do not normally permit such a separation.

As noted above, the film badge data for low and intermediate yield weapons fall close to a straight line. Such slight suggestion of lengthening in the apparent mean free path with distance which does appear in Fig. 3.2:2 occurs beyond about 3,000 yd, but is well within the experimental error of the measurements. Therefore, where extrapolation of the results of Fig. 3.2:2 to larger distances was required, the straight line was extended. This may lead to some slight underestimate of the predicted doses for distances larger than 3,500 yd at $\bar{\rho} = 0.9$ and for corresponding distances at other average air densities.

Comparison of Dose-Distance Results from Several Sources

It is of interest to compare the initial gamma dose-distance relation derived above and represented by Eq. 3.2:25 with two similar relations from alternate sources. The theoretical analysis of Malik[2] provides the basis for calculating the total initial gamma dose through its separation into the fission product and nitrogen capture components as given in Eq. 3.2:8. Thus, the conversion factors C_{fp} and C_{nc} and the apparent mean free paths in standard density air λ_{fp_0} and λ_{nc_0} can be calculated. For distances greater than 1300 yd from the point of burst this analysis yields

$$\frac{D_\gamma R^2}{W} = 3.18 \times 10^8 \, h_{fp} \, e^{-\frac{\bar{\rho}R}{284}} + 2.87 \times 10^8 \, h_{nc} \, e^{-\frac{\bar{\rho}R}{456}} \qquad (3.2:8)$$

For low and intermediate yield weapons where the hydrodynamic scaling factors are close to unity, Eq. 3.2:8 is approximately

$$\frac{D_\gamma R^2}{W} = 3.18 \times 10^8 \, e^{-\frac{\bar{\rho}R}{284}} + 2.87 \times 10^8 \, e^{-\frac{\bar{\rho}R}{456}} \qquad (3.2:26)$$

The calculations from which the numerical values of Eq. 3.2:26 are derived are approximate only, but they do at least permit separation of the total dose into its two constituents. It should be noted that Malik has applied his original analysis to both delivery rate and total dose calculations for four test bursts in the 10 to 50-KT yield range with reasonable agreement with experimental results.[2]

The analysis of experimental dose measurements by Harris and Vortman[12] indicates that the following equation can be used to represent the relationship between initial gamma dose and distance:

$$\frac{D_\gamma R^2}{W} = 2 \times 10^8 \, e^{-\frac{\bar{\rho}R}{380}}. \qquad (3.2:27)$$

Note that the effective hydrodynamic scaling factor is not explicitly included in Eq. 3.2:27; this equation may not be strictly comparable with the results presented in Eq. 3.2:25. Since in the low and intermediate yield range h_{eff} is not far from one, this should not be a major difference, however.

Fig. 3.2:3 shows the three curves represented by the equations previously presented. In the figure, $D_\gamma R^2/W \, h_{eff}$ and $D_\gamma R^2/W$ are plotted as functions of R for standard density air ($\bar{\rho} = 1.0$). The three equations are tabulated below.

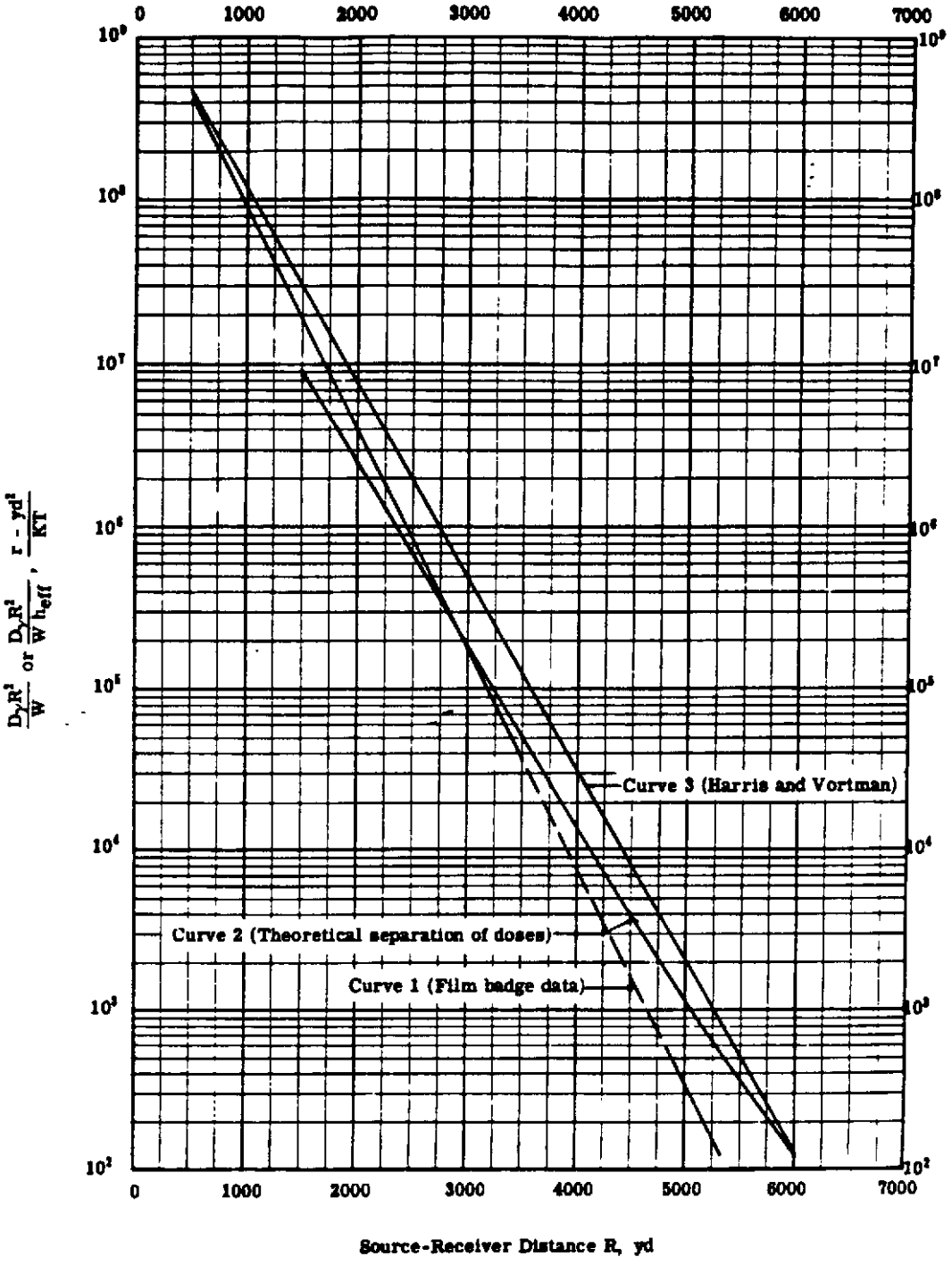

Fig. 3.2:3 Comparison of Initial Gamma Dose-Distance Results from Several Sources for Surface Bursts of Low and Intermediate Yield Weapons ($\bar{\rho} = 1.0$). The dashed line is extrapolated.

Curve 1 (analysis of film badge dose measurements)

$$\frac{D_\gamma R^2}{W h_{eff}} = 1.93 \times 10^8 \, e^{-\frac{\bar{\rho}R}{324}} \qquad (3.2:25)$$

Curve 2 (theoretical separation of doses)

$$\frac{D_\gamma R^2}{W} = 3.18 \times 10^8 \, e^{-\frac{\bar{\rho}R}{284}} + 2.87 \times 10^8 \, e^{-\frac{\bar{\rho}R}{406}} \qquad (3.2:26)$$

Curve 3 (Harris-Vortman experimental results)

$$\frac{D_\gamma R^2}{W} = 2 \times 10^8 \, e^{-\frac{\bar{\rho}R}{300}} \qquad (3.2:27)$$

Since the experimental film badge data only extended to about 3500 yd, Curve 1 is drawn as a solid line to this point only. The dashed portion of the line is extrapolated. Similarly since Eq. 3.2:26 does not hold below about 1500 yd, Curve 2 is not extended to shorter distances.

The maximum spread between the curves is a factor of four and for most of the data the spread is less than this. Discrepancies of this order are perhaps not surprising considering the uncertainties in both the experimental measurements and the theoretical calculations, and in the different means used to obtain the results. Thus the determination of the numerical coefficients and of the apparent mean free paths of Eq. 3.2:26 involve approximations of an undeterminable nature. Conversion of the detector reading into dose introduces errors, both those due to calibration and those due to the change of energy spectrum with distance, as previously noted in connection with the comparison of the LASL and ESL results. Curves 1 and 3, being based on weapon test results, include the effect of the earth surface and of the cloud rise on the dose while Curve 2 does not. Also, the hydrodynamic effect is treated differently in the three equations. Other factors may be important.

The analysis based on separation of the dose components yields the longest apparent mean free path (approximately 400 yd) while the film badge measurements yield a value of 324 yd. If the experimental measurements are to be believed, it would appear that Curve 2 underemphasizes the importance of the fission product gammas.

Determination of Effective Hydrodynamic Scaling Factor

The hydrodynamic effect is expected to be small for low and intermediate yields. (h_{eff} is equal to or close to unity). A proper treatment of the blast wave perturbation of the attenuating medium, therefore, is not essential for yields less than 100 KT although it becomes of dominant importance in the MT region. An approximate method of determining h_{eff} as a function of yield is shown below. This method ignores the dependence of h_{eff} on the average quiescent air density and on the source-receiver distance, the errors involved being comparatively small.

Equation 3.2:14 is the simplified dose-distance relationship applicable to low and intermediate yields.

$$D_\gamma = W h_{eff}\left[D_{fp} + D_{nc}\right] \qquad (3.2:14)$$

$$= W h_{eff}\left[\frac{C_{fp} \, e^{-\frac{\bar{\rho}R}{\lambda_{fp\phi}}}}{4\pi R^2} + \frac{C_{nc} \, e^{-\frac{\bar{\rho}R}{\lambda_{nc\phi}}}}{4\pi R^2}\right] \qquad (3.2:15)$$

Assuming that h_{eff} is not a function of R and $\bar{\rho}$, for given values of R and $\bar{\rho}$ the quantities inside the brackets are constant and the dose is proportional to W and h_{eff} only.

$$D_\gamma = k\, W\, h_{eff} \qquad (3.2{:}28)$$

For low yields where $h_{eff} = 1$ and at the same values of R and $\bar{\rho}$, the dose is then

$$\left(D_\gamma\right)_\ell = kW \qquad (3.2{:}29)$$

The relationship for h_{eff} is then

$$h_{eff} = \frac{D_\gamma}{(D_\gamma)_\ell} \qquad (3.2{:}30)$$

The effective hydrodynamic scaling factor is determined by plotting the measured dose at some fixed distance and air density against yield for as many shots as available in the low and intermediate yield range. The portion of the curve at low yields is found, as expected, to be approximated quite well by a straight line. This line and its extension represent $(D_\gamma)_\ell$, the dose to be expected in the absence of the blast effects. The ratio of $D_\gamma/(D_\gamma)_\ell$ is then h_{eff}. Fig. 3.2:4 presents the quantity $W\, h_{eff}$ as a function of the yield W.

Because the effects of air density and distance from the source are neglected, errors of up to ±30 percent in h_{eff} may be expected in some cases for 100 KT bursts. These errors are considered acceptable at present in the light of the several large uncertainties in the dose determination.

Calculation of the Initial Gamma Dose

The dose-distance relationship represented by Eq. 3.2:25 and plotted in Fig. 3.2:2 and 3.2:3 (Curve 1) has been extended to cover a range of air densities by the method described in Section 3.2.1. Values of $D_\gamma R^2/W\, h_{eff}$ have been plotted in Fig. 3.2:5 as a function of R with $\bar{\rho}$ as a parameter. The solid portions of the lines of Fig. 3.2:5 represent the original data or transformations of such data to other air densities. The dashed portions of the lines represent extrapolations. (Fig. 3.2:5 presents curves for $\bar{\rho}$ as low as 0.2. These low air densities are not applicable to surface bursts but are included here for convenience since Fig. 3.2:5 will also be used to calculate air burst doses.)

To find the initial gamma dose D_γ for a particular burst it is necesssary to know the yield W, the average air density $\bar{\rho}$, and the distance from the source R at which D_γ is desired. The quantity $D_\gamma R^2/W\, h_{eff}$ is found from Fig. 3.2:5 at the known values of $\bar{\rho}$ and R; $W\, h_{eff}$ is found at the known value of W from Fig. 3.2:4; the appropriate arithmetic produces D_γ, the initial gamma dose, in r.

PROBLEM 1

The initial gamma dose due to a low or intermediate yield weapon is required at a given point. The distance between the point of burst and the receiver, the average quiescent air density, and the bomb yield are known.

Solution

1. Find $W\, h_{eff}$ from Fig. 3.2:4 at the given yield W (in KT).
2. Find $D_\gamma/W\, h_{eff}$ at the given distance and average quiescent air density from Fig. 3.2:5.
3. The required dose in r is the product of the values of $W\, h_{eff}$ and $D_\gamma/W\, h_{eff}$ found in steps 1 and 2.

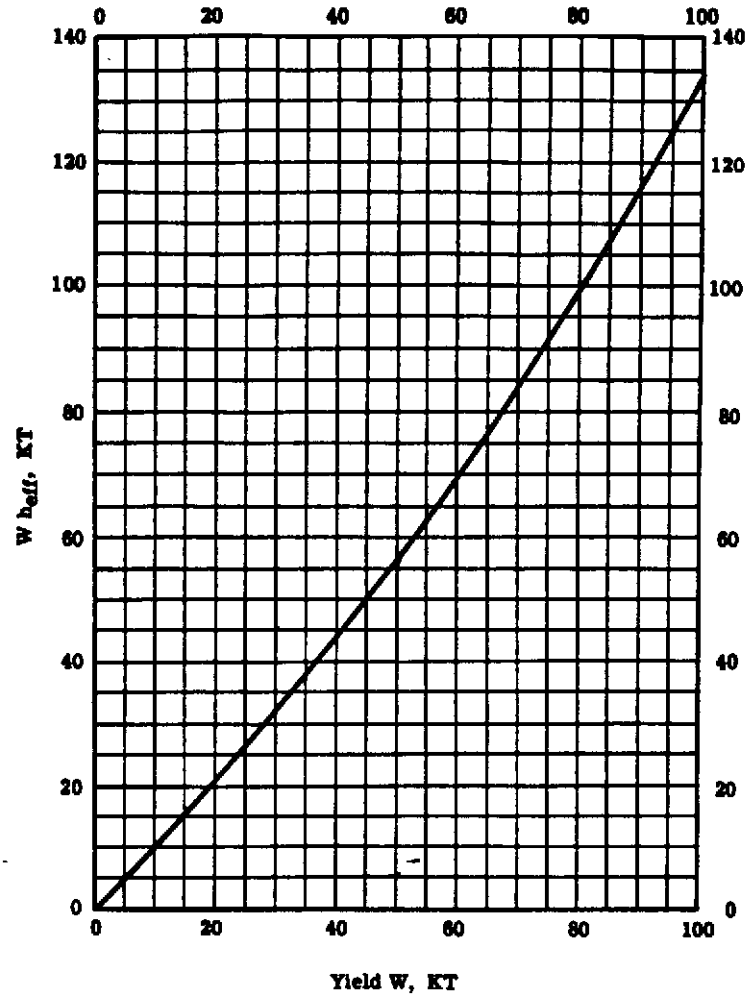

Fig. 3.2:4 W h_{eff} as a Function of Weapon Yield W for Surface and Air Bursts of Low and Intermediate Yield Weapons.

Example

What is the initial gamma dose at a distance of 2000 yd from the point of burst of a 40-KT weapon? The average air density is 0.9.

1. From Fig. 3.2:4 W h_{eff} is 44 KT.
2. From Fig. 3.2:5 D_γ/W h_{eff} at $\bar{\rho}$ of 0.9 and R of 2000 yd is 2.0 r-KT^{-1}.
3. The initial gamma dose is therefore (44) (2.0) = 88 r.

PROBLEM 2

At what distance from the burst point will a given dose be experienced? The average air density, and the weapon yield are known.

Solution

1. Find W h_{eff} from Fig. 3.2:4 and the given value of the yield W (in KT).

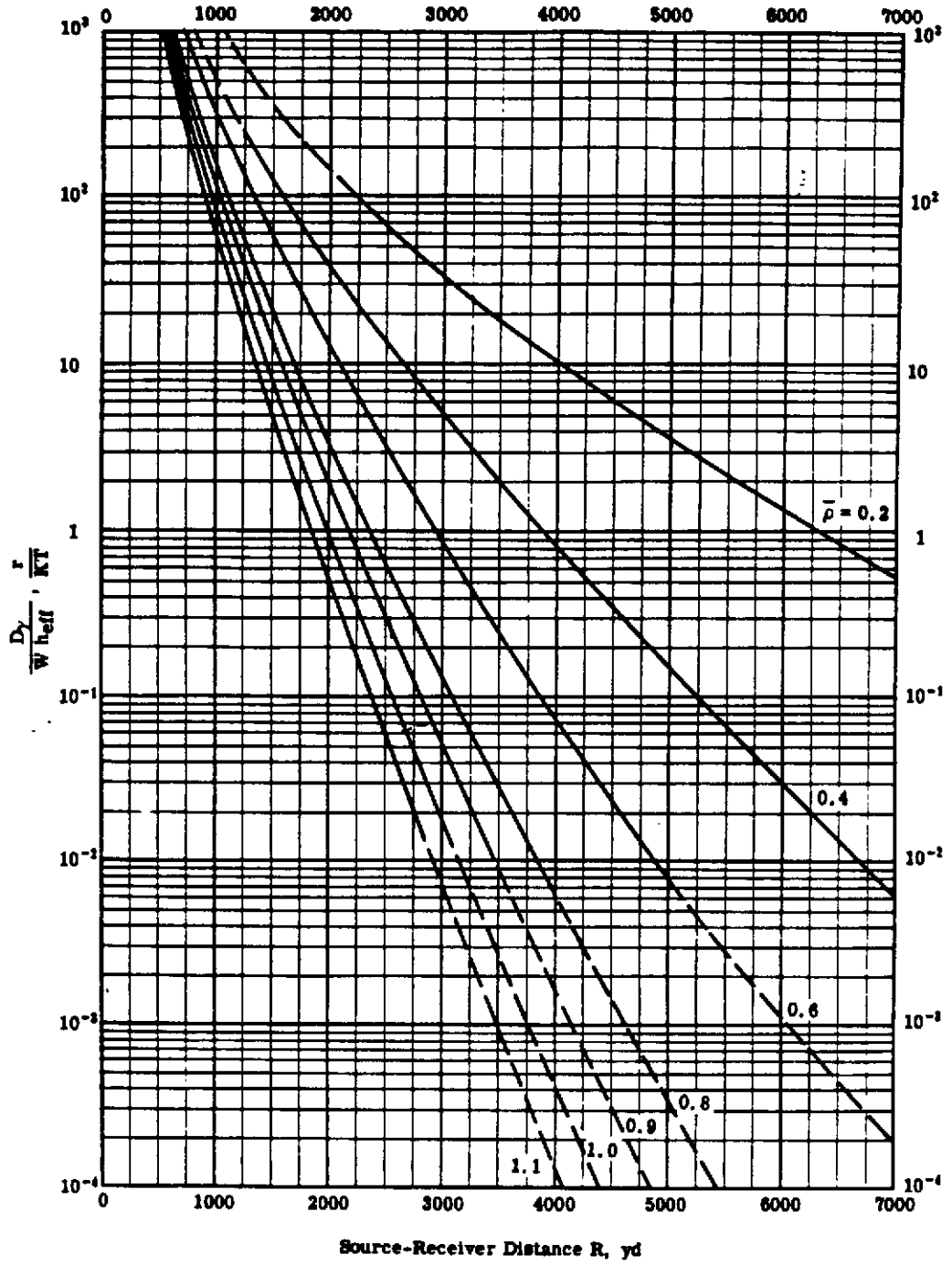

Fig. 3.2:5 Initial Gamma Dose-Distance Results for Surface and Air Bursts of Low, Intermediate, and High Yield Weapons for Several Average Air Densities. The average quiescent air density $\bar{\rho}$ is defined as the ratio of the actual air density to the air density at standard conditions (1.293×10^{-3} gm-cm^3). The value of $D_\gamma/W\,h_{eff}$ for surface bursts of all yields is read directly from the figure. The value of $D_\gamma/W\,h_{eff}$ for air bursts of all yields is obtained by multiplying the value read from the figure by a factor of 1.5.

2. Divide the given initial gamma dose by the value of W h_{eff} found in step 1.

3. Using the value of D_γ/W h_{eff} calculated in step 2, find the desired distance from Fig. 3.2:5 on the curve corresponding to the given air density.

Example

Find the distance from the point of burst at which an initial gamma dose of 100 r will be experienced for a 10-KT burst. The average air density $\bar{\rho}$ is 0.8.

1. From Fig. 3.2:4 at a yield of 10 KT the value of W h_{eff} is 10 KT.

2. The given initial gamma dose divided by the value of W h_{eff} is 100/10 = 10.

3. From Fig. 3.2:5 at $\bar{\rho}$ = 0.8 and D_γ/W h_{eff} = 10 the corresponding distance is 1700 yd. This is the required distance from the point of burst.

PROBLEM 3

What area will experience an initial gamma radiation dose greater than some given value? The initial gamma dose of interest, the average quiescent air density, the bomb yield, and the burst height are known.

Solution

1. Using the method of Problem 2, find the distance from the point of burst at which the given value of the dose will be experienced.

2. Find the distance from ground zero which corresponds to the source-receiver distance found in step 1, using the following relation.

   Distance from ground zero = $\sqrt{(\text{source-receiver distance})^2 - (\text{height of burst})^2}$

3. Convert the distance found in step 2 from yd to mi by dividing by 1760. Find the area of the circle of which this distance is the radius. This is the required area. More compactly,

$$\text{Required area (mi}^2) = \pi\left[\frac{\text{distance from ground zero (yd)}}{1760\ (\text{yd} \cdot \text{mi}^{-1})}\right]^2$$

Example

Find the area which will experience an initial gamma dose of more than 100 r for the conditions described in Problem 2. In addition to the information given in Problem 2 it is known that the burst height is 1400 yd.

1. The source-receiver distance found in Problem 2 was 1700 yd.

2. The distance from ground zero is $\sqrt{(1700)^2 - (1400)^2}$ = 960 yd.

3. The required area is $\pi\left(\frac{960}{1760}\right)^2$ = 0.93 mi^2.

Error

The probable error in the values of D_γ derived from the solid portions of the lines in Fig. 3.2:5 is the same as that in the experimental results themselves. Thus the probable error is about a factor of two, i.e., it is estimated that the probability is 50 percent that the computed dose is too large or too small by less than a factor of two. For the dashed portions of the lines the probable error may very well be larger because of the extrapolation involved, and at short distances also because of the questionable validity of the air density scaling procedure.

3.2.3 HIGH YIELD WEAPONS

Determination of the dose-distance relation for high yield weapons must again rely primarily on experimental measurements in the absence of adequate theoretical analysis. Unlike the situation for low and intermediate yield weapons, however, where experimental data are plentiful and reasonably consistent, the study of high yield bursts is seriously hampered by the small amount of data available and the incompleteness and inconsistency of these data. The poor documentation of radiation effects from high yield weapons is due principally to the experimental difficulties of measuring such effects and the relatively small number of high yield weapon tests which have been made. Under these circumstances only a very rough and simple treatment is presented and the associated errors may well be large.

From the curves included in this section it is possible to calculate the initial gamma dose for surface bursts of boosted fission and fusion weapons with yields from 100 KT to 20 MT, average quiescent air densities of 0.2 to 1.1, and source-receiver distances of between 500 and 6000 yd. For weapon yields less than 1 MT the dose results are probably good to within a factor of three. For weapon yields above 1 MT the results are probably no better than a factor of 10 and possibly of as much as 25.

Dose Measurements and Analysis

In the yield range of from 100 KT to 0.5 MT there are only the total dose measurements from [redacted] Total doses were obtained at seven source-receiver distances of from 1500 to 2800 yd. In the 0.5 to 1.0-MT range there is one total dose reading for Ivy King (0.55 MT)[10] at 1800 yd, and one incomplete reading at 1140 yd from which no useful information can be obtained for present purposes. In the yield range above 1 MT there are two complete total dose readings at 2400 and 4500 yd for Castle 4 (Union) (6.5 MT);[15] one incomplete dose rate curve measured at 2500 yd, and one total dose value at 4400 yd for Ivy Mike (10.5 MT);[10] and finally one incomplete dose rate curve at 2400 yd from Castle 1 (Bravo) (14.5 MT).[15] The incomplete dose records (Ivy Mike and Castle 1) show the dose which reached the receiver before the shock wave. For yields between 20 KT and 1 MT, and at the distances at which measurements have been made, as much as 50 to 90 percent of the dose may arrive after the shock wave, while for yields greater than 1 MT this may increase to as high as 99 percent of the total dose.

Table 3.2:1 summarizes the data for these high yield bursts. Information presented includes the test series and burst designation, the weapon type, the average quiescent air density between burst and receiver in units of standard air density, the actual distance between receiver and point of burst, and the value of the separation distance corrected to standard air density. In addition, there are presented the dose measurements D_γ and the calculated value of $D_\gamma R^2/W$ in $r - yd^2 - KT^{-1}$, where W is the total yield in all cases. Fig. 3.2:6 presents the calculated values of $D_\gamma R^2/W$ for the high yield shots plotted against the source-receiver distance adjusted to a standard air density ($\bar{\rho} = 1.0$). For Ivy Mike and Castle 4 where two data points are available these points are connected by straight lines. What justification there is for this course lies in the knowledge that at lower yields and over reasonable distances the initial gamma dose data fall close to a straight line when plotted as in Fig. 3.2:6.

In addition to the high yield values the low-intermediate yield curve of $D_\gamma R^2/W\ h_{eff}$, as shown in Fig. 3.2:2 but scaled to standard air density ($\bar{\rho} = 1.0$), is also included in Fig. 3.2:6. From the prior discussion of the hydrodynamic effect one would expect that a plot of $D_\gamma R^2/W$ against distance in the region where the variation of h_{eff} with yield is important would show separate curves for each yield with the highest yield producing the highest curve and the longest mean free path. At large enough distances the curves should all become parallel, while they should converge at zero distance. These characteristics are shown in general by all of the curves in Fig. 3.2:6, including the low-intermediate yield curve; because this curve is plotted as $D_\gamma R^2/W\ h_{eff}$ rather than $D_\gamma R^2/W$, it might not be expected to conform. However, since h_{eff} is close to unity in the low-intermediate yield range and does not vary appreciably with distance, the position and slope of the curve is not much affected; for this qualitative examination of the data, therefore, the low-intermediate yield curve may be considered to be $D_\gamma R^2/W$.

TABLE 3.2:1

Summary of High Yield Test Data

Test Series and Burst	Weapon Type	Yield W, MT	Average Air Density $\bar{\rho}$	Actual Source-Receiver Distance, yd	Adjusted Source Receiver Distance R, yd(1)	Dose Measurements D_γ, r		$D_\gamma R^2/W$, r-yd^2-KT^{-1}
						Incomplete	Complete	
[redacted]			0.897	1500	1345		11,000	1.15×10^6
				1650	1480		5,000	6.34×10^7
				1900	1705		1,500	2.53×10^7
				2100	1885		570	1.17×10^7
				2200	1975		380	8.58×10^6
				2500	2245		110	3.21×10^6
				2800	2510		36	1.31×10^6
Ivy King	Boosted fission	0.55	0.865	1140	—	Insufficient data		—
				1820	1575		8,000	4.81×10^7
Castle 4 (Union)	Fusion	6.5	0.902	2400	2165		16,500	1.37×10^7
				4500	4060		84	2.62×10^5
Ivy Mike	Fusion	10.5	0.89	2520	2245	15,000 r at 1 sec	120,000(2)	7.26×10^7
				4380	3900		1,800	3.29×10^6
Castle 1 (Bravo)	Fusion	14.5	0.904	2400	2170	12,000 r at 1 sec	96,000(2)	3.81×10^7

(1) The actual source-receiver distance is multiplied by the average air density $\bar{\rho}$ to obtain the adjusted source-receiver distance R for standard density air ($\bar{\rho} = 1.0$).

(2) It is estimated that from 5 to 20 percent of the dose is delivered in the first second after the burst. To get the complete dose readings the dose received within the first second after the burst is multiplied by eight.

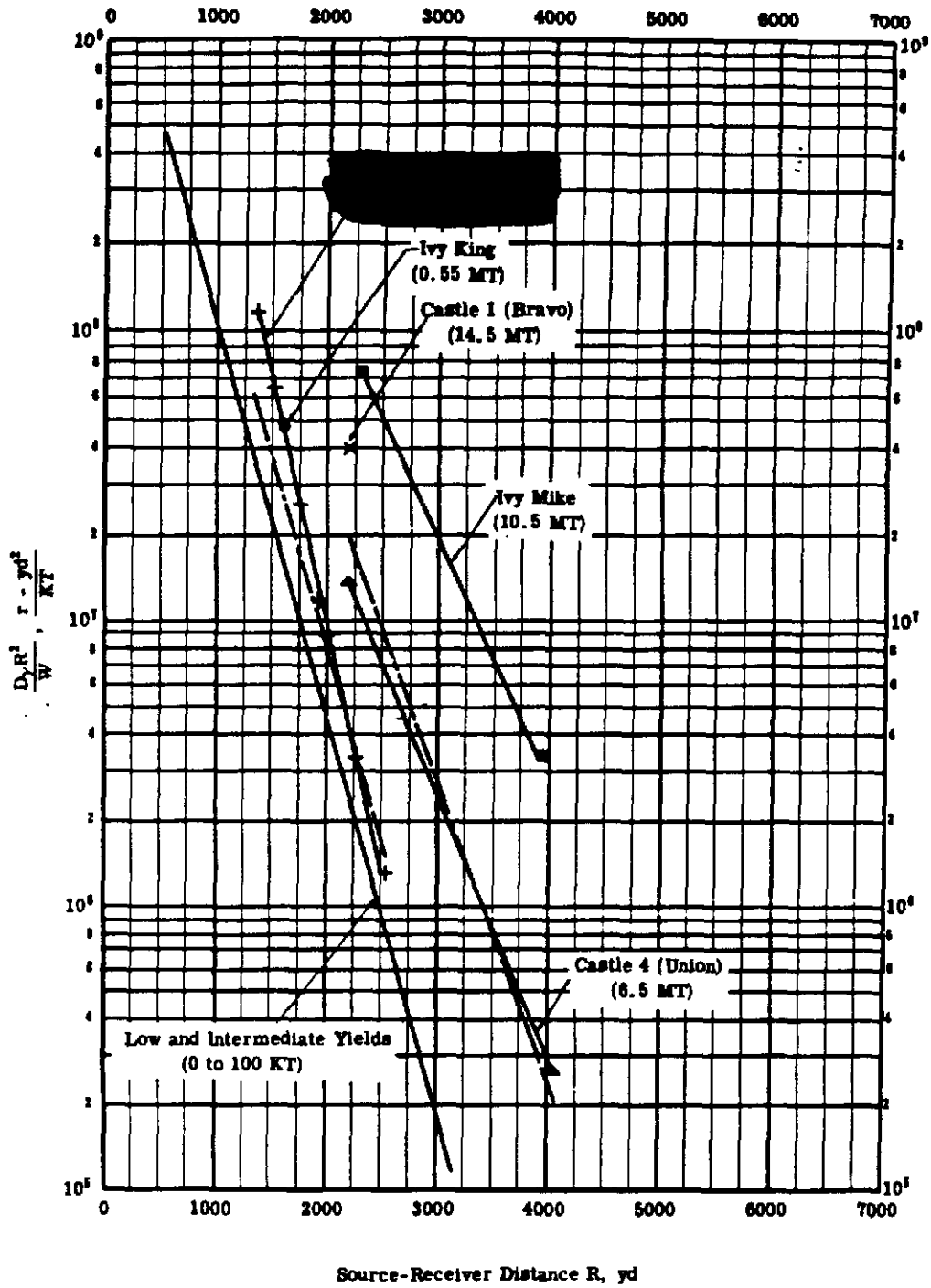

Fig. 3.2:6 Experimental Values of $D_\gamma R^2/W$ for Surface Bursts of High Yield Weapons as a Function of the Source-Receiver Distance R at Standard Air Density ($\bar{\rho} = 1.0$). The low and intermediate yield results are actually $D_\gamma R^2/W\ h_{eff}$ rather than $D_\gamma R^2/W$. The dashed lines are adjusted results for [redacted] and Castle 4.

[redacted]

The general agreement of Fig. 3.2:6 with theoretical expectation is shown in Table 3.2:2, where the test data are compiled in order of increasing yield. It is seen that both the dose values at a representative distance (2500 yd) and the mean free paths increase with increasing yield. The only exception to this trend is the mean free path o[redacted] which is much too short in comparison with either the high or low-intermediate yield shots.

Despite the general agreement of Fig. 3.2:6 with expectations there are serious discrepancies in the data. Thus, the Castle 1 (14.5 MT) point is lower than the corresponding point for Ivy Mike (10.5 MT) by a factor of about two, rather than being above as would be expected due to the higher yield of Castle 1. These two points are more uncertain than the other high yield data, however, since they are based on doses read up to one second after the burst only. The doses received up to one second are multiplied by a correction factor of eight to obtain the total doses. (The factor of eight is based on examination of complete dose delivery rate curves for other bursts which indicate that for this weapon type and yield from 5 to 20 percent of the total dose is delivered in the first second. The incomplete dose rate curves for Ivy Mike and Castle 1 are almost identical up to one second, supporting the use of the same multiplicative factor for both). The Ivy King (0.55 MT) data point also appears out of line, being high in comparison with the low-intermediate yield curve and the Castle 4 curve.

TABLE 3.2:2

Comparison of Gamma Doses and Mean Free Paths for Several Test Bursts

Shot	Yield, MT	Initial Gamma Dose at 2500 yd, r	Mean Free Path, yd
Low-intermediate yield weapons	0 to 0.10	8.8×10^5	324
[redacted]		1.3×10^6	260
Castle 4 (Union)	6.5	6.6×10^6	470
Ivy Mike	10.5	4.6×10^7	530

A more serious problem is presented by the [redacted] data. There are seven total dose readings from [redacted] which fall very nicely on a straight line between adjusted distances of 1300 to 2500 yd. The slope of the line appears to be considerably too steep, however, in comparison with both the low-intermediate yield and other high yield curves. Furthermore, the apparent mean free path for [redacted] shown on Fig. 3.2:6 (260 yd) is shorter than the best current estimate of the short mean free path component of the total dose. Fission product gammas have been calculated to have an apparent mean free path of 284 yd. (See Section 3.2.2). Nitrogen capture gammas have a much longer mean free path and it is hard to see how combining the two could produce radiation with a 260-yd value.

A second important discrepancy is the mean free path read from the Castle 4 (6.5 MT) data. The value of 470 yd seems somewhat longer than it should be.

While these data are inconsistent in terms of the simple model postulated for initial gamma radiation, it is not known if this is due to oversimplification in the model or to experimental errors. Further it is not clear which experimental values should be suspect if the reason for the inconsistencies does lie with the data rather than the model. Thus, there are several methods of resolving the problems posed by Fig. 3.2:6, depending on which data are accepted as most likely to be reliable.

For the present we will accept the curves for low-intermediate yields and for Ivy Mike as most likely to be reliable and adjust th[redacted]nd Castle 4 curves to the smallest degree necessary to achieve internal consistency. (This adjustment is determined not only by what is required to make Fig. 3.2:6 consistent but also by what is required to yield reasonable values of h_{eff}). Both

[redacted]

the Castle 1 and the Ivy King data points are disregarded. The adjusted curves for [redacted] and Castle 4 are shown in Fig. 3.2:6 as dashed lines.

Determination of Effective Hydrodynamic Scaling Factor

From the curves of Fig. 3.2:6 and the simplified dose equations of Section 3.2:1 it is now possible to establish values of h_{eff} for high yield weapons and standard density air as a function of yield and separation distance.

The simplified dose equations used to represent the low-intermediate (ℓi) yield and high (h) yield weapon results are

$$\begin{aligned} \left(D_\gamma\right)_{\ell i} &= (W)_{\ell i}\left(h_{eff}\right)_{\ell i}\left[D_{fp} + D_{nc}\right]_{\ell i} \\ \left(D_\gamma\right)_h &= (W)_h\left(h_{eff}\right)_h\left[D_{fp} + D_{nc}\right]_h \end{aligned} \qquad (3.2:14)$$

If we now make the assumption that D_{fp} and D_{nc} (the gamma doses due to fission products and nitrogen capture from a bomb of unit yield) are independent of yield, the effective hydrodynamic scaling factor for high yield weapons is simply

$$\left(h_{eff}\right)_h = \frac{\left(\frac{D_\gamma R^2}{W}\right)_h}{\left(\frac{D_\gamma R^2}{W h_{eff}}\right)_{\ell i}} \qquad (3.2:30)$$

Thus $(h_{eff})_h$ at $\bar{\rho} = 1.0$ can be determined directly from the adjusted data of Fig. 3.2:6 for several yields and separation distances.

The assumption that the component doses are independent of yield is equivalent to assuming either that the number of neutrons and gammas escaping from the bomb per KT and their energy distribution are both constant over very wide ranges of weapon yield, or, alternatively, that the values of C_{fp}, C_{nc}, λ_{fp_e} and λ_{nc_e} are independent of yield. Large changes in yield are usually accompanied by correspondingly large changes in weapon design, which would certainly affect the source characteristics of the neutrons and gammas. Thus, this assumption may not be a very good one. It is clear, for example, that fusion weapons will have a different neutron production per KT and neutron energy distribution than will fission weapons.

In the absence of any real understanding of how these quantities change with yield and since, if we accept this assumption, it appears that no more adjustment of the data is necessary to obtain consistent values of $(h_{eff})_h$ than would be necessary with more elaborate approaches, the present course seems reasonable.

Using the data of Fig. 3.2:6, with [redacted] and Castle 4 adjusted as shown, a plot of h_{eff} for high yield weapons was constructed. The values of h_{eff} determined for the low-intermediate yield weapons were used to determine the lower values of the plot. Interpolation between these points and the high yield values from Fig. 3.2:6 established a family of curves between 0.1 and 10.5 MT. A curve for 20-MT yield was also drawn but this is thought to be about as far as the meagre data should be extrapolated.

The family of curves of h_{eff} was scaled by the method described in Section 3.2.1 to average quiescent air densities ranging from $\bar{\rho} = 0.2$ to $\bar{\rho} = 1.1$; the scaled values are plotted in Fig. 3.2:7 through 3.2:13 for the several air densities. (The lower air densities are not applicable to surface bursts but are included here for convenience, since these figures will also be used to calculate air burst doses.)

[redacted]

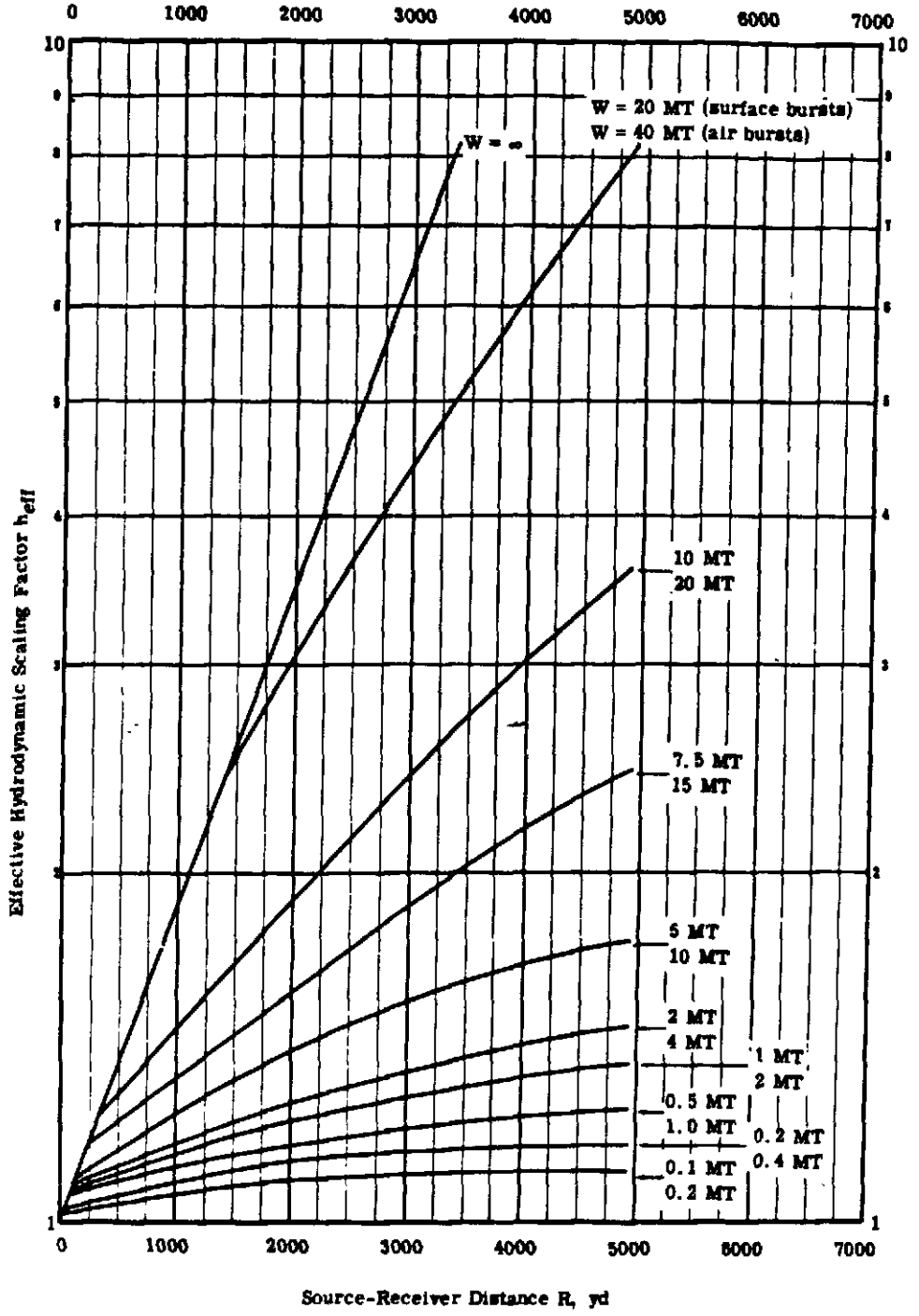

Fig. 3.2:7 Effective Hydrodynamic Scaling Factors for Surface and Air Bursts of High Yield Weapons ($\bar{\rho} = 0.2$).

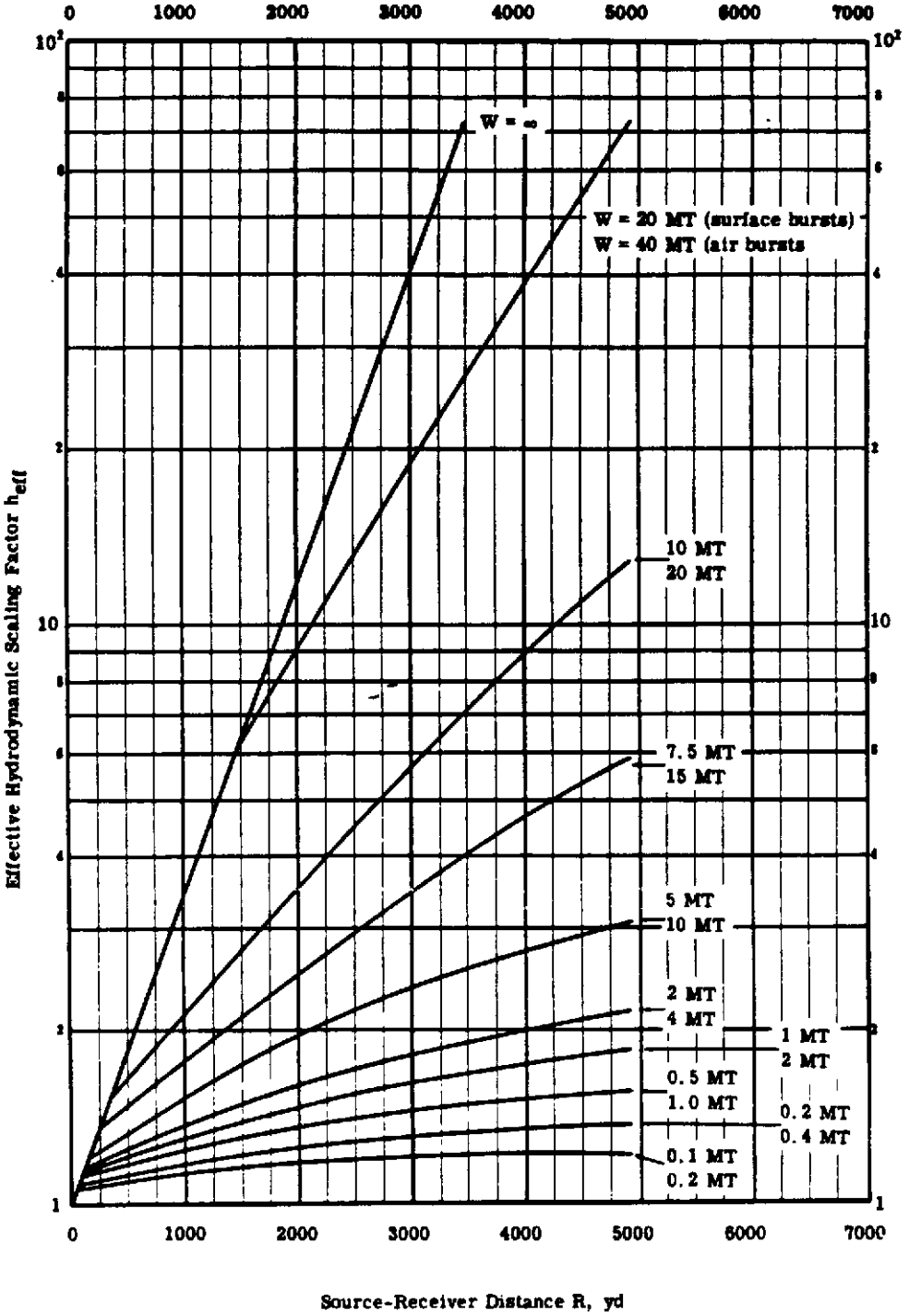

Fig. 3.2:8 Effective Hydrodynamic Scaling Factors for Surface and Air Bursts of High Yield Weapons ($\bar{\rho} = 0.4$).

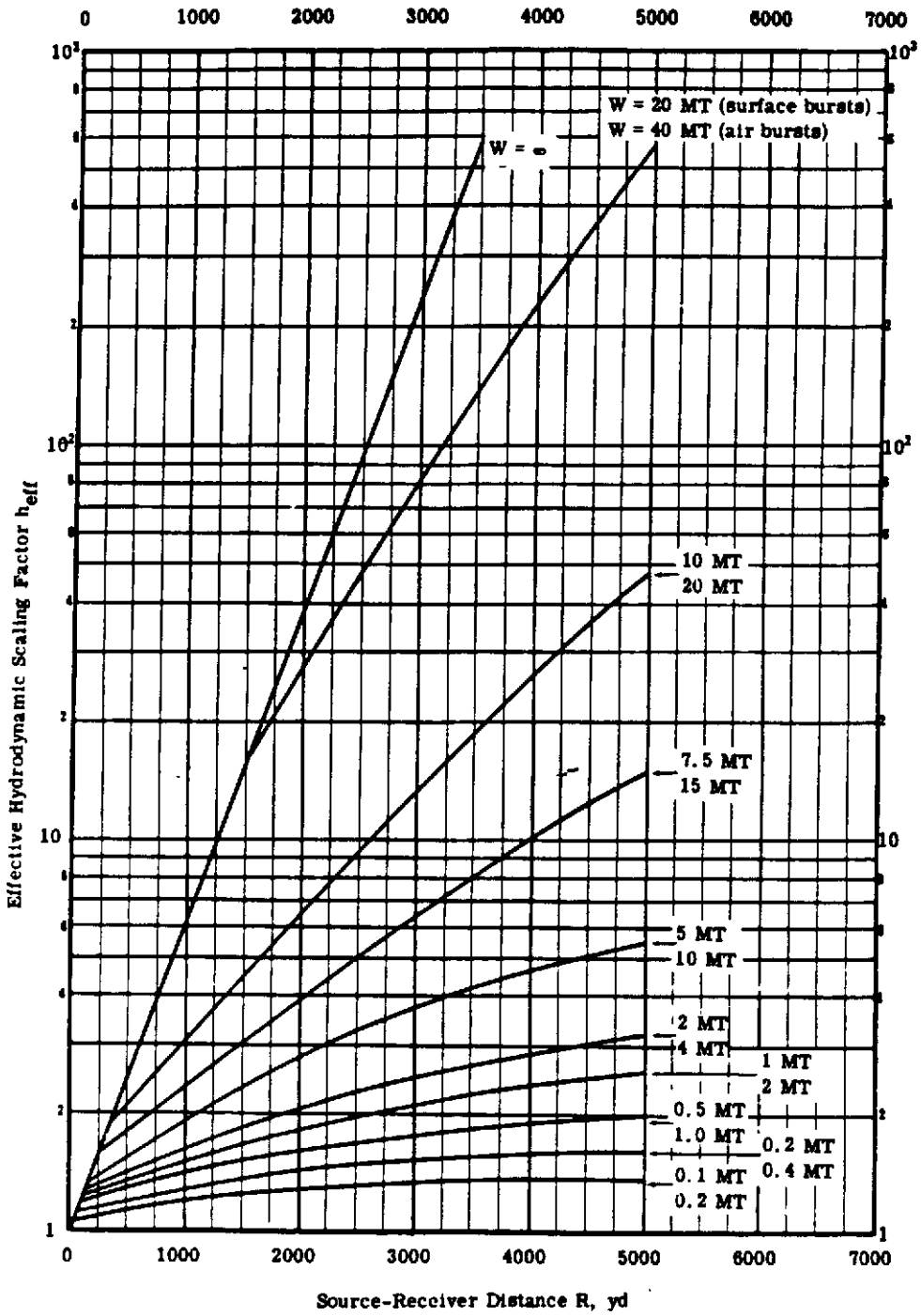

Fig. 3.2:9 Effective Hydrodynamic Scaling Factors for Surface and Air Bursts of High Yield Weapons ($\bar{\rho} = 0.6$).

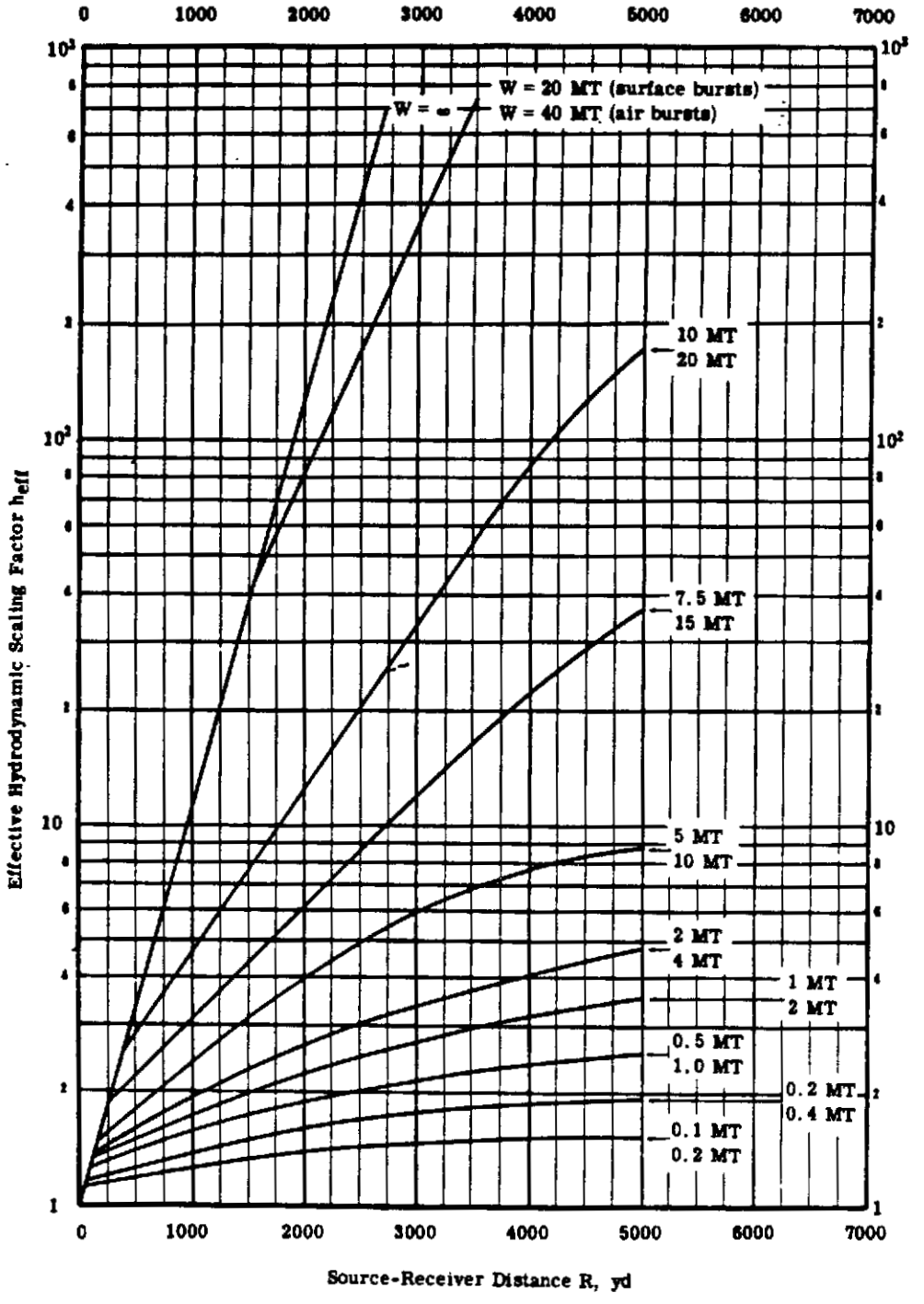

Fig. 3.2:10 Effective Hydrodynamic Scaling Factors for Surface and Air Bursts of High Yield Weapons ($\bar{\rho} = 0.8$).

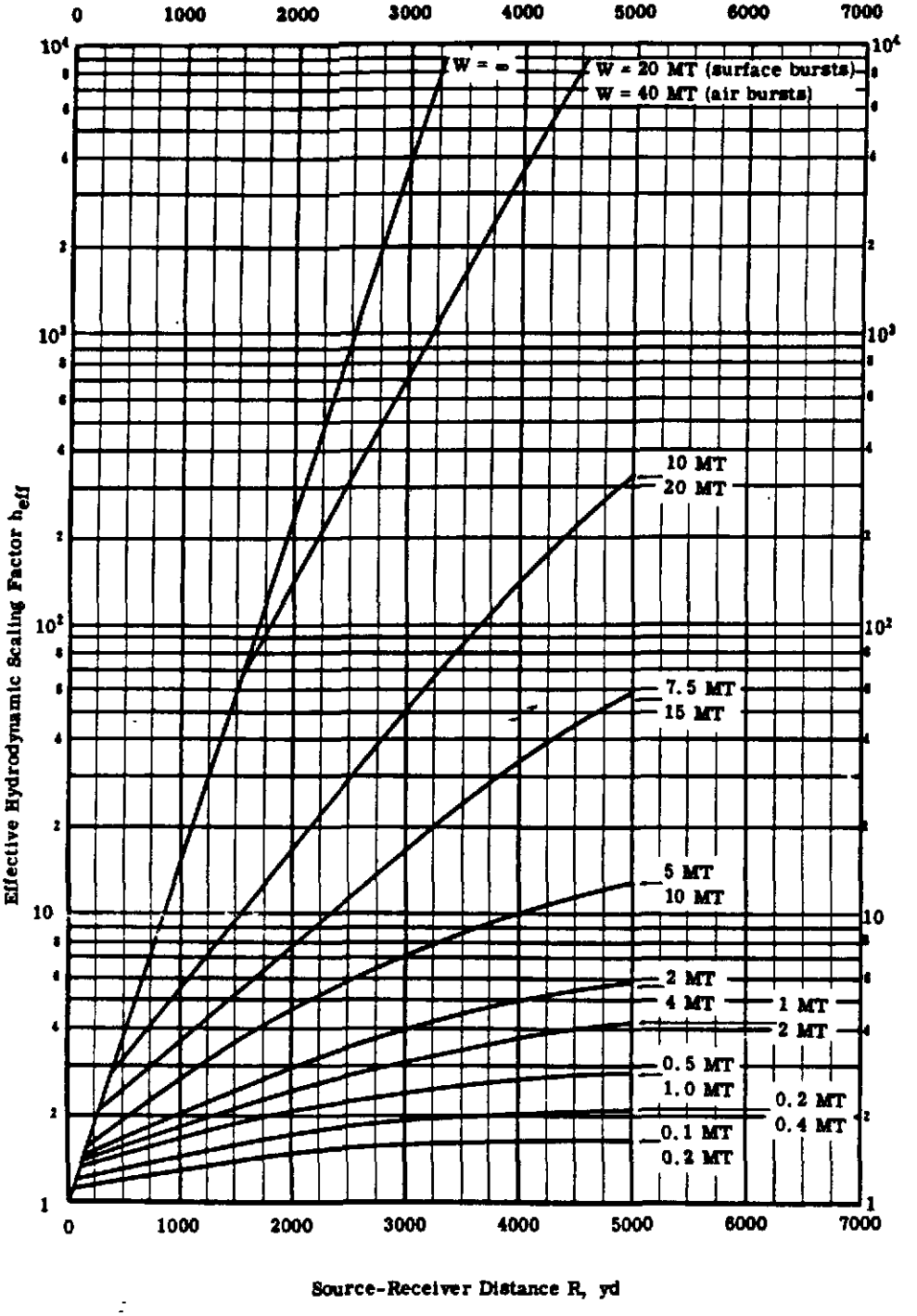

Fig. 3.2:11 Effective Hydrodynamic Scaling Factors for Surface and Air Bursts of High Yield Weapons ($\bar{\rho} = 0.9$).

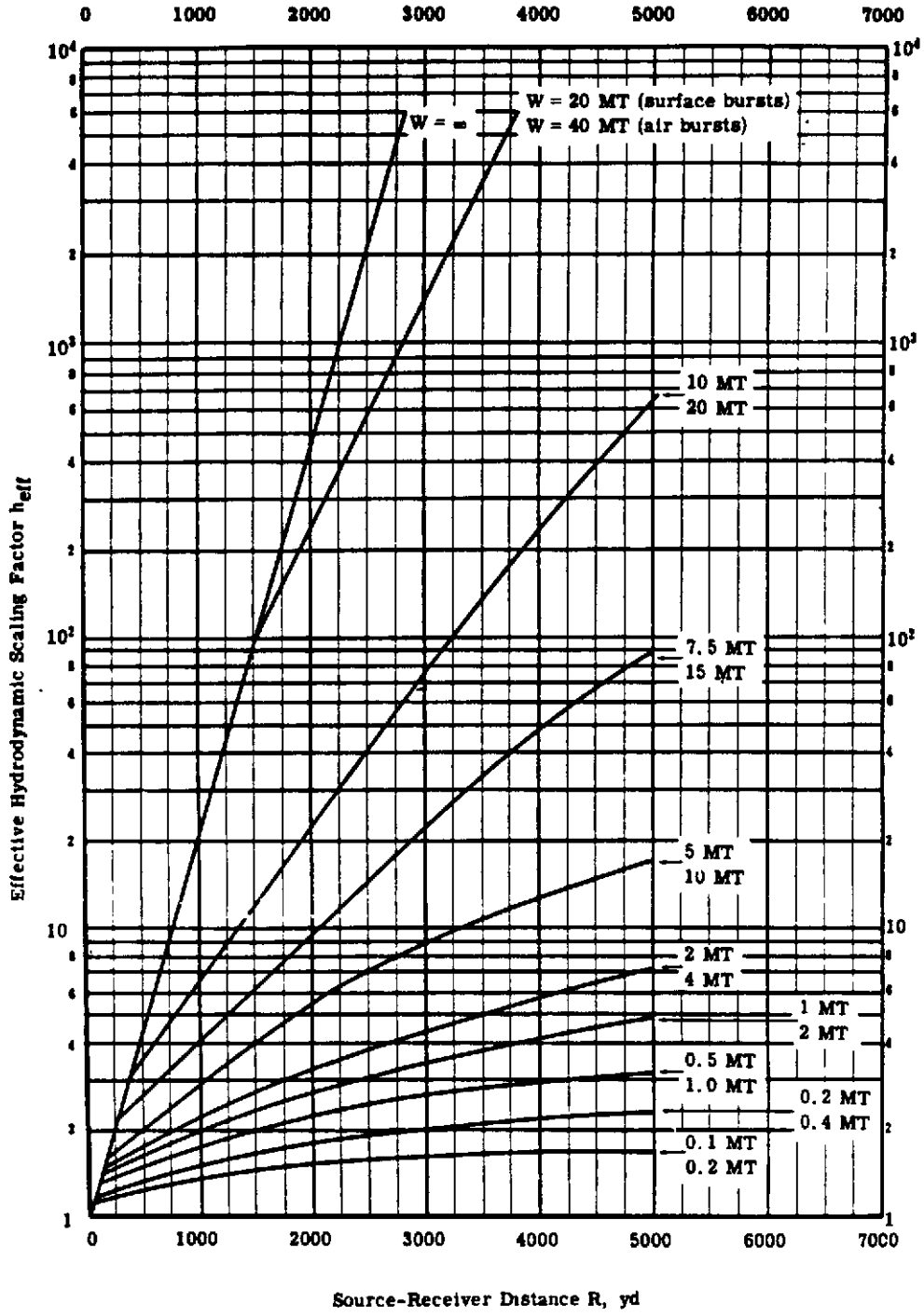

Fig. 3.2:12 Effective Hydrodynamic Scaling Factors for Surface and Air Bursts of High Yield Weapons ($\bar{\rho} = 1.0$).

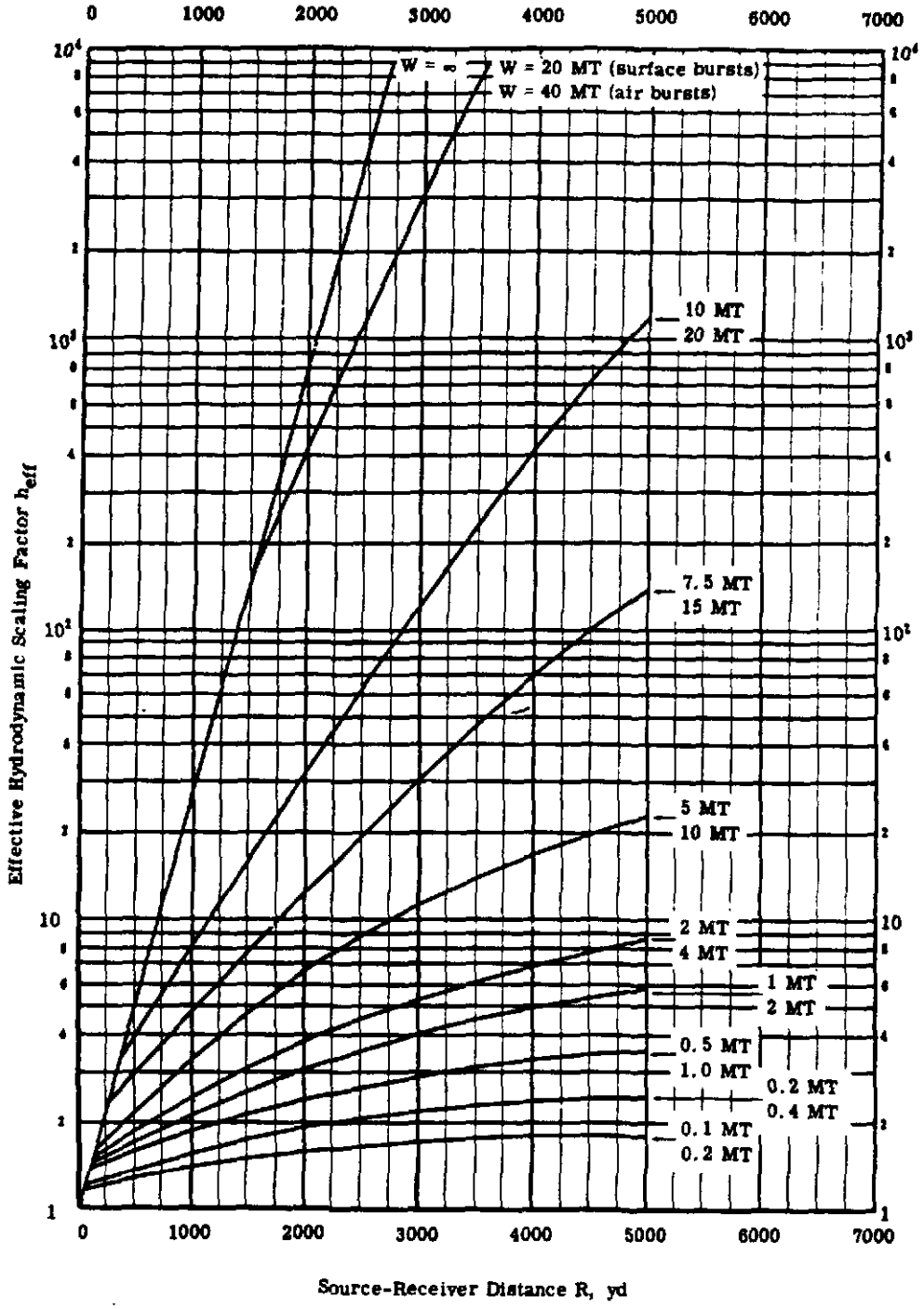

Fig. 3.2:13 Effective Hydrodynamic Scaling Factors for Surface and Air Bursts of High Yield Weapons ($\bar{\rho} = 1.1$).

Calculation of Initial Gamma Dose

The expression for the initial gamma dose for high yield weapons is obtained by transposing and rearranging Eq. 3.2:30.

$$\left(D_\gamma\right)_h = \left(\frac{D_\gamma R^2}{W\, h_{eff}}\right)_{fi} \frac{W\left(h_{eff}\right)_h}{R^2}. \qquad (3.2{:}31)$$

Thus, to determine the initial gamma dose it is necessary to know the weapon yield W, the average quiescent air density $\bar{\rho}$, and the source-receiver distance R. $(D_\gamma R^2/W\, h_{eff})_{fi}$ is found from Fig. 3.2:5 for the appropriate value of R and $\bar{\rho}$, and $(h_{eff})_h$ is found from Fig. 3.2:7 through 3.2:13 for the appropriate values of R, $\bar{\rho}$, and W. The initial gamma dose $(D_\gamma)_h$, in r, is determined by the indicated multiplication.

PROBLEM 4

The initial gamma dose due to a high yield weapon is required at a given point. The distance between point of burst and the receiver, the average quiescent air density, and the bomb yield are known.

Solution

1. Find the effective hydrodynamic scaling factor h_{eff} for the given average air density, the bomb yield, and the source-receiver distance, from the appropriate figure (Fig. 3.2:7 through 3.2:13.)
2. Find the value of $D_\gamma/W\, h_{eff}$ for the given average air density and source-receiver distance from Fig. 3.2:5.
3. The initial gamma dose is the product of h_{eff} (from step 1), $D_\gamma/W\, h_{eff}$ (from step 2), and the given yield W (in KT).

Example

A 0.8 MT bomb is detonated on the earth's surface. The average air density $\bar{\rho} = 0.9$. What is the initial gamma dose 3000 yd away from the point of burst?

1. From Fig. 3.2:11 ($\bar{\rho} = 0.9$) at 3000 yd and for a yield of 0.8 MT, the effective hydrodynamic scaling factor h_{eff} is 2.8.
2. From Fig. 3.2:5 at $\bar{\rho}$ of 0.9 and R of 3000 yd, $D_\gamma/W\, h_{eff}$ is 0.052 r-KT^{-1}.
3. The initial gamma dose is therefore (0.052) (2.8) (800) = 120 r.

PROBLEM 5

At what distance from the burst point will a given initial gamma dose be experienced? The average air density and the weapon yield are given.

Solution

1. Select several source-receiver distances estimated as well as possible to bracket the desired distance.
2. Using the method of Problem 4 compute the dose at each of the selected points until the given dose has been bracketed.

3. The desired source-receiver distance is obtained either by plotting the results for step 2 and interpolating or by actually calculating the dose for additional source-receiver distances within the region of interest found in step 2 until a satisfactory degree of approximation is achieved.

Error

For yields below 1 MT the dose computations are probably good to within a factor of three. This is because shock effects in this area are not so great as to cause complete distortion of the relatively well-known results for the low and intermediate yield regions. For yields greater than 1 MT, because of the glaring inconsistencies among the experimental measurements and of the very crude scaling techniques, an error factor of the order of 10 is quite possible over most of the region. In the region of very high yields, an error factor of the order of 25 is not inconceivable. This is an unfortunate but realistic estimate of the state of our knowledge, and points up the urgency of further work in this field.

3.3 DOSE-DISTANCE RELATIONS FOR AIR BURSTS

An air burst is one whose fireball does not intersect the earth. The initial gamma dose from high altitude bursts may be expected to differ from surface bursts for several possible reasons. With increasing altitude the gamma sources and particularly the nitrogen capture gammas behave less like point sources and the air-earth boundary is reduced to a minor role in determining the scattered dose. Also the hydrodynamic effect is quite different for a burst in free air, compared to one near the air-earth interface. In general, it is not expected that the initial gamma dose for low yield, high altitude bursts will be greatly different from that due to corresponding surface bursts; it is expected, however, that this difference will increase with yield and become of major importance for high yield weapons.

Inasmuch as there has been only a single air burst at very high altitude (Teapot 10), it is necessary for us to depend on the results of surface bursts to anticipate high altitude results. Fortunately the physics of the situation is simple enough to permit reasonable extension of surface burst data to all but low altitude, high yield air bursts.

3.3.1 LOW AND INTERMEDIATE YIELD WEAPONS

The only very high altitude burst on record in the low and intermediate yield region is Teapot 10 (3 KT, 32,000 ft burst height). The complicating effect of a widely varying quiescent air density was avoided by positioning the dose receivers for Teapot 10 at approximately the burst altitude rather than on the ground. (In addition to the high altitude Teapot 10 test, two moderately high altitude tests have been made, Upshot-Knothole 4 (11 KT, 6150 ft burst height) and Tumbler 3 (30 KT, 3450 ft burst height).) Teapot 9 was sensibly identical to Teapot 10 except that its burst height was 740 ft. The initial gamma dose measurements[1, 11] from the two shots indicate that when corrected to the same air density:

1. the high altitude dose was greater than the low altitude dose at all distances,
2. the average factor by which the high altitude dose was greater was 1.5, and
3. the factor was greater than 1.5 close to the burst point and less than 1.5 at large distances.

It had been expected that, when reduced to the same air densities, the shots would have given the same gamma dose at a given distance. The reason for the difference is still not fully understood. It is believed, however, that neutrons may have contributed a substantial portion of the apparent gamma dose. It is also possible that the nitrogen capture gamma ray dose may be affected at high altitudes by the greater diffusion length of neutrons before capture. The greater extension in space of the fireball and of the nitrogen capture source may be the cause of the decreased apparent mean free path.

In any case, it is recommended that to solve dose-distance problems for air bursts of low and intermediate yield weapons, the dose be calculated from Figs. 3.2:4 and 3.2:5 exactly as prescribed for surface bursts in Section 3.2.2 and then multiplied by a factor of 1.5. This treatment is conserv-

ative; more careful analysis and experimental work may result in a decrease in the value of the correction factor.

3.3.2 HIGH YIELD WEAPONS

In addition to the effects discussed in the preceding section, which, if significant, apply to air bursts for all ranges of weapon yield, there is one effect of variation of burst height which is peculiar to high yield weapons, and which in many cases may be dominant. This is the difference in the shock enhancement between high yield, high altitude bursts and high yield, surface bursts. From a burst close to the earth's surface there will be a direct shock wave and a reflected shock wave. As a result, the shock enhancement of the dose is greater for bursts near the surface than for high altitude bursts where there is no reflected shock wave.

For the moment we will consider only the limiting cases of a true surface burst (one detonated directly on the earth's surface) and a true high altitude burst (no reflected shock wave). If the earth is considered to be a rigid plane reflector, then the shock wave from a surface burst of a given yield is just equivalent to the shock wave from a high altitude burst of twice the yield[16]. For this reason we do not present graphs of the effective hydrodynamic scaling factors for high altitude bursts in this section. Instead we refer to Figs. 3.2:7 through 3.2:13 which have been labelled with yields appropriate for both surface and high altitude bursts. The solution of the dose-distance problems for high altitude, high yield bursts is basically the same as that given in Section 3.2.3, except that the value of $D_\gamma/W\ h_{eff}$ from Fig. 3.2:5 is multiplied by a correction factor of 1.5 (as described in Section 3.3.1) and that the effective hydrodynamic scaling factor is determined from Figs. 3.2:7 through 3.2:13 for the high altitude yield rather than for the surface yield.

For burst elevations intermediate between true surface and high altitude, an intermediate value of the effective hydrodynamic scaling factor and of the dose can be expected. It is clearly desirable that some criterion exist to determine when a burst is a high altitude burst in the sense that there is no reflected shock wave. One possible approach to such a criterion may be found in the plots of the hydrodynamic scaling factors. It has been noted previously that the hydrodynamic scaling factor is expected to level off and reach a constant value at some distance from the point of burst. The distance beyond which h_{eff} increases relatively little is a measure of the outer radius of the shock effect. If the burst height is greater than this distance, the magnitude of the direct shock wave will be quite small when it reaches the earth's surface and the reflected shock wave will be correspondingly unimportant. Thus, one may consult the curve from Figs. 3.2:7 through 3.2:13 for the given air density and weapon yield (air burst yield rather than surface burst yield). The distance at which h_{eff} no longer rises sharply but starts to level off may be considered as the minimum elevation for which a burst is a high altitude burst. It must be admitted that this method, while plausible, is untested and should be used accordingly.

PROBLEM 6

The initial gamma dose due to a high yield, high altitude burst is required at a given point. The distance between point of burst and receiver, the average quiescent air density, and the bomb yield are known.

Solution

1. Find h_{eff} for the given average air density, and source-receiver distance from the appropriate figure of the series (Figs. 3.2:7 through 3.2:13) using the curve with the proper air burst yield.
2. Find the value of $D_\gamma/W\ h_{eff}$ for the given average air density and source-receiver distance from Fig. 3.2:5.
3. The initial gamma dose is the product of h_{eff} (from step 1), $D_\gamma/W\ h_{eff}$ (from step 2), the given yield W (in KT), and the correction factor 1.5.

Example

A 0.8 MT bomb is detonated at an altitude of 28,000 ft. The average air density between point of burst and receiver is 0.4. What is the initial gamma dose 3,000 yd away from the point of burst?

1. From Fig. 3.2:8 ($\bar{\rho} = 0.4$) at 3,000 yd and at the air burst yield of 0.8 MT the value of h_{eff} is 1.4.
2. The value of $D_\gamma/W\ h_{eff}$ is 5.2 r-KT^{-1} from Fig. 3.2:5 at $\bar{\rho} = 0.4$ and R of 3,000 yd.
3. The initial gamma dose is, therefore, (1.4) (5.2) (800) (1.5) = 8750 r.

3.4 DOSE-DISTANCE RELATIONS FOR UNDERGROUND BURSTS

An underground burst is defined as one where the burst occurs below the ground surface. From the point of view of effects it is difficult to distinguish a burst not far below the surface from a surface burst.

In an underground burst, initial gamma radiation will come entirely from fission products and neutron-activated materials in the ground or in the weapon. One can safely assume that none of the neutrons will escape into the air and produce nitrogen capture gamma rays, unless the bomb is detonated within a few feet of the surface. In that case the burst should probably be interpreted as a surface burst. The extent to which soil material will be activated depends, of course, upon the composition of the soil. Although soil activation has been detected in the underground and surface shots in Nevada[17] and in the Marshall Islands surface shots,[18] there is no reason to believe that in either location it caused a substantial contribution to the initial gamma radiation dose. Consequently, in this treatment of underground bursts, fission products are considered to be the only source of initial gamma radiation.

3.4.1 LOW YIELD WEAPONS

To date there have been two underground detonations of nuclear weapons, both in low yield range, a 1.2 KT, 17 ft underground shot at Jangle[19,20] and a 1.2 KT, 67 ft underground shot at Teapot.[17] Because of the essential identity of the yields, the two bursts could have been directly compared to gain insight into the effects of depth of burial on the initial gamma radiation dose. Unfortunately only the Jangle underground shot was documented for initial gamma radiations; no such data were taken at the Teapot underground shot. Even back-extrapolation of the Teapot delivery rate curves taken at times greater than one minute is not possible because winds at Teapot had so perturbed the source material by that time that the dose rate-distance results were badly distorted. Such extrapolation, if it had been possible, might have allowed comparison with equivalent data taken at the Jangle underground shot.

Considerations which apply directly and almost uniquely to the analysis of underground burst initial radiations are:

1. the time at which the active material emerges from the ground,
2. the fraction of active material, including fission products and induced activities, which remains in the ground,
3. the amount and nature of induced activities, and
4. the extent to which the earth material intermingled with the active material affects the attenuation of radiation.

It is perhaps clear on intuitive grounds that two bombs of identical yield but at substantially different burial depths will have different initial gamma radiation characteristics. The same remark will apply to two bombs of different yields detonated at the same depth underground. The coupling between yield and depth and how the initial radiations depend upon these coupled parameters is not understood at all. With our present limited knowledge we are able to produce only dose-distance curves normalized to the measurements made at Jangle. The following expression[20] was used to generate the curves.

$$\frac{D_\gamma}{W} = \frac{(S_{fp}/W)\, C\, e^{-\mu_{t_0}\bar{\rho}R}\, B(\mu_{t_0}\bar{\rho}R)}{4\pi R^2} \int_0^{t_\gamma} \frac{dt}{1 + (0.7t)^{1.2}} \qquad (3.4:1)$$

where

D_γ = initial gamma dose from an underground burst

C = conversion factor, 1.39×10^{-13} r-yd^2-gamma^{-1}

S_{fp}/W = emission rate of fission product gammas per unit yield at burst time, gammas-sec^{-1}-KT^{-1}

μ_{t_0} = gamma ray total linear attenuation coefficient at standard air density

$\bar{\rho}$ = average air density in units of standard air density ($d_0 = 1.293 \times 10^{-3}$ gm-cm^{-3})

R = source-receiver distance, yd

$B(\mu_{t_0}\bar{\rho}R)$ = gamma ray buildup factor at $\mu_{t_0}\bar{\rho}R$ mean free paths from the source

t_γ = time after burst at which initial gamma dose period ends, sec

W = weapon yield, KT.

The effective energy of the fission product gamma rays is taken as 3 Mev and the values of μ_{t_0}, $B(\mu_{t_0}\bar{\rho}R)$, and C are all selected at this energy. The value of S_{fp}/W used in the calculation is 3.3×10^{22} gammas-sec^{-1}-KT^{-1}, and t_γ is taken as 60 sec in accordance with the previous and somewhat arbitrary choice of the initial gamma time period.

The curves presented in Fig. 3.4:1 were scaled from the experimental to other air densities by means of the scaling relation described in Section 3.2.1. To the extent that earth material mingled with active material and contributed importantly to the gamma ray attenuation, the scaling is in error. Due to the previously mentioned lack of understanding of the variation of dose with weapon yield and burial depth, it is advisable to consider that the curves of Fig. 3.4:1 apply only for yields which are between about 0.2 and 7.5 KT and for burial depths which are between 12 and 22 ft. We are unable to suggest procedures for computing doses for depths and yields outside this admittedly limited range.

PROBLEM 7

The yield and burial depth of an underground burst are given and lie within the range of applicability of Fig. 3.4:1, namely 0.2 to 7.5 KT and 12 to 22 ft underground. The initial gamma dose at a given receiver point is required. The distance of the receiver from ground zero and the average air density are known. (For the purposes of underground burst calculations the source-receiver distance will be taken as equal to the distance between ground zero and the receiver.)

Solution

1. From Fig. 3.4:1 read D_γ/W at the appropriate air density $\bar{\rho}$ and source-receiver distance R.
2. Multiply the value of D_γ/W from step 1 by the bomb yield W to obtain the initial gamma dose D_γ.

Example

A 3 KT burst is detonated 15 ft underground. The initial dose at a point 2000 yd from ground zero is required; the average air density is known to be 0.93.

1. At $\bar{\rho}$ of 0.93 and R of 2000 yd, Fig. 3.4:1 gives a value for D_γ/W of 1.2 r-KT^{-1}.
2. Multiplying this value of D_γ/W by the yield W gives an initial gamma dose of 3.6 r.

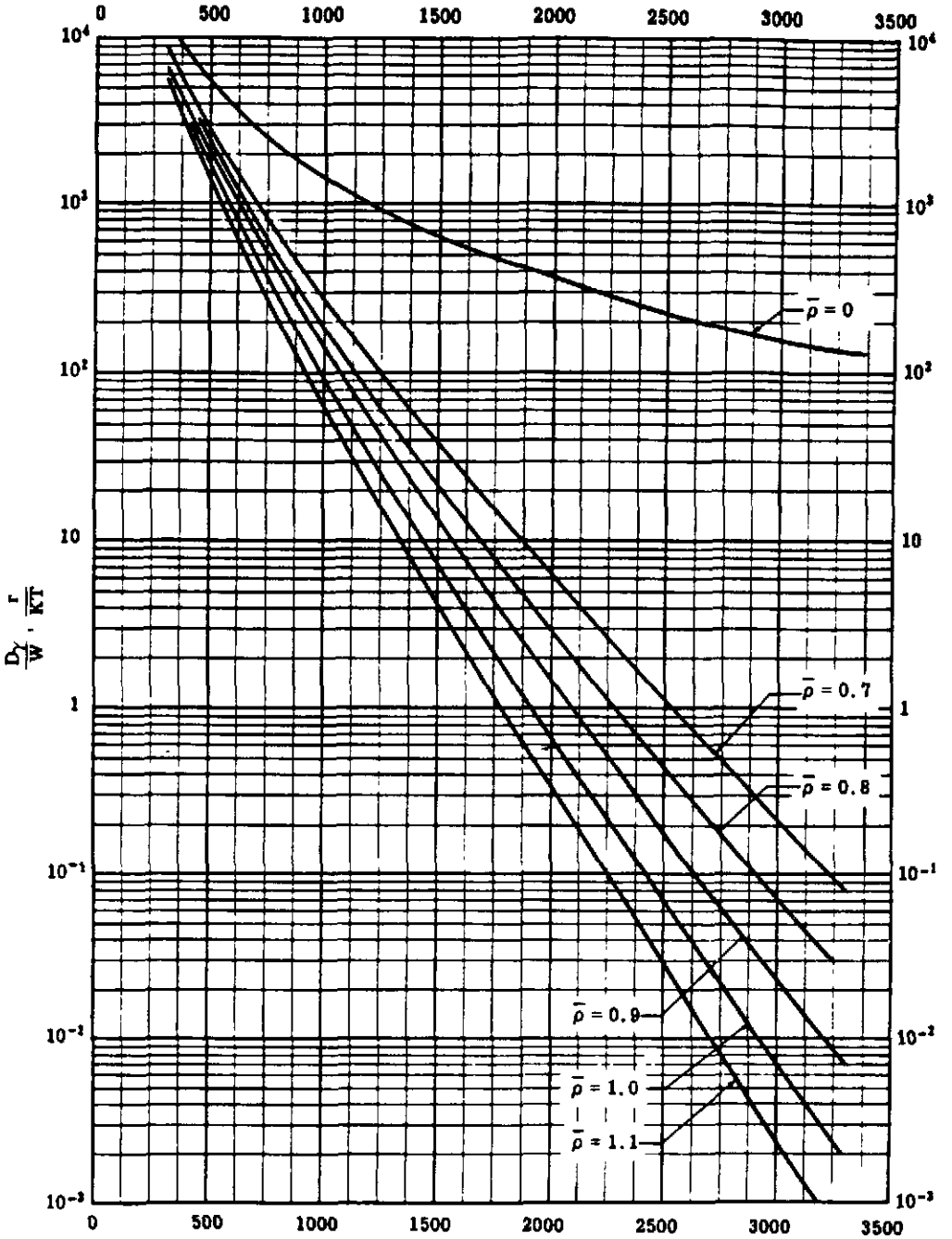

Fig. 3.4:1 Initial Gamma Dose-Distance Results for Underground Bursts of Low Yield Weapons for Several Average Air Densities. These curves are applicable only for yields between 0.2 and 7.5 KT and burial depths between 12 and 22 ft.

PROBLEM 8

The yield and burial depth of an underground burst are given and lie within the range of applicability of Fig. 3.4:1. The average air density is also known. Find the range within which a given initial gamma dose will be experienced.

Solution

1. Divide the given initial gamma dose by the given yield to obtain D_γ/W.
2. From Fig. 3.4:1 at the appropriate value of the average air density find at what distance the value of D_γ/W determined in step 1 is given. This is the desired distance.

Example

A 3 KT bomb is detonated 15 ft underground. The average air density is 0.93. At what range will an initial gamma dose of 1 r be experienced?

1. The desired dose divided by the bomb yield is $1/3 = 0.33$ r-KT^{-1}.
2. From Fig. 3.4:1 the distance at which D_γ/W is 0.33 is 2600 yd. This is the required distance.

Error

It is estimated that these methods, used within the prescribed limits, should produce results good within a factor of two, provided the soil at the point of burst is not too different from the soil at the Nevada test site. The error that would be introduced by a very different soil type is similar in origin, but not necessarily in magnitude, to the error that would be expected from a distinctly different burial depth. At the present time the effect of soil type cannot be estimated.

3.4.2 INTERMEDIATE AND HIGH YIELD WEAPONS

As has already been noted, the only experimental underground bomb bursts reported to date have been in the low yield range, the 1.2 KT Jangle shot and the 1.2 KT Teapot shot. There is no information about intermediate and high yield underground bursts. An acceptable scaling relation for initial gamma radiation dose would necessarily take into account:

1. variations in the gamma ray source with yield,
2. variations in the gamma ray source with depth, and
3. variations in the attenuating media with yield and depth,
   a. earth shielding, and
   b. hydrodynamic effect in two media.

There are no data or calculations available from which this scaling relation might be determined. It is not possible, therefore, at this time to make any sound predictions about the initial gamma dose from intermediate and high yield underground bursts.

3.5 DELIVERY RATE

The delivery rate at a point is the rate at which dose is received at the point. There are at least three general shapes of initial gamma radiation delivery rate curves, each characteristic of a

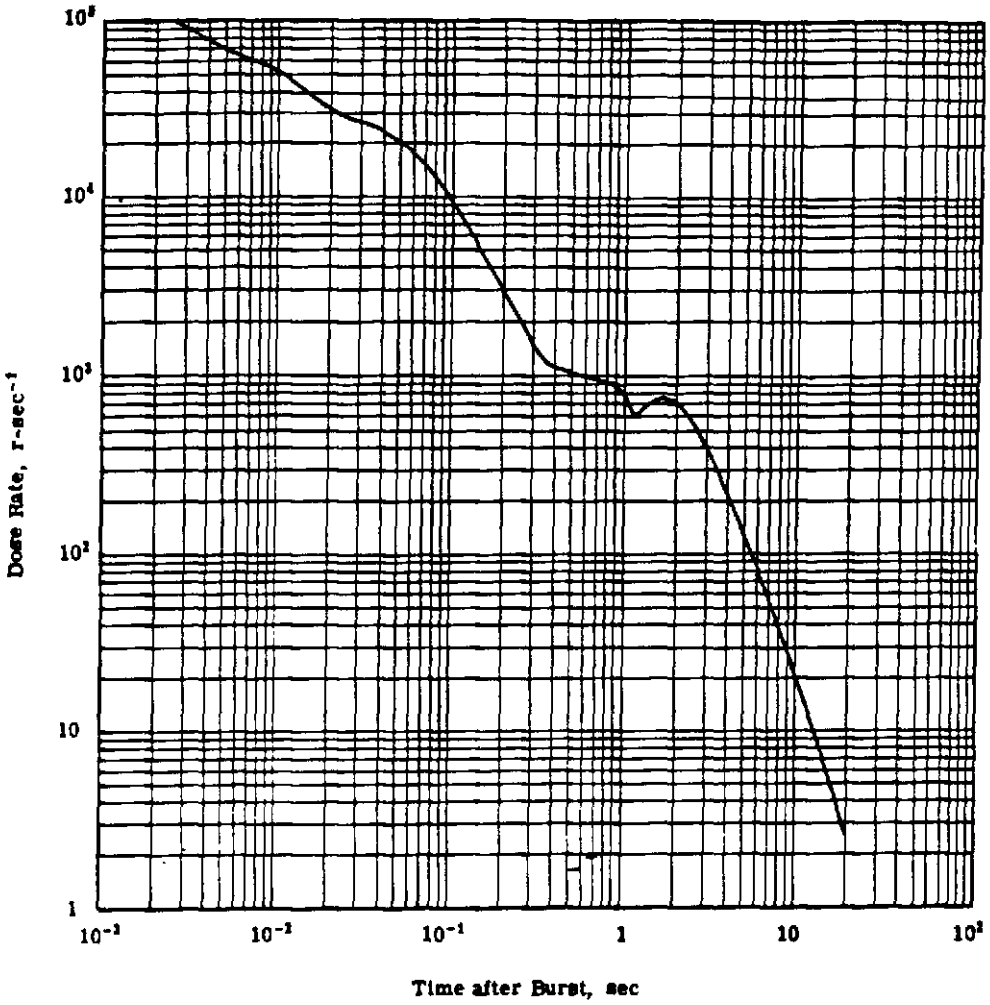

Fig. 3.5:1 Initial Gamma Radiation Delivery Rate for Buster Easy, 32-KT Yield, 1300-ft Burst Height, 1040 yd from Ground Zero.

different situation. Fig. 3.5:1 is a delivery rate curve of an intermediate yield weapon, Buster Easy (32 KT, 1300 ft burst height).[19] It shows a double hump, something like two rounded stairsteps. The first hump is due to nitrogen capture gamma radiation, the second to fission product gamma radiation. Fig. 3.5:2 is the delivery rate curve for the Jangle underground shot (1.2 KT, 17 ft underground).[19] It shows an early buildup and subsequent constancy during the period when the active material has just emerged from the ground, the fireball is expanding, and substantial amounts of earth material are falling away from the source and back to the ground. The subsequent fall-off in the curve appears to be controlled primarily by the decay rates of the fission products. Fig. 3.5:3 is a high yield delivery rate curve from Castle 4 (6.5 MT, surface burst).[15] It is a twin-humped curve beautifully illustrating the hydrodynamic effect. The first hump is due to the nitrogen capture gamma radiation. The second hump builds up to its maximum just after the passage of the shock wave and clearly depicts the tremendous magnification of dose caused by shock effects. Comparison of Figs. 3.5:1 and 3.5:3 is profitable in that practically the only qualitative difference between them is the presence of the shock wave in the latter. The reader should not be misled by the visual distortion introduced into Fig. 3.5:3 by reason of the fact that it is plotted on a logarithmic scale. To the eye the two humps appear about equal in area. If the same curve were plotted on a non-distorting linear scale, the first hump would be seen to have only about one percent the area of the second.

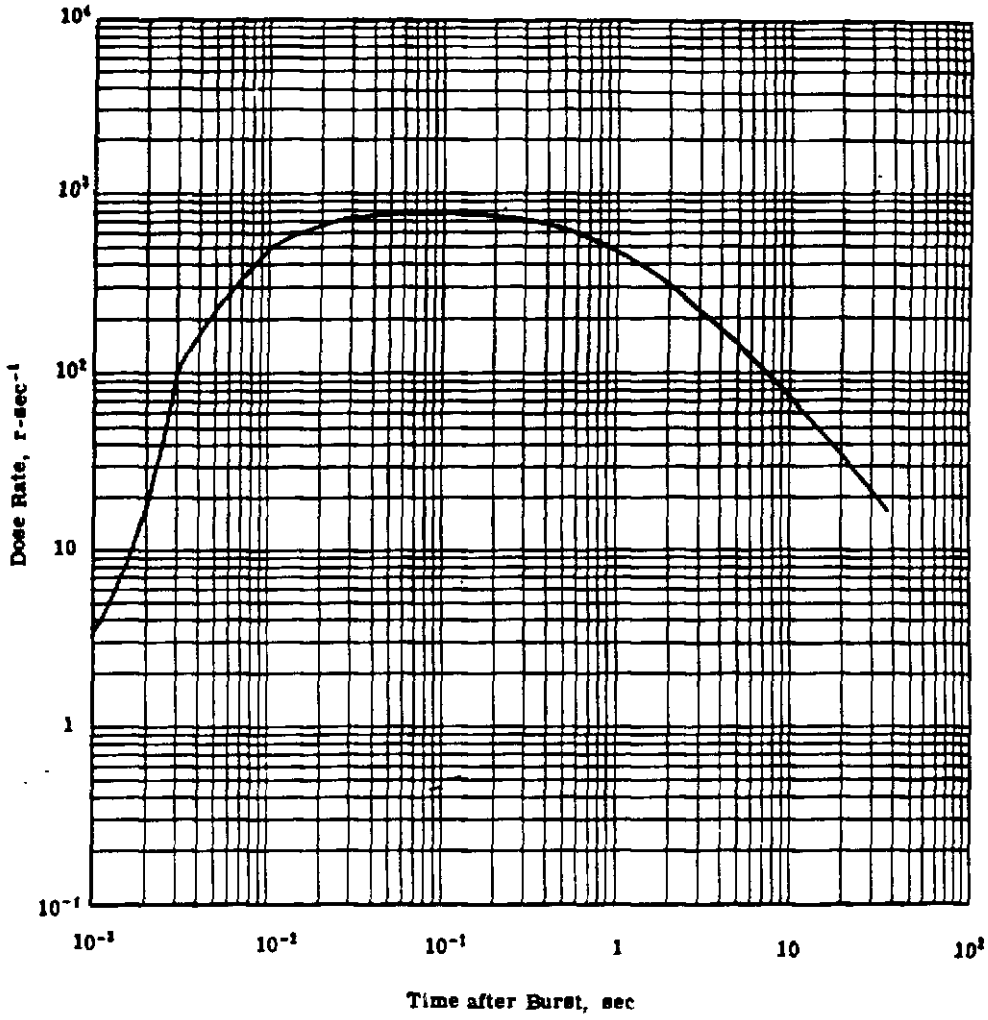

Fig. 3.5:2 Initial Gamma Radiation Delivery Rate for Jangle Underground, 1.2-KT Yield, 17-ft Underground, 500 yd from Ground Zero.

A compact way of permitting intercomparison of delivery rates on another basis is to show the fraction of the total dose which has been accumulated at any given time, i.e., integrate the delivery rate curves and normalize them to one. This is done in Fig. 3.5:4.

Curve A is the delivery rate for the Jangle underground shot at a point 500 yd from ground zero. It is believed that, barring such phenomena as hydrodynamic effect, this curve shape is representative of a very broad range of underground shots. It has the gradual and fairly uniform slope that can be expected for a dose that depends entirely on fission product decay. Changing the weapon yield or burial depth might cause displacement of the curve, but would probably effect no significant difference in its shape.

Curves B and C are representative of low or intermediate yield air or surface bursts. Curve B is based on experimental data taken at 1040 yd from ground zero at Buster Easy. It has two humps. The early one corresponds to the nitrogen gammas, and the later one corresponds to the fission product gammas. Curve C is an estimate of the situation that should prevail at distances of 5000 yd or more from ground zero. At those distances only the nitrogen gammas are important and the dose should

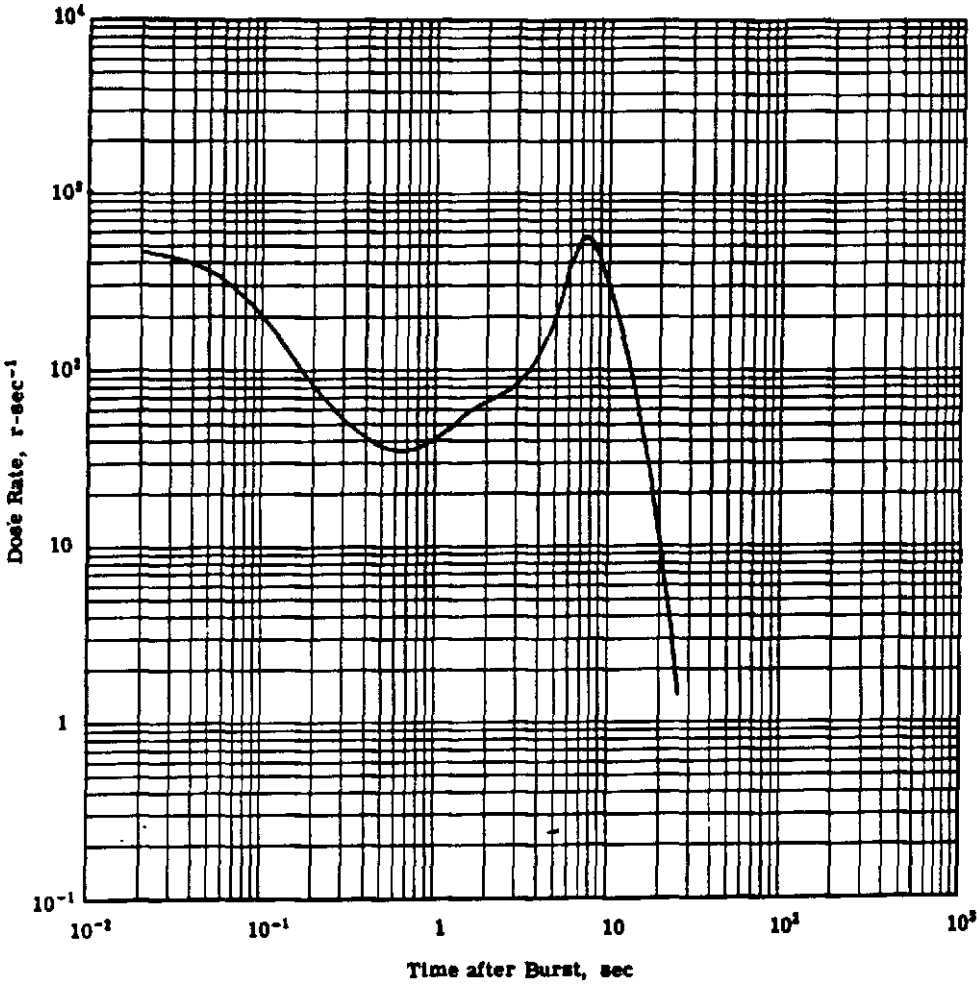

Fig. 3.5:3 Initial Gamma Radiation Delivery Rate for Castle 4 (Union), 6.5-MT Yield, Surface Burst, 4500 yd from Ground Zero.

reach its maximum rapidly. The two curves form a band which ought to comprehend, roughly, the curves characteristic of intermediate distances.

Curves D and E represent high yield. They were measured at Castle 4, 2390 and 4350 yd from ground zero, respectively. They display the hydrodynamic effect vividly. In Curve D most of the dose arrives at about 4 sec after the burst, for Curve E at about 7 sec. These times correspond roughly to the arrival of the rarefaction phase of the shock wave at the receiver. In this sense the dose for a high yield bomb may be considered to "travel" with the velocity of the shock wave. (See Section 3.2.1 for a fuller discussion of the hydrodynamic effect.)

3.6 INITIAL GAMMA RAY SPECTRUM

Because the radiation attenuation properties of media and of shielding materials and the susceptibility of living organisms and instruments to radiation effects are all heavily dependent upon the energy distribution of the radiation, knowledge of the energy spectrum of initial gamma radiation is of importance. The radiation spectrum observed at a particular receiver point will be different from

that observed at most other receiver points because the various energy components of the spectrum degrade differentially in passing through an attenuating medium. Knowledge of the initial gamma radiation spectrum at the source together with the existing knowledge of the spectral effects of the differential energy scattering and absorption cross sections[3] makes possible reasonably good approximations to the initial gamma ray energy spectrum at any point within about 8000 yd of the source.

3.6.1 INITIAL GAMMA RAY SPECTRUM AT THE SOURCE

Attempts were made at Operation Greenhouse to measure the initial gamma radiation spectrum.[21,22] While substantial information was obtained, affording new insight into early fission product decay processes, calibration and other difficulties prevent our relying heavily on the measured spectrum.

Recently, calculations of the initial gamma ray spectrum have been made by Borg and Eisenhauer.[4] A spectrum of great interest for weapons effects may be taken to consist entirely of gammas from two sources, namely fission product decay and neutron capture in atmospheric nitrogen. Infor-

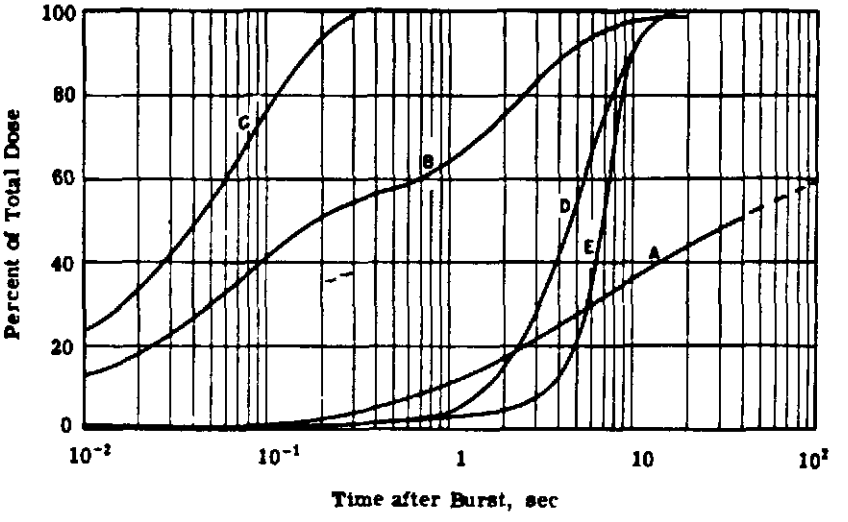

Fig. 3.5:4 Percent of Initial Gamma Dose Accumulated as a Function of Time under Various Burst and Receiver Conditions. A. Jangle Underground (1.2 KT, 17 ft underground, 500 yd from ground zero). B. Buster Easy (32 KT, 1300 ft burst height, 1040 yd from ground zero). C. Estimated for low and intermediate yield weapons, surface bursts, 5000 yd from ground zero. D. Castle 4 (6.5 MT, surface burst, 2390 yd from ground zero). E. Castle 4 (6.5 MT, surface burst, 4500 yd from ground zero).

mation about the fission product gamma rays has been obtained from reactor measurements and from short-time uranium irradiation experiments. The spectrum of nitrogen capture gamma rays has been determined by Kinsey et al.[23] (A third gamma source is the prompt radiation emitted during the fission process. Since only a relatively small fraction of the dose (~8 percent in some representative cases[19]) is contributed by the prompt gamma radiation, it is usually ignored in comparison with the fission product and nitrogen capture gammas.)

Some results of these calculations are presented in Fig. 3.6:1 for a representative low-intermediate yield (less than 100 KT) fission weapon. In Fig. 3.6:1 the gamma spectrum is approximated by the fraction of the total number of gammas which appear at each of several specific energies. It shows the composite spectrum due to both fission product and nitrogen capture gammas at an equivalent point source of radiation in an infinite homogeneous atmosphere. The relative contributions of

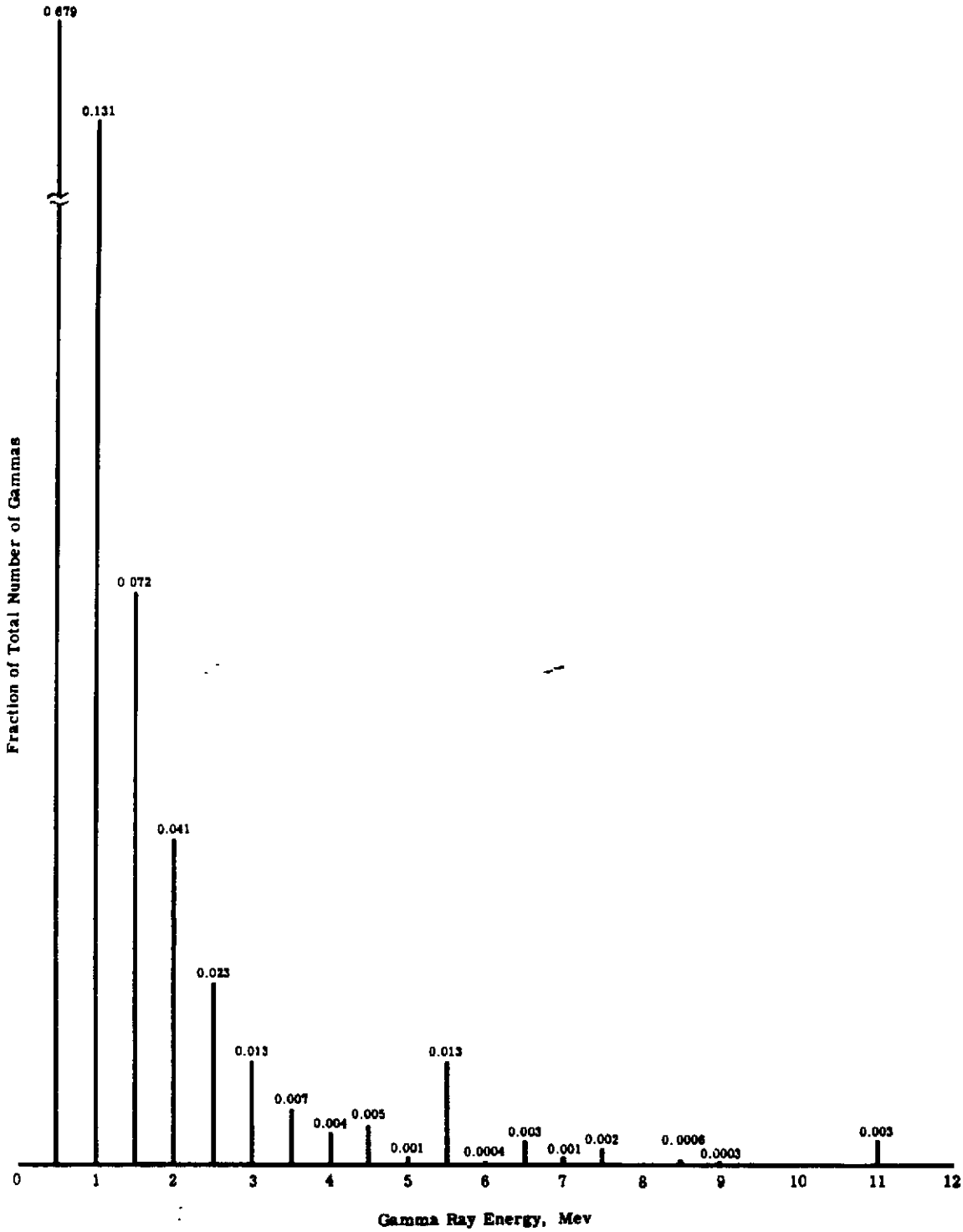

Fig. 3.6:1 Initial Gamma Ray Spectrum at an Equivalent Point Source.

fission product and nitrogen capture gammas to the composite spectrum are based on source strengths of 1.9 Mev of fission product gamma per fission and 0.5 Mev of nitrogen capture gamma radiation per fission. The spectrum given in Fig. 3.6:1 is taken to represent the average spectrum over the initial gamma period. Changes in the spectrum with time undoubtedly occur, but of necessity they are not treated in the present work.

The model used in the calculations has several defects. It ignores the spatial distribution of the fireball, the even broader spatial distribution of the nitrogen capture gamma ray source, and the change of quiescent air density with altitude.

In addition, several weapon design parameters which affect the nitrogen capture gamma ray source strength and spectrum have been approximated by an average value characteristic of the class of weapons exploded at the various past tests. Such parameters include the uranium-plutonium ratio, the ratio of non-fission to fission captures inside the weapon, and the neutron transmission factor of the weapon casing. The additional complications involved in a more refined treatment do not, in our opinion, justify the small increase in accuracy.

Fig. 3.6:1 includes no contribution to the nitrogen capture source due to fusion neutrons. Thus this figure is specifically unsuited for use with thermonuclear weapons.

While it is believed that Fig. 3.6:1 represents the best information at present available on the subject, it should be emphasized that the irradiation experiments and the reactor work upon which the fission product spectrum is based involve periods of time considerably longer than the almost instantaneous irradiation period of a weapon. Thus, the spectrum contains certain components of relatively long-lived fission products which are not wanted, and does not contain the very short-lived fission products which are wanted and which may contribute a substantial portion of the initial gamma ray dose. Further work to measure the initial spectrum directly is indicated.

3.6.2 SPECTRAL VARIATION WITH DISTANCE

It has been observed that the spectral composition of gamma radiation changes as the radiation progresses through an attenuating medium. This change is due to the fact that different energy components of the spectrum experience different degrees of absorption and degradation in passing through absorbing and scattering material.

Table 3.6:1 records $4\pi R^2$ times the number flux of gammas ϕ, in energy ranges of 0 to 0.75, 0.75 to 2, 2 to 4.5, 4.5 to 8, and 8 to 12 Mev.[3] The values of $4\pi R^2\phi$ are given as a function of the number of mean free paths traversed from a point source of one gamma per second, with source energies of 0.5, 1, 3, 6, and 11 Mev. The product $4\pi R^2\phi$ is dimensionless. If the gamma energy at the source E_s, is within the energy interval of interest at the receiver ΔE_i, then the value in Table 3.6:1 is

$$4\pi R^2\phi = e^{-\mu_{t_0}\bar{\rho}R}\left[1 + \int_{\Delta E_i}\left(4\pi R^2 e^{\mu_{t_0}\bar{\rho}R} I\right)\frac{dE}{E}\right] \qquad (3.6:1)$$

where the first and second terms within the bracket represent the unscattered and scattered gammas, respectively. If the gamma energy of the source is not in the energy interval of interest at the receiver, then the value in Table 3.6:1 is

$$4\pi R^2\phi = e^{-\mu_{t_0}\bar{\rho}R}\int_{\Delta E_i}\left(4\pi R^2 e^{\mu_{t_0}\bar{\rho}R} I\right)\frac{dE}{E}. \qquad (3.6:2)$$

The single term of Eq. 3.6:2 represents scattered gammas only, since there can be no unscattered gammas at the receiver under these circumstances.

TABLE 3.6:1

$4\pi R^2\phi$ for a Point Isotropic Source in Air with a Source Strength of One Gamma per Sec

Source Energy E_g, Mev	Number of Mean Free Paths $\mu_{t_0}R$	$4\pi R^2\phi$ Energy Range ΔE_i, Mev				
		0 to 0.75	0.75 to 2	2 to 4.5	4.5 to 8	8 to 12
0.5	1	2.06				
	2	2.14				
	4	1.02				
	7	1.55×10^{-1}				
	10	1.61×10^{-2}				
	15	2.57×10^{-4}				
	20	3.34×10^{-6}				
1	1	1.73	4.80×10^{-1}			
	2	1.70	2.21×10^{-1}			
	4	6.40×10^{-1}	4.33×10^{-2}			
	7	7.65×10^{-2}	3.31×10^{-3}			
	10	6.69×10^{-3}	2.31×10^{-4}			
	15	8.50×10^{-5}	2.43×10^{-6}			
	20	1.01×10^{-6}	2.31×10^{-6}			
3	1	1.12	1.66×10^{-1}	4.60×10^{-1}		
	2	8.62×10^{-1}	1.27×10^{-1}	2.04×10^{-1}		
	4	2.33×10^{-1}	3.66×10^{-2}	3.73×10^{-2}		
	7	2.02×10^{-2}	3.35×10^{-3}	2.61×10^{-3}		
	10	1.47×10^{-3}	2.44×10^{-4}	1.69×10^{-4}		
	15	1.48×10^{-5}	2.54×10^{-6}	1.59×10^{-6}		
	20	1.31×10^{-7}	2.42×10^{-8}	1.39×10^{-8}		
6	1	7.00×10^{-1}	1.01×10^{-1}	9.65×10^{-2}	4.16×10^{-1}	
	2	4.84×10^{-1}	7.26×10^{-2}	7.13×10^{-2}	1.71×10^{-1}	
	4	1.12×10^{-1}	1.88×10^{-2}	1.92×10^{-2}	2.78×10^{-2}	
	7	8.75×10^{-3}	1.55×10^{-3}	1.65×10^{-3}	1.74×10^{-3}	
	10	5.95×10^{-4}	1.06×10^{-4}	1.16×10^{-4}	1.04×10^{-4}	
	15	5.48×10^{-5}	1.03×10^{-5}	1.14×10^{-5}	8.96×10^{-7}	
	20	4.11×10^{-6}	8.88×10^{-8}	1.00×10^{-8}	7.33×10^{-9}	
10	1	4.94×10^{-1}	7.03×10^{-2}	6.02×10^{-2}	5.57×10^{-2}	3.97×10^{-1}
	2	3.18×10^{-1}	4.76×10^{-2}	4.27×10^{-2}	4.05×10^{-2}	1.57×10^{-1}
	4	6.93×10^{-2}	1.14×10^{-2}	1.09×10^{-2}	1.07×10^{-2}	2.40×10^{-2}
	7	5.09×10^{-3}	8.82×10^{-4}	8.83×10^{-4}	9.10×10^{-4}	1.41×10^{-3}
	10	3.37×10^{-4}	5.86×10^{-5}	5.96×10^{-5}	6.32×10^{-5}	8.04×10^{-5}
	15	3.07×10^{-6}	5.40×10^{-7}	5.63×10^{-7}	6.15×10^{-7}	6.56×10^{-7}
	20	2.16×10^{-8}	4.59×10^{-7}	4.79×10^{-8}	5.34×10^{-9}	5.19×10^{-9}

The terms used in Eq. 3.6:1 and 3.6:2 are defined as follows:

R = distance from source to point where the gamma spectrum is desired

ϕ = total (scattered and unscattered) number flux of gammas within the chosen energy range ΔE_i and at the point of interest

μ_{t_0} = total linear attenuation coefficient for gamma rays in standard density air at the chosen source energy E_g (See Fig. 3.6:2)

$\bar{\rho}$ = average quiescent air density

ΔE_i = chosen energy range

I = energy flux per unit energy interval within ΔE_i carried by scattered gammas for a source of one gamma per second at energy E_g

$4\pi R^2 e^{\mu_{t_0}\bar{\rho}R}$ I = differential energy spectrum.

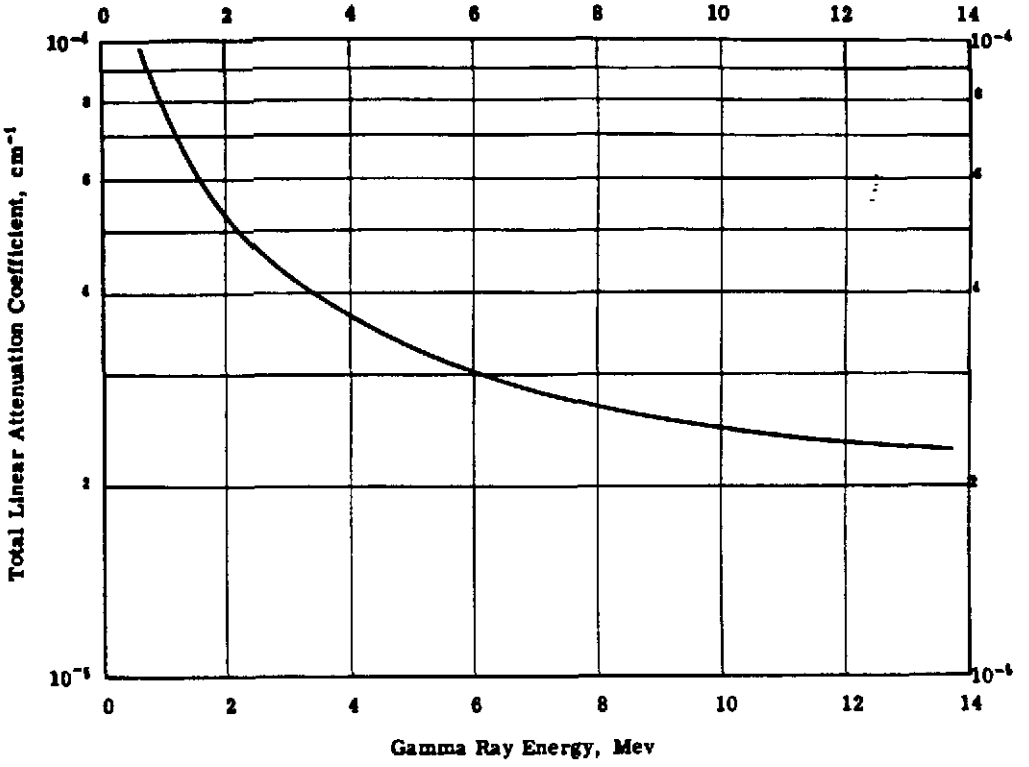

Fig. 3.6:2 Total Linear Attenuation Coefficient for Gamma Rays in Standard Density Air as a Function of Gamma Energy.

The differential energy spectra have been calculated for a number of media.[3] The values given in Table 3.6:1 are based on differential energy spectra for water since corresponding results for air are not available. This does not introduce serious errors because in the energy range in question water possesses gamma ray attenuation properties very closely resembling those of the atmosphere.

Table 3.6:2 is compiled directly from Fig. 3.6:1 and presents, for a typical fission weapon, the fraction of the total number of gammas at the source within the several energy ranges specified in Table 3.6:1.

Fig. 3.6:2 is a plot of the total linear attenuation coefficient for gamma rays in standard density air μ_{t0}, as a function of energy.[24] The attenuation coefficient is expressed in units of reciprocal cm. If R, the distance of a receiver point from the source, is expressed in cm, the number of mean free paths between the source and the receiver in standard density air is simply $\mu_{t0}R$.

Using Tables 3.6:1 and 3.6:2 and Fig. 3.6:2 the gamma spectrum can be estimated at various distant receiver points. The calculational methods are illustrated in the problems that follow. The spectral information obtained is of value in determining the effectiveness of various shielding materials and thicknesses.

It should be noted that the calculational methods which provide a means of estimating the gamma energy distribution also may be used to calculate a value of the total dose at the receiver. Such a calculation, while holding enough promise to warrant investigation, is not recommended at the present time for routine dose determinations because of the possible large errors in the results and the availability of the alternative and experimentally based methods (see Sections 3.2 and 3.3).

TABLE 3.6:2

Fraction of the Total Number of Gammas at the Source

Energy Range ΔE_i, Mev	Fraction of Total Gammas at Source
0 to 0.75	0.679
0.75 to 2	0.244
2 to 4.5	0.052
4.5 to 8	0.021
8 to 12	0.004
	1.000

PROBLEM 9

The distance between a gamma radiation source and a receiver is known. The intervening medium is air of known average density. The energy components of the source are known. Find the number of mean free paths between source and receiver for each energy component of the source.

Solution

1. From Fig. 3.6:2 find μ_{t_0} for each energy component of the source.
2. Multiply each value of μ_{t_0} found in step 1 by the source-receiver distance R (in cm) and by the average air density $\bar{\rho}$. The product $\mu_{t_0}\bar{\rho}R$ is the number of mean free paths for each energy.

The following conversion factors may prove helpful:

1 yd = 91.4 cm

1 ft = 30.5 cm

Example

A receiver is 2000 yd from a source of gamma radiation. The intervening medium is air of average density $\bar{\rho} = 1.0$. The source is composed of gamma rays of energies 0.5, 1, 3, 6, and 10 Mev. Find the number of mean free paths between source and receiver for each of the gamma ray energies.

1. From Fig. 3.6:2 the values of μ_{t_0} at the several energies of interest are as follows:

Source Energy, Mev	Total Linear Attenuation Coefficient μ_{t_0}, cm^{-1}
0.5	$10. \times 10^{-5}$
1	7.7×10^{-5}
3	4.3×10^{-5}
6	3.0×10^{-5}
10	2.5×10^{-5}

2. The source-receiver distance is 2000 yd or 1.83×10^5 cm and $\bar{\rho} = 1.0$. The number of mean free paths is obtained, therefore, by multiplying the value of μ_{t_0} listed above by 1.83×10^5.

Source Energy, Mev	Number of Mean Free Paths
0.5	18.3
1	14.1
3	7.9
6	5.5
10	4.6

PROBLEM 10

The energy distribution of a source of gamma radiation is known, as is the source-receiver distance. The intervening medium is air of known average quiescent air density. Find the energy distribution of the radiation at the receiver.

SOLUTION

1. Approximate the source spectrum by breaking it up into a number of energy groups.
2. Assume that the several energy groups may be represented by single average energies. For each of these energies compute the number of mean free paths between the source and the receiver by the method of Problem 9.
3. By interpolation in Table 3.6:1 find the energy distribution into each degraded energy group for each component of the approximate source.
4. Weight the energy distributions found in step 3 by the source spectrum of step 1.
5. Sum the components in each degraded energy group.
6. Normalize the spectrum by dividing each sum resulting in step 5 by the total of all such sums. The resulting spectrum will give the fraction of all gammas in each energy group, and the sum over all energy groups will be equal to unity.

Example

The energy distribution of a source of gamma radiation is taken to be that given in Table 3.6:2. The source-receiver distance is 2000 yd and the intervening medium is air of average quiescent air density $\bar{\rho} = 1.0$. Find the energy distribution of the radiation at the receiver.

1. The energy distribution from Table 3.6:2 is

Energy Range ΔE_i, Mev	Fraction of Total Gammas at Source
0 to 0.75	0.679
0.75 to 2	0.244
2 to 4.5	0.052
4.5 to 8	0.021
8 to 12	0.004
	1.000

2. Each of the energy groups listed above will be represented by the single energy used in Problem 9. The numbers of mean free paths are listed below as calculated in Problem 9 for these average energies, a source-receiver distance of 2000 yd and $\bar{\rho} = 1.0$.

Energy Range ΔE_i, Mev	Average Energy, Mev	Number of Mean Free Paths
0 to 0.75	0.5	18.3
0.75 to 2	1	14.1
2 to 4.5	3	7.9
4.5 to 8	6	5.5
8 to 12	10	4.6

3. Interpolation in Table 3.6:1 provides the following

Average Energy, Mev	Number of Mean Free Paths	$4\pi R^2\phi$ Energy Range ΔE_i, Mev				
		0 to 0.75	0.75 to 2	2 to 4.5	4.5 to 8	8 to 12
0.5	18.3	8.97×10^{-5}				
1	14.1	1.80×10^{-3}	6.20×10^{-5}			
3	7.9	1.27×10^{-2}	2.11×10^{-3}	1.63×10^{-3}		
6	5.5	5.69×10^{-2}	9.61×10^{-3}	9.84×10^{-3}	1.39×10^{-2}	
10	4.6	5.86×10^{-2}	9.61×10^{-3}	9.21×10^{-3}	9.10×10^{-3}	2.03 to 10^{-2}

4-5. Weighting the energy distribution found in step 3 by the source energy distribution from step 1 and summing the components in each degraded energy group provides the following:

Average Energy, Mev	Fraction of Total Gammas at Source, F	$F(4\pi R^2\phi)$ Energy Range ΔE_i, Mev				
		0 to 0.75	0.75 to 2	2 to 4.5	4.5 to 8	8 to 12
0.5	0.679	6.09×10^{-5}				
1	0.244	4.39×10^{-4}	1.51×10^{-5}			
3	0.052	6.60×10^{-4}	1.10×10^{-4}	8.48×10^{-5}		
6	0.021	1.19×10^{-3}	2.02×10^{-4}	2.07×10^{-4}	2.92×10^{-4}	
10	0.004	2.34×10^{-4}	3.84×10^{-5}	3.68×10^{-5}	3.64×10^{-5}	8.12×10^{-5}
	1.000	2.58×10^{-3}	3.66×10^{-4}	3.29×10^{-4}	3.28×10^{-4}	8.12×10^{-5}

6. The total of all sums from the above energy groups is 3.68×10^{-3}; by dividing the individual energy group totals by 3.68×10^{-3} we get the energy distribution at the receiver as shown below.

Energy Range ΔE_i, Mev			Fraction of Total Gammas at Receiver
0	to	0.75	0.701
0.75	to	2	0.099
2	to	4.5	0.089
4.5	to	8	0.089
8	to	12	0.022
			1.000

Fig. 3.6:3 presents both the gamma energy spectrum calculated above (receiver 2000 yd distant from point source) and, for purposes of comparison, the corresponding spectrum at the source given earlier in Table 3.6:2.

Error

It is not possible to speak about errors for this kind of calculation in precise numerical terms. It suffices to say that the methods delineated are quite crude and approximate. The results are, however, qualitatively correct, and sufficiently definitive for the purpose of making estimates of the relative effectiveness of shielding structures in field situations. For work where more precision is needed, reference should be made to the detailed procedures[3] upon which Table 3.6:1 is based. Lack of better information about the gamma source spectrum in large measure vitiates any present refinements in the techniques of computing energy degradation.

3.7 MILITARY SHIELDING

Gamma radiation incident upon a receiver from a given source can be reduced in only two ways:

1. by increasing the distance between source and receiver, and
2. by interposing absorbing materials between source and receiver.

Since, in general, the source-receiver distance is fixed, particularly for the initial radiations, it is really only through variation of the material shielding around the receiver that the dose can be controlled.

To evaluate the shielding effectiveness of any given configuration of materials it is necessary to have some notion of the directions from which the radiation may arrive and of the shielding values of the materials composing the structure. Because in traversing a medium such as air, gamma radiation can be scattered as well as absorbed, and because a scattering process can involve changes of direction as well as loss of energy, the radiation will not all travel along the line of sight from the source to the receiver. As the distance from the source to the receiver increases, an increasing fraction of the total radiation arrives at the receiver from directions other than the line of sight. While there have been no definitive measurements or calculations of the angular distribution of radiation at a receiver in the neighborhood of a nuclear explosion, experience in similar problems indicates that very substantial amounts of radiation may arrive at the receiver from directions markedly different from the line of sight.

Although there are some circumstances in military operations where a simple line-of-sight shield can provide adequate personnel protection, the more common situation requires all-around and top shielding and such protection should be provided wherever possible.

No generalized treatment of the military gamma shielding problem, either theoretically or experimentally based, can be presented at this time. The geometrical configuration of a structure bears importantly on its shielding effectiveness; the geometry of most practical structures and of the

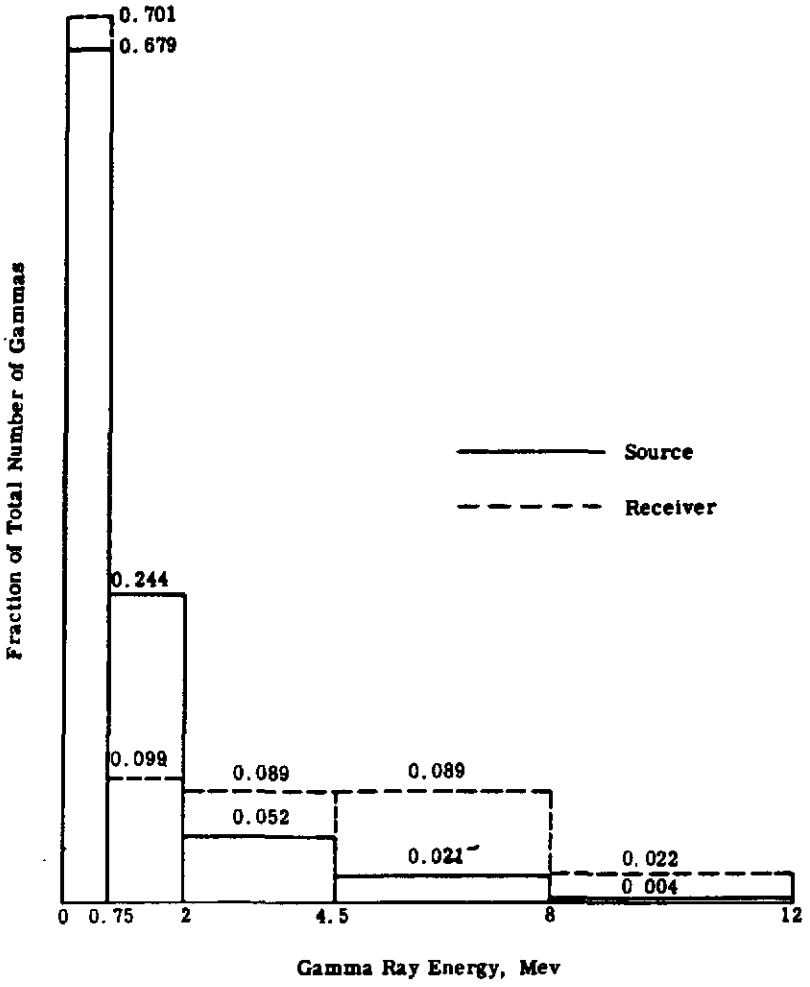

Fig. 3.6:3 Comparison of the Initial Gamma Ray Spectra at the Source and at a Receiver 2000 yd from the Source.

topography in which they are located cannot be simply described in a mathematical sense. It is extremely difficult, therefore, to compute the shielding effectiveness of a given structure with reasonable accuracy. The computational problem is compounded by the general lack of information on the distribution of the radiation at the receiver in intensity, energy, and angle. Generalizations based on experimental measurements are equally difficult because the data are limited, are distributed over a variety of structural types, and often lack internal consistency.

Under these circumstances it is felt that at present the best way to determine the shielding effectiveness of a given configuration of materials is to estimate it from experimentally measured values for similar structures under similar conditions.

To this end the most pertinent and comprehensive test results,[25,26] notably from Teapot, are summarized below for various shelters, field fortifications, foxholes, armored vehicles, and vehicle trenches. These results were obtained in real structures under conditions which approximated real military situations, but they should always be used with the understanding that they apply strictly to a particular situation and will vary to an extent depending on the actual situation of interest. Specific soil types, burst heights, and weapon characteristics may all be expected to have some effect on shielding effectiveness.

The results are conveniently presented in terms of the gamma dose transmission factor T, defined as the ratio of the dose measured inside the shielding structure to the dose measured outside. As the shielding effectiveness of a configuration goes up, the transmission factor goes down. As noted above, the transmission factor for a given configuration is not unique but depends on the conditions under which the doses are measured. Further, for different structures the value of the transmission factor may vary widely. Some structures with thick earth covers provide transmission factors of 10^{-4}, which is virtually complete protection. The transmission factor at the bottom of foxholes may be as low as 0.05, while armored vehicles may have average transmission factors as high as 0.7.

The transmission factors and related descriptive information are presented in Tables 3.7:1 through 3.7:7 and Figs. 3.7:1 and 3.7:2. Table 3.7:1 presents a description of the several shelters tested at Teapot while Table 3.7:2 presents the corresponding transmission factors and line-of-sight thicknesses from the detector to the point of burst. Table 3.7:3 presents a description of the field fortifications tested for gamma shielding at Teapot and Table 3.7:4 lists the fortification transmission factors and line-of-sight thicknesses. The transmission factors for 1-man, 2-man, and prone foxholes resulting from measurements at several shots in the Ranger and Teapot series are given in Table 3.7:5. These data are also plotted as a function of distance from ground zero in Figs. 3.7:1 and 3.7:2. Finally, Tables 3.7:6 and 3.7:7 present a limited number of transmission factor values for armored vehicles and vehicle trenches, respectively.

Some of the data presented are clearly questionable and where such discrepancies appear in Tables 3.7:2 and 3.7:4 (shelters and fortifications), they are indicated by an asterisk. Since the foxhole data are plotted in Figs. 3.7:1 and 3.7:2, the possible inconsistencies are best determined from the figures rather than from Table 3.7:5.

Despite these questions several general results may be noted. For covered shelters or fortifications the vertical variation of dose, at least between 20 and 50 in. from the structure floor, is of negligible importance. Horizontal variation, on the other hand, may have a more pronounced effect. The very limited data available indicate, for example, that moving close to the wall nearest ground zero from a central point within a structure may reduce the transmission factor by a factor of three or four. At the point of emergence from the shelter the transmission factors will, of course, be close to or equal to one and therefore the increase in the transmission factor between the interior and the entrance will be largest for the most effectively shielded structures. This type of increase may be quite large; for the shelters and fortifications tested at Teapot it varied from less than 2 to more than 200. Thus, position within the structure at the time of burst will have an important effect on the dose received.

A first attempt has been made to correlate the foxhole transmission factor data from Ranger[26] and Teapot[25] in Figs. 3.7:1 and 3.7:2. While questions can be raised about a substantial portion of the data, even from a single test shot, there appears to be enough consistency on the whole to justify such an attempt. Fig. 3.7:1 presents the spread of values of the transmission factor as a function of distance from ground zero for Ranger Shots 2 through 5. All four shots were made at the same location and with burst heights which varied between 1,000 and 1,500 ft. In most cases, several readings were taken at each depth and thus the values presented may be taken to represent the average transmission factor at the depths indicated. Additional data were taken on 1-man and prone foxholes and these data are reported in Table 3.7:5. They are not, however, plotted in Fig. 3.7:1 since the uncertainty in the values of the transmission factors for a single type of foxhole appears to be greater than the spread between types or, for that matter, the orientation of the foxhole to the burst point. Using these data, estimated boundary curves are drawn for the transmission factors at three depths. It should be noted that the boundary curves are all drawn decreasing monotonically with increasing distance from ground zero, although the data for the lower two depths at 1,600 yd seem to indicate a change in slope. It is conceivable that at distances and depths where the major dose component is scattered, such a change in slope actually does occur; some of the Teapot data also suggest this possibility. However, because of the many variables involved and because of the considerable scatter in the available data, this question must be left open for further investigation.

Fig. 3.7:2 presents the data from individual foxholes from Teapot Shots 11 and 12. The burst heights for Shots 11 and 12 were 300 and 400 ft, respectively, and the locations and soil characteristics

TABLE 3.7:1

Description of Shelters

OCE – The three OCE (Office, Chief of Engineers) shelters (UK-3.8a, UK-3.8b, UK-3.8c) are identical, buried[1], flat-roofed, box-shaped structures with walls of reinforced concrete (side walls 19 in. thick, end walls 15 in. thick) and beam-supported steel roofs (1/2 in. thick). The structures are 8 ft high, 10 ft wide, and 21 ft long, oriented with the long side facing ground zero. All three structures are 300 yd distant from ground zero. The principal difference between the structures is the thickness of the earth cover (1, 4, and 8 ft). Each structure has a single entrance tunnel with one right angled turn.

OCE-Duplex – The single OCE-duplex shelter (UK-3.7) is basically similar to the structures described above. It is a two-room, buried, box-shaped and flat-roofed cell with reinforced concrete walls (side walls 19 in. thick, end walls 15 in. thick) and a beam-supported steel roof (1/2 in. thick). The structure is 7 ft high, 8 ft wide, and 19 ft long. It is positioned 300 yd from ground zero with the long side facing ground zero. The earth cover is 2 ft thick. There is a baffled entrance at each end of the structure, one of these entrances having three right turns and the other, seven.

Navy Armco – There are two Navy Armco structures, one at 500 yd (TP-F-3.6-a-1) and the other at 767 yd (UK-3.15) from ground zero, both above ground and long-side-on to the blast. They are half-cylindrical, Quonsut-hut type structures made of 1/8 in. and 1/16 in. thick corrugated steel, respectively. The shelters are both 12 ft high at the crown, 25 ft wide, and 48 ft long and are covered by an earth embankment which is approximately flat over the structure proper and then tapers off to the normal ground level. The TP structure is covered with earth, with a vertical thickness of 3 1/2 ft at the crown and increasing to about 15.5 ft at the edges of the cylinder. The vertical thickness of the earth cover is zero at the crown of the UK structure and increases to about 12 ft at the edges. There is one entrance at the end of each of the Armco structures, a straight length of corrugated steel cylindrical pipe, approximately 12 ft long and 6 ft in diameter.

BuDocks – The BuDocks (Navy Bureau of Yards and Docks) shelter is above ground, 1633 yd from ground zero, and side-on to the blast. It is a box-shaped structure with a gabled roof. The walls and roof are made of precast panels of reinforced concrete, 2 in. thick. It is 13 1/2 ft high at the peak, 22 ft wide, and 48 ft long. The entrance is at the end of the shelter and is fitted with a blast door. There is no earth cover on top or sides.

Instrument Shelters – There are five instrument shelters (3.28j, 3.28c, 3.28h, 3.28f, 3.28e) positioned from 333 to 2200 yd from the point of burst. They are all box-shaped structures with flat roofs. The walls and roofs are made of reinforced concrete. Some of the instrument shelters were semi-buried (3.28j and 3.28c) while the others were above ground. None of them has earth covering on the roof but they all have earth embankments piled up at the sides. The dimensions of the shelters vary, 3.28j being 7 1/2 ft high, 8 ft wide, and 29 1/2 ft long; 3.28c being 7 1/2 ft high, 8 ft wide, and 15 1/2 ft long; 3.28e, 3.28f, and 3.28h all being 7 1/2 ft high, 8 ft wide and 17 ft long. Similarly, the thickness of the concrete walls and roof varies, 3.28j having walls and roof 2 1/2 ft thick; 3.28i having walls and roof 1 1/2 ft thick; 3.28e and 3.28f having walls and roof 10 in. thick; and 3.28h having walls and roof 9 in. thick. The entrance arrangements also vary, two of the shelters (3.28j and 3.28c) having two steel hatches (2 1/2 ft square) in the roof while the others have a door in the wall farthest from ground zero and a cut in the embankment at that wall.

---

[1] For present purposes shelters and fortifications will be classified as buried (those completely below the normal ground level), semi-buried (those partly below normal ground level), and aboveground (those completely above normal ground level). While the buried structures are usually completely surrounded by earth on sides and top, semi-buried and aboveground structures may or may not be earth-covered.

TABLE 3.7:2

Transmission Factors for Shelters (Teapot, Shot 12)[1]

Shelter	Code	Distance from Ground Zero, yd	Vertical Thickness of Earth Cover, ft	Inside Shelter				Near Shelter Entrance			
				Detector Height above Floor, in.	Transmission Factor	Line-of-Sight Thickness, ft		Detector Height above Floor, in.	Transmission Factor	Line-of-Sight Thickness, ft	
						Concrete	Earth			Concrete	Earth
OCE	UK-3.8a	300	1	26 to 44[2]	0.33[2]	1.75[2]	8.6[2]	—	0.011*[3]	1.1	12.4
	UK-3.8b	300	4	26 to 44	0.00012	1.75	15	—	0.0029[4]	1.1	19.4
	UK-3.8c	300	8	26 to 44	0.0000013	1.75	25	—	0.0029[4]	1.1	19.4
OCE duplex	UK-3.7	300	2	26 to 44	0.0020	1.2	12.3				
Navy Armco	TP-F-3.6-a-1	500	[3.5 at crown 15.5 at edges]	Front[5]							
				20	0.009*[3]	0	17				
				38	0.0014*	0	18				
				Rear[5]							
				20	0.0007*	0	14				
				38	0.01*	0	13				
	UK-3.15	767	[0 at crown 12 at edges]	Rear[5]							
				20	0.064	0	11				
				38	0.065	0	9.5				
BuDocks	UK-3.12a	1633	0	26 to 44	0.059	0.16	0				
Instrument shelter	3.28j	333	0	26 to 44	0.0019	3.5 to 6.5	0 to 3.5	36	0.0045	2.75	11.7
	3.28c	767	0	44	0.0079	1.5	13	42	0.011	1.5	15
	3.28h	2200	0	44	0.018	0.75	16	42	0.026	0.75	14
	3.28f	1467	0	44	0.025	0.83	14.5	42	0.055	0.83	11.5
	3.28e	1667	0	44	0.018	0.83	15	36	0.038	0.83	12.5

(1) Measured at Teapot, Shot 12 (24KT yield, 400-ft burst height).[25]

(2) When there was little or no change in the transmission factor at the two heights at which it was measured, these heights are indicated together with the average value of the measured transmission factor and the average line-of-sight thicknesses. When there was a marked change with height, the individual rather than average values of the transmission factors and line-of-sight thicknesses are given.

(3) When the measured value of the transmission factor is uncertain or clearly inconsistent, an asterisk is placed next to the value in question.

(4) The vertical portion of the entrance tunnel was shared by the two shelters, UK-3.8b and UK-3.8c, so that the two values of the transmission factor near the entrance actually came from the same measurement.

(5) "Front" refers to detectors mounted near the wall of the Navy Armco structures nearest ground zero. "Rear" refers to detectors mounted near the far wall.

TABLE 3.7:3

Description of Fortifications

A-1, A-2, A-3 – The A-type fortifications are semi-buried, T-shaped machine gun emplacements, approximately 8 ft high, with the bar of the T 21 ft long and 7 ft wide and the stem 7 ft long and 7 ft wide. They are located 333, 383, and 467 yd from ground zero, respectively. There is an open entrance at each end of the bar and the end of the stem contains the machine gun port. The stem of the T faces away from the burst point. The earth cover is 5 ft thick and the roof and walls of the fortification are of timber.

B-1, B-2, B-3 – The B-type fortifications are buried, box-shaped structures, 7 ft high, 8 ft wide, and 12 ft long. They are made in two 8 ft by 6 ft sections and are located at 333, 383, and 467 yd from ground zero. There is a single entrance which makes one right turn before reaching the surface. The B-3 structure is identical to the B-1 and B-2 structures except that the entrance of the outer 8 ft by 6 ft section is equipped with a blast door and the inner section is made into a CBR (Chemical, Biological, Radiological) shelter by lining the walls with diffusion board. The earth cover is 5 ft thick and the roof and walls of the fortification are timber. The long side of the structure faces the burst point and the entrance to the structure is on that side.

G-3 – The G-3 fortification is the same as the B type except that logs are used for the roof and walls instead of cut timber. It is positioned at 467 yd from ground zero.

D-2 – The D-2 fortification is a buried, box-shaped bunker, 9 ft high, 11 ft wide and 20 ft long. It is positioned with the long side facing the burst point and has an entrance at each end, each of which makes two right turns before reaching the surface. The walls and roof are of timber, the earth cover is 5 ft, and the structure is 383 yd from ground zero.

H-3 – The H-3 fortification is a semi-buried, upright cylinder capped with a prefabricated plywood dome. The cylindrical portion of the fortification is approximately 3 ft high and 8 ft in diameter. The dome is 9 ft in diameter and has an 8 in. high by 2 ft long gun port facing away from the burst point. The entrance to the fortification is a short tunnel, with one right turn, and is on the side closest to the burst point. The walls of the structure are of timber and the earth cover is approximately 3 ft at the top of the dome.

I-3 – The I-3 fortification is an 8 ft length of 4 ft diameter corrugated steel pipe buried in the ground with the axis of the pipe side-on to the burst point. An open trench at one end of the pipe serves as the single entranceway and this end is covered with the wooden wall and door. The earth cover is approximately 4 ft thick above the top of the pipe.

TABLE 3.7:4

Transmission Factors for Fortifications (Teapot, Shot 12)[25]

Fortification	Distance from Ground Zero, yd	Vertical Thickness of Earth Cover, ft	Inside Fortification			Near Fortification Entrance			Near Wall Closest to Ground Zero		
			Detector Height above Floor, in.	Transmission Factor	Line-of-Sight Thickness[1] ft	Detector Height above Floor, in.	Transmission Factor	Line-of-Sight Thickness[1] ft	Detector Height above Floor, in.	Transmission Factor	Line-of-Sight Thickness[1] ft
A-1	333	5	26	0.10	7	29	0.18	8.5			
A-2	383	5	26	0.051	10	29 to 47	0.17	12	——	0.012	——
A-3	467	5	26 to 44	0.041	11.5	29 to 47	0.093	13	——	0.013	——
B-1	333	5	26	0.0013	15.5	29	0.034	14.5			
B-2	383	5	26 to 44	0.00040	20.5	29 to 47	0.013	19.5			
B-3	467	5	26 to 44	0.00030	25	29 to 47	0.012	24			
G-3	467	5	26 to 44	0.00043	25	29 to 47	0.014	24	——	0.0024*[2]	——
D-2	383	5	26 to 44	0.00024	20				——	0.000054	——
H-3	467	3 at top of dome	26 to 44	0.026	5.5						
I-3	467	4 at top of cylinder	26	0.016	10						

[1] The line-of-sight thicknesses are given in terms of thickness of earth but may be considered to be total values including the relatively thin wooden walls and/or roofs of the fortifications.

[2] When the measured values of the transmission factor are uncertain or clearly inconsistent, an asterisk is placed next to the value in question.

TABLE 3.7:5

Transmission Factors for Foxholes[25, 26]

Test	Shot Number	Weapon Yield, KT	Burst Height, ft	Distance from Ground Zero, yd	Foxhole Type[2]	Foxhole Orientation to Ground Zero	Transmission Factor[1] Distance Below Ground Surface				
							48 in.	32 in.	24 in.	16 in.	12 in.
Ranger	3 to 5	0.9 to 22	1000 to 1500	400	2 man	side-on	0.15 to 0.30	0.40 to 0.93		0.75 to 0.95	
				800	prone	side-on			0.29 to 0.31		0.47 to 0.60
					1 man	side-on	0.12	0.15 to 0.20		0.29 to 0.36	
					2 man	side-on, 45°, & head-on	0.11 to 0.24	0.20 to 0.30		0.41 to 1.00	
				1200	prone	side-on			0.20 to 0.55		0.30 to 0.75
					2 man	side-on, 45°, & head-on	0.09 to 0.15	0.13 to 0.30		0.25 to 0.70	
				1800	2 man	side-on	0.12 to 0.47	0.17 to 0.50		0.25 to 0.53	
				2000	2 man	side-on	0.11	0.14		0.31	
							58 in.	40 in.	22 in.		
Teapot	11	1.5	300	300	1 man	side-on	0..2	0.24	0.52		
					2 man	side-on	0.24	0.29			
				600	1 man	side-on		0.18	0.25		
					2 man	side-on	0.18	0.18	0.18		
				1000	1 man	side-on	0.20				
					2 man	side-on	0.13	0.17	0.22		
							42 in.	24 in.	6 in.		
Teapot	12	24	400	488	1 man	side-on		0.29	>0.51		
					1 man	head-on		0.30	>0.51		
					2 man	side-on		>0.51[3]	0.25[3]		
				750	2 man	side-on	0.082	0.14	>0.03		
				1500	2 man	side-on	0.06	0.08	0.26		
				2000	1 man	side-on	0.08	0.08	0.18		
					1 man	head-on	0.05	0.08	0.39		
					2 man	side-on	0.07		0.42		

(1) Questionable values of the transmission factor are not indicated in this table. The values that do not appear to be consistent with the smooth curves drawn in Fig. 3.7:2 are so indicated in the figure, however.

(2) The Ranger 2-man foxholes were 2 ft wide, 6 ft long and 4 ft deep, the 1-man foxholes were 2 ft wide, 3.5 ft long and 4 ft deep, and the prone foxholes were 2 ft wide, 6 ft long, and 2 ft deep. The Teapot 2-man foxholes were 2 ft wide, 6 ft long, and 5 ft deep while the 1-man foxholes were 2 ft wide, 3 1/2 ft long, and 5 1/2 ft deep.

(3) These values of the transmission factors appear to have been reversed and are plotted in what is thought to be the correct positions in Fig. 3.7:2.

TABLE 3.7:6

Transmission Factors for Armored Vehicles[25]

Vehicle	Transmission Factor within Vehicle[1]		
	Minimum	Maximum	Average
M48 Tank, 90-mm Gun	0.04	0.18	0.1
AIV-M59 Personnel Carrier	0.48	1.0	0.7
T97 Self-Propelled 155-mm Gun	0.31	1.0	0.6

(1) These transmission factors were measured at Teapot Shots 1 (1.2-KT yield, 762 ft burst altitude), 4 (43-KT, 500 ft), 5 (3.6-KT, 300 ft), 8 (15-KT, 500 ft), and 12 (24-KT, 400 ft).

TABLE 3.7:7

Transmission Factors for Vehicle Trenches (Teapot, Shot 12)[25]

Distance of Trench from Ground Zero, yd	Transmission Factor Inside Trench
700	0.6
900	0.2

for the two bursts were not the same. In some cases these data represent single readings at a given depth while in others several readings were averaged. With few exceptions and these only at 2,000 yd from ground zero the Shot 12 data fall into a consistent pattern. The curves drawn are based primarily on the results of Shot 12. The Shot 11 results have considerably less internal consistency and also tend to be above the corresponding Shot 12 results. Differences in soil type for the two locations may be partly responsible for the differences between Shots 11 and 12 but no explanation is offered for the poor internal consistency of Shot 11.

The vertical variation of the transmission factor within the foxholes is, as expected, larger than that within covered shelters and fortifications. Thus, the transmission factor may decrease by as much as a factor of 10 in going from 10 to 50 in. below the ground surface. Conversely, the horizontal variation of the transmission factor is much less than that in underground shelters, because of the relatively small size and open construction of the foxhole. The lowest transmission factor at a given depth will, however, still be next to the face or faces of the foxhole closest to ground zero.

Despite the discrepancies and uncertainties of the foxhole data it is recommended that for the present Figs. 3.7:1 and 3.7:2 be used to estimate transmission factors for air bursts with burst heights of 1,000 to 1,500 ft and 300 to 500 ft, respectively. Interpolation or extrapolation to other burst altitudes may be made based on these figures but always with an appreciation of the inaccuracies in the original results.

To assist in those cases where it is not possible to find a tested structure or fortification sufficiently similar to the device whose shielding characteristics are desired, a simple and rough

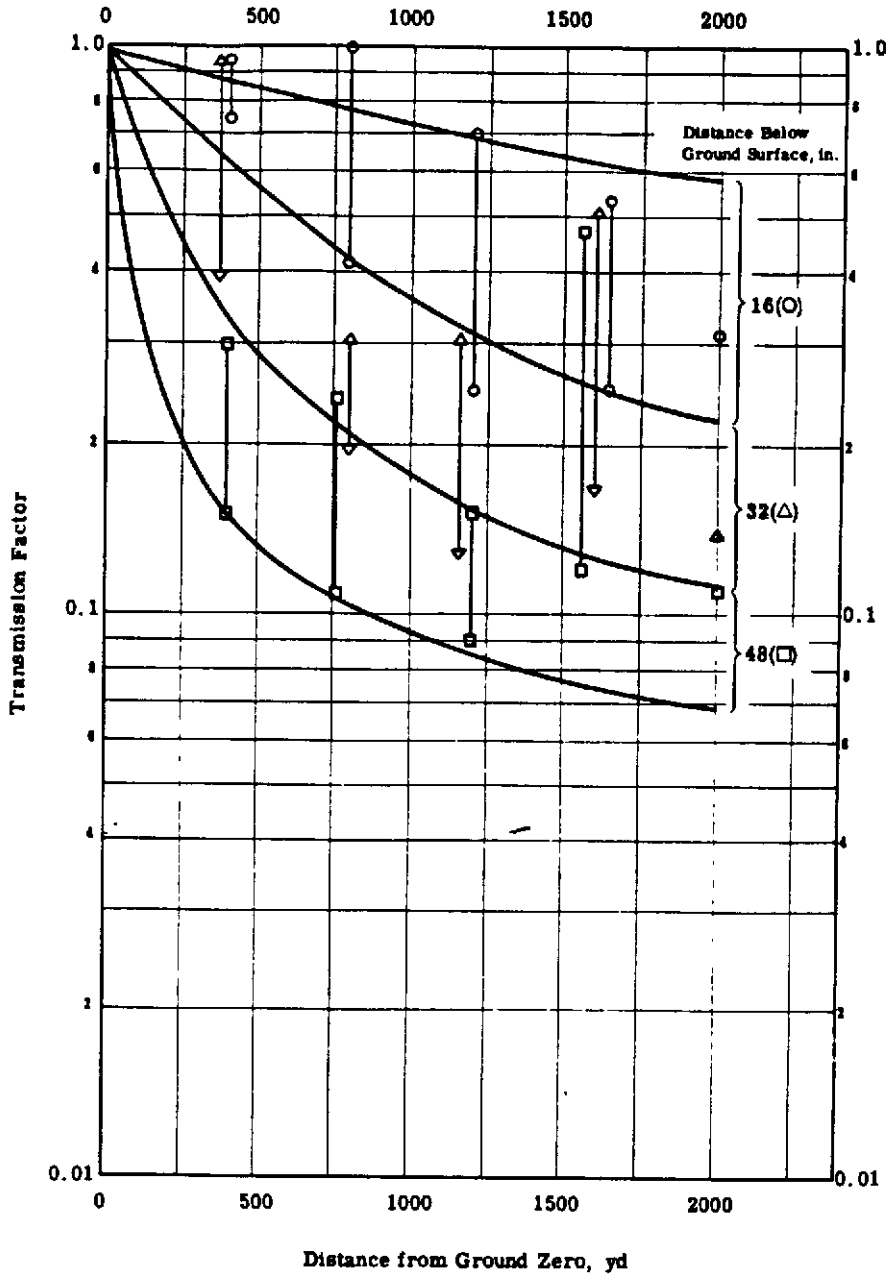

Fig. 3.7:1 Transmission Factors for Foxholes (Ranger Shots 2 through 5).

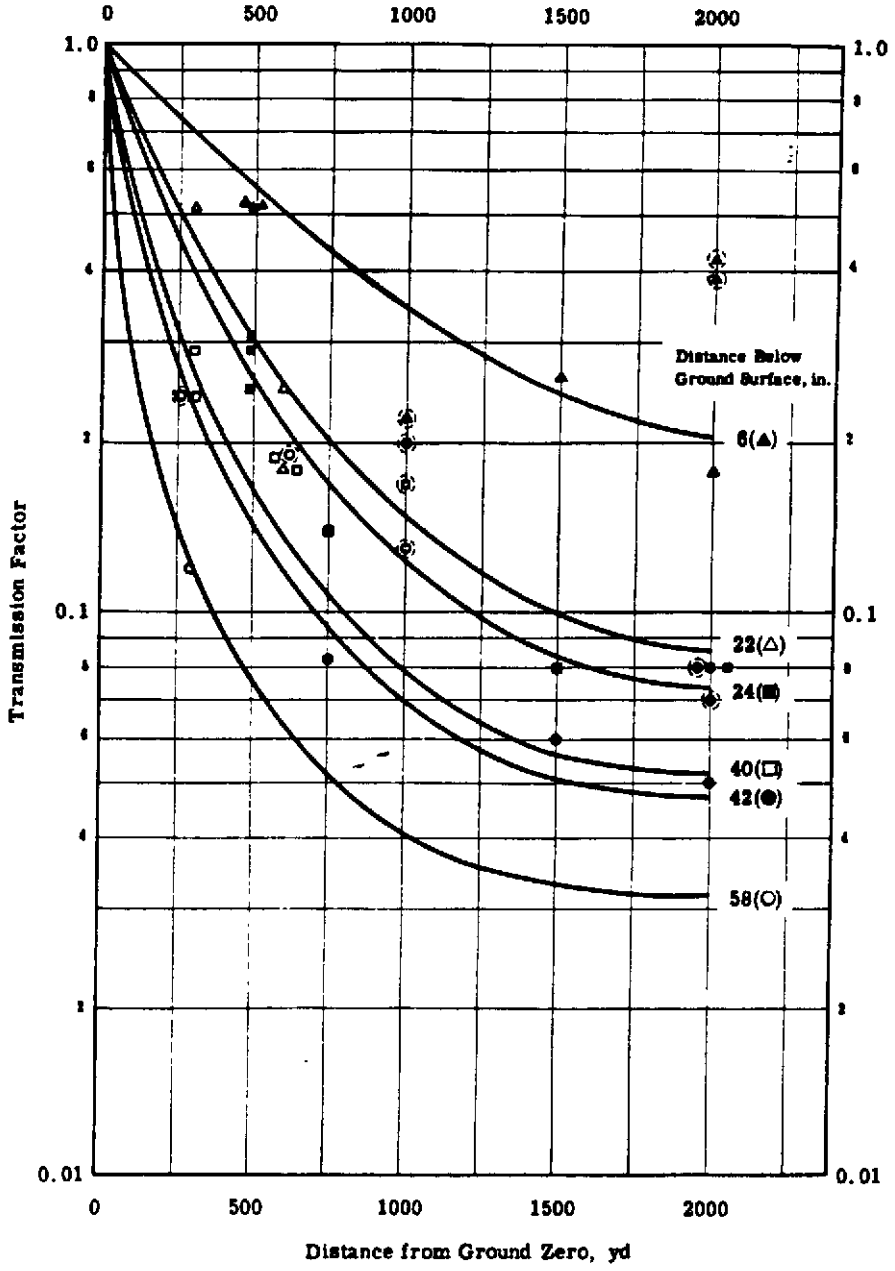

Fig. 3.7:2 Transmission Factors for Foxholes (Teapot Shots 11 and 12). Data points which are circled appear to be inconsistent with the transmission factor curves as drawn.

TABLE 3.7:8

Transmission Factors for Standard Thicknesses of Five Common Shielding Materials as a Function of Gamma Ray Energy

Material	Standard Thickness	Transmission Factor, Gamma Ray Energy, Mev							
		0.25	0.5	1	2	3	4	5	6
Water	1 ft	0.37	0.36	0.38	0.45	0.50	0.53	0.54	0.56
Iron	1 in.	0.45	0.54	0.60	0.63	0.65	0.65	0.63	0.63
Concrete	1 ft	0.089	0.083	0.091	0.15	0.19	0.22	0.23	0.25
Lead	1 in.	0.001	0.065	0.27	0.44	0.44	0.39	0.36	0.33
Sand	1 ft	0.061	0.068	0.099	0.14	0.15	0.15	0.15	0.15

calculational procedure is possible. For this purpose we may define an approximate form of the transmission factor

$$T_e = e^{-\mu_t x} \tag{3.7:1}$$

where, for a given material, μ_t is the total linear attenuation coefficient and x is the thickness

If we choose some standard thickness of material x_s and determine the corresponding value of the transmission factor T_{es}, then any other thickness x of this material will yield a transmission factor

$$T_e = e^{-\mu_t x} = e^{-\mu_t x_s\left(\frac{x}{x_s}\right)} = (T_{es})^{\frac{x}{x_s}} \tag{3.7:2}$$

Similarly, if several different materials compose the shield, then the combined transmission factor will be

$$T_{e(1,2,3)} = e^{-(\mu_{t1}x_1 + \mu_{t2}x_2 + \mu_{t3}x_3)} = T_{e1}T_{e2}T_{e3} \tag{3.7:3}$$

Eqs. 3.7:2 and 3.7:3 demonstrate a very important rule applicable to approximate shielding calculations, namely that when several different materials or thicknesses of the same material are added together in a shield, the composite transmission factor is equal to the product of the transmission factors of the individual layers. Hence, the transmission factor for two layers of equal thickness of a given material is the square of the transmission factor for a single layer.

Table 3.7:8 presents the transmission factor T_{es} (as a function of gamma energy) for arbitrarily selected standard thicknesses of the five most common shielding materials. Using Eq. 3.7:3 and the values of T_{es} given in Table 3.7:8, the composite transmission factors can be roughly estimated for structures made up of the materials listed and for gammas of a known energy and energy distribution.

The values of T_{es} given in Table 3.7:8 indicate that the materials listed are most effective against the lower energy (say below 0.5 Mev) gamma rays. Further, in the gamma energy range of interest the shielding effectiveness of most materials decreases with increasing gamma energy, reaches a minimum value, and then slowly increases. (This is not true of materials of low atomic weight where the shielding effectiveness decreases continuously with energy in this range.) For many

important gamma shielding materials the transmission factor does not vary appreciably within the range of interest (say 0 to 15 Mev) above about 3 Mev. Since there are relatively few fission gammas above about 4 Mev, an average value of 3 or 4 Mev is often used for approximate shielding calculations in the absence of detailed spectral information. This choice is usually conservative.

PROBLEM 11

A radiation shelter has uniform structural composition on all sides and on top. Its material composition is known together with the thickness of each component. It is exposed to radiation of known energy distribution. Find the average gamma ray transmission factor available within the shelter.

SOLUTION

1. Divide the thickness of each component material x, by the standard thicknesses x_s as given in Table 3.7:8.
2. From Table 3.7:8 read the standard thickness transmission factor T_{es} appropriate to each material and at each energy which is present in the spectral distribution.
3. For a given energy and material take the standard thickness transmission factor T_{es} and raise it to the x/x_s power where x/x_s is the number of standard thicknesses for this material as found in step 1. This is now the transmission factor T_{e1} for the actual thickness of the given material.
4. Repeat step 3 at the same energy for all other materials in the shield to obtain T_{e2}, T_{e3}, etc.
5. Multiply together all the values of T_{e1}, T_{e2}, T_{e3}, etc., found in steps 3 and 4 to obtain $T_{e(1,2,3,\ldots)}$ the over-all gamma ray transmission factor for the structure at the given energy.
6. Repeat steps 3, 4, and 5 for each other energy. The resulting numbers comprise a set of energy-dependent gamma transmission factors. These factors are weighted by the known gamma energy distribution to obtain the over-all transmission factor for the structure.

In general, instead of doing the computation in such detail, it will be done for only a single energy characteristic of the entire gamma energy spectrum. The energy-dependent set of transmission factors is not useful unless the radiation energy distribution is known. Such information will not generally be available, although it can be calculated approximately by the methods of Section 3.6.

Example

The walls and ceiling of a shielding structure are made of 2 in. of iron and 6 in. of sand. The gamma energy distribution is not known and a 3 Mev average energy is assumed in the absence of the spectral information. Find the gamma ray transmission factor of the structure.

1. From Table 3.7:8 the standard thicknesses of iron and sand are 1 in. and 1 ft, respectively. Thus, the structure is made up of two standard thicknesses of iron and one-half standard thickness of sand.
2. From Table 3.7:8 the transmission factors for standard thicknesses of iron and sand at 3 Mev are 0.65 and 0.15, respectively.
3. The gamma ray transmission factor for 3-Mev gammas and two standard thicknesses of iron is $(0.65)^2 = 0.42$.
4. The transmission factor for 3-Mev gammas and one-half standard thickness of sand is $(0.15)^{1/2} = 0.39$.
5. The transmission factor for the shelter is then (0.42) (0.39) = 0.16 when the gamma rays are assumed to be 3 Mev.

3.8 REFERENCES

1. H.K. Gilbert and E.B. Doll. ITR-1153. June 1955. (Secret)
2. J.S. Malik. LA-1620. Jan. 1954. (Secret)
3. H. Goldstein and J.E. Wilkins, Jr. NYO-3075. June 1954. (Unclassified)
4. D.C. Borg and C. Eisenhauer. AFSWP-502B. Jan. 1955. (Secret)
5. M. Ehrlich. WT-81. May 1952. (Secret)
6. E. Storm. WT-408. Mar. 1952. (Secret)
7. R.G. Larrick et al. WT-522. Sept. 1952. (Secret)
8. E. Storm. WT-549. July 1952. (Secret)
9. E. Storm. WT-201. June 1952. (Secret)
10. J.S. Malik. WT-634. Feb. 1954. (Secret)
11. R.G. Larrick. ITR-1115. May 1955. (Secret)
12. P.S. Harris and L.J. Vortman. SC 33-56-51. Feb. 1956. (Secret)
13. E. Storm. LASL. Private Communication. June 1955.
14. M. Ehrlich. NBS. Private Communication. June 1955.
15. P. Brown and G. Carp. ITR-913. May 1954. (Secret)
16. S. Glasstone et al. The Effects of Atomic Weapons. U.S. Government Printing Office. Sept. 1950. (Unclassified)
17. J.G. Graham and G. Carp. ITR-1118. May 1955. (Confidential)
18. C.F. Miller. AFSWP-895. Jan. 1955. (Secret)
19. J.S. Malik. WT-356. June 1956. (Secret)
20. M.G. Schorr and E.S. Gilfillan. WT-391. June 1952. (Secret)
21. H.F. Gibson et al. WT-76. Apr. 1952. (Secret)
22. J.W. Motz et al. WT-107. 1953. (Secret)
23. B.B. Kinsey et al. Can. J. Phys. 29.2. Jan. 1951. (Unclassified)
24. J. Moteff. APEX-176. Dec. 1954. (Unclassified)
25. J.R. Hendrickson et al. ITR-1121. May 1955. (Secret)
26. P.R. Cerar. WT-201. June 1952. (Secret)

[redacted]

Chapter 4

NEUTRON RADIATION

4.1 INTRODUCTION

Neutron radiation is emitted at the time of a nuclear explosion and adds to the gamma radiation dose discussed in Chapter 3, although it is usually smaller in magnitude. Neutron radiation is most important at short distances from the point of burst, when the burst is at high altitude, or when the weapon has a very thin casing. Under these circumstances, or combinations of such circumstances, the neutron dose may exceed the gamma dose.

Experimental data on neutron radiation were much less complete than on gamma radiation before the Teapot (1955) series of test bursts. The work of Harris[1] on the Teapot series, however, has considerably improved the situation and present results can now, with some reservations, be interpreted in terms of basic phenomenological theory which is well understood.

Section 4.2 presents a discussion of the mechanisms of neutron generation. Section 4.3 describes the experimental methods, both physical and biological, used for measuring neutron radiation effects and then presents a summary of the most significant experimental results. Section 4.4 derives the total flux-distance relations for neutrons for the most important situations and describes the scaling of these relations for various conditions. Some of this material is nearly the same as that given in Chapter 3. The major limitations of these relations are also discussed. In Section 4.5 dose-distance relations are provided for the prediction of total neutron dosage in most operational situations. It should be noted that the accuracy and scope of such predictions are limited by the inadequacy of the experimental methods and the incompleteness of the theory. Moreover, experimental measurements do not yield consistent results for all types of bursts and burst environments. Section 4.6 discusses the relative importance of neutron radiation as compared to the other mechanisms of bomb damage. Sections 4.7 and 4.8 provide limited information on the neutron energy spectra and delivery rates, respectively. Finally, Section 4.9 presents information on military shielding against neutrons. In this area current deficiencies of quantitative information are perhaps even greater than in the dose-distance relationships.

Throughout this treatment of neutron radiation the approach taken is to attempt to correlate, empirically, experimental results with simple theoretical calculations, rather than to attack the problem from the point of view of fundamental theory.

4.2 THEORY OF NEUTRON GENERATION

4.2.1 INFLUENCE OF WEAPON DESIGN

Neutron generation characteristics, specifically the neutron source strength and energy distribution, are controlled primarily by the weapon design. Three separate effects are involved.

1. The number of neutrons produced per KT and the initial energy spectrum depend on whether fusion or fission is the production process.

2. The number of neutrons absorbed by non-fission processes within the weapon is dependent on its design and construction. This dependence, characterized by the capture to fission ratio α, is not strong. The value of α [redacted] for weapons which have thus far been tested, most values clustering well within these limits.

3. The neutrons which are not captured in the weapon components will be degraded in energy in penetrating the weapon casing, especially when the latter contains hydrogenous material (such as high explosive). Asymmetries in the construction of the weapon will result in asymmetries in the flux or dose-distance relations.

The discussion of neutron generation which follows is therefore based on the classification of weapons as fission, boosted fission, and fusion.

4.2.2 FISSION WEAPONS

Neutrons are released from the weapon core as a result of the nuclear fission reaction, which occurs during the explosion of a fission weapon. Their number is given by $1.3 \times 10^{23} (\nu - 1 - \alpha) W$ where 1.3×10^{23} is the number of fissions per kiloton, ν is the average number of neutrons per fission ($\nu = 2.5$ for U^{235}, 2.95 for Pu^{239}), α is the ratio of the number of nonfission neutron captures in the weapon components (including the fissionable material) to the number of fission captures, and W is the fission weapon yield in KT.

Values of α have been calculated by Malik[2, 3] considering captures in the weapon core only and ignoring those ocurring in the high explosive shell. (High explosive is composed primarily of nitrogen and hydrogen; captures in the explosive occur predominantly in the nitrogen.) In the one specific case in which Malik makes an estimate, [redacted] of the neutrons born are captured in the high explosive. This is because the mean lifetime of the neutron in normal density high explosive [redacted] is much longer than the time required for the expansion of the weapon to a negligible density. Thus, most of the neutrons that enter the high explosive get through it without being captured.

The explosive may be very effective, however, in degrading neutrons in energy because of the large energy losses involved in collision with its hydrogen constituent. In some of the older weapons with very thick high explosive shells [redacted] most of the neutrons were probably slowed down all the way to velocities and energies characteristic of bomb thermal temperature (approximately 1 kev in energy). Bomb thermal temperature may be loosely defined as the temperature of the weapon components at a time just after completion of the nuclear reaction. The components have then expanded just enough so that the weapon reactivity has dropped below critical. The weapon diameter has approximately doubled in size by this time.

In the newer type weapons [redacted] the high explosive shell is much thinner and therefore less effective in degrading neutrons in energy. A substantial fraction of neutrons now appear outside the weapon at nearly fission neutron energies.

In a gun-type weapon high explosive is lacking except at the weapon ends. Fast neutrons escape most easily in the direction in which no high explosive is present. Thus, there occur asymmetries in the dose-distance relations which are not present in spherical implosion-type weapons. The fast neutron flux per unit energy yield for gun-type weapons is naturally higher than for spherical implosion weapons. [redacted]

The number of fast neutrons emerging from the weapon is, therefore, a rather strong function of weapon type. The total number of neutrons emerging from a weapon with a given fission yield, however, is less sensitive, depending only on α, which varies [redacted] (The few captures in the high explosive are ignored.)

[redacted]

4.2.3 BOOSTED FISSION WEAPONS

Boosted fission weapons are usually merely unboosted fission weapons to which a very small amount of deuterium has been added. The direct fusion yield from this deuterium is very small compared to the fission yield. About half of the fusion neutrons are very energetic (14 Mev), however, and they augment the fission yield appreciably by causing additional fissions to occur. Fusion neutrons are especially effective in causing fission[5,6] in U^{238}. The fission threshold energy for U^{238} is about 1.5 Mev and for this reason neutrons resulting from the fission process are quite ineffective in initiating fission in U^{238}.

The same general considerations discussed under fission weapons apply to the generation of neutrons in boosted fission weapons. The difference between the fission and boosted fission weapons of the same design is only that the yield of the boosted weapon may be appreciably higher and that the neutron spectrum may be very slightly higher, due to the presence of the relatively small number of 14-Mev fusion neutrons.

4.2.4 THERMONUCLEAR WEAPONS

For a given yield, thermonuclear weapons produce a larger number of neutrons (1.2 to 2.1 x 10^{24} *neutrons-KT*$^{-1}$) *than fission or boosted fission weapons* (~2.6 x 10^{23} *neutrons-KT*$^{-1}$). [redacted] The number of neutrons per KT of total yield will, therefore, be intermediate between the values given above; in addition, the neutron energy spectrum for thermonuclear weapons will be higher than for fission or boosted fission weapons. Due to reasons of security classification, details concerning the design and construction of thermonuclear weapons are unavailable and therefore no discussion of the neutron attenuation processes within the weapon is possible here.

4.3 EXPERIMENTAL METHODS AND RESULTS

The physical quantities of interest required to establish an understanding of neutron radiation effects include the total flux, the neutron energy spectra, the dose (in rep), and the delivery rate. The biological quantities of importance are the dose (in rem) for the specific biological effects of interest and the corresponding RBE. There are as yet no completely satisfactory methods of measuring any of these quantities and there are large gaps and inconsistencies in the available experimental data. It is of value, nevertheless, to describe the current experimental methods. The short summary which follows is intended to illustrate in broad outline these methods and the approximations and weaknesses inherent in much of the experimental data. It is not intended to be a textual introduction to the field of instrumentation for the study of neutron radiation.

Following the description of the methods of measurement, the most pertinent and reasonable of the experimental results are presented. This discussion leans heavily upon the Teapot test results of Harris[1] for fission and boosted fission weapons. The data for thermonuclear weapons are much less satisfactory.

4.3.1 PHYSICAL EXPERIMENTAL METHODS

Measurements of neutron flux and spectra have been performed primarily by activation detectors. These detectors depend on the conversion of certain elements into radioactive species as a result of neutron capture. Activation detectors are usually made in the form of thin foils or wafers and in this form are nearly isotropic in sensitivity to neutron direction. Neutrons which have a high energy at the source (relative to the particular detector) may, therefore, suffer one or more collisions in transit (with associated energy loss and change of direction) and still be detected, along with those neutrons that remain unscattered. If the value of the unscattered flux is desired separately, it can be obtained by the use of neutron-collimating systems in conjunction with the detector. In the absence of such collimating devices, activation detectors measure total flux (scattered and unscattered) in a specific energy range which depends on the detector.

[redacted]

Other devices have been used for neutron measurements with varying success, such as ionization chambers, fission fragment cameras, and germanium detectors.

Threshold Activation Detectors

An important class of activation detectors is known as threshold detectors. These detectors depend on a neutron reaction which will not occur except with neutrons above a specific non-zero energy. For threshold detectors the number of active atoms formed at the time of the bomb burst, therefore, is proportional only to that part of the neutron flux that is above the threshold energy. At later times the number of active atoms decreases at the rate characteristic of the particular reaction product. For irradiation times short compared to the mean life of the reaction product and for detectors small enough to avoid depression of the neutron flux the total number of active atoms in a threshold detector at time after burst t is

$$N = e^{-\lambda_d t} V \int_0^\infty \Sigma(E)\, \phi(E)\, dE \qquad (4.3:1)$$

where

λ_d = decay constant for the activated reaction product

$\Sigma(E)$ = macroscopic activation cross section

$\phi(E)$ = neutron flux per unit energy to which the detector was exposed

V = volume of detector

E = neutron energy

It is usually assumed that the activation cross section rises sharply at the threshold to some value and remains constant at this value above the threshold energy. Thus

$$\Sigma(E) \approx \Sigma \text{ for } E > E_{thr}$$

$$\Sigma(E) \approx 0 \text{ for } E < E_{thr}$$

where

E_{thr} = threshold energy

Σ = macroscopic cross section above the threshold energy

The total neutron flux ϕ above the threshold is then

$$\phi = \frac{N e^{\lambda_d t}}{V\Sigma} \qquad (4.3:2)$$

where

$$\phi = \int_{E_{thr}}^\infty \phi(E)\, dE \qquad (4.3:3)$$

The activity or rate of decay is related to the number of active atoms by the decay constant

$$A = \frac{dN}{dt} = \lambda_d N \qquad (4.3:4)$$

and therefore

$$\phi = \frac{A e^{\lambda_d t}}{\lambda_d V \Sigma} \qquad (4.3:5)$$

To determine the activity A the detector is placed in a predetermined position with respect to a conventional counting device. In many cases the detector is placed within the counter to avoid radiation losses in penetrating the counter window. Since the counting device is usually not 100 percent efficient, it measures a quantity A_c which is only a fraction of the detector activity A. Calibration of the detector-counter system is therefore required. This is performed by exposing an identical detector to an artificially produced neutron flux of known magnitude whose energy spectrum is as close as possible to that of the bomb radiation. (A nuclear reactor is generally used for this purpose to simulate bomb fission neutrons. To simulate 14-Mev bomb fusion neutrons a high energy particle accelerator is used to bombard a suitable target.)

Further adjustments in the calculation must be made in some situations, for example when the decay constant λ_d is so large that the activity will change appreciably during the time of measurement.

The most commonly used threshold detectors are discussed individually below and are listed in Table 4.3:1 together with the threshold energy and the nuclear reaction involved.

The most reliable of the threshold detectors in past experimental tests has been sulphur (3 Mev threshold).[7,8] Fission threshold detectors have only recently proven successful for detection of neutron radiation of intermediate energies.[1,31] Early results showed rather poor consistency.[9,10] Pu^{239}, when shielded against thermal neutrons by 2 cm of boron, measures the neutron flux above about 4 kev. The effective threshold can be varied somewhat by changing the thickness of the boron absorber. Np^{237} has a threshold at about 750 kev and U^{238} has a threshold at about 1.5 Mev. (Using U^{238} detectors, one must carefully avoid contamination of the U^{238} by U^{235}.) A complication resulting from the use of fission threshold detectors is brought about by the formation of many different active fission products, each of which follows its own exponential decay rate. The gross fission products decay at an over-all rate which is then the sum of a number of exponentials. Procedures for fission threshold detectors must be modified accordingly. This may be done by replacing the exponential in Eq. 4.3:5 by another time-dependent function determined experimentally from gross fission product decay. Alternatively one might measure the activity of two similar detectors, one exposed to the known flux used for calibration and the other exposed to the unknown flux, at equal times after exposure. (The energy spectra of the two fluxes should be closely similar.) The unknown flux would then be simply

$$\phi = \phi_k \frac{A_{cu}(t)}{A_{ck}(t)} \qquad (4.3:6)$$

where

ϕ_k = total known neutron flux used for calibration

$A_{cu}(t)$ = activity of detector exposed to unknown flux as measured by counter at time t

$A_{ck}(t)$ = activity of detector exposed to known calibration flux as measured by counter at time t

Such a procedure is, of course, also applicable to nuclear reactions where the product follows the exponential decay law.

TABLE 4.3:1

Characteristics of Neutron Threshold Detectors

Detector	Threshold Energy	Reaction[1]
Pu^{239}	4 kev[2]	$_{94}Pu^{239} + {}_0n^1 \rightarrow$ Fission products*[3] + prompt neutrons Fission products* $\rightarrow$ Fission products + delayed neutrons + beta and gamma radiation
Np^{237}	750 kev	$_{93}Np^{237} + {}_0n^1 \rightarrow$ Same as above
U^{238}	1.5 Mev	$_{92}U^{238} + {}_0n^1 \rightarrow$ Same as above
S^{32}	3 Mev	$_{16}S^{32} + {}_0n^1 \rightarrow {}_{15}P^{32*} + {}_1p^1$ $_{15}P^{32*} \xrightarrow{14.3 \text{ days}} {}_{16}S^{32} + {}_{-1}\beta^0$
I^{127}	9.5 Mev	$_{53}I^{127} + {}_0n^1 \rightarrow {}_{53}I^{126*} + 2\,{}_0n^1$ $_{53}I^{126*} \xrightarrow{13 \text{ days}} {}_{54}Xe^{126} + {}_{-1}\beta^0$
As^{75}	10.5 Mev	$_{33}As^{75} + {}_0n^1 \rightarrow {}_{33}As^{74*} + 2\,{}_0n^1$ $_{33}As^{74*} \xrightarrow{17.5 \text{ days}} {}_{34}Se^{74} + {}_{-1}\beta^0$ (53%) $_{33}As^{74*} \xrightarrow{17.5 \text{ days}} {}_{32}Ge^{74} + {}_{+1}\beta^0$ (47%)
Zr^{90}	12.5 Mev	$_{40}Zr^{90} + {}_0n^1 \rightarrow {}_{40}Zr^{89*} + 2\,{}_0n^1$ $_{40}Zr^{89*} \xrightarrow{33 \text{ days}} {}_{39}Yt^{89} + {}_{+1}\beta^0$

(1) Symbols used are ${}_0n^1$ (neutron), ${}_1p^1$ (proton), ${}_{-1}\beta^0$ (electron), and ${}_{+1}\beta^0$ (positron).

(2) Pu^{239} shielded by 2 cm of boron has a threshold energy of approximately 4 kev.

(3) The * is used to indicate that the atom or atoms are in an unstable state.

Zirconium has proven particularly useful for measuring the flux of 14-Mev fusion neutrons by means of the (n, 2n) reaction which has a 12.5 Mev threshold. Such (n, 2n) reactions usually suffer from competition from a (γ, n) reaction which yields the same activated product. This can be compensated for by exposing both unshielded and lead-shielded zirconium detectors. There are other competing reactions; to eliminate them, advantage may be taken of the characteristic positron emission of the zirconium (n, 2n) reaction by using a coincidence spectrometer, which registers only positrons.

Arsenic (10.5 Mev threshold) and iodine (9.5 Mev threshold) also depend on (n, 2n) reactions and suffer from (γ, n) competition. They have been successfully used, however, for instance at Tumbler-Snapper.[5]

Other Activation Detectors

Not all activation detectors are threshold detectors. Certain activation detectors are used to determine the neutron flux below a given energy (the cutoff energy). These detectors are usually exposed to the neutron flux in pairs, one detector bare and the other shielded by a material with a sharp

neutron cross-section resonance to define the cutoff energy. These materials are opaque to neutrons with energies below the resonance but transparent to those with energies above the resonance. (The high cross-section materials commonly used for this purpose are cadmium and indium.)

The number of active atoms in the bare and shielded detectors at time t after exposure to a short duration neutron flux are

$$N_b = e^{-\lambda_d t} V \int_0^\infty \Sigma(E)\, \phi(E)\, dE$$

$$N_s = e^{-\lambda_d t} V \int_{E_c}^\infty \Sigma(E)\, \phi(E)\, dE \qquad (4.3:7)$$

where

N_b = total number of active atoms formed in the bare detector

N_s = total number of active atoms formed in the shielded detector

E_c = cutoff energy

If a proper average value of the cross section $\bar{\Sigma}$ is known for the energy region below E_c, then the total flux in this region is

$$\phi = \frac{(N_b - N_s)\, e^{\lambda_d t}}{V\bar{\Sigma}} = \frac{(A_b - A_s)\, e^{\lambda_d t}}{\lambda_d V\bar{\Sigma}} \qquad (4.3:8)$$

where

A_b = activity of the bare detector

A_s = activity of the shielded detector

More often the correct average cross section is not known and it is necessary to assume a value from which a corresponding value of the flux is calculated.

The activation detector of this type which is of most interest and which has the best reliability is gold, used with and without cadmium shielding. The gold-cadmium detectors are used to measure thermal neutrons; the average value of the gold cross sections usually being taken as the thermal cross section.

Deficiencies of Activation Detectors

The several deficiencies of activation detectors are listed below. Not all of these deficiencies apply to every type of detector, however.

1. The active isotope may be produced by competing reactions which obscure the neutron capture reaction.
2. The lifetime of the radioactive products may be quite short. Gold with a 2.7-day half life may be taken as a particular example.

3. Activation detectors usually employ isotopes with cross sections which are rather complicated functions of energy. Since the flux is usually calculated by assuming the cross section is constant over some well-defined energy range and zero elsewhere, the result is inherently inaccurate to some degree.

Previous to the Teapot test series, sulphur (above 3 Mev) and gold (thermal) detectors were the most reliable of the activation detectors. These detectors completely miss, however, the energy region of greatest biological interest, which lies at about 1 Mev. The Teapot tests[1] (low yield weapons) successfully utilized the fission threshold detectors to cover this energy gap. Fission detector data on high yield weapons[9, 10] are in a much less satisfactory state.

Other Detector Types

In addition to activation detectors, attempts have been made to utilize several other devices to detect weapon neutrons. Ionization chambers[1] and germanium detectors have been tried, but thus far without yielding fully satisfactory results. Ionization chambers can be made roughly tissue-equivalent; they would, in principle, then measure the dose directly in rep. One disadvantage of ionization chambers is that they have a limited range of sensitivity and thus are useful only for neutron fluxes within a restricted range of intensities.

The conductance characteristics of germanium are altered by exposure to fast neutrons, but are essentially unaffected by gammas. Calibration of germanium detectors, however, is difficult.

Neutron delivery rate data are available for only a few bursts and usually only at one station.[2, 3, 5, 11] Delivery rates have been studied by means of fission fragment catcher cameras and ionization chambers containing fissionable materials. In the camera a cellophane ribbon is passed at constant speed in front of a mass of fissionable material. The ribbon collects fission fragments whose activity at any location is proportional to the neutron delivery rate. In the ionization chamber, the fissionable material is usually coated on one of the plates. The fission fragments cause an ionization current proportional to the rate of fission within the chamber and, in turn, to the neutron delivery rate.

In either of these devices if the fissionable material is U^{235}, only the slow neutron delivery rate is measured, since the U^{235} fission cross section is largest at low energies. If U^{238} is used, the delivery rate of neutrons above a threshold energy of approximately 1.5 Mev is measured. The U^{238} is customarily shielded by cadmium in order to eliminate fissions in the U^{235} impurity which is inevitably present.

Although experimental data on delivery rates for intermediate energy neutrons are lacking, the experiments using U^{238} do set upper bounds on the time of neutron arrival, since high energy neutrons will certainly arrive before the intermediate energy neutrons.

4.3.2 BIOLOGICAL EXPERIMENTAL METHODS

For convenience we repeat here some necessary definitions which are important to an understanding of biological damage due to neutrons and of the experimental procedures for measuring such damage.

A roentgen equivalent physical or rep is defined as that amount of ionizing radiation of any type which, when absorbed in one gram of organic tissue, will deposit 93 ergs of energy.

A roentgen equivalent man (or mammal) or rem is defined as that amount of ionizing radiation which, when absorbed in mammalian tissue, will cause the same biological damage as the absorption of one rep of 400-kev gamma radiation. Naturally, this unit is dependent on the particular biological effect chosen. It may be lethality, drop in white blood cell count, weight loss of the spleen and/or thymus gland at the end of a specified time, whole body weight loss, cataract formation or any other chosen effect. Those mentioned are the most common.

The relative biological effectiveness or RBE is defined as the ratio of the dose in rem to the dose in rep. The value of the RBE thus depends on the biological effect chosen and for neutrons also depends upon the energy spectrum.

An example of the relationships between these quantities may clarify their meaning. A specific biological effect of a given neutron dosage is found to be the same as that from 150 rep of 400-kev gamma rays. The biological neutron dose is then known to be 150 rem. If the physical neutron dose is known to be 100 rep, the RBE is 1.5.

The biological dosimetry experiments[1, 12, 13, 14, 15] which have been conducted at the various bomb tests have generally used mice for reasons of convenience. (Other animals such as monkeys, dogs, hamsters, rabbits, etc., have also been used on occasion.) The biological effects chosen for study included weight loss of the spleen and/or thymus after 5 days, the drop in the white blood cell count, the whole body weight loss, and the survival time (for doses in the supralethal range). Spleen and/or thymus weight loss experiments using mice produced the most consistent and easily interpretable results. For illustrative purposes these experiments will be described below, although the methods discussed could be applied to any other experimental animal and chosen biological effect.

The mice were exposed at ground level beneath 7 in-thick lead hemispheres. The lead served to shield out gamma radiation which in most cases would have contributed the larger dose. (The use of the shields still does not provide completely clear-cut results, since lead degrades the incident neutron energy spectrum. In addition, there is a residual gamma dose inside the hemispheres due to gamma rays generated in the lead by the inelastic scattering of fast neutrons.) Together with the mice, activation detectors were placed under the lead to allow determination of the neutron dose in rep. Finally the relationship between gamma dose in rep and biological damage was determined by exposing mice of the same genetic and physical characteristics to known doses of 400-kev gamma rays. The animals were sacrificed and the spleen and thymus weight loss measured.

A comparison of the 400-kev gamma dose (in rep) and the neutron dose (in rep) which each produced the same spleen-thymus weight loss yields the neutron dose (in rem). This is simply equal numerically to the 400-kev gamma dose (in rep). The RBE is then the ratio of the neutron dose (in rem) to the neutron dose (in rep).

4.3.3 EXPERIMENTAL RESULTS

Fission and Boosted Fission Weapons

Early work[12, 13, 14] on fission and boosted fission test bursts used sulphur and gold activation detectors. The experimental results were highly scattered and exhibited some logical inconsistency in the correlation of biological dose with the results of the physical measurements.

The work of Harris[1] at the Teapot test series, if it proves to be reproducible, will have resolved many of the questions raised by the earlier results. For fission and boosted fission weapons, his work has experimentally established invariance of the shape of the neutron flux energy spectrum with distance from the point of burst and within the energy range of interest. Thus, this invariance does not include thermal neutrons and probably not the 14-Mev neutrons from fusion in boosted fission weapons. For an invariant energy spectrum the dose (in rep) is proportional to the total flux in any arbitrarily specified energy range independent of distance. (The fact that the thermal flux is not included in this invariance is not overly important since, as will be demonstrated below, its contribution to the total dose is relatively small. Similarly, the 14-Mev neutrons from boosted fission weapons, while individually quite damaging, are not present in sufficient number to make an important contribution to the total dose.) The spectral invariance has been demonstrated to hold from 200 to 1500 yd for Teapot tower shots. There would appear to be no obvious reason why it should not hold for larger distances as well.

The physical measurements of flux were made using gold, plutonium, neptunium, uranium, and sulphur activation detectors. Semilog plots of $R^2\phi$ as a function of R for each of these detectors except gold were very satisfactorily parallel.

Table 4.3:2 presents recommended[1] values of the factors used to convert the neutron flux within specified energy ranges to dose (in rep). For convenience the limits of the energy ranges chosen

correspond to the energy limits of the pertinent activation detectors from thermal energy (gold) to 12.5 Mev (zirconium). These conversion factors were computed theoretically from first collision theory.

From these conversion factors and the flux measurements from the appropriate activation detectors, Harris was able to compute, as a function of distance, the dose (in rep), both total and within the specified energy ranges.

It is seen that for fluxes of the same order of magnitude the thermal neutron dose (in rep) may be neglected in comparison to the higher energy dose. Thus, to produce a dose of a given number of rep requires a thermal neutron flux about 20 times as large as the Pu-Np flux (4 kev to 0.75 Mev) and 55 times as large as the S-Zr flux (3 to 12.5 Mev). In general the thermal flux resulting from a bomb burst is comparable in magnitude to the total non-thermal flux[1] and the dose due to thermal neutrons can therefore be ignored.

TABLE 4.3:2

Neutron Flux-Dose Conversion Factors[1]

Neutron Energy Range	Detectors	Conversion Factors, rep-cm^2-neutron^{-1}
Thermal	Gold	2.9×10^{-11} [31]
4 kev to 0.75 Mev	Pu^{239}-Np^{237}	1.0×10^{-9}
0.75 Mev to 1.5 Mev	Np^{237}-U^{238}	2.5×10^{-9}
1.5 Mev to 3.0 Mev	U^{238}-S^{32}	3.2×10^{-9}
3.0 Mev to 12.5 Mev	S^{32}-Zr^{90}	3.9×10^{-9}
> 12.5 Mev	Zr^{90}	6.5×10^{-9} [16]

Zirconium detectors (12.5-Mev threshold), customarily used to measure the 14-Mev neutrons from fusion, were not employed at Teapot. Therefore, the energy distribution of neutrons above 3 Mev from boosted fission weapons and the variation of this distribution with distance was not observed at the Teapot series. However, previous test data have invariably shown the apparent mean free path for zirconium neutrons to be shorter than that for the corresponding sulphur neutrons[5] and thus spectral invariance is not expected to hold for the portion of the spectrum due to 14-Mev fission neutrons in boosted weapons. The number of these high energy neutrons is small compared to the number of fission neutrons and their effect is not expected to be significant.

Along with the physical measurements made at Teapot, the biological damage of bomb neutrons to mice under lead shields was measured in terms of rem (spleen-thymus weight loss criterion) by the methods described in Section 4.3:2. Then, knowing the neutron dose as a function of distance in both rem and rep, the mouse spleen-thymus RBE was determined.

Previous experimental studies on the biological effects of radiation have established the following basic facts on the relationships between physical and biological dose due to neutrons and gammas.

1. Any specific biological effect, such as mouse spleen-thymus weight loss, increases monotonically with both neutron and gamma doses.
2. The biological damage, measured by any specific criterion, for a given gamma dose is approximately independent of the gamma energy spectrum for all energies greater than 100 kev. This situation does not hold for neutrons where, for a given neutron dose, the biological damage does vary with the neutron energy spectrum.

[redacted]

3. In general, a given neutron dose (in rep) does not do the same amount of biological damage as a numerically equal gamma dose (in rep). Of course the given value of the neutron dose may result from a wide variety of neutron spectra but the non-equality of biological damage due to an equal dose of neutrons and gammas appears to hold for all bomb neutron spectra of interest.

4. For any constant neutron spectrum the neutron dose (in rep) which produces a given amount of biological damage, using any specific damage criterion, is proportional to the gamma dose (in rep) which produces the same amount of biological damage. The factor between neutron and gamma dose (in rep) appears to remain constant over the entire sublethal and lethal dose range.

5. The RBE for neutrons is defined as the neutron dose (in rem) over the neutron dose (in rep). Further, the neutron dose (in rem) is equal to the gamma dose (in rep) which does the same biological damage. Thus from (4) the neutron RBE for specific biological effects and for a constant neutron energy spectrum is constant within the sublethal and lethal dose range.

The results of Harris at Teapot are consistent with the paragraphs above. For the unboosted weapons tested (and therefore for the particular approximately invariant neutron energy spectrum associated with unboosted fission weapons) the mouse spleen-thymus RBE was found to be quite constant and equal to 1.7, over the dose range 100 to 1,000 rem.[1] (As pointed out later, this is not the value recommended for human use.) This value is considerably lower than the values 5 to 20 in other experiments and for other damage criteria, particularly cataract formation. As the dose increases into the supralethal range, the value of the RBE decreases. Thus at 10,000 rem the mouse spleen-thymus RBE seems to drop to about 1.2 and at still higher supralethal doses it drops to as low as 0.6 in some cases. The implication seems to be that some sort of saturation effect occurs for supralethal doses.

The Teapot series included [redacted] The spectrum from these boosted weapons was somewhat different from the unboosted fission weapons (see Section 4.7). The effect of the difference in spectrum is probably not large, however, and the mouse spleen-thymus RBE for boosted fission weapons is thought to be only slightly different than that for unboosted fission weapons.

The RBE depends not only on the damage criterion but also on the mammal involved. Extrapolation of mouse spleen-thymus data to man inevitably involves serious approximations. One important consideration in such extrapolation is the self-shielding property of large bodies. A mouse is essentially a thin film for neutrons but man's internal organs are somewhat protected by the thickness of his outer surfaces. For this reason the use of 1.3 as spleen-thymus weight loss RBE for man is recommended.[16,17]

Other organs, the eye for instance, may be more sensitive to neutrons and the RBE for cataract formation is larger. The RBE of 1.3 is, however, recommended for acute response to neutron radiation in situations of military operational significance.

Several other results of the Teapot experiments are worth noting.

1. Activation detectors were placed both inside and outside the lead shields used to protect the mice from gamma rays. The neutron dose (in rep) inside the shields was found to be 50 percent of that outside.

2. The gamma dose (in rep) inside the shields was only 7 to 10 percent of the total dose and thus did not interfere appreciably with interpretation of neutron damage.

3. The gamma dose inside the shield was shown to result from inelastic scattering of neutrons. This was indicated by the fact that the gamma dose within the shield decreased with distance from the point of burst with an apparent mean free path characteristic of the bomb neutrons rather than of the bomb gammas. (The bomb gamma apparent mean free path is considerably longer than that for bomb neutrons.)

[redacted]

4. When the neutron dose is below the saturation level, the neutron and gamma radiation doses (both in rem) appear to be additive to within the limits of experimental error. It may be presumed that there is also a saturation effect for gammas somewhere in the high dose region and that the Teapot gamma doses were below this level. There is little experimental evidence available on this point.

5. The value of 700 ± 160 rem is recommended as the neutron LD_{50} dose for mice. (LD_{50} is the dose which will be fatal to 50 percent of the irradiated population.) This number is the subject of some controversy and must be considered uncertain. (See Section 2.4.1).

Of the several Teapot test results the one of most significance would appear to be the invariance of the flux energy spectrum with distance. This result represents a very important simplification in the prediction of neutron dosage. At the present time, however, the principle of spectral invariance should be regarded as tentative since it is possible that eventual improvement of the measurements may destroy the simplicity of the concept and thus increase the complexity of neutron dose calculations.

In the following sections, the principle of spectral invariance will be used to the fullest extent and will be assumed to hold for all distances. Further, the Teapot results in general will be used as the basis for calculation of neutron doses for all fission and boosted fission weapons. This seems to be the most reasonable approach to take in the light of our present understanding.

Fusion Weapons

Present evidence seems to indicate that the spectral invariance of the neutron flux does not apply to high yield (thermonuclear) weapons. The Teapot tests did not include any fusion weapons and existing data[9,10] for such weapons are much less complete and consistent than for the Teapot series. The phenomenological approach of Brode[18] will be followed in the treatment of fusion weapons.

4.4 FLUX-DISTANCE RELATIONS

There is at present no single theoretical or empirical flux-distance relation which treats all weapon designs and the entire neutron energy range. Relations which hold for one weapon type and energy range do not necessarily hold for another design and energy range. It is necessary, therefore, to analyze each class of weapons and its associated neutron characteristics separately; this is the approach that is followed below. Both theoretical arguments and experimental results are used in deriving the several flux-distance relations but in all cases their approximate nature should be fully appreciated.

The variation in neutron behavior for different weapon types results from the very wide spread of possible neutron energies. Thus, the highest energy neutrons are at about 14 Mev and result from the fusion reaction. Most of the fission neutrons emerge from the weapon in the range between about 4 Mev and 1 kev. These relatively high energy neutrons then slow down as a result of collision with the surrounding media and are eventually captured. A large number of neutrons are slowed down all the way to thermal energy (about 0.025 ev) and diffuse at this energy before capture. Thus the ratio of high to low neutron energy at a given receiver may be as large as 10^9.

The actual neutron spectrum and flux at the receiver are strongly dependent on the neutron characteristics at the source and, therefore, on the weapon design. The specific design characteristics of importance are the total yield, [redacted] and the neutron attenuation produced by the weapon components. The differences between the flux-distance relations given in this section are more probably caused by [redacted] and in the neutron attenuation due to weapon components than by variations in the weapon yield. The first two factors determine the energy spectrum of neutrons emerging from the weapon. The only effect of variation in the weapon yield (in the absence of the blast wave or hydrodynamic effect on the attenuating media - see Section 4.8) is a corresponding linear variation in the intensity of the neutron flux.

In the treatment that follows, flux-distance relations are presented for fission/boosted fission and fusion weapons separately. Further, an additional broad classification is made on the basis of neutron energy. Neutrons are considered to be thermal (those measured by gold detectors) and non-thermal (those measured by plutonium or higher threshold-energy detectors). This distinction is made because of the major differences in the behavior of thermal and non-thermal neutrons and because of the negligible thermal neutron contribution to the dose (in either rep or rem). In fact, the flux-distance relations for thermal neutrons are of little practical importance and are presented primarily for completeness and because they have in the past been useful for analyzing results from the older-type fission weapons. No flux-distance relation is presented for thermal neutrons from fusion weapons.

4.4.1 NON-THERMAL NEUTRONS FROM FISSION AND BOOSTED FISSION WEAPONS

For fission and boosted fission weapons, and those with thick and thin high explosive casings, the neutrons that determine the character of the biologically important portion of the flux are those that start from the point of burst in the Mev range and reach the receiver before slowing down to thermal. Analysis of weapon test results indicates that to a reasonably good approximation the flux-distance relation for these non-thermal neutrons from fission and boosted fission weapons can be represented by an equation of the form resembling that used for unscattered neutrons from a point source.

The flux of unscattered neutrons from a monoenergetic point source in an infinite homogeneous medium and integrated over all time, is given exactly by

$$\phi_u = \frac{S}{4\pi R^2} e^{-\mu_t R} \qquad (4.4:1)$$

where

S = source strength, total number of neutrons produced

R = distance from source to detector

μ_t = total linear attenuation coefficient for neutrons at the source energy

Similarly, the total non-thermal neutron flux (scattered and unscattered) from the polyenergetic source of weapon neutrons, again in an infinite homogeneous medium and integrated over all time, has been found to be given approximately by

$$\phi = \frac{S}{4\pi R^2} e^{-\mu R} = \frac{S}{4\pi R^2} e^{-\frac{R}{\lambda}} \qquad (4.4:2)$$

where

μ = apparent linear attenuation coefficient

λ = apparent mean free path.

The value of μ may be considerably smaller than that of μ_t. It may be useful to think of Eq. 4.4:2 in terms of the buildup factor discussed in Chapter 3. The buildup factor for non-thermal neutrons from fission and boosted fission weapons is then

$$e^{-(\mu - \mu_t)R}$$

a form which has some theoretical justification.[19]

Despite the fact that Eq. 4.4:2 is only an approximation, when appropriate values of S and μ are empirically chosen for the particular circumstances, it fits experimental non-thermal flux-distance data over a wide range of conditions; semi-log plots of $R^2\phi$ as a function of R usually give good straight line fits. Eq. 4.4:2 fits both fission and boosted fission results and further both thick and thin casing weapons of each type. This appears to be true even though what information is available shows a wide spread of neutron energies from these weapons and some variation in the energy spectra between types (see Section 4.7).

As pointed out in Section 4.3:1 non-thermal neutron flux measurements are usually made with threshold activation detectors. This type of detector measures the total flux above a prescribed threshold energy. The agreement of Eq. 4.4:2 with experimental results seems to hold not only for the total non-thermal flux but also for the portions of the flux above the individual threshold energies.

There are some circumstances in which Eq. 4.4:2 does not appear to hold. Thus, it has been noted previously that it does not apply to thermal neutrons. It also does not seem to fit the very high energy (14-Mev) fusion neutrons. Finally it should not be used for distances too close to the source point, since it holds best for measurements at some distance, that is for $\mu R >> 1$.

Some experimental data for non-thermal neutrons have been analyzed using a summation of several terms[5] such as given in Eq. 4.4:2 but with different values of S and μ in each term. The several terms then represent different neutron energy groups. Such superpositions can usually be approximated well enough by the single term of Eq. 4.4:2 with average values of S and μ characteristic of the entire spectrum.

4.4.2 NON-THERMAL NEUTRONS FROM FUSION WEAPONS

Fusion weapons produce large numbers of 14-Mev neutrons from the DT reaction. Because of their high energy and abundance as compared to fission neutrons (with an average energy of about 1 Mev), these 14-Mev neutrons characterize the flux of biological importance for fusion weapons.

The few neutron flux measurements that are available from fusion weapons are only poorly fitted by Eq. 4.4:2. The reasons for this difference in behavior are not definitely known but several possibilities can be suggested. In the higher energy range (above 5 Mev) inelastic scattering is likely to be an important mechanism for neutron slowing-down, while for fission neutrons elastic collision is the primary mechanism. Inelastic collisions will degrade neutrons in energy much more rapidly than elastic collisions and change the flux-distance relation correspondingly.

Also, Eq. 4.4:2 is known to be a poor approximation for small values of μR, even for fission neutrons. Since μ generally becomes smaller at large neutron energies[5, 9, 10] deviations from Eq. 4.4:2 at any fixed R are expected to be greater for the case of thermonuclear weapon bursts with their large 14-Mev component. Finally, the blast wave or hydrodynamic effect, if it is significant, would be greatest for the fusion (high yield) weapons, whereas its effect would be much less and probably negligible for the low and intermediate yield fission and boosted fission weapons.

A revised relation which better fits experimental data from the Castle series of fusion weapon tests has been devised empirically by Brode.[18]

$$\phi = \frac{S}{4\pi R^2} e^{-R\frac{\mu_1\mu(R^2 + R_1^2)}{\mu_1 R^2 + \mu R_1^2}} = \frac{S}{4\pi R^2} e^{-\frac{R(R^2 + R_1^2)}{R^2\lambda + R_1^2\lambda_1}} \qquad (4.4:3)$$

where the constants μ_1, μ, and R_1 are adjusted to fit the experimental results. This equation has the special property that

$$\phi \approx \frac{S}{4\pi R^2} e^{-\mu_1 R} \quad \text{for } R \ll R_1$$

$$\phi \approx \frac{S}{4\pi R^2} e^{-\mu R} \quad \text{for } R \gg R_1 \qquad (4.4:4)$$

Experimental results indicate that the apparent mean free path for short distances (λ_1) is considerably longer than that for large distances (λ).

4.4.3 THERMAL NEUTRONS FROM FISSION AND BOOSTED FISSION WEAPONS

As previously noted, thermal neutrons are of less interest that the higher energy neutrons. Nevertheless, a relation for thermal neutrons from fission and boosted fission weapons is sometimes used to analyze radiation effects. The relation usually used gives the flux as a function of distance from a point source of monoenergetic non-thermal neutrons which slow down, in an infinite homogeneous medium, according to Fermi age theory. By a simple integration the thermal flux may be shown to be[2, 20]

$$\phi = \frac{S e^{K^2\tau}}{4\pi dR}\left[\frac{e^{-KR}}{\sqrt{\pi}} \operatorname{erfc}\left(\frac{-R + 2K\tau}{2\sqrt{\tau}}\right) - \frac{e^{KR}}{\sqrt{\pi}} \operatorname{erfc}\left(\frac{R + 2K\tau}{2\sqrt{\tau}}\right)\right] \qquad (4.4:5)$$

where

$$\operatorname{erfc} x = \int_x^\infty e^{-y^2}\, dy \text{ (x and y serve only to define the erfc function)}$$

S = source strength, total number of monoenergetic non-thermal neutrons produced

τ = average Fermi age at which the non-thermal neutrons either become thermal or are captured

d = diffusion coefficient for thermal neutrons

K = reciprocal of the diffusion length for thermal neutrons.

For $R \gg K\tau$ and $R \gg \sqrt{\tau}$ this simplifies to

$$\phi = \frac{S e^{K^2\tau}}{4\pi dR} e^{-KR} \qquad (4.4:6)$$

Equations 4.4:5 and 4.4:6 have been most useful in gaining an understanding of thermal neutron flux measurements due to bursts of the older-type fission and boosted fission weapons.[21] They should, however, be applied with great caution to the most recently designed fission/boosted fission weapons.

The thick explosive casings of the older type weapons degraded most neutrons to energies approaching those characteristic of bomb thermal temperature (1 kev). Thus, the major source of thermal neutrons is very crudely monoenergetic and of relatively low energy. For low energy neutrons the distance traveled while diffusing at thermal energies is significant compared to the distance traveled while slowing down to thermal. Under these circumstances the thermal neutron flux should follow Eq. 4.4:5 or 4.4:6 for small and medium distances from the source.

The newer weapon designs, on the other hand, have thin casings and the emerging neutrons are spread over a wide energy range. They are, on the average, of higher energy, therefore, and travel a short distance while diffusing as compared to the distance traveled while slowing down. Most of the neutrons may be expected to penetrate the high explosive casing while still fast and to remain fast through the intervening air until they are close to the point of capture. (The neutron mean free path is longest at high energy). They then suffer their first collision, slow down to thermal, and are captured, all in the close vicinity of the point of first collision. The spatial distribution of the thermal neutron flux should then follow[2] that of the non-thermal flux (Eq. 4.4:2) and Eqs. 4.4:5 and 4.4:6 do not seem applicable, particularly at any appreciable distance from the source. If Eq. 4.4:5 or Eq. 4.4:6 applies at all in these circumstances, it would apply only for distances relatively close to the source.

The common practice of analyzing thermal neutron flux data by the use of semi-log plots of $R\phi$ rather than $R^2\phi$, therefore, seems debatable at least in some cases,[22] i.e., for fission weapons with thin high explosive shells and at large distances from the point of burst.

4.4.4 EFFECT OF VARIATIONS IN ATMOSPHERIC DENSITY AND HUMIDITY

The atmosphere is not, of course, as assumed for the flux-distance relations given above, an infinite homogeneous medium. Atmospheric density and humidity both vary with position and both characteristics affect the neutron attenuation properties.

Air density varies roughly exponentially with altitude. The preceding relations remain good approximations in spite of this variation if, as in Chapter 1, factors like $e^{-\mu R}$ are replaced by appropriate average values.

$$e^{-\mu R} = e^{-\int_0^R \mu dx} = e^{-\bar{\mu} R} \qquad (4.4:7)$$

Also since

$$\mu = \rho \mu_0 \qquad (4.4:8)$$

$$e^{-\rho \mu_0 R} = e^{-\mu_0 \int_0^R \rho dx} = e^{-\bar{\rho} \mu_0 R} \qquad (4.4:9)$$

where

μ = apparent linear attenuation coefficient for air

μ_0 = apparent linear attenuation coefficient for air at density d_0

$\bar{\mu}$ = average apparent linear attenuation coefficient for air between point of burst and receiver

ρ = air density expressed in units of d_0

$\bar{\rho}$ = average air density between point of burst and receiver, expressed in units of d_0

d_0 = density of pure dry air at standard conditions (1.293×10^{-3} gm-cm^{-3})

Methods of calculating $\bar{\rho}$ have been described in Section 1.8. Taking the variation of air density into account Eq. 4.4:2 then becomes

$$\phi = \frac{S}{4\pi R^2} e^{-\mu_0 \bar{\rho} R} = \frac{S}{4\pi R^2} e^{-\frac{\bar{\rho} R}{\lambda_0}} \qquad (4.4:10)$$

where

λ_0 = apparent mean free path for neutrons in air at standard conditions

Similar substitutions can be made in the other flux-distance relations.

The composition of air also varies but to a lesser degree. While the ratio of oxygen to nitrogen content remains fixed, the relative concentration of water vapor may vary considerably from point to point. This is of some small importance in the slowing down and diffusion of neutrons. The properties of moist air differ from those of dry air because of the hydrogen content of water, a collision with hydrogen involving a much larger energy loss than collisions with either oxygen or nitrogen.

The equilibrium vapor pressure of water at 30°C (100°F) is, however, only about 50 mm of mercury or 6.5 percent of standard atmospheric pressure. This represents 100 percent relative humidity; in most cases the relative humidity and, therefore, the water vapor content are considerably less. Approximate estimates have indicated that, under typical conditions at sea level, water vapor changes the apparent mean free path of neutron radiation by only about 2 percent. Thus, at least at sea level, water vapor plays a minor role, and may usually be neglected. At higher elevations this may be less true.

The interpretation of present experimental data is that perturbations of the flux due to atmospheric water vapor content are much less than the errors in the measurements themselves. The effect of water vapor content will, therefore, be neglected.

4.4.5 SCALING RELATIONS FOR VARIATION OF AVERAGE QUIESCENT AIR DENSITY AND WEAPON YIELD

Experimental data from weapon test bursts cannot be applied directly to situations far different than those of the original test. They cannot be applied, in particular, to situations where the average quiescent air density between the point of burst and the receiver varies markedly from that of the original test. When the data are fitted to flux-distance relations such as Eqs. 4.4:2 to 4.4:6 they can, however, be scaled for such variations. This is possible because the attenuation coefficients and similar quantities appearing in the several flux-distance equations are either directly or inversely proportional to air density.

$$\begin{aligned} \mu &= \rho \mu_0 \\ d &= \frac{1}{\rho} d_0 \\ K &= \rho K_0 \\ \tau^{\frac{1}{2}} &= \frac{1}{\rho} \tau_0^{\frac{1}{2}} \end{aligned} \qquad (4.4:11)$$

Thus, for the non-thermal flux from fission and boosted fission weapons Eq. 4.4:10 applies

$$\phi = \frac{S}{4\pi R^2} e^{-\mu_0 \bar{\rho} R} \qquad (4.4:10)$$

$$\frac{\phi R^2}{S} = \frac{e^{-\mu_0 \bar{\rho} R}}{4\pi}$$

Since $\bar{\rho}$ and R are the only variables on the right side of the equation and they appear only as the product $\bar{\rho}R$,

$$\frac{\phi R^2}{S} = f(\bar{\rho}\, R) \qquad (4.4:12)$$

Therefore, if the quantity $\phi R^2/S$ is known for some distance R_1 and average density $\bar{\rho}_1$, then the same value of $\phi R^2/S$ holds for any other density $\bar{\rho}_2$ and distance R_2, (but for the same value of S) chosen such that

$$\bar{\rho}_1 R_1 = \bar{\rho}_2 R_2$$

The same relation restated is

$$\frac{\phi_1 R_1^2}{S} (\bar{\rho}_1 R_1) = \frac{\phi_2 R_2^2}{S} (\bar{\rho}_2 R_2) \qquad (4.4:13)$$

Eq. 4.4:13 is then the scaling relation required for transferring not the flux, but rather the quantity $\phi R^2/S$, to other air densities. The flux itself can be scaled for different air densities by the following relation which is clearly identical to Eq. 4.4:13

$$\phi_1(\bar{\rho}_1, R_1) = \left(\frac{\bar{\rho}_1}{\bar{\rho}_2}\right)^2 \phi_2(\bar{\rho}_2, R_2) \qquad (4.4:14)$$

These same equations will also hold for scaling the thermal flux thick casing fission weapons. Only slight modification of Eq. 4.4:14 is required to obtain the scaling relation for the non-thermal flux from fusion weapons. This modification is

$$\phi_1(\bar{\rho}_1, R_1, R_{i1}) = \left(\frac{\bar{\rho}_1}{\bar{\rho}_2}\right)^2 \phi_2(\bar{\rho}_2, R_2, R_{i2}) \qquad (4.4:15)$$

where

$$\bar{\rho}_1 R_1 = \bar{\rho}_2 R_2$$
$$\bar{\rho}_1 R_{i1} = \bar{\rho}_2 R_{i2}$$

It may also be desired to scale to different weapon yields as well as for different air densities. Since the yield W is proportional to the source strength S, Eqs. 4.4:14 and 4.4:15 can be generalized giving

$$\phi_1(\bar{\rho}_1, R_1, W_1) = \frac{W_1}{W_2} \left(\frac{\bar{\rho}_1}{\bar{\rho}_2}\right)^2 \phi_2(\bar{\rho}_2, R_2, W_2) \qquad (4.4:16)$$

$$\phi_1(\bar{\rho}_1, R_1, R_{i1}, W_1) = \frac{W_1}{W_2} \left(\frac{\bar{\rho}_1}{\bar{\rho}_2}\right)^2 \phi_2(\bar{\rho}_2, R_2, R_{i2}, W_2) \qquad (4.4:17)$$

Eqs. 4.4:14 through 4.4:17 are useful for relating burst situations which are characterized by the same type of empirical flux-distance relation. They will not properly scale between situations which are best described by different flux-distance equations.

With this reservation these scaling relations should apply independent of the change in weapon yield. If in the future they are found not to agree with experimental results for high yield weapons, it

[redacted]

is most probably because of the perturbation of the attenuating medium (the hydrodynamic effect). At present this effect is not thought to be a significant factor for neutron radiation although further and more conclusive study is certainly needed.

4.4.6 MAJOR DEFICIENCIES IN FLUX-DISTANCE RELATIONS

The flux-distance relations presented above, although quite useful, remain limited by their empirical and approximate nature. Certain reservations in their application should be noted and some of the most important of these are listed below.

1. In nearly all realistic situations the ground surface plays an important role, even if the point of burst or the receiver is not actually at the surface. The ground or water medium both scatters and absorbs neutrons differently from air, and this difference may greatly affect the scattered dose. The importance of the second medium as a sink for neutrons as compared to its importance as a reflector depends on several factors. In general it may be expected to act primarily as a reflector at distances close to the neutron source. The second medium will thus increase the flux close to the interface over the free air flux. At large distances from the source, however, the second medium would be expected to behave primarily as a sink and reduce the flux below the free air value. A very low order approximation to the proper flux at or near the media interface can be made by multiplying the free air flux by a constant chosen so as to fit experimental results. This factor probably lies between the values of 0.5 and 2.0.

2. The approximate nature of the flux-distance relations makes the problem of scaling from one set of circumstances to another difficult and uncertain. This is particularly true for scaling from low to high altitudes. The distances of operational significance for high altitudes are equivalent to the distances close to the burst point at low altitude. It is at these short distances that the measured doses show the greatest departure from the point source exponential relationship upon which the scaling relations are based.

3. The non-homogeneity of the attenuating media has not been fully considered. Normal variations in atmospheric density and humidity have been discussed previously. However, the blast wave perturbation of the atmosphere and the removal of the high explosive shell may have an effect on the delayed neutron flux and possibly even on the prompt thermal neutron flux. A detailed examination of the time behavior of the neutron delivery rates is necessary to resolve this question. (A discussion of neutron delivery rates is presented in Section 4.8.)

4.5 DOSE-DISTANCE RELATIONS

In this section are presented those results which are directly usable in predicting neutron doses (in rem). These results are given as separate sets of curves for fission/boosted fission, and thermonuclear weapons, together with associated tables. Illustrated problems are provided to demonstrate proper use of these curves and tables. Finally a general discussion of the dose-distance relations and their origins is presented.

4.5.1 CALCULATION OF TOTAL NEUTRON DOSE

Calculation Based on Weapon Type and Yield

The dose-distance relations are given in the form of a family of curves of the total neutron dose D, divided by the weapon yield W and by two constants, k_s depending on the weapon type and k_g depending on the receiver environment. The term $D/k_s k_g W$ is given as a function of the slant range R, from the point of burst to the receiver, with the average air density $\bar{\rho}$ between the source and receiver as a parameter. The dose (in rem) is based on the use of an estimated RBE for damage to the human spleen-thymus which, in turn, is derived from experimental mouse spleen-thymus data. As previously noted (see Sections 2.3 and 4.3.3) the spleen-thymus RBE is taken to be equivalent to the RBE for acute

[redacted]

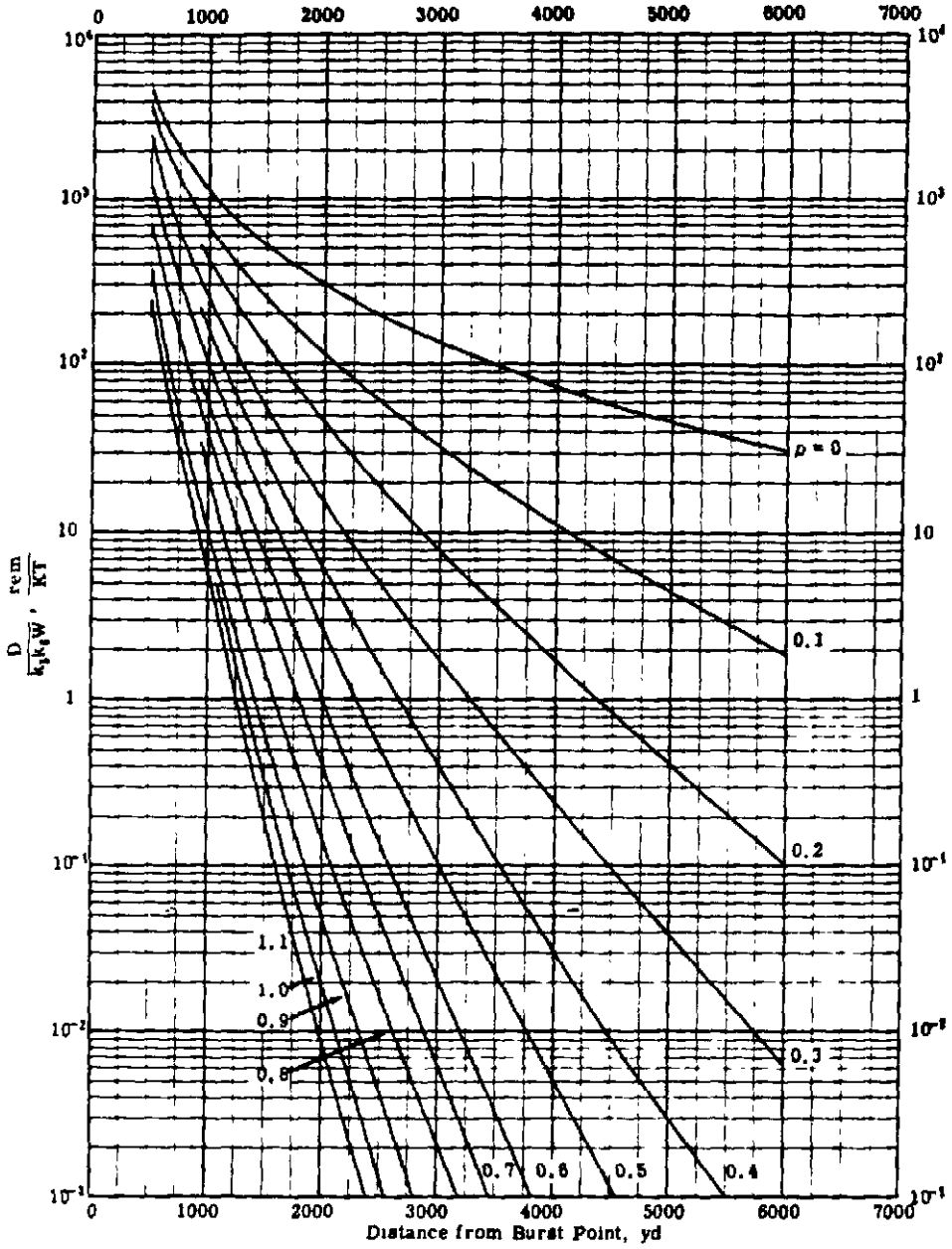

Fig. 4.5:1 Neutron Dose as a Function of Distance for Fission and Boosted Fission Weapons.

response in situations of military operational significance. Therefore the biological doses calculated below should also be taken as based on acute response, at least until better data become available.

Figure 4.5:1 presents curves suitable for fission and boosted fission weapons while Fig. 4.5:2 presents corresponding curves for fusion weapons. Table 4.5:1 shows, for a variety of boosted and unboosted fission weapons, the empirical formulas upon which the dose-distance curves are based and the corresponding values of k_s. (The value of k_s for fusion weapons is taken to be 1.0.) The table further describes the weapons as regards their general type and, where available, gives the thickness of their high explosive shell.

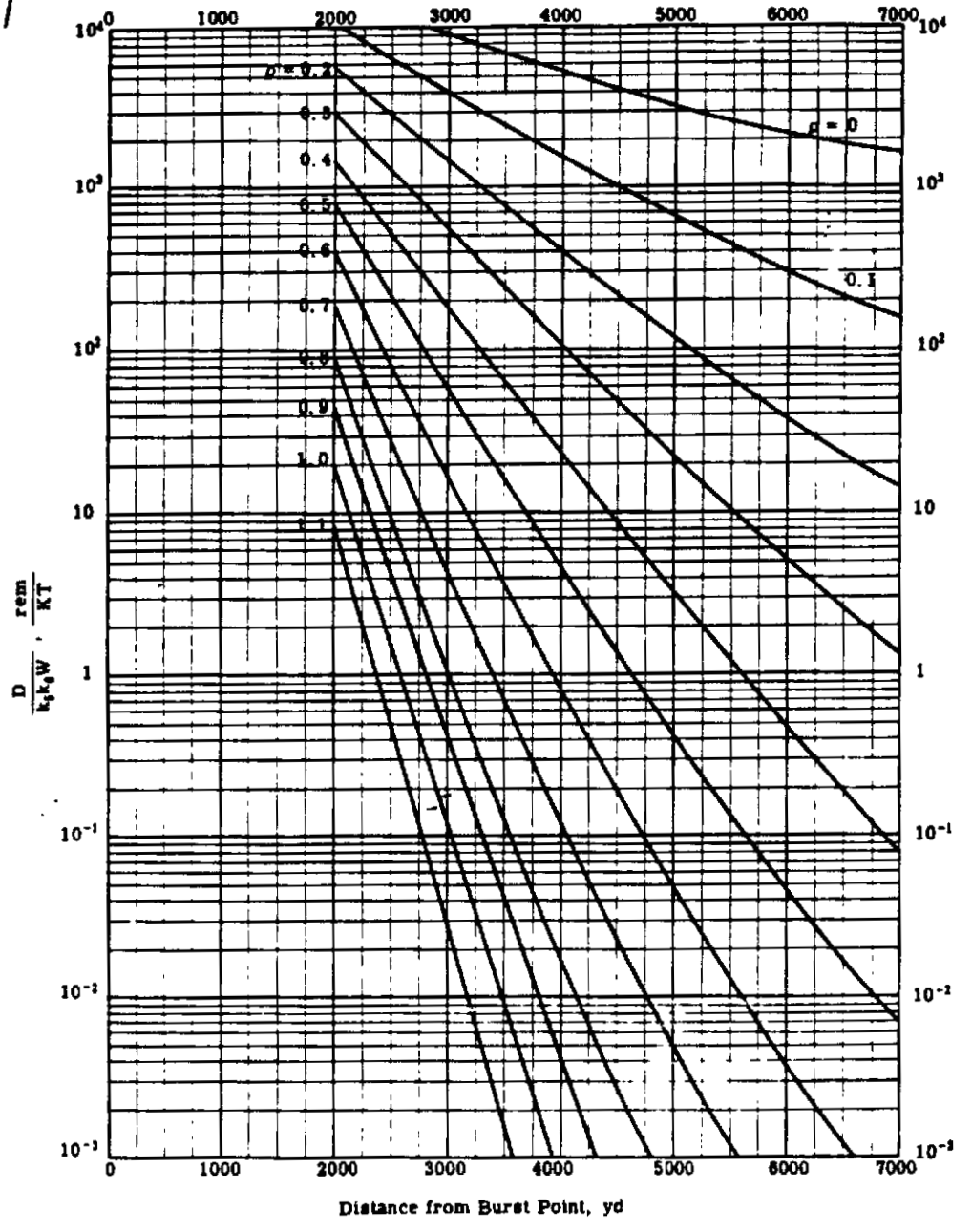

Fig. 4.5:2 Neutron Dose as a Function of Distance for Fusion Weapons

[redacted] The k_s factor for boosted weapons would be expected to differ from that for an equivalent unboosted weapon [redacted]

The values of k_s given in Table 4.5:1 are based on weapons previously tested.[1,16] For cases where the weapon of interest is listed, the value of k_s may be selected directly. For future or unlisted weapons k_s should be estimated by comparison with the most similar listed weapon types.

Page 128 is deleted.

Table 4.5:2 gives values for the factor k_e as a function of the environment of the receiver

Table 4.5:3 lists estimated probable error factors in the dose; these values represent the best present judgment of the authors. The probable error factors are intended to include both the inadequacies of the equations used to represent the dose-distance relations and the uncertainties in the constants used in these equations. The probable errors are given for receiver distance of 500 and 6000 yd and for bursts in standard atmospheric air ($\bar{\rho} = 1.0$) and in vacuum ($\bar{\rho} = 0$). An error factor should be interpreted in the following way. If the error factor is three, the probability is 50 percent that the proper value of D is less than one third or more than three times the value obtained by use of Figs. 4.5:1 and 4.5:2 and Tables 4.5:1 and 4.5:2.

TABLE 4.5:2

Receiver Environment Factors (k_e) for Dose-Distance Calculations

Receiver Environment	k_e
On or within 10 ft of the ground surface	1.0
On or within 10 ft of the surface of the sea	0.7
In free air	1.5

TABLE 4.5:3

Probable Error Factor in Dose-Distance Calculations[1]

Weapon Type	Probable Error Factor			
	R = 500 yd		R = 6000 yd	
	$\rho = 0$	$\rho = 1.0$	$\rho = 0$	$\rho = 1.0$
Unboosted fission	3	2	6	4
Boosted fission	3	2	6	4
Fusion (thermonuclear)	8	5	15	10

(1) It is estimated that the probability is 50 percent that the computed dose is too large or too small by more than this factor.

Calculation Based on Sulphur Neutron Flux

The principle of spectral invariance of the neutron flux[1] established at Teapot permits direct conversion of sulphur neutron flux to total physical dose (in rep) or to biological dose (in rem) for unboosted and boosted fission weapons. Such a calculational procedure may be useful in very rough calculations.

Factors for converting sulphur neutron fluxes to physical dose (in rep) may be calculated from the values of sulphur neutron dose as a percentage of the total dose listed in Table 4.7:1 for three major weapon types and the conversion factor for the S-Zr neutron flux from Table 4.3:2.

Using the RBE values derived from the work of Harris[1,16,17] the physical dose (in rep) can be converted to biological dose (in rem). The value recommended for acute response of humans to fission weapon neutrons is 1.3 rem-rep^{-1}. It may be assumed, as a low order approximation that this RBE value also holds for boosted fission weapons. Table 4.5:4 presents the several conversion factors for the three fission and boosted fission weapons for which some spectral information is available.

The classification of weapon types into only three categories is most certainly incomplete and is subject to future extension. In general the accuracy of the conversion factors is rather poor, as a result of our limited knowledge both of the energy spectrum and of its variation as a function of weapon design.

The values in Table 4.5:4 should not be confused with the entries in Table 4.3:2. The latter gives the partial dose (in rep) due to neutrons in a specified energy range. The conversion factors listed in Table 4.5:4 give the total dose (in rep and rem) due to all neutrons.

Since the principle of spectral invariance has not been extended to fusion neutrons, Table 4.5:4 should not be used to determine the total dose from fusion weapons.

TABLE 4.5:4

Factors for Conversion of Sulphur Neutron Flux to Total Dose

Weapon Type	Conversion Factors: To Physical Dose, $\frac{\text{rep-cm}^2}{\text{neutron}}$	Conversion Factors: To Biological Dose for Human Acute Response, $\frac{\text{rem-cm}^2}{\text{neutron}}$
Unboosted fission weapon with thick casing	10×10^{-8}	13×10^{-8}
Unboosted fission weapon with thin casing	5×10^{-8}	7×10^{-8}
Boosted fission weapon	3×10^{-8}	4×10^{-8}

PROBLEM 1

A nuclear weapon of known type and yield is exploded in a given environment. The distance from the receiver to the point of burst, the receiver environment and the average air density (in units of 1.293×10^{-3} gm-cm^{-3}) between the points are also given. It is required to determine the total neutron dose at the receiver.

Solution

1. From Fig. 4.5:1 or Fig. 4.5:2 (whichever is appropriate) read the value of $D/k_e k_s W$ for the given distance R from point of burst to receiver and for the given average air density $\bar{\rho}$.
2. From Table 4.5:1 read the value of k_e for the weapon type exploded.
3. From Table 4.5:2 read the value of k_s for the environment of the point at which the dose is being computed.

4. Form the product

$$D = \left(\frac{D}{k_s k_e W}\right) k_s k_e W$$

where W is the yield in KT. The number D is the total neutron dose in rem.

Example

A 5-KT, [redacted] weapon is exploded at the ground surface. It is required to determine the total neutron dose at a point 2000 yd distant, also at the surface. The average air density $\bar{\rho}$ between the points is 0.9, in units of standard atmospheric density.

1. For R = 2000 yd and $\bar{\rho} = 0.9$, Fig. 4.5:1 gives

$$\frac{D}{k_s k_e W} = 6.0 \times 10^{-2} \quad \text{rem-KT}^{-1}$$

2. For a [redacted] weapon, from Table 4.5:1

$$k_s = 6.15$$

3. When the point at which the dose is desired is on the surface, from Table 4.5:2

$$k_e = 1.0$$

4. We compute, for a yield W of 5 KT

$$D = \left(\frac{D}{k_s k_e W}\right) k_s k_e W = (6.0 \times 10^{-2})\ (6.15)\ (1.0)\ (5.0)$$

$$D = 1.8 \text{ rem}$$

The total neutron dose at the required point is 1.8 rem.

PROBLEM 2

A nuclear weapon of known type and yield is exploded in a given environment. The average air density in the vicinity of the burst and the receiver environment are also given. It is required to determine the horizontal distance at which the total neutron dose drops below a specified value.

Solution

1. From Table 4.5:1 read the value of k_s for the weapon type exploded.
2. From Table 4.5:2 read the value of k_e for the environment of the point at which the dose is to drop below the specified value.
3. Form the quotient

$$\frac{D}{k_s k_e W}$$

where D is the specified total neutron dose (in rem) and W is the yield (in KT).

4. From Fig. 4.5:1 or Fig. 4.5:2 (whichever is appropriate) for the computed value of $D/k_s k_g W$ and the given value of the average air density $\bar{\rho}$, read the distance R at which the total neutron dose drops below D rem.

Example

A 5-KT, [redacted] weapon is exploded over the surface of the sea. The average air density at sea level is 1.0. It is required to determine the horizontal distance at which the total neutron dose D drops below 200 rem.

1. From Table 4.5:1 for a [redacted] weapon

$$k_s = 6.15$$

2. From Table 4.5:2, when the point at which the dose is desired is over the surface of the sea,

$$k_g = 0.7$$

3. For a dose D of 200 rem and for a yield W of 5 KT we calculate

$$\frac{D}{k_s k_g W} = \frac{200}{(6.15)\ (0.7)\ (5.0)} = 9.3\ \text{rem-KT}^{-1}$$

4. For an average air density $\bar{\rho}$ of 1.0 and for the above value of $D/k_s k_g W$, from Fig. 4.5:1, R = 1000 yd. Beyond this distance the total neutron dose will be less than 200 rem.

PROBLEM 3

The neutron flux due to the explosion of a fission weapon is known, as read by a sulphur threshold detector at a given point. Find the total neutron biological dose (in rem) received at the point in question.

Solution

1. From Table 4.5:4 read the conversion factor from sulphur flux to the biological dose for the weapon type exploded.
2. Multiply this value for the conversion factor by the sulphur neutron flux. The product is the biological dose (in rem).

Example

A thin casing, unboosted fission weapon is exploded and produces a sulphur neutron flux of 10^9 neutrons-cm^{-2} at the receiver. Find the corresponding total neutron dose (in rem).

1. From Table 4.5:4 the value of the flux-dose conversion factor is 7×10^{-8} rem-cm^2-neutron^{-1}.
2. The total biological neutron dose is then

$$D = (10^9)\ (7 \times 10^{-8}) = 70\ \text{rem}$$

4.5:2 DISCUSSION OF DOSE-DISTANCE RELATIONS

Fission and Boosted Fission Weapons

The curves and tables given in Section 4.5:1 for fission and boosted fission weapons are based heavily on the Teapot test results of Harris[1] although attention has also been paid to prior experimental work.[5, 7, 8, 11, 12, 13, 14, 22, 23]

The Teapot results indicate that the biological dose D (in rem) is linearly related to the non-thermal neutron flux as given for fission and boosted fission weapons by Eq. 4.4:2. Thus

$$D = k_\gamma \phi = \frac{k_\Gamma S}{4\pi R^2} e^{-\frac{\bar{\rho} R}{\lambda_0}} \qquad (4.5:1)$$

Since the source strength S is proportional to the weapon yield W, and the 4π can be included in the constant

$$D = \frac{k_g W}{R^2} e^{-\frac{\bar{\rho} R}{\lambda_0}} \qquad (4.5:2)$$

The value of k_g is constant for a given weapon type and receiver environment. If the effects of these two factors are transferred to the left side of the equation through the use of the previously defined k_δ and k_θ,

$$\frac{D}{k_\delta k_\theta W} = \frac{k_g}{R^2} e^{-\frac{\bar{\rho} R}{\lambda_0}} \qquad (4.5:3)$$

[redacted]

Results from many series of test shots for low and intermediate yield fission and boosted fission bursts have shown apparent mean free paths for sulphur neutrons (scaled to standard density air) remarkably independent of weapon type. Thus the results on a wide variety of weapons give $\lambda_0 = 210 \pm 7$ yd. Since the neutron spectrum of importance is approximately invariant with distance, the apparent mean path for all biologically damaging neutrons may be taken as equal to that for sulphur neutrons.

If weapon type has any influence on the apparent mean free path, it falls within the magnitude of the error quoted above. We may, therefore, expect errors in the dose calculations of the order of

$$e^{-\left(\frac{\bar{\rho} R}{\lambda_0}\right)\left(\frac{\Delta\lambda_0}{\lambda_0}\right)}$$

due to uncertainty in the apparent mean free path. This error is about a factor of 3 at 6000 yd. The probable error in the dose listed in Table 4.5:3 includes that due to the mean free path.

The inadequate treatment of the effect of the ground surface has been discussed briefly in Section 4.4.6. In a very simple way this effect may be considered to depend on two factors, the environment at the burst point and the environment at the receiver. A rough correction has been made for the

effect of variations in the receiver environment through the use of the k_6 term. No corresponding correction is presently practicable for the effect of the environment at the burst point in the face of the very limited knowledge available on this subject. (An attempt is made, however, to include the additional uncertainty in the results from non-surface bursts as compared to surface bursts by estimating two probable error factors (Table 4.5:3) for average air densities of $\rho = 0$ and $\rho = 1.0$).

A test of the over-all effect of the ground surface on the dose was included in the Teapot series. [redacted] Both the burst point and the receivers were at the ground surface for Teapot 9 while both the burst point and the receivers were at approximately 35,000 ft for Teapot 10. When the neutron flux measurements[23] made at these tests were plotted as $R^2\phi$ and as a function of R on semilog paper, neither the same zero intercept nor the same apparent mean free path (when scaled to the same air density) was found. The experimental errors in the measurements were so great, however, that these results are not considered conclusive.

Fusion Weapons

The experimental results[9,10] of neutron flux and dose measurements for thermonuclear weapons are much less complete than the corresponding fission weapon results and also much less consistent. It was felt preferable, therefore, to base the present methods partly on the phenomenological approach of Brode[18] rather than on the experimental measurements alone.

The dose is considered to be given by the following equation, which is a combination of Eqs. 4.4:2 and 4.4:3.

$$\frac{D}{k_s k_6 W} = \frac{A_1(1-M)}{R^2}\, e^{-\frac{\bar{\rho}R\left[R^2+\left(\frac{R_{i0}}{\bar{\rho}}\right)^2\right]}{R^2\lambda_0+\left(\frac{R_{i0}}{\bar{\rho}}\right)^2\lambda_{i0}}} + \frac{A_2(1-M)}{R^2}\, e^{-\frac{\bar{\rho}R}{\lambda_0}} + \frac{A_3(M)}{R^2}\, e^{-\frac{\bar{\rho}R}{\lambda_0}} \qquad (4.5{:}4)$$

The first term represents the dose due to 14-Mev fusion neutrons. The second term represents the dose due to the lower energy fusion neutrons and the third term represents the dose due to fission neutrons.

The values of the constants to be inserted in Eq. 4.5:4 are

$k_s = 1.0$

$M = 1/2$

$A_1 = 1.43 \times 10^{11}$ rem-yd^2-KT^{-1}

$A_2 = 8.0 \times 10^{10}$ rem-yd^2-KT^{-1}

$A_3 = 1.0 \times 10^{19}$ rem-yd^2-KT^{-1}

$R_{1_0} = 3160$ yd

$\lambda_{1_0} = 210$ yd

$\lambda_{1_3} = 330$ yd

The term k_s and its value of unity are inserted in the equation for fusion weapons merely to make the notation consistent with that for fission weapons. M represents the ratio of fission to total yield and the value of 1/2 is roughly correct [redacted]

The value of A_1 is calculated from

$$A_1 = \frac{(1.05 \times 10^{24})\ (2.86 \times 10^{-5})\ (0.5)}{(4\pi)\ (91.4)^2} = 1.43 \times 10^{11} \text{ rem-yd}^2\text{-KT}^{-1} \qquad (4.5{:}6)$$

There are 1.05×10^{24} 14-Mev fusion neutrons generated per KT under conditions of partial burn. The conversion factor from flux to dose (in rem) is taken[18] to be 2.86×10^{-5} rem-cm^2-neutron^{-1}. A transmission factor of 0.5 is assumed for neutron penetration of the weapon components. This value is quite approximate and may be low for the newer weapon types. There are 91.4 cm-yd^{-1}. The calculated value for A_1 is clearly uncertain but it is believed that there is little point in attempting to further refine its accuracy until more consistent and reliable measurements become available.

A_3 is chosen as an average value for fission weapons. Since the low energy fusion neutrons (to a very coarse approximation) are comparable to the fission neutrons in energy, the ratio A_2/A_3 should be approximately equal to the ratio of the number of low energy fusion neutrons generated per KT of fusion yield to the number of fission neutrons generated per KT of fission yield. This ratio is $1.05 \times 10^{24}/1.3 \times 10^{23}$ or about 8, thus, $A_2 = 8A_3$. There are probably large errors associated with the choice of values for A_2 and A_3 but these errors are not particularly important since the second and third terms of Eq. 4.5:4 are small relative to the first. Almost all of the dose comes from the 14-Mev fusion neutrons.

The values of R_{1_0} and λ_{1_0} were obtained by fitting Eq. 4.5:4 to Castle results. The value of λ_{1_3} was obtained from fission weapon results.

As has been indicated in Table 4.5:3, the over-all errors in the prediction of neutron dose from thermonuclear weapons are believed to be much greater than those from fission weapons.

4.6 RELATIVE IMPORTANCE OF NEUTRON RADIATION

The relative importance of neutron radiation must be judged by comparison with all other weapon phenomena capable of inflicting damge. Such phenomena include initial gamma radiation, residual gamma and beta radiation (fallout), thermal radiation, and blast damage. Several of these are incommensurate since they involve damage effects of entirely different types, and proper definition of a comparative criterion is difficult.

Comparison of neutron and gamma radiation, however, is relatively straightforward. The apparent mean free paths for fission product and nitrogen capture gamma radiation are much longer than those for neutron radiation.[1, 2, 5, 6] The total neutron energy released at the point of burst, however, is comparable to or greater than the corresponding gamma energy. There exists, therefore, a spherical volume surrounding the point of burst within which the neutron dose is greater than and outside of which the neutron dose is less than the gamma dose. This equal-dose radius is dependent on a number of factors, including the weapon type, and yield burst height, and burst environment.

Based on the results of Section 4.5 and of Chapter 3, equal-dose radii can be determined for specific situations. Thus, for surface bursts ($\rho = 1.0$) over land of a 20-KT, unboosted, [redacted] weapon the equal-dose radius is less than 500 yd, where both neutron and gamma doses are in rem; for a

20-KT, boosted, [redacted] weapon under the same conditions the equal-dose radius is about 1800 yd. At high altitudes the radius increases as attenuation due to the medium decreases and the fixed attenuation due to distance (the R^2 effect) assumes increased relative importance. Somewhat differently we could say that at any fixed distance from the source neutron radiation is more important compared to gamma radiation at high altitudes than at low.[24] Thus, at an altitude of about 44,000 ft ($\rho = 0.2$) the equal-dose radii for a 20-KT, unboosted, [redacted] and a 20-KT, boosted, [redacted] weapon are less than 500 yd and greater than 7000 yd, respectively.

For high yield thermonuclear weapons the situation is more complicated. The neutron dose per KT is increased because the fusion process is more productive of neutrons than the fission process. However, the gamma dose is also greatly enhanced because of the hydrodynamic effect. The removal of the attenuating medium by the blast wave occurs at a time when the fission product gamma source is still relatively strong but when the neutron source has probably disappeared. Although the uncertainties are much larger, based on the results given in Section 4.5 and in Chapter 3, one can estimate equal-dose radii for the high yield weapons comparable to those given above.

A somewhat broader study of the damage effects of low and intermediate yield weapons due to other mechanisms involved in the explosion, in addition to neutron and gamma radiation, has been conducted by Ifland.[6] We may, following Ifland, define for any particular phenomenon a critical radius such that for smaller distances from the point of burst the damage is greater than a suitably defined critical level, and for larger distances the damage is less than the critical level. Blast damage, neutron, gamma, and thermal radiation were considered for yields of 2 and 20 KT, altitudes of 0 and 40,000 ft, and low (thick explosive shell) and high (thin explosive shell) neutron flux weapons. The critical damage levels chosen are 400 rem for neutrons, 400 rep for gammas, and 18 cal-cm^{-2} for thermal radiation. (Thermal radiation at this level is sufficient to heavily damage 0.016-in. polished aluminum aircraft skin.) The blast damage criterion cannot be simply defined and the reader is referred to Ifland's report[6] for the details of this definition.

TABLE 4.6:1

Comparison of Critical Radii Due to Several Damage Mechanisms[6]

Weapon Type	Yield, KT	Burst Altitude, ft	Critical Radius, yd: Neutron Dose (400 rem)	Gamma Dose (400 rep)	Thermal Radiation (18 cal-cm^{-2})	Blast Damage to B-29 Type Aircraft(1): Nose-On	Most Vulnerable Orientation
Low neutron flux	20	0	700	1300	1700	850	2300
Low neutron flux	20	40,000	1900	2900	1800	1100	2100
High neutron flux	20	0	1200	1400	1700	850	2300
High neutron flux	20	40,000	3200	3300	1800	1100	2600
High neutron flux	2	40,000	2400	1800	600	500	1200

(1) See Reference 6 for criteria of blast damage.

Results of the comparison are shown in Table 4.6:1. The critical radius for neutrons is less than the critical radius for gammas except for the high neutron flux, 2-KT weapon at high altitude. As expected, the relative importance of the neutron dose compared to the gamma dose increases with increasing altitude and with decreasing thickness of the high explosive shell. At high altitudes the neutron radius also tends to become larger than the critical radius for thermal radiation and/or blast damage.

4.7 NEUTRON ENERGY SPECTRUM

Experimental test bursts previous to the Castle series usually included instrumentation only for sulphur (3-Mev threshold energy) and gold (0.3 ev cutoff energy) neutrons, thus omitting the entire energy spectrum between 0.3 ev and 3 Mev. (Gold neutrons, as indicated in Section 4.3, contribute negligibly to the biological effect.) Fission detectors, which cover the missing range, did not yield results easily interpretable until the Teapot series,[1] although they were tried at Castle for thermonuclear weapons but without very consistent results. Use of fission detectors at Teapot, however, established the energy distribution over the energy range of interest for several weapon types. (The fission detector results also established the invariances of these spectra with distance - see Section 4.3.3.)

Table 4.7:1 shows the percent of the total neutron flux and dose (in rep) in the various energy ranges of interest for unboosted and boosted fission weapons, based on the Teapot data. Conversion of flux to dose (in rep) may be accomplished by means of the factors listed in Table 4.3:2. The spectra are given independent of distance and are classified into three broad categories of weapon type. This classification is almost certainly incomplete and subject to extension. At the present time, however, the effect of further differences in weapon type lies within the error of the measurements.

The Teapot results do not show the energy distribution above 3 Mev of the 14-Mev fusion neutrons from boosted fission weapons since no detector with a threshold energy greater than 3 Mev (sulphur) was used. All neutrons with energies above 3 Mev were included in the sulphur detector results and examination of Table 4.7:1 indicates that the contribution of the 14-Mev neutrons to either the flux or dose (in rep) is not large.

[redacted]

No information corresponding to that given in Table 4.7:1 for fission and boosted fission weapons is presently available on the neutron energy spectra from thermonuclear weapons. As previously noted, spectral invariance of fusion neutrons cannot be assumed at this time; it is probable that consideration of the variation of the spectrum with distance will be necessary.

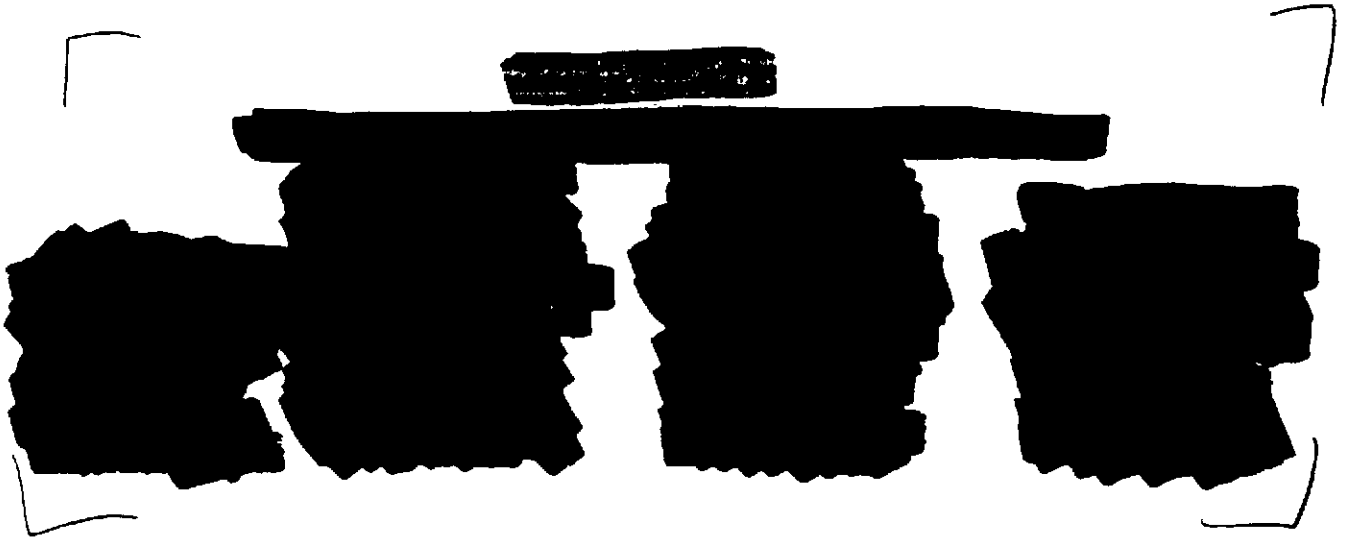

4.8 DELIVERY RATES AND THE HYDRODYNAMIC EFFECT

The preceding sections have dealt almost exclusively with the neutron flux or dose integrated over all time. Implicit in this treatment has been the assumption that all or most of the neutrons arrive at the receiver almost simultaneously with the time of burst, i.e., before the blast wave has any appreciable effect. This appears to be a reasonable assumption on the basis of our present understanding of neutron time behavior.

The following paragraphs discuss the neutron delivery rate and its relationship to the hydrodynamic effect. The discussion will consider first the prompt and then the delayed neutrons. Finally, some of the very limited experimental delivery rate measurements will be presented.

4.8.1 PROMPT NEUTRONS

Prompt fission neutrons are those which are born at the time of the fission reaction. This reaction is completed very quickly, within 5×10^{-8} sec. The fusion reaction produces only prompt neutrons and proceeds even more rapidly than fission. Thus, all prompt neutrons are emitted essentially simultaneously with the time of burst.

Those prompt neutrons from either fission or fusion which arrive at the receiver while still at high energy and corresponding high speed (a 3-Mev neutron travels at a speed of about 2.6×10^{7} yd-sec^{-1}) must do so without suffering many collisions in transit. It may be inferred, therefore, that they arrive after only a very small transit time and before the blast wave. (The speed of the blast or shock wave is less than 10^{3} yd-sec^{-1} except for very short distances from the point of burst.) Traveling ahead of the blast wave, they should be unaffected by it.

The remaining neutrons are either slowed down by collisions within the weapon, or in the air. Those neutrons which are slowed down in the weapon may become trapped in the high explosive shell. This entrapment is only temporary and of short duration since even low yield weapons expand very rapidly, releasing the neutrons to the atmosphere in the process. (A 20-KT fission weapon will have expanded to about 50 ft in diameter in about 100 microseconds.) Once the low energy neutrons are released from the weapon, they travel at somewhat reduced average velocities. (Thermal neutrons, for example, travel only at about 2400 yd-sec^{-1} between collisions. Their average speed is much less than this since they travel more by the random process of diffusion than by the relatively straight line path characteristic of fast neutrons.) Thus, the low energy and particularly the thermal neutrons may fall behind the shock front and experience blast wave enhancement.[9,10]

The lifetime of these (neutrons) is quite short, however, and so therefore is the time over which they are exposed to the blast wave. The mean lifetime of any neutron slowing down in standard density air is only about 0.07 sec and is independent of its original energy. A neutron released at bomb thermal energy (approximately 1 kev) will slow down to 0.5 ev in about 0.0027 sec. (For air of less than standard density, neutrons will live longer on the average.) Since the blast wave effect is quite small at short times after the blast, it may have some influence on the lower energy prompt neutrons, but their short lifetime precludes any major blast wave effect.

The neutrons which are slowed down in air behave in the same general fashion as those slowed down in the high explosive shell, once the latter are released from the weapon. The preceding discussion therefore applies in general to both neutrons slowed down in air and in the weapon casing.

It would seem that the prompt neutron flux and dose, due both to the biologically damaging fast neutrons and the less important low energy and thermal neutrons, should be delivered very quickly - well within one second. As a consequence, the blast wave effect should be unimportant for prompt neutrons.

4.8.2 DELAYED NEUTRONS

A small fraction of the fission neutrons is emitted from the fission products rather than at the time of the nuclear reaction.[25,26] They are therefore somewhat delayed in time of emission and appear later in the delivery rate curve.

Fission of U^{235}, U^{238}, and Pu^{239} has, in each case, produced the same six major groups of delayed neutrons. The half lives of the precursors of these groups of neutrons vary from 0.15 to 54 sec and the delayed neutron energies vary from 0.25 to 0.62 Mev. The relative abundance of each group depends on the fissionable material and to a much lesser extent on the energy of the neutrons causing fission. The most important characteristics of the delayed neutrons from U^{235}, U^{238}, and Pu^{239} are tabulated by group in Table 4.8:1. The relative abundance of the delayed neutrons varies from 0.23 to 1.47 percent of the total number of neutrons produced for these three fissionable materials.

If their relative abundance and energy were the only factors which determined the magnitude of the delivery rate of delayed neutrons, these neutrons could be safely neglected in comparison to the prompt neutrons. Because of the late emission time, the importance of the delayed neutrons may be multiplied, however, by the blast effects, particularly for intermediate and high yield weapons.

TABLE 4.8:1

Delayed Neutron Characteristics for U^{235}, U^{238}, and Pu^{239}

Half Life of Delayed Neutron Precursor, sec	Delayed Neutron Energy, Mev	Percent of Total Fission Neutrons		
		U^{235}	U^{238}	Pu^{239}
54	0.25	0.03	0.01	0.01
22	0.56	0.15	0.15	0.06
5.8	0.43	0.13	0.23	0.04
2.1	0.62	0.28	0.60	0.09
0.45	0.42	0.09	0.35	0.03
0.15	—	0.01	0.13	0.00
		0.69	1.47	0.23

The attenuation of delayed neutrons is reduced relative to that of prompt neutrons by two separate effects of the blast: (1) the removal of the hydrogenous high explosive shell, and (2) the compression effect on the atmosphere between the neutron source and the receiver. Thus the exponential for prompt neutrons traveling through the high explosive and the unperturbed medium is

$$e^{-(\mu_e R_e + \mu_{atm} R_{atm})}$$

where the subscripts e and atm refer to the explosive and atmosphere, respectively. The exponential for delayed neutrons in the non-homogeneous atmosphere is

$$e^{-\int_0^R \mu_{atm}(r,t)\,dr}$$

and is a function of both position (r) and time (t). The second exponential will be larger and in some cases it may conceivably be considerably larger than the first.

The magnitude of these blast effects on the delayed neutron flux and dose has not yet been properly evaluated. Based on the little that we do know, the effects are believed to be small for weapons of current design, primarily because these weapons have thin high explosive casings and the corresponding value of $\mu_e R_e$ is relatively small.

It would appear, therefore, that neither the relative abundance of the delayed neutrons nor the multiplying effect of the blast is large enough to make the delayed neutron dose a significant part of the total neutron dose.

4.8.3 EXPERIMENTAL RESULTS

Experimental data on delivery rates are rare and not very reliable. Determination of delivery rates by theoretical calculation is difficult and here, too, little has been done.

Thermal (both prompt and delayed) neutron delivery rates were measured at Greenhouse using fission fragment cameras. Unpublished results show a definite second maximum in the delivery rate curve; this is ascribed to blast wave enhancement. This finding tends to substantiate the argument given above, namely that the thermal neutrons fall behind the blast wave due to their relatively low velocity and random path. Attempts were also made at Greenhouse to measure fast neutron delivery rates using U^{238}. These results were inconclusive, however, because of contamination of U^{238} by U^{235}, which is sensitive to thermal neutrons.

Figure 4.8:1 shows the results of essentially thermal neutron delivery rate experiments at Buster Baker[11] (3.5 KT) and at Tumbler Snapper 4 (also known as Snapper 1) (19 KT).[5]

It is seen that for both Buster Baker and Tumbler-Snapper 4 the dose was received within about one second of the burst. Both yields, however, were too low to expect any second maximum in the curves due to blast wave enhancement.

If blast wave enhancement of the neutron flux or dose does occur and is in any way important for high yield bursts, the proper flux-and dose-distance equations will not be in the form of either

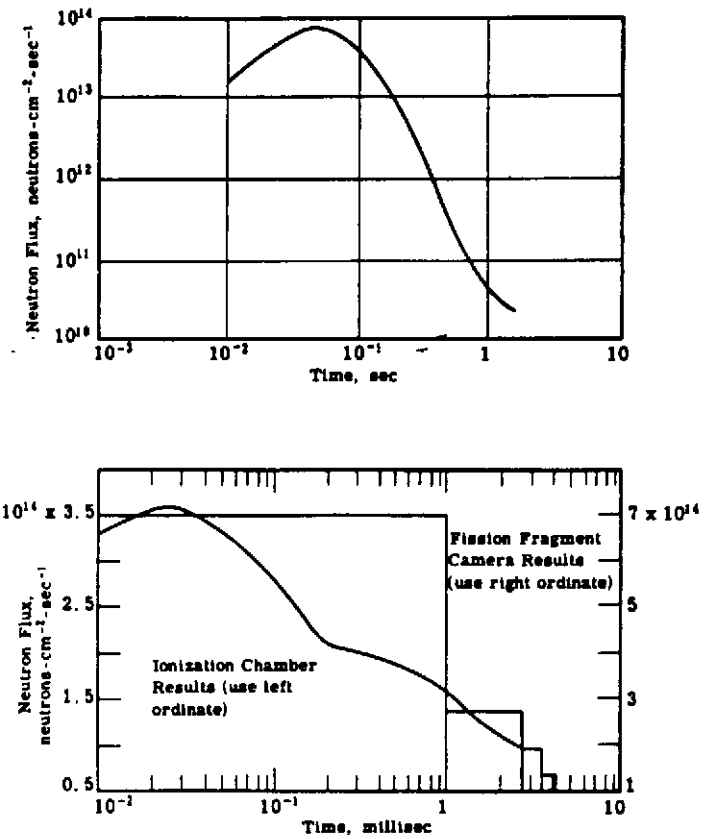

Fig. 4.8:1 Thermal Neutron Delivery Rates from Buster Baker and Tumbler-Snapper 4

Eq. 4.4:2 or of Eq. 4.4:3. They should resemble Eq. 4.4:3 in that the apparent mean free path at small distances should be longer than at large distances. The change in apparent mean free path with distance should, however, be yield dependent in a way not suggested by either Eq. 4.4:2 or 4.4:3. It would be possible in principle, of course, to use Eq. 4.4:2 in combination with a hydrodynamic scaling factor as was done in Chapter 3. Sufficient data for determining such factors are not known at this time.

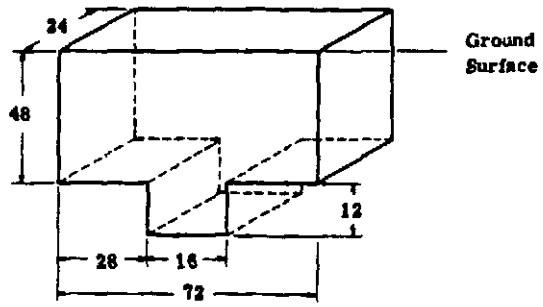

Sketch of Foxhole (all dimensions in inches)

Fig. 4.9:1 Neutron Flux Transmission Factors for Two-Man Foxholes

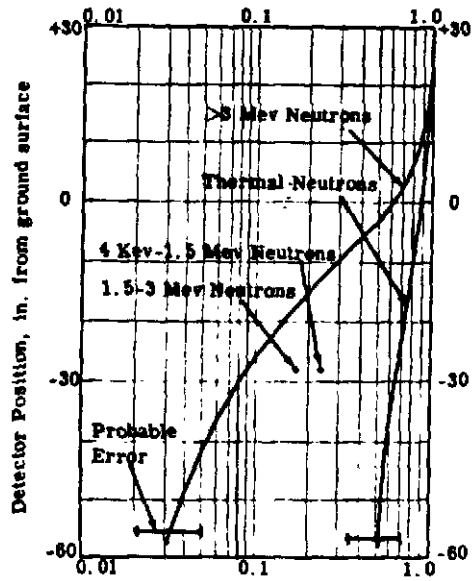

4.9 MILITARY SHIELDING

The protective effects of shielding have been investigated[27,28] experimentally primarily using sulphur (3-Mev threshold) and gold (thermal) neutron detectors. As previously noted, these detectors do not cover the energy range of greatest biological importance and data obtained from them are therefore of somewhat limited value. In addition, there have been a few experiments during the Teapot series which utilized fission detectors for the energies between thermal and 3 Mev. Direct biological experiments (see Section 4.3) to determine the shielding effectiveness of military structures have not been performed. A broad review made[29] of the data on neutron shielding experimental results sharply points up the very wide scatter in the experimental results. In addition to this lack of consistent experimental results, thus far there has been no satisfactory calculational procedure for the effects of shielding on the neutron flux or dose.

In these circumstances only representative experimental data from specific test bursts and for the detectors actually used can be presented. The material given can be applied, at least crudely, to future situations, although greater discrepancies will arise the further the conditions of interest are from those under which the data were obtained.

The data are presented in the form of flux transmission factors. The flux transmission factor is defined as the ratio of the flux inside the shield to the open air flux at the same position (both fluxes in the same specified energy range). Transmission factors are given for foxholes, vehicle trenches, soil, and protective structures of various designs.

Fig. 4.9:1 shows transmission factors for two-man foxholes obtained[27] by averaging data from Teapot bursts 3, 11, and 12 (all tower shots). The accuracy is probably not better than a factor of 1.5 for the sulphur and 1.3 for the gold neutron flux transmission factors. It is seen that the gold neutrons persist in quantity to considerable depths, while the sulphur neutrons are attenuated more easily. The data show considerable scatter which seems to exhibit little correlation, even with distance from ground zero. Points are also plotted for intermediate energy neutron between 4 kev and 1.5 Mev and between 1.5 and 3 Mev, as measured by Np^{237}, Pu^{239}, and U^{238} fission detectors.

TABLE 4.9:1

Neutron Flux Transmission Factors for Field Structures from Teapot Shot 12

Structure	Instrument Position	Distance from Ground Zero, yd	Flux Transmission Factors				
			Distance Above Floor				
			20 in.	26 in.	38 in.	44 in.	In Entranceway
OCE - 1 ft earth cover		300		S 5.0×10^{-3} Au 2.0×10^{-3}		S 6.0×10^{-3} Au 2.1×10^{-2}	S 2.0×10^{-3} Au 2.3×10^{-2}
OCE - 4 ft earth cover		300		S 1.4×10^{-5} Au 1.1×10^{-4}		S 1.3×10^{-5} Au 7.1×10^{-5}	S 4.5×10^{-4} Au 4.9×10^{-3}
OCE - 8 ft earth cover		300		S 1.4×10^{-6} Au 1.1×10^{-6}		S $<1.0 \times 10^{-7}$ Au 1.7×10^{-6}	S 4.5×10^{-4} Au 4.9×10^{-3}
OCE - Duplex		300		S 5.1×10^{-5} Au 3.6×10^{-4}		S 6.4×10^{-5} Au 3.9×10^{-4}	
Instrument shelter		317		S 8.0×10^{-5} Au 3.1×10^{-3}		S 5.9×10^{-5} Au 3.1×10^{-3}	
Navy Armco-3 1/2-ft earth cover on crown	Near wall toward ground zero	500			S 2.2×10^{-4} Au 4.6×10^{-3}		
	Near wall away from ground zero	500	S 2.0×10^{-4} Au 4.9×10^{-3}				
Navy Armco-no earth cover on crown	Near wall toward ground zero	767	S 1.7×10^{-3} Au 1.5×10^{-1}		S 1.8×10^{-3} Au 1.7×10^{-1}		
	Near wall away from ground zero	767	S 5.3×10^{-3} Au 2.1×10^{-1}		S 5.9×10^{-3} Au 2.1×10^{-1}		
BuDocks		1633		S 3.9×10^{-1}		S 3.5×10^{-1}	

Vehicle trenches at 700 yd from ground zero were tested for shielding effect at Teapot 12 (24 KT)[27]. Sulphur neutron flux transmission factors varied with position from 0.25 to 0.37, while gold transmission factors varied from 0.69 to 0.88.

Transmission factors for soil were measured at Upshot-Knothole[30] using sulphur and gold detectors. The measurements were made for soil thicknesses up to 3-1/2 ft and distances from ground zero between 400 and 750 yd. The average flux transmission factor reported for sulphur neutrons is 0.1 per ft of soil.

Sulphur and gold flux transmission factors for several protective structures both above and below ground were also measured at Teapot 12.[27] The results of these measurements are presented in Table 4.9:1.

The OCE underground structures were reinforced concrete cells with beam-supported, earth-covered roofs. The cells were 10 ft wide, 21 ft long and 8 ft high. The thickness of the earth cover varied from 1 to 8 ft.

The OCE-Duplex underground structure was similar in construction but had two rooms. The structure was positioned so that each room was side-on to the blast. The building was 8 ft wide, 19 ft long, 7 ft high, and had 2 ft of earth cover.

The two Navy Armco structures were above ground and of the Quonset-hut type, constructed of 10 gauge (0.14 in) corrugated steel plate. They were 25 ft wide, 48 ft long and 12 ft high. In one case 3 1/2 ft of earth cover was used on the crown, with the earth thickness on the sides increasing to about 15 1/2 ft. In the other case there was zero thickness of earth at the crown and about 12 ft of earth at the sides.

The Bureau of Docks structure was a precast concrete gable shelter above ground. It was 22 ft wide, 48 ft long, and 13.5 ft high.

The instrument shelter was 9 ft wide, 29-1/2 ft long and 12 1/2 ft high. It was constructed of 2 1/2 ft thick concrete and was partially underground. The portion of the sides of the shelter protruding above ground was banked with earth but no earth cover was used on the shelter roof.

Further information on these structures is contained in Section 3.7.

4.10 REFERENCES

1. P.S. Harris et al. ITR-1167. May 1955. (Secret)
2. J.S. Malik. LA-1620. Jan. 1954. (Secret)
3. J.S. Malik. WT-634. Feb. 1954. (Secret)
4. E.B. Doll and H.K. Gilbert. ITR-1153. June 1955. (Secret)
5. C.L. Cowan. WT-555. June 1952. (Secret)
6. P.W. Ifland. AFSWP-500. April 1953. (Secret)
7. G.A. Linenberger and W. Ogle. SS-18. Feb. 1949. (Secret)
8. H. Scoville et al. SS-19. June 1948. (Secret)
9. T.D. Hanscome and D.K. Willett. ITR-914. May 1954. (Secret)
10. T.D. Hanscome and D.K. Willett. NRL Report 4403. (Secret)
11. C.L. Cowan et al. WT-416. June 1952. (Secret)
12. J.T. Brennan et al. WT-43. 1951. (Secret)
13. R.E. Carter et al. WT-528. April 1953. (Secret)
14. R.E. Carter et al. WT-747. Dec. 1953. (Secret)

15. V.P. Bond et al. WT-793. Sept. 1953. (Secret)
16. P.S. Harris. LASL. Private Communication. Aug. 1955.
17. P.S. Harris. Proc. Tripartite Conference on Weapons Effects. Nov. 1955. (Secret)
18. H.L. Brode. RM-1523. Aug. 1955. (Secret)
19. J.J. Taylor. WAPD-RM-217. Jan. 1954. (Unclassified)
20. P.R. Wallace and J. LeCaine. MT-12. Aug. 1943. (Unclassified)
21. B.R. Suydam. WT-103. March 1951. (Secret)
22. T.D. Hanscome and D.K. Willett. WT-524. Feb. 1953. (Secret)
23. T.D. Hanscome and D.K. Willett. ITR-1116. May 1955. (Secret)
24. F.H. Shelton. SC-3363 (TR). April 1954. (Secret)
25. S. Glasstone and M. Edlund. Elements of Nuclear Reactor Theory. D. Van Nostrand Co. Inc. Nov. 1952. (Unclassified)
26. D.J. Hughes et al. Phys. Rev. 73. 111. 1948. (Unclassified)
27. J.R. Hendrickson et al. ITR-1121. May 1955. (Secret)
28. T.G. Walsh. WT-383. May 1952. (Secret)
29. P.S. Harris and L.J. Vortman. SC-33-56-51. Feb. 1956. (Secret)
30. E. Tochilin et al. WT-795. Sept. 1953. (Secret)
31. G.S. Hurst et al. Rev. Sci. Instr. 27. 3. Mar. 1956. (Unclassified)

Chapter 5

RESIDUAL GAMMA RADIATION

5.1 INTRODUCTION

Fallout is the name applied to radioactive debris from a nuclear detonation which, after some residence in the atmosphere, settles upon the earth's surface. It is a significant source of radiation only for high yield weapons, say of the order of 0.5 MT or greater, and for bursts which are low enough to allow the fireball to intersect the earth's surface. Some fallout occurs in small but measurable amounts at places thousands of miles removed from the point of burst. It is not at this time known to what extent deleterious effects may result from the radiations associated with this far-ranging fallout. The present study, however, is not concerned with fallout in relatively distant areas but rather with fallout in regions within a few hundred miles of the burst where activity is deposited in such amounts as to create an immediate hazard to health and safety.

Until the Greenhouse and Jangle test series (1951) there had been very little investigation of fallout phenomena. The particle and monitoring studies at Jangle and the accidental contamination of a number of Marshallese, Americans and Japanese as a result of the Castle test focused attention on the problem. Considerable effort has been subsequently devoted to fallout. Some of the fruits of this effort as well as some of the remaining unanswered questions are dealt with in discussion which follows.

This chapter covers such matters as the mechanisms by which fallout occurs, some of the devices used to compute and predict fallout patterns with some results, the rate of decay of fallout, the means of scaling experimentally observed fallout patterns to conditions other than those which prevailed during the experiment, the time of arrival of the contaminant, shielding, and some lesser associated topics. For most of the material there are large gaps in our current understanding, and what is presented frequently contains ambitious extrapolations from what is known. It is to be hoped that with further time and effort our understanding of these matters will come to rest on a firmer basis.

An excellent study of the physical phenomenology of fallout has been made in Project Aureole.[1]

5.2 MECHANISM OF FALLOUT

When a nuclear weapon explodes, the temperatures are high enough to vaporize the bomb and casing materials. As the hot gases rise and cool, these materials condense to particles of the order of one micron diameter at most. These particles, in the absence of other large particles to adhere to, remain suspended in the atmosphere for long periods of time and, generally speaking, settle out in low concentration over much of the earth's surface. Occasionally, local meteorological conditions cause a heavier than average deposition at some place. There then arises the phenomenon of fallout at places remote from the point of burst.

If, however, the burst occurs sufficiently close to the surface that the earth is intersected by the fireball, earth is mingled in the fireball with the bomb and casing materials. The earth particles are very much larger than the bomb particles, probably because much of the earth does not vaporize.[2,3] Active material accumulates on or in many of these particles, rendering them highly radioactive. These

particles fall in the gravitational field with velocities modified by the air resistance. They are carried horizontally from the point of burst by the winds at the various altitudes through which they fall.

The active particles begin settling upon the earth in important quantity immediately after the burst, and about one day later the fallout pattern is essentially complete. The contour of the contaminated region is, in most cases, roughly oval in shape (although substantial distortions from this shape may occur) with the elongated portion indicating the downwind direction for the effective wind averaged over altitude. The area of contamination and the intensity within that area depend principally on the wind field and the bomb yield.

Rain, snow, or hail can accelerate fallout somewhat since active particles are caught by the precipitation and brought to the ground more rapidly than otherwise. Higher intensities of activity may result over small areas. This scavenging may not be too important, however, because for the high yield bursts the active material probably spends much of the time at altitudes higher than those at which water vapor collects.

The following is a listing of the principal parameters which determine fallout dose and dose rate contours. Our knowledge of most of these parameters is quite scant, and our ability to predict fallout patterns is thereby severely limited.

1. Yield and type of bomb
2. Burst height
3. Soil type
4. Shape of cloud and stem
5. Height of cloud
6. Fraction of activity scavenged by particles
7. Spatial distribution of particles within cloud
8. Particle shape and density
9. Particle distribution in size
10. Distribution of activity among particles by size
11. Law governing atmospheric resistance to fall of particles
12. Wind vector field as a function of time and of the three space coordinates
13. Response of particles to forces exerted by wind
14. Lateral diffusion of particles

The items in the foregoing list are not all independent. A complete specification of atmospheric and soil conditions, of weapon type and yield, and of burst position would, in principle, fully determine the problem. At present, however, it is not known how to proceed to a solution from these initial conditions without making further assumptions about the details of the mechanism, and, in particular, without invoking most of the above parameters.

5.3 COMPUTATION MODELS

A number of organizations have addressed themselves to the problem of computing fallout patterns from given data about the nature of the bomb, the burst, and meteorological conditions. The preceding section listed fourteen parameters as determining the fallout pattern. Each of the computation models which have been devised treats some of these parameters differently from the other models. Hence, for some input conditions, in particular for those conditions where the wind direction varies strongly with altitude, the results produced using one model can differ markedly from the results

produced using another model. Figs. 5.3:1 and 5.3:2 present two wind fields, Conditions A and B, respectively, and the hypothetical fallout patterns based on these wind fields and calculated by several of the computation models. (The wind fields shown were actually observed at potential target areas.) It is clear that there is a wide disagreement on the nature of the fallout pattern to be expected in wind fields such as Condition A (Fig. 5.3:1). On the other hand, in spite of some spread in the results, there is approximate general agreement on the pattern of fallout to be expected in wind fields such as Condition B (Fig. 5.3:2).

These examples are cited for the following reasons:

1. To show that there is nothing like unanimity of opinion as to how to predict fallout. In the poor state of our present knowledge it is necessary to use the material of this chapter only in the realization that it represents best estimates and that it can contain considerable error.
2. To point up the need for the development of better techniques to compute fallout.
3. To stress the need of extensive further observations at weapons tests to evaluate the parameters of fallout, which are so inadequately known.

There is no sound criterion at present available against which to judge the validity of the results from the various models. The fallout from the Jangle surface shot was fairly well recorded; there was a partial record made of fallout from the Castle Bravo shot in the Marshall Islands; and the patterns from some of the tower shots in Nevada were very sketchily recorded. ARDC claims to have duplicated the fallout patterns for several of these shots including Jangle surface and Castle Bravo;[5] Rand Corporation claims to have reproduced the Castle Bravo pattern,[6] and USNRDL the Jangle surface pattern. Yet these three agencies show no agreement whatever in Fig. 5.3:2. The reason for this disagreement lies in the large number of unknown parameters in the calculation. When the solution is known beforehand and with judicious selection of values, almost any model can be made to produce a desired pattern. Furthermore, because there are so many arbitrary parameters available, a given model can be forced to agree with a good number of measured situations. This gives no guarantee, however, until agreement has been found in many qualitatively different situations, that the model will necessarily produce a correct pattern in a situation where the result is not known a priori.

It seems advisable to select from among the presently available models that which appears to be the most promising, even though the bases for selection are indirect. Evaluating the models as to (1) the experience of the agency, (2) the techniques and facilities used by the agency, and (3) the general credibility of the assumptions, we are led to choose the Rand model from among those now existent. This should not be taken as a blanket endorsement of the Rand method or condemnation of other methods. We believe that the Rand method can be improved by incorporating into it some of the better features of models of other agencies, that it can undoubtedly be improved as more information becomes known, and that events of the future need not necessarily establish it as the best of the methods now available. Nevertheless, if an interim reliance is to be placed on one of these methods, our choice would be the one developed by Rand.

The Rand model contains the following features.[6, 7]

1. Only surface bursts are handled (in common with most other models).
2. The cloud and stem are taken as cylinders of different dimensions. The coarse over-all diameters used in the Castle Bravo computation, however, are noticeably less than those actually observed.
3. Rand has a general scheme of cloud heights which admits variation with weapon yield, season, and geographical location.[8]
4. The spatial distribution of particles within the cloud is exponential, following the surrounding atmosphere.

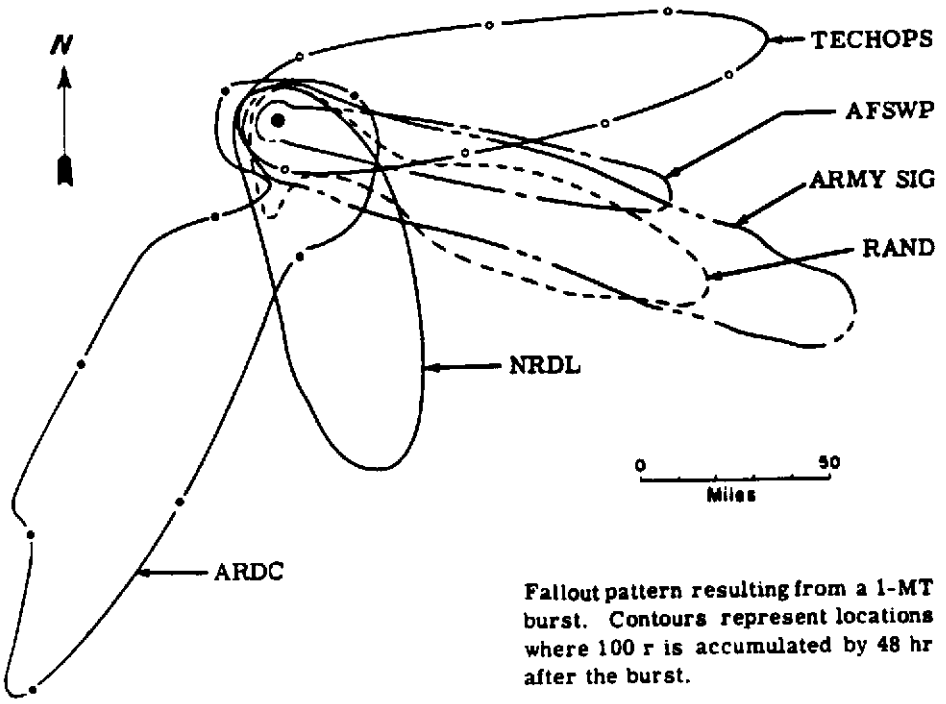

Fallout pattern resulting from a 1-MT burst. Contours represent locations where 100 r is accumulated by 48 hr after the burst.

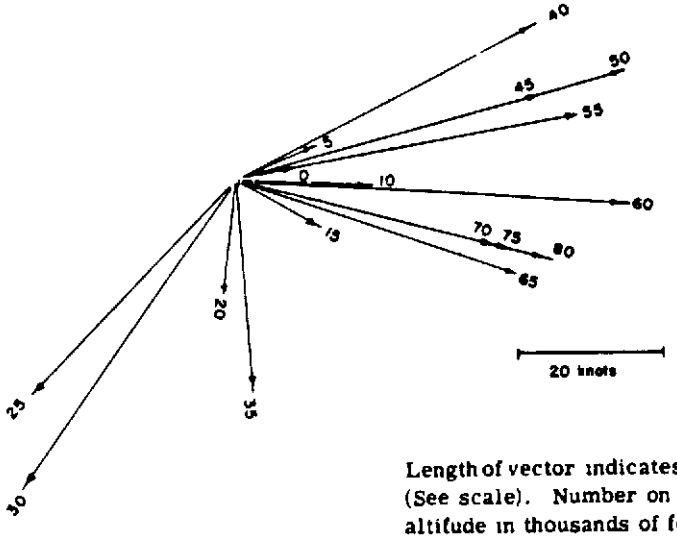

Length of vector indicates wind speed. (See scale). Number on vector gives altitude in thousands of feet.

Fig. 5.3:1 Wind Field and Fallout Pattern for Condition A

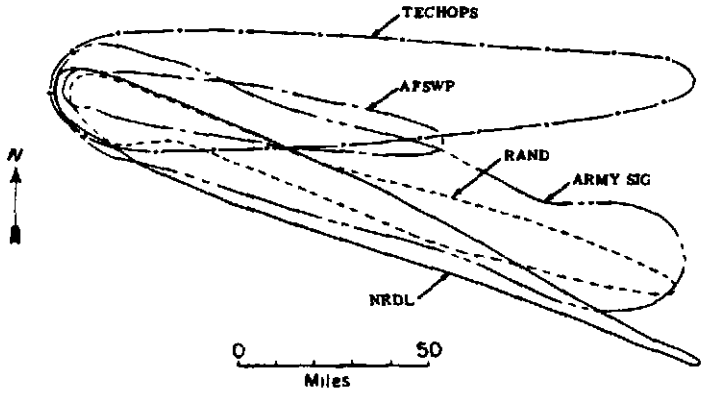

Fallout pattern resulting from a 1-MT burst. Contours represent locations where 100 r is accumulated by 48 hr after the burst.

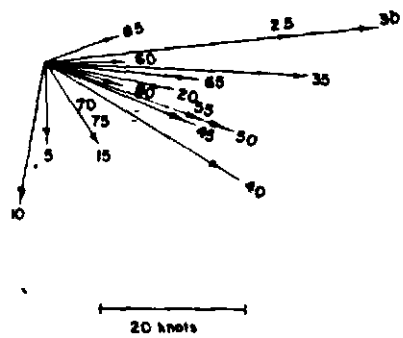

Length of vector indicates wind speed. (See scale). Number on vector gives altitude in thousands of feet.

Fig. 5.3:2 Wind Field and Fallout Pattern for Condition B

5. The cloud contains 90 percent of the activity, the stem 10 percent. ARDC has assumed 80 percent in the stem and 20 percent in the cloud for surface bursts. It is principally because of disagreement over this parameter that such large differences occurred in the proposed solutions to the previously cited example.

6. Particles are taken to be spheres and a corresponding aerodynamic law of fall is used. The assumptions of Technical Operations and USNRDL of irregularly shaped particles with corresponding laws of fall seem superior.

7. The activity distribution by size of particles is chosen ad hoc to fit the Jangle surface shot fallout pattern. It would seem preferable to use the size distribution observed in the USNRDL sampling even if there is some question as to the adequacy of the sample size.

8. Particles are assumed to move laterally with the local wind velocity (which varies with altitude) but without diffusion.

9. The wind may be varied in time.

10. The computation is coded for a high speed computing machine, thus adding immeasurably to its value.

Comparative discussions of other models can be found elsewhere.[9]

For defensive purposes it will be necessary to have a means of computing fallout which is much quicker than the method indicated above. Either a rapid and reliable approximation or an analogue simulator or both are desirable. Until such time as our understanding has progressed to the point where we are able to compute reliable patterns by long and tedious methods on digital computers, however, there can be little hope of developing the required short methods.

5.4 DECAY OF ACTIVITIES

Some of the most important information related to fallout is that concerned with the decay of activity. The reasons for its importance are twofold: (1) it has direct application in many operational situations, and (2) the facts about it are quite well known.

A source of activity, by the very reason of its radioactivity, becomes weaker with time. The process is referred to as decay. The decay characteristics of most nuclides which might be found in fallout debris are rather well known. It is therefore possible to construct total decay functions and simplified analytical approximations for them and to glean substantial results from their manipulation.

The low energy components of the fission product gamma radiation have not been thoroughly studied up to this time and their contribution to the total radiation remains unknown. As a consequence, there is some uncertainty in the average fission product energy and in the time variation of that average. Nevertheless, barring quite radical changes in the radiological potentialities of the weapon, the results presented in this section should be applicable within moderate limits of error - perhaps 25 to 50 percent.

Some of the questions that can be answered by the methods of this section are as follows:

1. If the dose rate at a given location and time after burst is known, what is the dose rate at any other time at the location?
2. If at some location the dose rate is known at a given time after burst, how much dose will be accumulated at the point during any time interval?
3. If the time required to reach an uncontaminated zone from some point within the fallout area by the most direct route is known, together with the shielding available during transit and the shielding available at the starting point, at what time should evacuation be undertaken to minimize the accumulated dose?

One very important restriction must be placed on the use of the methods described below. They should not be applied at any time before fallout is substantially complete. Before then, the dose rate expressed as a function of time depends mainly on rate of transport of material by the wind and very little on decay.

Experimental measurements[10] have been made of the activity encountered at Castle Bravo due to fission products and material activated by bomb neutrons. Based on these measurements and on the assumption that the average gamma ray energy is not a strongly variant function of time, the corresponding dose rates can be calculated. Fig. 5.4:1 is a plot of dose rates based on the Castle Bravo measurements; the rates are presented as the ratio of the dose rate at time t to the dose rate 1 hr after the burst. This ratio is called F(t) for convenience. Thus,

$$F(t) = \frac{\dot{D}(t)}{\dot{D}(H+1)} \qquad (5.4:1)$$

where

$\dot{D}(t)$ = dose rate t hours after the burst

$\dot{D}(H+1)$ = dose rate 1 hr after the burst.

Therefore, if the dose rate is known at any one time t_b, it can be found for any other time t_a from Fig. 5.4:1 and the simple relation

$$\dot{D}(t_a) = \frac{F(t_a)}{F(t_b)} \dot{D}(t_b). \qquad (5.4:2)$$

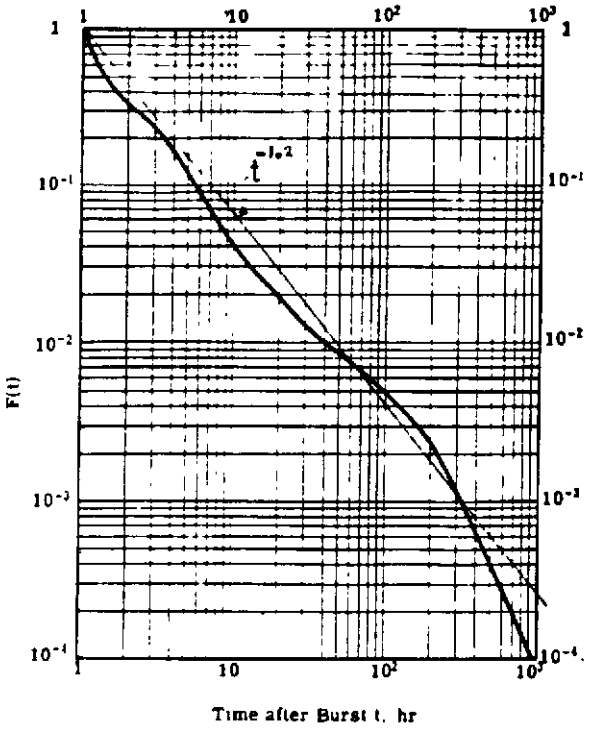

Fig. 5.4:1 F(t) as a Function of Time after Burst

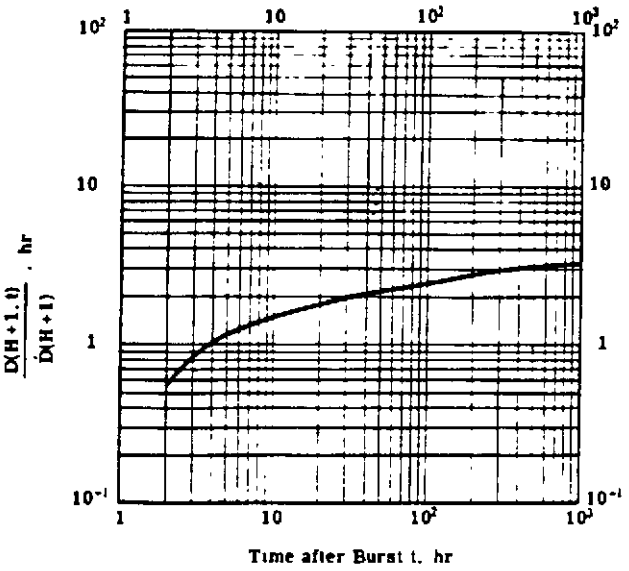

Fig. 5.4:2 $\frac{D(H+1,t)}{\dot{D}(H+1)}$ as a Function of Time after Burst

Fig. 5.4:2 is a plot of the variation with time of the dose accumulated between 1 hr after the burst and any later time t, divided by the dose rate at 1 hr after the burst. Thus, Fig. 5.4:2 presents

$$\frac{D(H+1,t)}{\dot{D}(H+1)} = \frac{\int_{H+1}^{t} \dot{D}(t')\,dt'}{\dot{D}(H+1)} = \int_{H+1}^{t} F(t')\,dt' \qquad (5.4:3)$$

where $D(H+1,t)$ = dose accumulated between 1 and t hr after the burst.

If, after the fallout is complete, the dose rate is known to be $\dot{D}(t_k)$ at some time t_k, then

$$\dot{D}(H+1) = \frac{\dot{D}(t_k)}{F(t_k)} \qquad (5.4:4)$$

and the dose accumulated between 1 and t hr after the burst is

$$D(H+1,t) = \frac{\dot{D}(t_k)}{F(t_k)} \left(\frac{D(H+1,t)}{\dot{D}(H+1)}\right) = \frac{\dot{D}(t_k)}{F(t_k)} \int_{H+1}^{t} F(t')\,dt' \qquad (5.4:5)$$

Similarly we may calculate the dose accumulated at a given location during any time period after fallout is complete. If the dose rate at a given location at any time t_k after fallout is complete is $\dot{D}(t_k)$, the expression for the dose accumulated during the time period t_m to t_n ($t_n > t_m$) is

$$D(t_m, t_n) = D(H+1, t_n) - D(H+1, t_m)$$

$$= \frac{\dot{D}(t_k)}{F(t_k)} \left(\frac{D(H+1, t_n)}{\dot{D}(H+1)} - \frac{D(H+1, t_m)}{\dot{D}(H+1)} \right) \qquad (5.4:6)$$

$$= \frac{\dot{D}(t_k)}{F(t_k)} \left(\int_{H+1}^{t_n} F(t) - \int_{H+1}^{t_m} F(t)\, dt \right)$$

Thus, $D(t_m, t_n)$ can be found from the known value of $\dot{D}(t_k)$ and from Figs. 5.4:1 and 5.4:2.

Finally, if there is an uncontaminated area within a reasonable distance, it may be of importance to evaluate the destrability of remaining in a place of shelter within the fallout field as compared to evacuation. It is possible, using the relations given above, to determine the time at which the shelter should be evacuated to minimize the total dose received from fallout. As above, this method can be applied only if fallout is complete before the time of evacuation. Assume the following:

1. that the transmission factor available within a shelter at a point inside the fallout field is T_s and that the transmission factor available during transit (the shelter afforded by a vehicle) is T_v. (The dose transmission factor of any shielding structure is defined as the ratio of the dose rate inside the structure to the dose rate outside.)
2. that the dose rate encountered in transit through the contaminated area falls off linearly, with time of transit, from the dose rate at the point of departure.

Then, if

t_k = some time after fallout is complete and at which the dose rate is known at the point of interest
t_ℓ = any convenient time after fallout is complete at the point of interest
t_m = time at which the point is to be evacuated
t_n = time at which the uncontaminated area is reached
$\dot{D}(t_k)$ = known dose rate at time t_k
D_A = dose accumulated from time t_ℓ to time t_m in the absence of shielding
D_B = dose accumulated during time of transit if there is no shielding during transit
$D_T(t_m)$ = total dose accumulated from t_ℓ to the time that the uncontaminated area is reached t_n

$$D_B = \frac{\dot{D}(t_k)}{F(t_k)} \left[\int_{t_m}^{t_n} F(t) \left(1 - \frac{t - t_m}{t_n - t_m} \right) dt \right] \qquad (5.4:7)$$

$$D_T(t_m) = D_A + D_B$$

$$= \frac{\dot{D}(t_k)}{F(t_k)} \left[T_s \int_{t_f}^{t_m} F(t)\, dt + T_v \int_{t_m}^{t_n} F(t) \left(1 - \frac{t - t_m}{t_n - t_m} \right) dt \right] \qquad (5.4:8)$$

It is clear from physical considerations that if $T_s \geq T_v$ evacuation should be immediate. If however $T_s < T_v$ it is necessary to examine the derivatives of Eq. 5.4:8 with respect to t_m to determine the optimum evacuation time. For this condition the optimum evacuation time is found to be that at which t_m satisfies the following equation.

$$F(t_m) = \frac{T_v}{T_s} \left(F(t_m) - \frac{1}{t_n - t_m} \int_{t_m}^{t_n} F(t)\, dt \right) \qquad (5.4:9)$$

Fig. 5.4:3 is derived from Eq. 5.4:9 and gives the values of t_m, the time after the bomb burst at which evacuation should be started to minimize the dose received, as a function of T_v/T_s. The transit time $t_n - t_m$ is given as a parameter.

Even in the absence of adequate methods to predict dose and dose rate patterns, the information which is available about decay rates is extremely useful. It is to be presumed that in the event of a nuclear attack by an enemy power, affected areas will be metered for dose rates at the earliest possible moment. The knowledge of the time behavior of the metered activity would then permit informed on-the-spot planning of personnel and material disposition.

PROBLEM 1

The dose rate is known to be $\dot{D}(t_a)$ r-hr^{-1} at a given location at (1) H+1 hr and (2) H+t_a hr. For each of these two cases calculate the corresponding dose rate t_b hr after the time of burst.

Solution

1. From Fig. 5.4:1 read $F(t_b)$, i.e., the value of $F(t)$ when $t = t_b$.
2. For case (1) the required solution is

$$\dot{D}(t_b) = \dot{D}(t_a)\, F(t_b)$$

3. For case (2) read from the same figure $F(t_a)$ as well as $F(t_b)$. The required solution is

$$\dot{D}(t_b) = \dot{D}(t_a) \frac{F(t_b)}{F(t_a)}$$

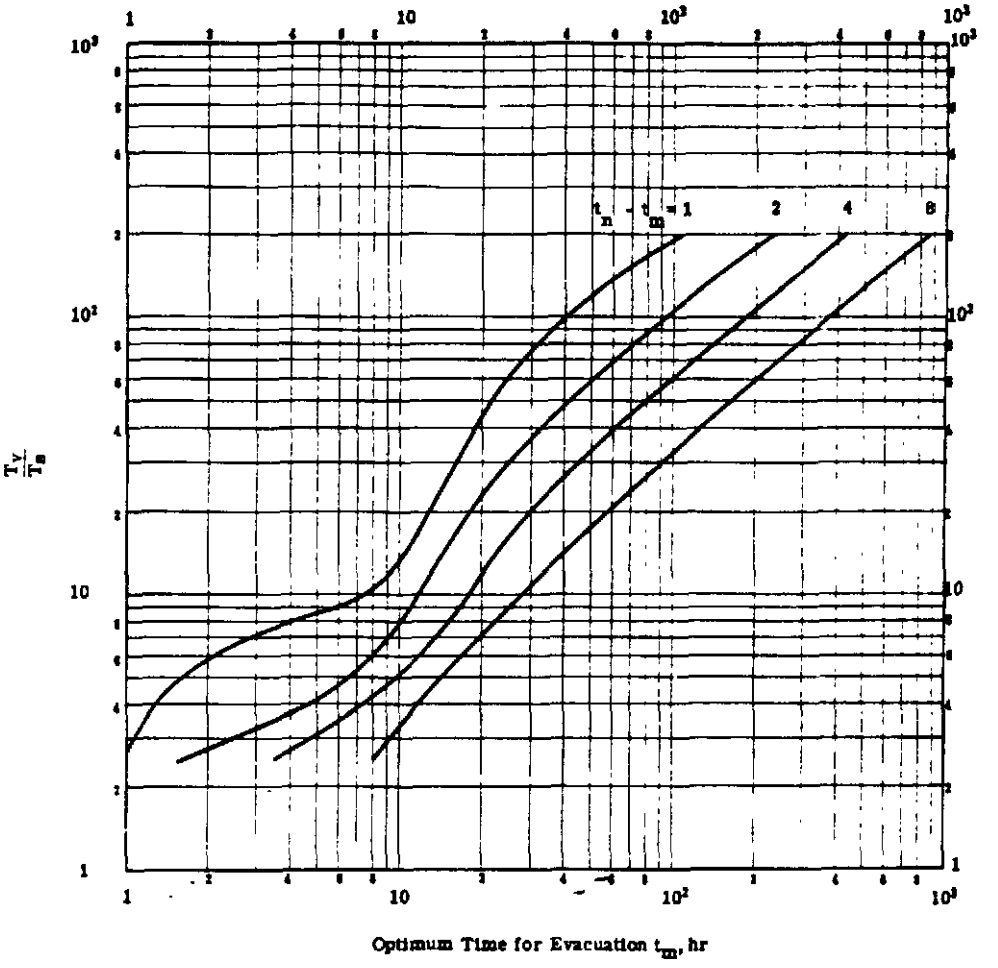

Fig. 5.4:3 Optimum Time for Evacuation of a Shelter Within the Fallout Field as a Function of T_V/T_S and the Transit Time $t_n - t_m$

Example

The dose rate at a point is required at H+10 hr. The dose rate at that point is known to be 400 r-hr^{-1} at (1) H+1 hr and (2) at H+5 hr. (Fallout is complete by H+1 hr.)

1. From Fig. 5.4:1, F(10) = 0.04
2. For case (1) the dose rate at 10 hr is

$$\dot{D}(10) = (400)\,(0.04) = 16 \text{ r-hr}^{-1}$$

3. For case (2), F(5) = 0.13 and the dose rate at 10 hr is

$$\dot{D}(10) = (400)\,\frac{(0.04)}{(0.13)} = 123 \text{ r-hr}^{-1}$$

PROBLEM 2

The dose rate at a point within the fallout field is known to be $\dot{D}(t_k)$ r-hr^{-1} at time t_k. It is desired to know what the accumulated dose at that point will be in the time interval t_m to t_n. Fallout was complete at that point before time t_f, which was earlier than t_k or t_m.

Solution

1. From Fig. 5.4:1, find $F(t_k)$.

2. From Fig. 5.4:2, find the values of $\int_{H+1}^{t_n} F(t)\,dt$ and $\int_{H+1}^{t_m} F(t)\,dt$.

3. The required accumulated dose is

$$D(t_m, t_n) = \frac{\dot{D}(t_k)}{F(t_k)}\left(\int_{H+1}^{t_n} F(t)\,dt - \int_{H+1}^{t_m} F(t)\,dt\right) .$$

Example

Fallout was complete at a point at H+5 hr. The dose rate at that point at H+6 hr is 50 $r\text{-}hr^{-1}$. How much dose accumulates at the point between H+5 and H+10 hr?

1. From Fig. 5.4:1, $F(6) = 0.09$

2. From Fig. 5.4:2, $\int_{H+1}^{10} F(t)\,dt = 1.5$, $\int_{H+1}^{5} F(t)\,dt = 1.2$

3. The required accumulated dose is

$$D(5, 10) = \frac{50}{0.09}\,[1.5 - 1.2] = 167\ r.$$

PROBLEM 3

Fallout was complete at a point before time t_ℓ. There is a shelter at the point whose shielding affords a gamma ray transmission factor of T_S. An evacuation vehicle is available and it has a gamma ray transmission factor of T_V. Assume that there is an uncontaminated area available and that it takes $t_n - t_m$ hr to reach this area. Further, assume that during transit the dose rate (outside the vehicle) falls off linearly with time from the dose rate at the point of departure (outside the shelter). At what time after the burst should the shelter be evacuated to minimize the total dose received?

Solution

1. Compute the ratio T_V/T_S.

2. For the value of T_V/T_S and the known values of $t_n - t_m$, find the corresponding value of t_m from Fig. 5.4:3.

[redacted]

Example

A shelter affords a transmission factor of 0.08. An evacuation vehicle is available which affords a transmission factor of 0.8. It will take 8 hr to reach an uncontaminated area. At what time after the burst (and after fallout is complete) should the shelter be evacuated to minimize the total dose received?

1. The ratio $T_v/T_s = 0.8/0.08 = 10$
2. From Fig. 5.4:3 for $T_v/T_s = 10$ and $t_n - t_m = 8$ hr, the value of t_m is 28 hr after the time burst. This is the time at which the shelter should be evacuated. Note that the result is independent of the dose rate. It holds as long as the radiation decays in time in a manner which is proportional to F(t), Fig. 5.4:1.

5.5 ISODOSE RATE CONTOURS

The isodose rate contours, along with the total integrated dose contours to various times, provide the greater part of the results of a fallout computation. The Rand Corporation calculations[11] appear to be the most comprehensive and possibly the best of those currently available.

It will probably never be possible to calculate a dose or dose rate pattern that can be believed literally in detail. However, a fair indication of areas of lethal, dangerous, and tolerable dose, some general notion of dose gradient, and an idea of the perturbations in pattern shape to be expected from input perturbations, like changes in the speed or direction of the wind, can well be hoped for.

Local differences in conditions within the fallout area also lead to very significant local fluctuations in patterns.

If a pattern is desired for a specific set of conditions, the pattern should be computed specifically for those conditions. There is at present no rapid way to make such a calculation. There is no very accurate way of deducing a pattern for one set of conditions from a known pattern for a different set. In short, until our grasp of the mechanics of fallout computations becomes much more sure and sophisticated, it is advisable to develop and maintain a rather extensive library of fallout patterns computed for many different situations.

Figs. 5.5:1 through 5.5:4 are downwind isodose rate patterns at H+1 hr. They are for two different yields and two different effective wind speeds. They are scaled from an idealized version of the experimentally determined patterns encountered at Castle Bravo.[12] As such, they do not purport to be the patterns encountered for any specific set of conditions. Rather, they are presented as an aid in making only roughly quantitative evaluations of the general potential of high yield weapons.

Except in the unusual situation when there are practically no winds aloft, the region around ground zero is contaminated chiefly by the large (say above 500-micron) particles which fall out of the cloud and stem. These particles fall so rapidly that they are little affected by the wind field. The extent of the pattern is determined roughly by the maximum dimensions of the cloud. The pattern centers close to ground zero, subject only to relatively small displacements by the wind; the controlling parameters are the soil, which determines the number of large particles available, and the yield, which determines the extent of the cloud. The downwind pattern, on the other hand, is controlled principally by the wind field.

The calculation of fallout patterns close to ground zero proceeds in much the same fashion as the calculation of downwind patterns. Accurate knowledge of large particle sizes and activity is considerably more crucial, however. For calculation of downwind patterns it is assumed that there is a time and height of cloud stabilization from which particles start falling. This assumption is not applicable for ground zero fallout patterns because the large particles begin to fall back to earth in important quantities very soon after the burst and before the cloud has attained anything close to maximum height. The objection can be partly met by deliberate alteration of the assumed spatial distribution of large particles. It is appropriate to make provision for these differences when setting up a computation.

[redacted]

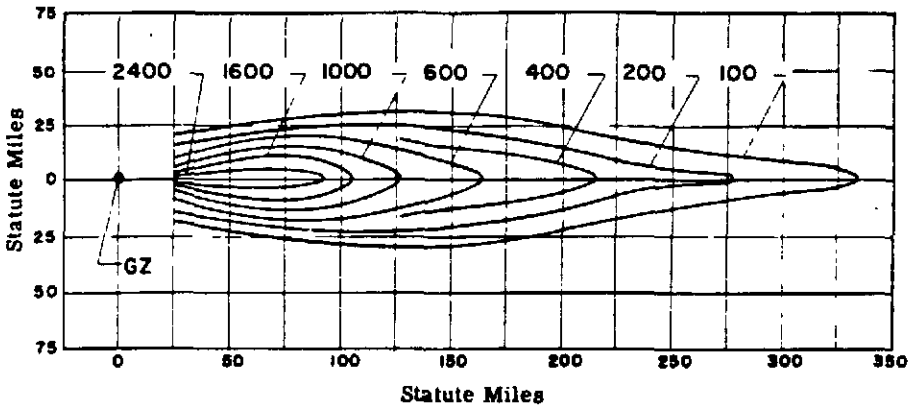

Fig. 5.5:1 Downwind Isodose Rate Pattern at H + 1 hr for 15-MT [redacted] Burst, 15-Knot Wind. Contours give dose rates in $r\text{-}hr^{-1}$.

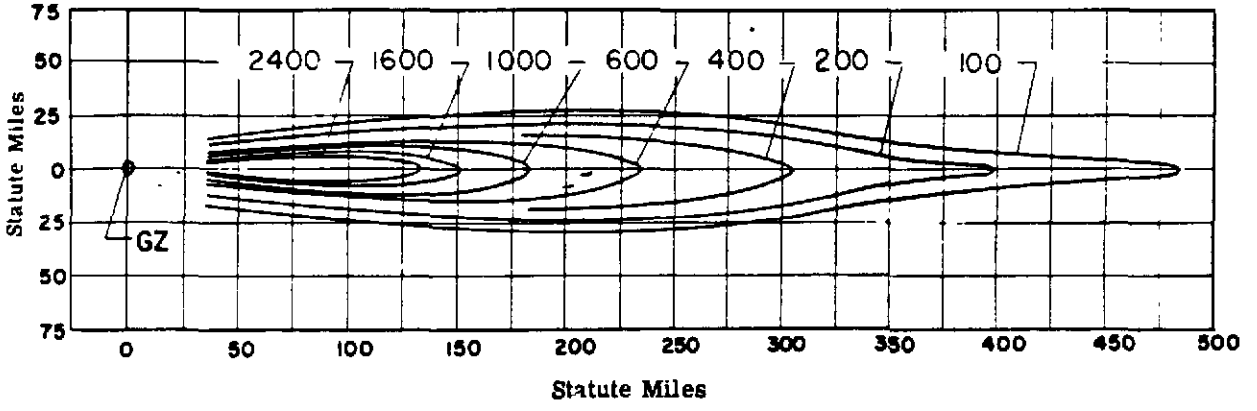

Fig. 5.5:2 Downwind Isodose Rate Pattern at H + 1 hr for 15-MT [redacted] Burst, 30-Knot Wind. Contours give dose rates in $r\text{-}hr^{-1}$.

Fig. 5.5:5 is a ground zero isodose rate pattern at H+1 hr for a 15-MT blast scaled by AFSWP from the Ivy Mike shot.[12] It is presented as the standard for planning in the 0.5 to 100 MT range. Since the ground zero pattern depends heavily upon the fraction of large particles available, Fig. 5.5:5 is strictly applicable only to coral sands such as those encountered in the Marshall Islands.

It is important to note that the isodose rate patterns in Figs. 5.5:1 through 5.5:5 are drawn for a reference time of H+1 hr. These patterns represent the dose rates at H+1 hr if the fallout were complete by that time, a condition which is rarely the case. For those cases where the fallout is complete by H+1 hr and the dose rate is desired at H+1 hr the value is read directly from the appropriate figure: For those cases where fallout is complete by H+1 hr and the dose rate is desired at a later time the dose rate value at H+1 hr is corrected by the methods described in Section 5.4 and the curve given in Fig. 5.4:1. For the more usual situation in which fallout is not complete by H+1 hr the dose rate can also be determined from Fig. 5.5:1 through 5.5:5 and Fig. 5.4:1, but only for times after fallout is complete. Figs. 5.5:1 through 5.5:5 cannot be used to calculate isodose contours for any time before completion of fallout.

[redacted] [redacted]

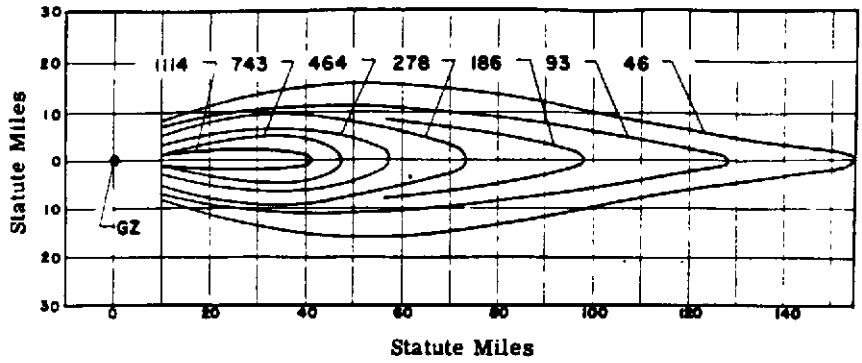

Fig. 5.5:3 Downwind Isodose Rate Pattern at H + 1 hr for 1.5-MT [redacted] Burst, 15-Knot Wind. Contours give dose rates in $r\text{-}hr^{-1}$.

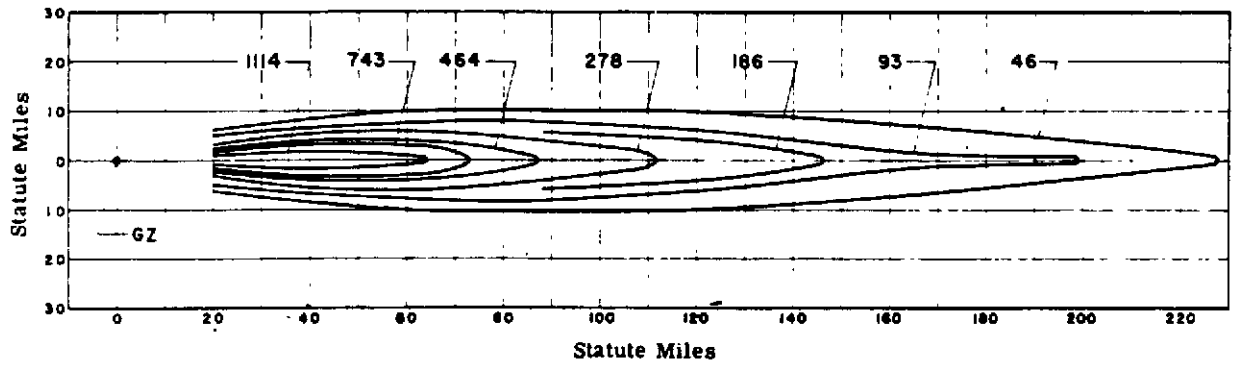

Fig. 5.5:4 Downwind Isodose Rate Pattern at H + 1 hr for 1.5-MT [redacted] Burst, 30-Knot Wind. Contours give dose rates in $r\text{-}hr^{-1}$.

It is worth remarking that in none of the diverse models of computing fallout and for none of the weapons considered, has any agency reported[4] a region where the H+1 hr dose rate substantially exceeded 10,000 $r\text{-}hr^{-1}$. There is no obvious physical mechanism which forces such a limit, and it may be that its apparent existence is merely fortuitous. Nevertheless, its persistent recurrence requires mention.

5.6 DETERMINATION OF EFFECTIVE WIND VECTORS, THE AREA OF FALLOUT AND THE TIME OF ARRIVAL

Military and civil authorities whose installations lie in the vicinity of a high yield atomic burst require specific information on the probable characteristics of the fallout, if maximum defense measures are to be taken when necessary. Prompt determination of the fallout characteristics and efficient use of the time before fallout commences can lead not only to the saving of lives but to the maintenance of the installation in a more operational condition following fallout than might otherwise have been possible.

The specific questions of primary importance are as follows:

1. In what direction from ground zero will the fallout occur, i.e., what are the effective wind vectors?

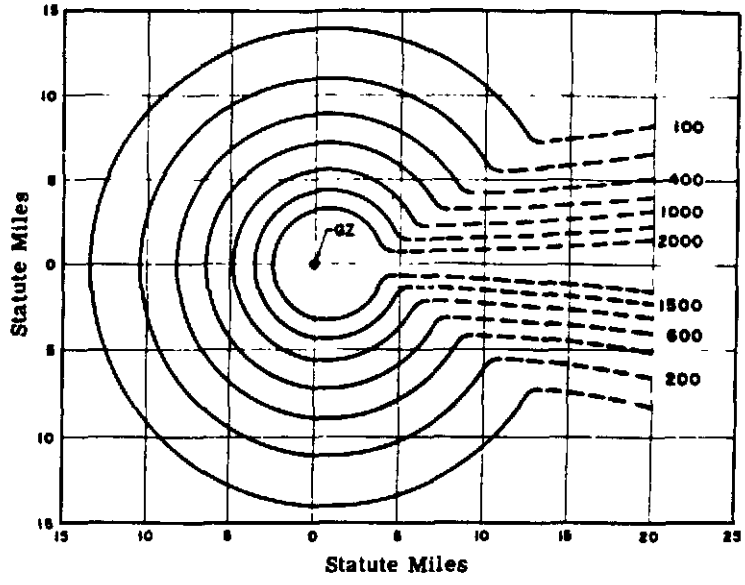

Fig. 5.5:5 Ground Zero Isodose Rate Pattern at H + 1 hr for 15-MT [redacted] Burst. Contours give dose rates in $r\text{-}hr^{-1}$.

2. Over what areas will the fallout occur, both in the vicinity of ground zero and in the area of downwind fallout?

3. What will the fallout time period be, i.e., when will it first arrive and how long will it last, both in the vicinity of ground zero and the downwind fallout area?

4. What are the dose rates to be expected in the fallout areas, both ground zero and downwind?

The first three of these questions are covered in the material that follows. The last question has been discussed to the degree presently possible in Sections 5.4 and 5.5.

In general these questions have to be answered in the order presented but their relative importance will vary depending on the situation. As the distance from ground zero increases, the importance will tend to shift from (4) toward (1). Thus, if the installation is in the vicinity of ground zero, fallout will occur almost immediately and the only question of importance involves the dose rates to be expected. At somewhat greater distances but still close enough so that fallout, if it does occur, will come shortly after the burst, the prime consideration is the length of time available for preparation. For very distant locations the major question is the direction from ground zero in which fallout will occur.

There is another factor which varies with distance from ground zero, namely the time available to determine the answers to the questions given above. For points close to ground zero very little time can be devoted to calculations since immediate action is required. Thus, only the simplest and quickest calculational methods are possible, which necessarily introduce the largest uncertainties into the results. The dangers inherent in such fast but inaccurate results may be considerable. It may be advisable, therefore, to determine for each installation an extensive catalog of calculated results for relatively nearby bomb bursts, based on prevailing weather variations and the most accurate methods available. The presently available methods may be used for initial determinations of such a catalog for simple wind situations but more accurate methods are needed and should be actively sought.

Completely adequate methods of determining quantitative answers are unknown at present and the best of the available methods are quite complex. The paragraphs below attempt to present relatively simple methods of obtaining the required information. It should be emphasized, however, that these

methods are applicable only to correspondingly simple wind fields. Where the wind field is complex, there appears to be no simple way of replacing the field with an effective wind vector or vectors and a more detailed calculation than given here seems mandatory.

The data required to estimate effective winds, fallout areas, and fallout time periods are:

1. distance and direction of the installation from point of burst,
2. wind field between point of burst and the installation,
3. height and diameter of atomic cloud at time of stabilization,
4. size range of fallout particles and
5. rates of fall of particles in size range and for altitudes of interest.

Items 1 through 3 will be known in general only after the bomb burst or may be assumed for calculation of given situations of interest before the event. Items 4 and 5 are characteristics which are known before the event.

5.6.1 DETERMINATION OF THE EFFECTIVE WIND VECTOR

Wind speed and direction may vary markedly with altitude at a given location. The composite of directions and speeds is known as the wind field and this field is of primary importance in determining the fallout pattern. It is to be expected that the wind field will not necessarily remain constant over any large area such as that between the point of burst and the installation. In a real situation the wind data available will be fragmentary at best and may have been measured at some distance from either ground zero or the installation. Under these circumstances nothing is gained by considering the additional complications introduced by variations in wind field and the assumption will be made, of necessity, that a wind field is known which does not vary over the entire area between ground zero and the installation.

With a knowledge of the wind field and the fallout particle characteristics it is possible to calculate the effective wind vectors. An effective wind vector is defined as the single vector which would produce the same fallout pattern as the wind field itself, for all particles starting at a given altitude. It should be noted that the effective wind vector is thus a function of altitude.

Table 5.6:1a, based on USNRDL calculations,[6] presents the time required for particles of irregular shape to fall through various altitudes in the atmosphere. The data are presented for particles from 50 to 1000 microns in diameter. (The 50-micron data are extrapolations of the USNRDL results.) While these data are thought to cover most of the range of interest,[13] additional information on the fall rates of particles less than 100 microns in diameter is highly desirable and fallout calculations should include the range of smaller particle sizes. Examination of the data in Table 5.6:1a indicates that, for the particle sizes and altitudes considered, the relative amount of time spent in any layer of altitude is almost independent of particle size. Table 5.6:1b gives the fractional total fall time for each altitude zone. These are averaged values for all particles between 50 and 1000 microns; they are given for particles starting their fall at 20,000-ft intervals with an upper limit of 100,000 ft.

From Table 5.6:1b and a known wind field, which is not too complex, an effective wind vector for each of the 20,000-ft intervals in altitude can be calculated. Thus, to determine the effective wind vector for a given altitude multiply each wind vector at that altitude and below by the corresponding fraction of total fall time found from Table 5.6:1b. Adding the weighted winds vectorially will give the effective wind for the particles falling from the given altitude.

PROBLEM 4

A high-yield bomb has been detonated sufficiently close by so that a particular installation may lie in the fallout field. The location of the burst, the height and diameter of the atomic cloud at, or close to, the time of stabilization, and the wind field in the area between ground zero and the installation are known.

TABLE 5.6:1

Characteristics of Irregularly Shaped Falling Particles

a. Partial Fall Time as a Function of Particle Size

Particle Size, microns	From, ft / To, ft	Partial Fall Time, hr 20,000 / 0	40,000 / 20,000	60,000 / 40,000	80,000 / 60,000	100,000 / 80,000
1,000		0.31	0.24	0.19	0.14	0.09
700		0.47	0.34	0.27	0.20	0.15
400		0.80	0.63	0.50	0.37	0.28
200		1.67	1.33	1.00	0.87	0.69
100		4.00	3.44	2.63	2.32	2.55
50 (extrapolated)		(11.)	(9.5)	(7.5)	(6.5)	—

b. Fraction of Total Fall Time Spent in Each Altitude Zone as a Function of Initial Height of Particle

Initial Particle Height, ft	From, ft / To, ft	Fraction of Total Fall Time Spent in Falling 20,000 / 0	40,000 / 20,000	60,000 / 40,000	80,000 / 60,000	100,000 / 80,000
100,000		0.31	0.24	0.19	0.15	0.11
80,000		0.34	0.27	0.22	0.17	—
60,000		0.42	0.32	0.26	—	—
40,000		0.56	0.44	—	—	—
20,000		1.00	—	—	—	—

c. Total Fall Time as a Function of Particle Size

Particle Size, microns	From, ft	Total Fall Time, hr 20,000	40,000	60,000	80,000	100,000
1,000		0.31	0.55	0.74	0.88	0.97
700		0.47	1.08	1.08	1.28	1.43
400		0.80	1.43	1.93	2.30	2.58
200		1.67	3.00	4.00	4.87	5.56
100		4.00	7.44	10.07	12.39	14.94
50 (extrapolated)		(11.)	(20.5)	(28.)	(34.5)	—

Compute the effective wind vectors for particles falling from several heights, starting from the maximum cloud height.

Solution

1. Tabulate the wind direction and speed as a function of altitude with the height of the top of the cloud as an upper limit.
2. Group the wind vectors in 20,000-ft altitude intervals. Determine the average wind vector for each altitude interval. The average wind vector may be determined by inspection if the spread in direction is not large or by vector addition and averaging if the spread is large.
3. Multiply the average wind speeds from (2) by the weighting factors (fraction of total fall time) for the corresponding altitude zones and starting altitudes found in Table 5.6:1b. Do this for particles starting at the top of each altitude interval.
4. Add the winds resulting from (3) vectorially for each starting altitude. This can be done either graphically on polar coordinate (circular) graph paper or numerically. The vector sum gives the effective wind speed and direction for particles starting at the several altitudes.

Example

An installation lies 200 miles due east of the point of a high-yield atomic explosion and thus possibly within the fallout path. The installation commander has been given the following information.

1. The active cloud will probably attain a maximum height of 80,000 ft and stabilized diameter of 60 miles.
2. The wind field is given below for 5000-ft increments of altitude.

Find the effective wind vectors for particles falling from 80,000, 60,000, 40,000, and 20,000 ft.

1. The wind field is as follows:

Altitude, thousand ft	Wind Speed, miles-hr^{-1}	Wind Direction, °
0	0	–
5	11	10
10	20	325
15	14	280
20	19	265
25	34	260
30	47	265
35	37	305
40	27	290
45	23	310
50	28	300
55	20	280
60	11	285
65	21	305
70	7	295
75	8	285
80	10	250

Note that the wind direction is measured from the compass heading from which the wind arrives, with 0° being due north and 90° being due east.

2. The wind fields averaged over 20,000-ft altitude zones are as follows:

Altitude, thousand ft	Average Wind Speed, miles-hr^{-1}	Average Wind Direction, °
0 - 20	12	305
20 - 40	33	275
40 - 60	22	295
60 - 80	12	285

The average wind vectors for the three altitude zones between 20,000 and 80,000 ft were determined by inspection, since the variation in wind direction is not large. The average wind vector for 0 - 20,000 ft required vector addition because of the larger spread in wind direction.

3. Using the results of (2) and the weighting factors from Table 5.6:1b, the weighted average wind speed is calculated for particles starting from the several altitudes.

Particle Starting Altitude, thousand ft	Altitude Zone, thousand ft	Average Wind Speed, miles-hr^{-1}	Weighting Factor	Weighted Average Wind Speed, miles-hr^{-1}	Average Wind Direction, °
80	0 - 20	12	0.34	4.1	305
	20 - 40	33	0.27	8.9	275
	40 - 60	22	0.22	4.8	295
	60 - 80	12	0.17	2.0	285
60	0 - 20	12	0.42	5.0	305
	20 - 40	33	0.32	10.6	275
	40 - 60	22	0.26	5.7	295
40	0 - 20	12	0.56	6.7	305
	20 - 40	33	0.44	14.5	275
20	0 - 20	12	1.00	12.0	305

4. By vector addition, as shown in Fig. 5.6:1 for 80,000 ft, the effective winds for particles starting from each of the several altitudes are as follows:

Particle Starting Altitude, thousand ft	Effective Wind Speed, miles-hr^{-1}	Effective Wind Direction, °
80	20	290
60	21	285
40	21	285
20	12	305

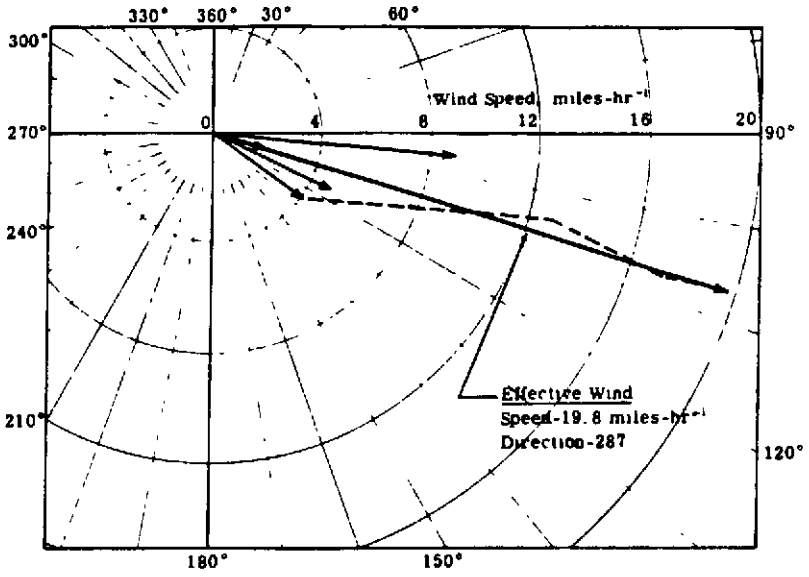

Fig. 5.6:1 Graphical Determination of Effective Wind Speed and Direction for Particles Falling from 80,000 ft (Problem 4)

5.6.2 DETERMINATION OF THE FALLOUT AREA

Fallout may be considered to occur over two separate areas – the region around ground zero and the region around the effective wind vectors. It is most convenient to discuss these areas separately as the fallout characteristics of each are quite different.

The immediate area around ground zero will almost certainly experience fallout. Further, this fallout may cover a wide region; it occurs very shortly after the burst and is essentially independent of the wind field. The rapidity and wide coverage of this fallout is the result of two factors – the very rapid initial expansion of the cloud diameter, particularly after it has reached its stable (maximum) height, and the very rapid fall of the heaviest particles in the cloud. These particles start falling before the cloud has even begun to approach its stabilized height.

While the available data are incomplete, experience at Castle gives the magnitude of the ground zero fallout area. A 15-MT weapon will produce a cloud with about a 70-mile diameter at 10 min after the burst. Moreover, although the cloud has reached its stable height by this time, its diameter may still be growing rapidly. It is the diameter at the end of the period of rapid expansion which is of most interest, since it determines both the maximum extent of the fallout around ground zero and the time at which the normal atmospheric dispersing forces become important in determining the downwind fallout.

The stabilized cloud diameter is a function of both weapon yield and atmospheric conditions, particularly tropopause height. Unfortunately, the data available on cloud diameters for high yield weapons are not complete, giving values at 10 min rather than at the end of the growth period. Further, no corrections for atmospheric variations are made. In the absence of anything better we are forced to use the 10-min diameters, even though these data will tend to underestimate the fallout area around ground zero. It is suggested, therefore, that the area around ground zero which receives immediate fallout be taken as having the diameters shown below as a function of bomb yield.

[redacted]

TABLE 5.6:2

Atomic Cloud Diameters for High-Yield Weapons at 10 min after Burst

Yield, MT	Cloud Diameter, miles
1	20
5	30
10	50
15	70

As is true for the other aspects of fallout, there are no completely reliable calculational methods for determination of downwind fallout, but there are three alternative approximate methods which can be suggested. The methods differ in the length of time required and the probable accuracy of the results, the quickest method giving the roughest result. Choice of a particular method will depend on the urgency of the individual situation.

The first two methods (A and B) define the entire fallout area in order to determine if fallout will occur at a given location. Method A gives only the outside angle of the probable fallout area. Method B, while somewhat more involved, gives an indication of the length of the fallout area as well as its width around the effective wind vectors. If the installation falls either within or some distance away from the areas found by either A or B, the probability of fallout occurring is clear. If, on the other hand, the installation lies near the boundary of the fallout area, the judgment of the observer is required to estimate the possible danger. Further, neither method as presently outlined requires any statement on the distribution of the active material with altitude at the time of stabilization. (It is implied, however, that there is some active material at all heights below the maximum height of the cloud.) When the actual distribution of activity with altitude is definitely determined, the effective wind vectors for altitudes with unimportant amounts of active materials may be neglected. Present indications are that a large part of the activity is concentrated in the cloud; based on this, the effective wind vectors for the highest altitudes should be more heavily weighted. In the examples presented in this section the effective wind vectors will, however, all be given equal weight.

The third method (C) provides a very rapid means of determining whether fallout will or will not occur at a given installation but it does this without defining the entire fallout area.

Method A

For very simple wind fields a sector can be drawn around the wind vectors for altitudes below the maximum height of the cloud. It is then assumed that the angles of this sector when applied to the cloud diameter define the area within which fallout will occur.

Method B

For wind fields which are somewhat more complicated but still not so complex as to invalidate use of any approximate method, it is possible to use the effective wind vectors at various altitudes to estimate the fallout area. The individual vectors presumably indicate the lines about which the fallout concentrates due to particles starting from a given altitude. The network of vectors then outlines the total area covered by particles falling from all altitudes. The choice of the range of altitudes to be used depends on one's estimate of the initial distribution of radioactive material with altitude. The most conservative assumption is that the active materials are distributed over all altitudes up to the maximum. The outer angles of the area defined by the several effective wind vectors, when applied to the cloud diameter, give the fallout area.

[redacted]

Method C

Fig. 5.6:2 presents graphically the data of Table 5.6:1c, the total fall time for given particle sizes as a function of the altitude from which the fall starts. In addition to these data, estimates are necessary of the maximum wind velocity in the general direction of the installation from ground zero, the maximum cloud height, and the separation distance. Assuming that the particles travel with the maximum wind velocity at all times, the approximate arrival time can be calculated. Knowing this time (which is equal to the fall time) and assuming that the particles start from the maximum cloud

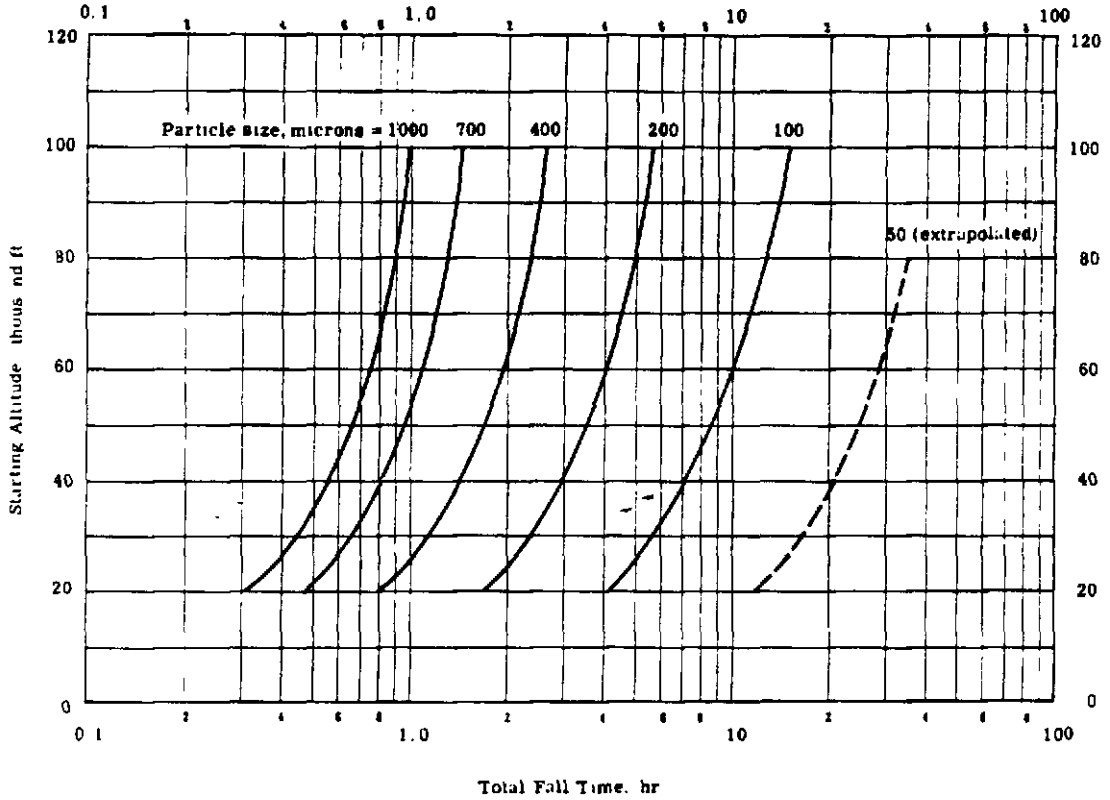

Fig. 5.6:2 Total Particle Fall Time as a Function of Starting Altitude

height, Fig. 5.6:2 will provide the size of the largest particle that will arrive at the installation. If this particle is below the size which contributes importantly to fallout (say 50 microns), then fallout will probably not occur. If it is much larger than 50 microns, fallout should be expected. This method is conservative since it assumes that the particles travel with the highest wind velocity throughout, directly toward the installation, and start falling from the maximum altitude, a combination of circumstances which is unlikely.

PROBLEM 5

For the situation described in Problem 4 calculate the probable area of fallout and whether fallout will occur at the installation.

Solution

Method A (simple wind fields)

1-2. Same as Problem 4

3. Plot the average wind vectors on polar coordinate (circular) graph paper with the origin taken as ground zero. Draw the sector best defined by these vectors, disregarding or assigning relatively small weight to vectors near the boundaries of the sector.

4. Draw the cloud centered at ground zero with the diameter assumed at stabilization. Expand the sector found in (3) so that it is tangent to the cloud diameter. The area defined by this enlarged sector is the probable fallout area.

5. Plot the position of the installation and observe if it falls within or near the boundaries of the enlarged sector found in (4).

Method B (wind field of intermediate complexity)

1-4. Same as Problem 4

5. From Table 5.6:1c determine the total number of hours necessary for the 50-micron particle to fall from the several starting altitudes to zero altitude.

6. Multiply the effective wind speeds for each starting altitude by the corresponding total fall time from (5) and plot the resulting maximum fallout distance vectors on polar coordinate paper.

7. Draw the cloud centered at ground zero with the diameter assumed at stabilization. Move the network of maximum fallout distance vectors found in (6) to the outer dimension of the cloud. The area defined by the vectors is the probable fallout area.

8. Plot the position of the installation and observe if it falls within or near the boundaries of the area found in (7).

Example

For the conditions described in the first example determine the fallout area and whether the installation lies within its boundaries.

Using Method A

1-2. The wind field and average winds are as tabulated in Problem 4.

3. The average wind vectors for the altitude zones of interest (80-60,000, 60-40,000, 40-20,000, 20,000-0 ft) are plotted in Fig. 5.6:3.

4. The cloud and the expanded sector are plotted in Fig. 5.6:3. The expanded sector is then the assumed fallout area. (Note that the wind vectors and linear dimensions are not to the same scale.)

5. The installation is plotted 200 miles due east of ground zero. It can be seen to fall just within the probable fallout area; fallout can therefore be expected, but it will probably be of relatively low intensity.

Using Method B

1-4. The wind field, average winds, and effective wind vectors are as calculated in Problem 4.

5. From Table 5.6:1c the total fall time for 50-micron particles as a function of starting altitude is as follows.

Initial Particle Height, thousand ft	Total Fall Time for 50-micron Particles, hr
80	34.5
60	28.0
40	20.5
20	11.0

6. The effective wind speed for each starting altitude is multiplied by the corresponding total fall time from (5) to yield the maximum fallout distance. The maximum fallout distance vectors from ground zero are plotted in Fig. 5.6:4.

Initial Particle Height, thousand ft	Total Fall Time for 50-micron Particles, hr	Effective Wind Speed, miles-hr^{-1}	Maximum Fallout Distance, miles	Effective Wind Direction, °
80	34.5	20	690	290
60	28.0	21	590	285
40	20.5	21	430	285
20	11.0	12	130	305

7. The cloud and the networks of fallout vectors starting from the outer diameter of the cloud are plotted in Fig. 5.6:4. The envelope drawn around the networks of vectors then defines the fallout area.

8. The installation location is plotted 200 miles due east of ground zero and it is seen to fall outside but near the boundary of the fallout area. The prudent conclusion would be again (as in Method A) that fallout is likely to occur at the installation but in relatively moderate amounts.

It is worthwhile to compare the fallout areas as determined by the two methods. It is clear that the direction of the fallout area is the same but this is not surprising since the winds are all generally in the same direction. The widths of the fallout zones, however, are somewhat different since Method A yields an area which continually expands with increasing distance from the burst point while Method B produces an area which is of roughly equal width for most of its length before it closes up. The latter method thus seems to agree more closely with measured results and this may justify the extra effort required for the calculation.

PROBLEM 6

For the situation described in Problem 4 determine if fallout occurs at the installation.

Solution

Method C

1. Determine the highest wind velocity in the general direction of the installation from ground zero.

2. Determine the separation distance between active material and installation by subtracting the cloud radius at stabilization from the distance from ground zero to the installation.

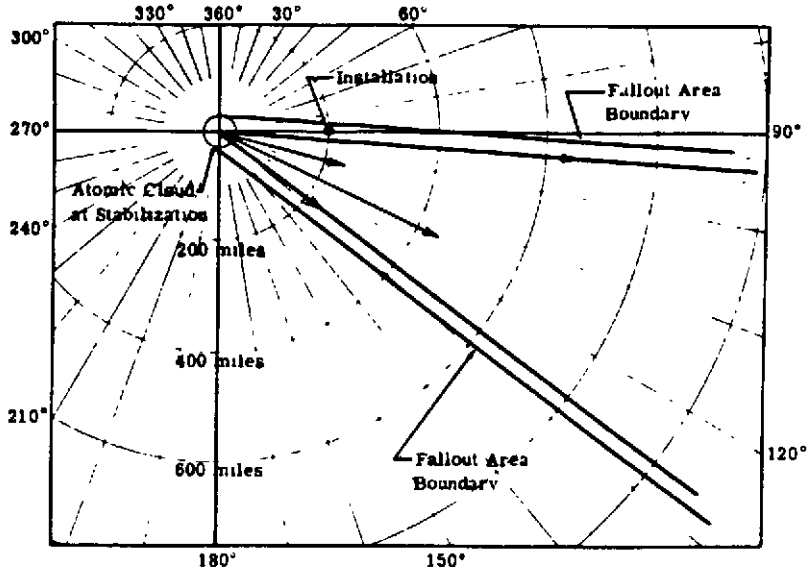

Fig. 5.6:3 Determination of Fallout Area (Problem 5 – Method A)

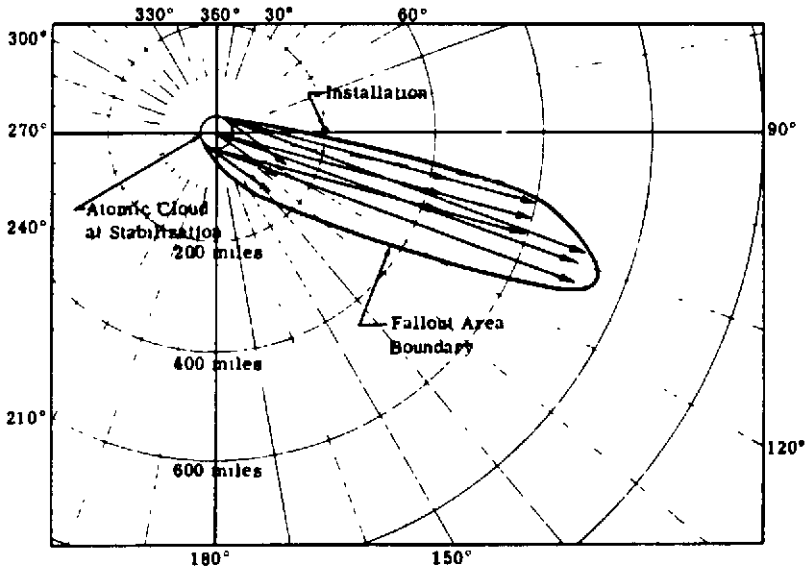

Fig. 5.6:4 Determination of Fallout Area (Problem 5 – Method B)

3. Divide the separation distance found in (2) by the wind velocity found in (1) to obtain the approximate time of arrival.

4. From Fig. 5.6:2, at the time found in (3) and the maximum cloud height, read the particle size to be expected at the arrival time. If this is 50 microns or less, there probably will be no appreciable fallout. If it is much larger than 50 microns, fallout should be expected.

Example

For the conditions described in the first example determine if the installation will receive fallout.

Using Method C

1. The maximum wind velocity in the general direction of the installation is about 45 knots.
2. The separation distance is 200-30 = 170 miles.
3. The approximate time of arrival is 170/45 or about 4 hr.
4. Fig. 5.6:2 indicates that particles falling from the maximum cloud height of 80,000 ft in 4 hr are 250 microns in diameter. Fallout may therefore be expected to occur.

5.6.3 DETERMINATION OF FALLOUT TIME PERIOD

The final question to be answered, once it is known that fallout is likely to occur, regards the time of arrival of fallout and the length of the fallout period. In the absence of violently variable wind fields, it may be generally expected that in the area around ground zero fallout will start essentially immediately and last for 1 or 2 hr. For regions a few hundred miles downwind, fallout might not start until 10 or 15 hr after the burst and last an equally long period. These are very coarse statements, subject to the caprice of the wind. A wind that doubled back on itself in time could even lead to two separate fallout periods at the same spot.

A more thorough examination of the fallout time period is presented below, again considering fallout around ground zero and downwind separately.

The available data on ground zero fallout arrival time are sparse and conflicting. Thus, after Ivy Mike, fallout arrived at lagoon stations (5 to 15 miles from ground zero) at about 45 min after burst time, but after the Castle tests the time of arrival at lagoon stations was only about 6 min. No explanation for the conflict is offered. Using these data, a rough estimate would be that fallout would probably arrive in the area around ground zero (with the diameter previously indicated) within about 30 min of the burst. For practical purposes it may be well to consider that it arrives immediately.

From the information determined in the preceding sections, fallout arrival time downwind of the burst point can be easily calculated. If the installation lies in the middle of the fallout area, the time of arrival is obtained by dividing the separation distance between active material and the installation by the largest of the calculated effective wind speeds. Note that the separation distance is not the distance between burst point and installation but rather it is this distance less the radius of the stabilized cloud. This reduced distance is used since the active material is transported to the cloud radius almost immediately after the burst by cloud expansion.

If the installation is not at or close to the middle of the fallout area, as will be true in most cases, the question arises as to the proper value of the separation distance or alternatively the proper value of the wind speed. For simple wind fields and distances far from the point of burst the errors introduced by the use of the separation distance and the effective wind speed, as determined for points on the effective wind vector, are small and can be neglected in comparison with the inherent uncertainties of the method. For wind fields which produce broad rather than elongated fallout areas or for locations close to ground zero, the importance of choosing the correct separation distance (or effective wind speed) is greater. Two simple alternatives are possible – using the separation distance as previously defined or using this separation distance multiplied by the cosine of the angle between the ground zero-installation heading and the effective wind vector. In either case the effective wind speed is used. The second approach is the more conservative of the two but it may very well be over-conservative since it implies that fallout particles are traveling even faster toward the installation than

along the effective wind vector. It is recommended, therefore, that to determine time of arrival throughout the fallout area at both close and distant points from ground zero the separation distance be divided by the highest effective wind velocity, ignoring the cosine multiplication.

Similarly, an estimate of the time of arrival of particles from other starting altitudes may be obtained by dividing the separation distance by the effective wind velocity for particles starting at the altitude of interest.

Information on the particle sizes involved during fallout (and indirectly an estimate of when fallout will end) can be obtained by an examination of Fig. 5.6:2. Knowledge of the arrival time for particles starting from a given altitude from Fig. 5.6:2 will allow an estimate to be made of the particle sizes corresponding to that arrival time. Assume a separation distance of 100 miles and an effective wind speed of 20 miles-hr^{-1} for particles starting at 80,000 ft. The arrival time of these particles is 5 hr and from Fig. 5.6:2 the particle size arriving at the receiver from 80,000 ft is about 200 microns. Using other known effective wind speeds allows a rough estimate to be made of the distribution in time of fallout particle size at a given location.

Further, knowing the smallest particle size which makes an appreciable contribution to the fallout allows an estimate to be made of the end of the fallout period. This would be the time after which only particles smaller than the given size arrive at the installation.

PROBLEM 7

For the situation described in Problem 4 calculate the probable time of arrival of fallout, the particle sizes which arrive as a function of time, and the probable end of the fallout period.

Solution

1. Determine and tabulate the effective wind vectors by the method outlined in Problem 4.
2. Determine the distance between ground zero and the installation and subtract from this distance the radius of the atomic cloud at stabilization. This is the separation distance.
3. Divide the separation distance found in (2) by the effective wind velocities found in (1). The shortest time found by this division is the time of arrival.
4. Using the times found in (3) and the corresponding initial particle altitudes, read from Fig. 5.6:2 the particle sizes which arrive at each time and from each altitude. The end of fallout will be taken as the time after which no particles larger than some chosen size (say 50 microns) arrive.

Example

1. From Problem 4 the effective wind vectors for each initial particle altitude are as follows:

Initial Particle Altitude, thousand ft	Effective Wind Speed, miles-hr^{-1}	Effective Wind Direction, °
80	20	290
60	21	285
40	21	285
20	12	305

2. The distance between ground zero and the installation is 200 miles. The radius of the stabilized cloud is 30 miles. Thus, the separation distance is 170 miles.

3. The time of arrival of particles starting at various altitudes is as follows:

Initial Particle Altitude, thousand ft	Effective Wind Speed, miles-hr^{-1}	Time of Arrival at Installation, hr
80	20	8.5
60	21	8.1
40	21	8.1
20	12	14.2

Thus fallout will arrive at the installation at about 8 hr after the burst.

4. From the results of (3) and Fig. 5.6:2 the time distribution of particle sizes and the probable end of the fallout period can be estimated.

Time of Arrival at Installation, hr	Estimated Particle Size, microns
8.1	95
8.1	115
8.5	130
14.2	40

Note that the particle size does not decrease smoothly with time. The sizes given should be considered as characteristic of the distribution that actually arrives at a given time. If one accepts 50 microns as the lower limit of particle size of importance, one can estimate that after 13 or 14 hr the fallout is essentially complete.

5.7 DELIVERY RATES

A knowledge of delivery rates during the fallout period is in itself not of major practical interest. What is important, however, is the dose rate measured at a given installation as a function of time. The value of delivery rate information is that dose rate curves may be derived from delivery rates. An installation commander with the knowledge of dose rates may be able to estimate the total dose to be delivered some hours before his meters could provide this information.

There are in fact several different kinds of fallout delivery rates which may be considered but very little information is available on any of them. This is primarily because they are very difficult to determine, either by calculation or by measurement in the field.

It is necessary to distinguish between these different kinds of delivery rates. There is first, the delivery rate of fallout material in terms of the weight delivered per unit time and unit area. This delivery rate is determined by the total number of particles and their size distribution, both as a function of time of arrival. (Part of the required data for calculation of the weight delivery rate could be provided by the methods of Section 5.6). Second, since each unit weight of fallout material is emitting radiation, there is also a delivery rate in terms of dose rate (say r-hr^{-1}) per unit time and unit area. This dose delivery rate will be a function not only of the particle number and size distribution but also of the activity content per particle and the decay characteristics of this activity. Third, there is a dose delivery rate in which all the activity is corrected back to some reference time, such as 1 hr after burst. This corrective dose delivery rate has the advantage that its value is not complicated by the decay of the active material.

The delivery rate of most interest is the dose delivery rate. If it can be calculated for a given situation, its integral over time will yield the expected dose rate as a function of arrival time. The

calculated dose rate curve could then be compared with actual fallout measurements during the initial part of a comparable, actual fallout period. At some time, as a result of this comparison, it may be possible to predict the rest of the dose rate curve. What information there is available about the dose delivery rate within the fallout period indicates that the rate reaches its maximum early and then tapers off. This early maximum is caused not only by the differential in the times of arrival of particles of various sizes but also by the continuous decay of the activity.

In the absence of any comparison between dose rates based on calculated delivery rates and actual measurements, the importance of the delivery rate determination is uncertain. For some situations, where the wind field is complex, it may very well be impossible to calculate valid delivery rates, but in any case this kind of situation is generally beyond the level of the present treatment. Even for simple wind fields the delivery rate calculation is quite complicated and requires large amounts of data which are presently unavailable. Further, depending on the shape of the delivery rate curve, the time savings in prediction of total dose may not be large enough to be particularly useful. Under such circumstances all that the commander of an installation can act on is the dose rate actually being received at a given time during the fallout period. Using the methods of Section 5.4, a calculation can be made of the total dose which would be received between the time of measurement and any time up to 1000 hr after the burst, but only due to the active material accumulated up to the time of measurement. (The dose received after 1000 hr is relatively small.) At some level of the measured dose rate or of the predicted total dose, the installation commander would initiate appropriate measures, e.g., evacuation.

Nevertheless, while it is unlikely that a precise determination of delivery and dose rates can be made a priori, on account of the sensitive dependence on many inaccessible parameters, it is possible that the general shape and extent of these rates for various classes of bursts and wind conditions can be determined. Even information of this nature may be valuable in anticipating, on the basis of incomplete metering, the extent of fallout at a given point.

5.8 SCALING WITH YIELD AND EFFECTIVE WIND VELOCITY

One of the most closely reasoned methods for scaling dose and dose rate contours is that developed at USNRDL.[14] This method provides a device for scaling the downwind pattern with yield when wind conditions remain constant, and for scaling with changes in average wind conditions when yields remain constant. By successive application of the two principles, it is possible to scale for simultaneous changes in yield and average wind conditions. The USNRDL method was devised for weapons which develop their entire energy release from the fission process. The formulae will be presented first for fission weapons and then will be extended to cover weapons which derive only part of their energy from the fission process.

A remark should be made at this point about the meaning of average wind. Strictly speaking, the wind scaling procedure applies only if every component of the wind field is multiplied by the same number, and if the relative angles between all components remain unchanged. Such severe restrictions, if rigorously met, however, would so limit the application of the method as to destroy its usefulness. It is believed that a good approach to the real situation can be achieved by replacing the entire wind field with a reasonably chosen average wind. (Such a choice will probably lead to bad results only in those cases where the wind fields under comparison show marked qualitative differences. A case in point would be one where a wind field with no shear was compared to one with a great deal of shear.) The meaning of average wind is not well defined. If the determination is to be made before the event, it is recommended that time of arrival calculations (see Section 5.6) be made at several points downwind, and that the average wind be taken as the average of the quotients of downwind distance and time of arrival. It should be possible, within the framework of the assumptions discussed in Section 5.6, to determine the downwind direction fairly well by inspection in many cases. If the determination is to be made after the event, the downwind distances and times of arrival can be taken from experimental measures.

There are five assumptions basic to the USNRDL procedure.

1. The total amount of activity in the cloud varies directly with the total energy release, W.

2. The height and linear dimensions of the cloud vary in the same way with yield, and this variation can be expressed in the form W^{ϵ}.

3. For a given soil the relative size distribution of the particles is independent of yield. Or, the same fraction of the total activity is included in any given particle size range.

4. The relative spatial distribution of active particles of any given size in the cloud is independent of yield. That is, homologous volumes contain the same particle sizes for all yields.

5. The rate of fall for particles of a given size is independent of yield. The rate of fall of active particles depends only on particle size.

While some of the above assumptions are subject to question, they are all probably reasonably good for scaling purposes as long as the scaling is not between yields that are very different. A reasonable guess as to the extent of their validity might be for yields that differ by no more than a factor of 50 from the standard case.

The scaling law which results from the assumptions given above is

$$\ell_a = \ell_b \left(\frac{W_a}{W_b}\right)^{k_{10}}$$

$$\dot{D}_a = \dot{D}_b \left(\frac{W_a}{W_b}\right)^{k_{11}} \qquad (5.8:1)$$

where

k_{10}, k_{11} = empirical constants

ℓ = any linear dimension of a given contour

$\dot{D}$ = dose rate on contour

W = weapon yield

USNRDL recommends the values of $k_{10} = k_{11} = 1/3$ and these values will be used here. Thus,

$$\ell_a = \ell_b \left(\frac{W_a}{W_b}\right)^{\frac{1}{3}}$$

$$\dot{D}_a = \dot{D}_b \left(\frac{W_a}{W_b}\right)^{\frac{1}{3}} \qquad (5.8:2)$$

(There is some question as to the proper values of the exponents. For example, Technical Operations[15] believes that $k_{11} = 1/2$ rather than $1/3$.)

Scaling with yield in the vicinity of ground zero requires an approach different from that for downwind scaling. The following assumptions are made.

1. The activity available on large particles scales linearly with the yield.

2. The cloud radius to heights of interest scales as the one-third power of the total yield.

3. The regions contaminated lie almost directly below the cloud.

[redacted]

It then follows

1. that the radius of a contour will scale as the one-third power of the total yield W, and
2. that the dose rate value of a scaled contour will scale as the areal concentration of activity, which will be the ratio of the activity scaling to the square of the linear scaling, i.e.,

$$\frac{W}{(W^{\frac{1}{3}})^2} = W^{\frac{1}{3}} \qquad (5.8:3)$$

Fortuitously, therefore, the same form of scaling law applies to ground zero as to the downwind region, but for different reasons.

It is further found empirically that the total area inclosed by a given dose rate contour does not depend very sensitively on the average, or effective, wind.

The scaling law plus the empirical statement about the areal constancy of dose rate contours can be restated for pure fission weapons as follows:

> At constant effective wind velocity, the shape-determining linear parameters of the isodose rate contours scale as the cube root of the total yield, and the areas scale as the two-thirds power of total yield. At the same time, the isodose rate intensities of the respective contours scale also as the cube root of the total yield.

In extending the formulae to weapons which develop only a fraction of the total yield from fission, it is only necessary to change the first of each of the above groups of assumptions.

The first of the five assumptions concerning downwind scaling becomes:

1. The total amount of activity in the cloud varies directly with the fission yield;

while the first assumption concerning scaling in the vicinity of ground zero is changed to:

1. The activity available on large particles scales linearly with fission yield.

The result is, then, that the contour shapes and sizes are functions of total yield of the weapon, whereas the dose rate contour values are determined by the amount of contaminant available; i.e., the fission yield.

Thus, if a dose rate on a particular contour is known for a pure fission weapon, the dose rate on the same contour for a weapon which is part fission and part fusion is:

$$\dot{D} = \dot{D}_F \left(\frac{Y}{W}\right) \qquad (5.8:4)$$

where

$\dot{D}$ = dose rate on a contour for a part fission weapon.

$\dot{D}_F$ = dose rate on the same contour for a pure fission weapon of the same total yield.

Y = fission yield.

W = total weapon yield.

[redacted]

Formulae (5. 8:2) are then generalized to:

$$\ell_a = \ell_b \left(\frac{W_a}{W_b}\right)^{\frac{1}{3}}$$

$$\dot{D}_a = \dot{D}_b \left(\frac{Y_a}{W_a}\right)\left(\frac{W_b}{Y_b}\right)\left(\frac{W_a}{W_b}\right)^{\frac{1}{3}} = \dot{D}_b \left(\frac{Y_a}{Y_b}\right)\left(\frac{W_b}{W_a}\right)^{\frac{2}{3}} \qquad (5.8:5)$$

where

ℓ = any linear dimension of a given contour.

$\dot{D}$ = dose rate on the contour.

Y = fission yield.

W = total weapon yield.

At constant yield, areas within isodose rate contours probably remain constant, but the downwind extent varies directly as the cube root of the wind velocity, and the crosswind extent varies inversely as the cube root of the wind velocity. This relation is verified (Dugway tests) only for winds whose velocities do not exceed 25 knots.[16] For winds less than 5 knots these statements do not apply. The dynamics of the active cloud overshadow the effects of such winds. It is anticipated, however, that wind velocities at the high altitudes to which high yield clouds rise will, in general, exceed 5 knots by a considerable amount.

Figure 5.5:1 is an idealized downwind fallout pattern from the Castle series for a 15-MT [redacted] bomb with an effective wind of 15 knots. It can be used as the basis for scaling to other yields and effective wind velocities following the above prescription.

Figure 5.5:5 is an idealized ground zero pattern, based on the Mike test, for a [redacted] 15-MT total-yield bomb and a 15-knot wind. It can be used as the basis for scaling to other yields following the method described above.

This scaling method should be regarded as quite rough, although rapid. The errors may be quite large and in fact for some cases at the Teapot tests the error was as much as a factor of three.[17]

PROBLEM 8

A downwind isodose rate contour pattern for a specific fission and total yield and effective wind velocity is given. The scaled pattern for a different fission and total yield and effective wind is required.

Solution

1. From the given pattern, Figure 5.5:1, choose a set of points properly dispersed to permit mapping the pattern. The set should include the maximum downwind and crosswind distances for each of a number of contours.
2. Compute the cube root of the ratio of the required total yield to the given total yield.
3. Compute the two-thirds root of the ratio of the given total yield to the required total yield.
4. Compute the ratio of the required fission yield to the given fission yield.
5. Compute the cube root of the ratio of the required effective wind speed to the given effective wind speed.

6. Compute the reciprocal of the number found in step (5).

7. For each point selected in step (1) perform the following operations.

   a. Multiply the downwind and the crosswind distances of the point each by the number found in step (2). The resulting numbers are, respectively, the downwind and crosswind coordinates of the corresponding point in a new contour which has been scaled for yield but not for wind speed.

   b. Multiply the value of the dose rate on the contour from which the point was selected by the numbers found in steps (3) and (4). The result is the dose rate value of the point found in (7a), scaled for yield only.

   c. Multiply the new downwind distance found in (7a) by the number found in step (5). The result is the downwind coordinate of the point scaled for both wind speed and yield. The associated dose rate value is that found in (7b).

   d. Multiply the new crosswind distance found in (7a) by the number found in step (6). The result is the crosswind coordinate of the point scaled for both wind speed and yield. The associated dose rate value is that found in (7b).

   e. Plot the point at the coordinates found in (7c) and (7d) with the dose rate value from (7b). Repeat for enough points to permit the sketching of isodose rate contours.

Example

The downwind isodose rate contour pattern for a [redacted] 15-MT total yield bomb at an effective wind speed of 15 knots is given in Figure 5.5:1. Construct the corresponding dose rate pattern for a [redacted] 1.875-MT total yield bomb at an effective wind speed of 30 knots.

1. The points will be characterized in the following manner: (125,30)-100 means the coordinates are 125 miles downwind, 30 miles crosswind, and the dose rate value is 100 r-hr^{-1} at H+1. A representative set of points might then be (125,30)-100, (335,0)-100, (100, 24)-200, (277,0)-200, (90, 22)-400, (215,0)-400, (80,20)-600, (165,0)-600, etc. The computation will be performed only for the point (125,30)-100, which is sufficiently general to illustrate the method.

2. $\left(\frac{1.875}{15}\right)^{\frac{1}{3}} = \left(\frac{1}{8}\right)^{\frac{1}{3}} = \frac{1}{2}$

3. $\left(\frac{15}{1.875}\right)^{\frac{2}{3}} = \left(8\right)^{\frac{2}{3}} = 4$

4. [redacted] $= \left(\frac{1}{8}\right)$

5. $\left(\frac{30}{15}\right)^{\frac{1}{3}} = 2^{\frac{1}{3}} = 1.26$

6. $\frac{1}{1.26} = 0.79$

7. a. $1/2 \times 125 = 62.5$ miles
   $1/2 \times 30 = 15$ miles

   b. $4 \times \frac{1}{8} \times 100$ r-hr^{-1} $= 50$ r-hr^{-1}

   c. $1.26 \times 62.5 = 79$ miles

d. 0.79 x 15 = 12 miles

e. The point (125,30)-100 therefore transforms into the point (79,12)-50. The process is repeated until there are enough transformed points to construct an isodose rate pattern.

PROBLEM 9

The isodose rate contour pattern in the vicinity of ground zero is given for a specific fission and total yield. Compute the isodose rate contour pattern for a different fission and total yield.

Solution

1. Choose a set of points along a ray from the center of Figure 5.5:5. Note the radial distance from the center and the associated dose rate for each point.
2. Compute the cube root of the ratio of the required total yield to the given total yield.
3. Compute the two-thirds root of the ratio of the given total yield to the required total yield.
4. Compute the ratio of the required fission yield to the given fission yield.
5. For each point selected in step (1) perform the following operations.
   a. Multiply the radial distance by the number found in step (2). This is the radial distance of the transformed point.
   b. Multiply the dose rate associated with the point by the numbers found in steps (3) and (4). This is the dose rate associated with the transformed point.
   c. Construct a circle about ground zero whose radius is equal to the number found in (5a). This is the isodose rate contour at H + 1 hour whose value is the dose rate found in (5b). An arc of perhaps 60° of this circle facing downwind would have a somewhat higher associated dose rate, in general, on account of wind perturbations. Also, the center of the circle would be somewhat displaced and its shape a bit distorted by the wind. The full circle approximation about ground zero is, however, about as good as reasonably can be expected from the use of simple methods.

Example

Although they are less involved, the procedures for scaling of ground zero isodose contours are similar enough to those of Problem 8 so that a separate example is omitted.

5.9 SCALING WITH HEIGHT OF BURST

The methods of predicting fallout discussed so far are applicable only to surface bursts. It is, therefore, desirable to scale for bursts at some height above the earth's surface. Fallout occurs in appreciable amounts only when there are earth particles in the fireball capable of scavenging the active material. Further, it appears that such scavenging particles are present in the fireball in quantity only when the fireball intersects the earth. There is clearly some relation between the amount of earth included in the fireball and the amount of activity that is scavenged. We shall assume it is linear. We shall assume also that the amount of earth in the fireball is proportional to the volume intersected by the fireball.

Let

x_f = effective fireball radius (for a weapon of a given yield the minimum burst height at which there is no appreciable fallout).

4. The required dose rate is

$$\dot{D}(H+1) = 0.46 \times 2000 = 920 \text{ r-hr}^{-1}$$

5.10 ENERGY SPECTRA OF FALLOUT GAMMA RADIATION

The energy spectrum of fallout gamma radiation is subject to variation with weapon type. The fission product portion of the spectrum is invariant for any given fissionable material, e.g., U^{235}, U^{238}, Pu^{239}, U^{233}. Moreover, indications are that there is very little variation in the fission product distribution among the three commonly used fissionable materials: U^{235}, U^{238}, and Pu^{239}. Hence, to a good order of approximation, we can expect the fission product part of the gamma radiation spectrum to be invariant.

The great floods of neutrons released in nuclear explosions, especially in thermonuclear weapons, can be captured in nearby materials, sometimes causing them to become radioactive.

There have been observed negligible but detectable components of the spectrum which rose from the activation of earth materials by neutrons, e.g., activated calcium in the Marshall Islands and activated aluminum in Nevada.[18,19] These activities constituted only a very few percent of the total and could safely be neglected. The several past undersea test shots have not shown activation of sodium sufficient to contribute importantly to the fallout spectrum.

Neutron-absorbing materials may be deliberately placed in or around a thermonuclear bomb to increase the radiological hazard. In such a case the fallout gamma radiation spectrum would almost certainly be altered.

Barring peculiar burst environments or deliberate addition of neutron absorbers to the bomb, however, *it is probable that the fallout gamma radiation spectrum characteristic of the Castle type* bombs will hold rather well for other thermonuclear weapon types.

The energy spectrum of gamma rays in fallout changes with time. That is because (1) nuclides with shorter half lives will decay faster and vanish from the spectral structure, and (2) some nuclides, which are not produced directly but occur as products of the decay of other nuclides, do not appear perceptibly in the spectral structure until after some lapse of time.

Fig. 5.10:1 presents 11 charts of the energy spectrum at different times ranging from 1 hr to 20 days after detonation. They are constructed from analytical curves of decay with the fission product and neutron activation components relatively weighted to afford agreement with the experimental determinations of the spectrum at Castle.[18,20] *Since these determinations began at approximately 5 days* after detonation, the spectral data here presented for times earlier than 5 days are possibly not as accurate as the data for later times.

In the absence of detailed study of the lower energy end of the fission product spectrum, fission product gammas with energies less than 0.1 Mev have been ignored. Further, the induced activities include strong components of radiation below 0.1 Mev which have been lumped into the 0.1 to 0.4 Mev range. While these low energy gamma components are not negligible, their treatment here simply makes the spectrum appear somewhat harder, i.e., of higher energy, than it really is. In turn, this leads to a slight apparent reduction in the shielding effectiveness of materials. (From the defensive viewpoint this is conservative.)

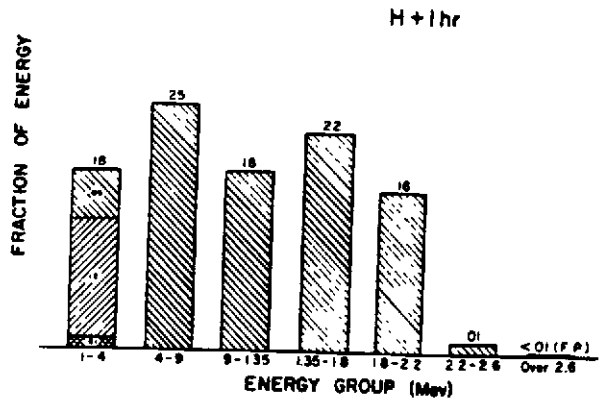

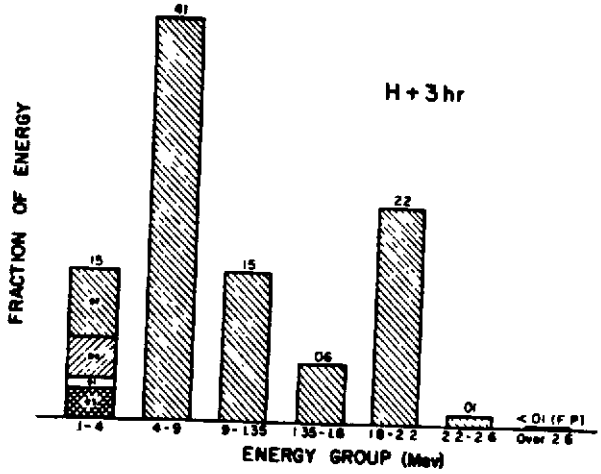

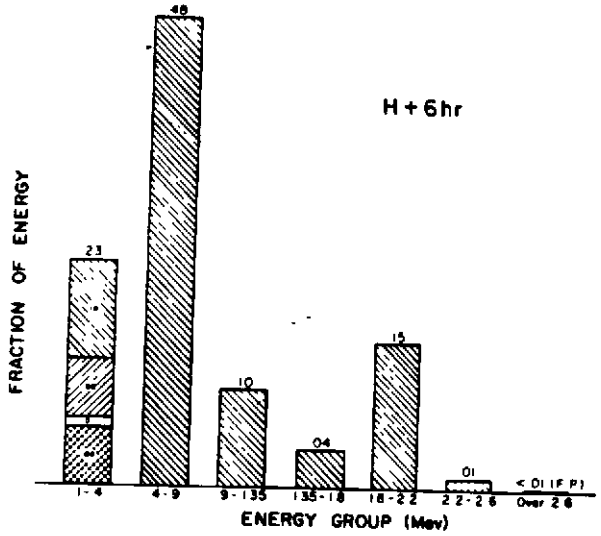

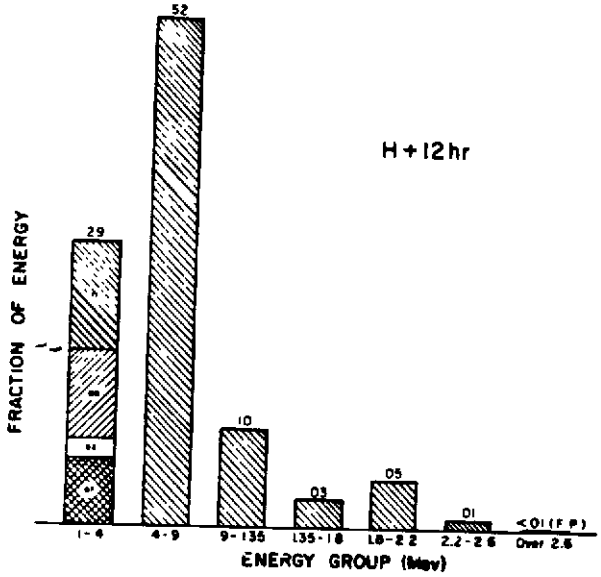

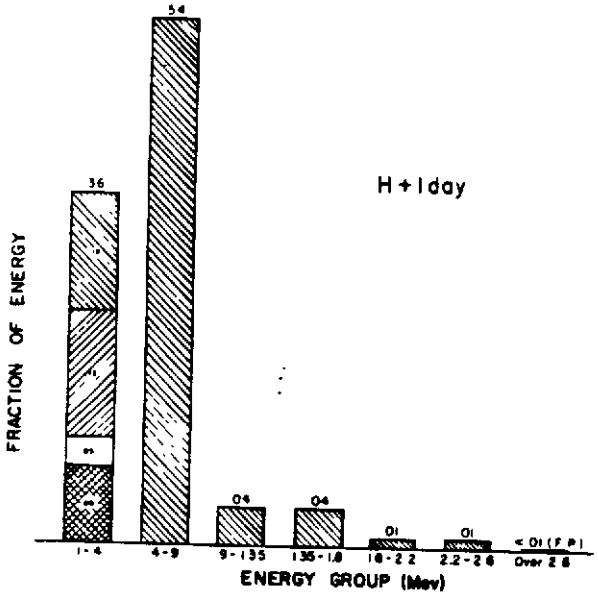

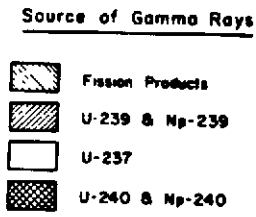

Fig. 5.10:1 Gamma Ray Energy Spectrum Histograms

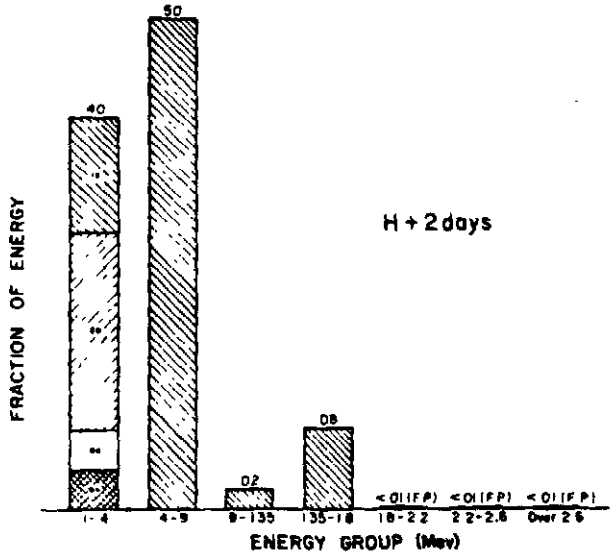
H + 2 days
FRACTION OF ENERGY
ENERGY GROUP (Mev)
1-4
4-9
9-13.5
13.5-18
18-22
22-26
Over 26

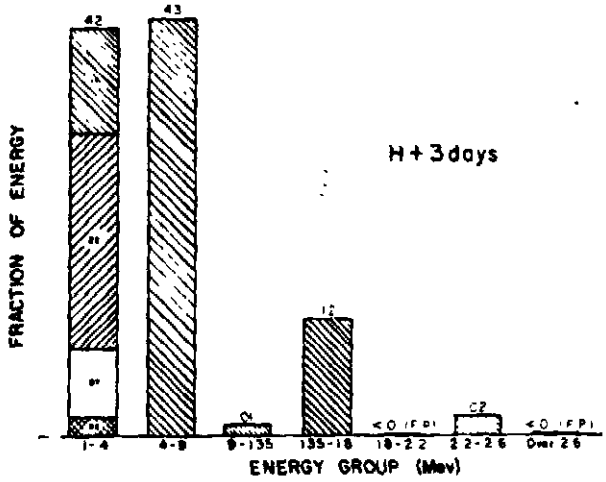
H + 3 days
FRACTION OF ENERGY
ENERGY GROUP (Mev)
1-4
4-9
9-13.5
13.5-18
18-22
22-26
Over 26

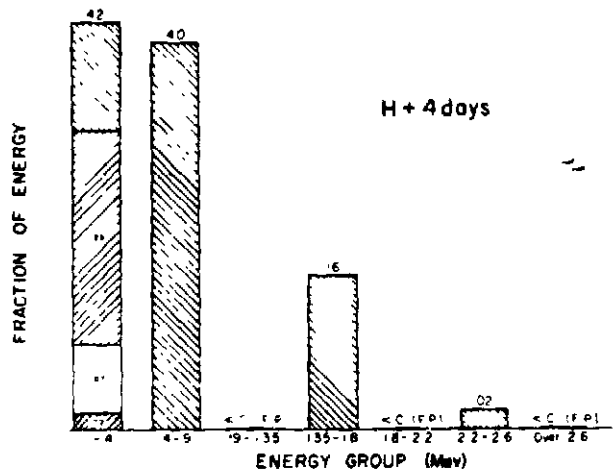
H + 4 days
FRACTION OF ENERGY
ENERGY GROUP (Mev)
1-4
4-9
9-13.5
13.5-18
18-22
22-26
Over 26

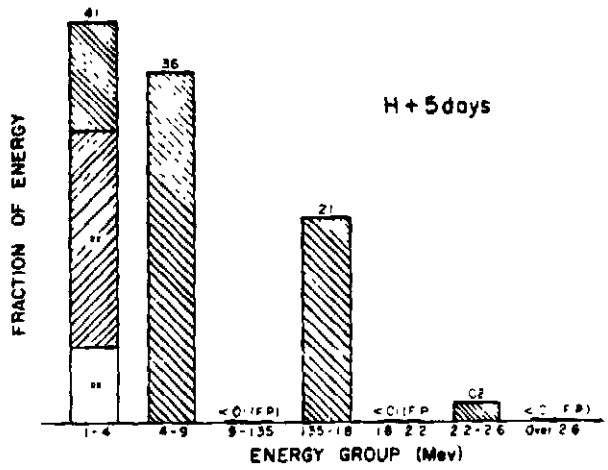
H + 5 days
FRACTION OF ENERGY
ENERGY GROUP (Mev)
1-4
4-9
9-13.5
13.5-18
18-22
22-26
Over 26

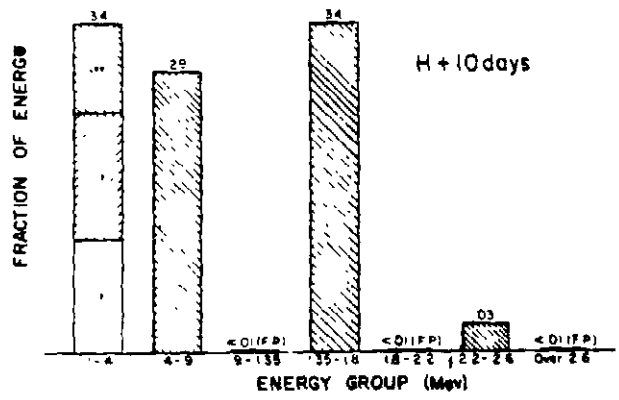
H + 10 days
FRACTION OF ENERGY
ENERGY GROUP (Mev)
1-4
4-9
9-13.5
13.5-18
18-22
22-26
Over 26

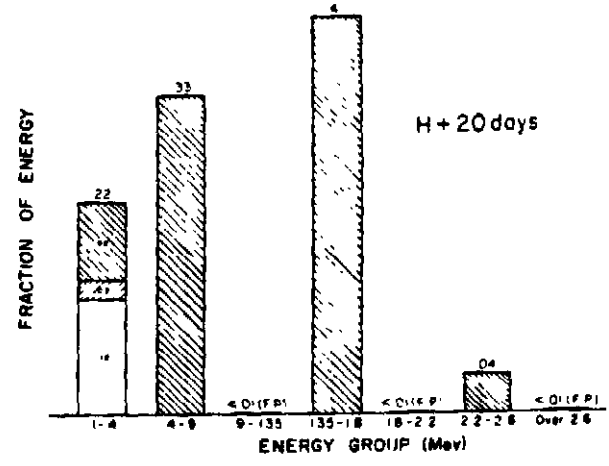
H + 20 days
FRACTION OF ENERGY
ENERGY GROUP (Mev)
1-4
4-9
9-13.5
13.5-18
18-22
22-26
Over 26

5.11 SHIELDING FROM RESIDUAL GAMMA RADIATION

The only mechanisms for reducing the gamma dose delivered from a source to a receiver are:

1. increasing the separation of source and receiver, and
2. interposing gamma-absorbing material between source and receiver or (better still) surrounding the receiver or source with gamma-absorbing material.

Within the fallout area there is very little opportunity to use separation distance as a means of attenuation because the fallout source is spread more or less uniformly over a broad region. To the extent that there are local non-uniformities, distance attenuation can be used by avoiding the hot spots.

Of much greater significance is the use of gamma-absorbing material to shield against the radiation. Actually all materials are gamma-absorbing but some are more effective or more convenient than others. A fairly accurate rule of thumb for selecting gamma-shielding materials is that for a given thickness of material the gamma-absorption effectiveness increases with the electron content per unit volume of the material. This is because a large portion of the gamma-absorption and scattering processes are simply reactions between gamma rays and electrons. The electron content per unit volume is the product of the electron content per unit weight and the density of the material. Since for most materials (except those containing a large concentration of hydrogen) the electron content per unit weight is approximately constant, the gamma-shielding effectiveness of a given thickness of material increases with the density of the material and is approximately independent of its composition. This is equivalent to saying that equal weights of most nonhydrogenous materials provide about the same shielding protection, assuming the same shielding geometry. (Within this broad statement it is also true that in general the materials of high atomic number and high density make the most effective gamma shields, particularly for gamma rays below about 0.5 Mev and above about 4 Mev.)

A convenient method of characterizing the shielding effectiveness of a given material and geometry is through the use of the dose transmission factor

$$T = \frac{D_i}{D_j} \qquad (5.11:1)$$

where

D_i = physical dose received at the inner face of a given material and geometry due to a polyenergetic source of gammas

D_j = physical dose received at the outer face of a given material and geometry due to a polyenergetic source of gammas.

Instead of the expression given above we will use an approximate and more easily calculated form for rough determination of the shielding effectiveness of a given structure. Thus

$$T_e = e^{-\mu_t x} \qquad (5.11:2)$$

where

μ_t = total linear attenuation coefficient for gammas of an appropriate average energy

x = thickness of shielding.

In general, T_e will not be equal to T as defined in Eq. 5.11:1. The use of T_e, while adequate for present purposes, would not be suitable for all others, for example for calculations involving the strong source and thick shield associated with nuclear reactors.

A corresponding expression for T_e which may be used when there are a number of slabs of different composition in the shield is

$$T_{e(1,2,3)} = e^{-(\mu_{t1} x_1 + \mu_{t2} x_2 + \mu_{t3} x_3)} = e^{-\mu_{t1} x_1} e^{-\mu_{t2} x_2} e^{-\mu_{t3} x_3} = T_{e1} T_{e2} T_{e3} \quad (5.11:3)$$

where the subscripts indicate different materials. Eq. 5.11:3 demonstrates the important rule, applicable to approximate calculations, that when several materials are added together in a shield their transmission factors are multiplied to obtain the transmission factor for the combined shield.

The shielding effectiveness of any material depends on the energy of the impinging radiation. The energy spectrum of the fallout radiation is time dependent, as shown in Section 5.10. The shielding effectiveness of a material varies, therefore, with time. For most of our present purposes, the time variation of shield effectiveness need not be considered, as it is relatively slight.

The only circumstance in which time variation becomes worthy of attention is when there is a strong component of relatively short-lived and highly penetrating radiation. If it were contemplated to remain in the fallout region for several weeks and if active sodium were present in quantity, the shield should be assigned one value during the important lifetime of sodium and another for the remainder of the time.

Fig. 5.11:1 is a plot of the transmission factor of one foot of soil (specific gravity = 2) from 1 hr to about 23 days after the burst. During this period the transmission factor varies from a maximum value of 0.164 to a minimum value of about 0.136. The 3-hr transmission factor, which is close to the maximum, is taken as the average value. Since the activity decays quite rapidly with time and a substantial portion of the dose is delivered early, the 3-hr choice is quite realistic.

The shield evaluations of this section are based upon the energy spectra of Section 5.10.

Table 5.11:1 presents nominal values of gamma ray transmission factors T_e, as a function of thickness, for several common materials. The specific gravity is also presented. These values, though approximate only, may be used to evaluate most simple shielding configurations.

The foregoing material is presented to permit evaluation of the relative shielding effectiveness of various common materials in the absence of more accurate methods. A better a priori evaluation can be made by computing, or making educated assumptions about, the anticipated external residual source distribution and calculating by Monte Carlo methods the radiation transport through the actual shield composition and configuration. The best evaluation is made by metering the shield interior under actual operational conditions.

While the characteristics of a shield are not the same for the long-lived, broadly distributed residual gamma source as they are for the short-lived and much more directional initial gamma source, a fair notion of the relative effectiveness of various shielding installations may be had by reference to Section 3.7 which deals with shielding against the initial gamma radiation.

While it is difficult to make exact quantitative statements, some general remarks about shielding in a residual radiation field may be offered.

Because the residual source is well distributed and because the radiation has the capability of being scattered through angles, or, so to speak, of turning corners, an adequate shield must surround the receiver completely. (Such exceptions to this rule as may occur for the case of residual radiation are quite special.)

A radiation shelter can be prepared in advance and especially designed for its purpose. The most commonly recommended shelter is an underground excavation with 3 to 5 ft of earth above. The access corridor to such a shelter should, where possible, have a bend in it so that gamma radiation cannot find a straight-line path into the shelter, since even though gamma rays can be scattered around corners they suffer considerable attenuation in the process.

all Islands who breathed, ate and drank contaminated air, food, and water for as long as 4 days, conclude that the internal radiation effects were low compared to the external effects observed. No conclusions can yet be drawn, however, about the long range effects of such radiation.

6.7 REFERENCES

1. Armed Forces Medical Policy Council. Handbook of Atomic Weapons for Medical Officers. DA Pam 8-11. June 1951. (Unclassified)
2. R. I. Condit et al. AD-95(H). April 1949. (Confidential)
3. E. P. Cronkite et al. WT-923. Oct. 1954. (Confidential)
4. G. Young and E. P. Blizard. ORNL-420. Nov. 1949. (Unclassified)
5. G. W. Imrie, Jr. and R. Sharp. WT-1120. (Confidential)
6. F. L. Bouquet et al. USNRDL-420. (Confidential)
7. C. Sondhaus. USNRDL-394. Dec. 1952. (Confidential)
8. H. F. Hunter and N. E. Ballou. ADC-65. Feb. 1949. (Unclassified)
9. E. Tochilin and P. Howland. WT-26. Aug. 1951. (Secret)
10. E. Tochilin et al. WT-372. April 1952. (Secret)
11. F. S. Goulding and G. Cowper. CREL-529. Jan. 1953. (Unclassified)
12. J. D. Teresi and A. Broido. Tech. Memo 18. USNRDL. Nov. 1954. (Unclassified)
13. J. T. Brennan. WT-746. Dec. 1953. (Secret)
14. L. V. Spencer. Phys. Rev. 98. 1597. June 1955. (Unclassified)
15. J. Moteff. APEX-176. Dec. 1954. (Unclassified)
16. The Effect of Atomic Weapons. Appendix D. USGPO. Sept. 1950. (Unclassified)
17. L. D. Gates, Jr. and C. Eisenhower. AFSWP-502A. Jan. 1954. (Unclassified)
18. United Kingdom Medical Research Council. The Hazards to Man of Nuclear and Allied Radiations. Her Majesty's Stationery Office. June 1956. (Unclassified)

Page 204 is blank.

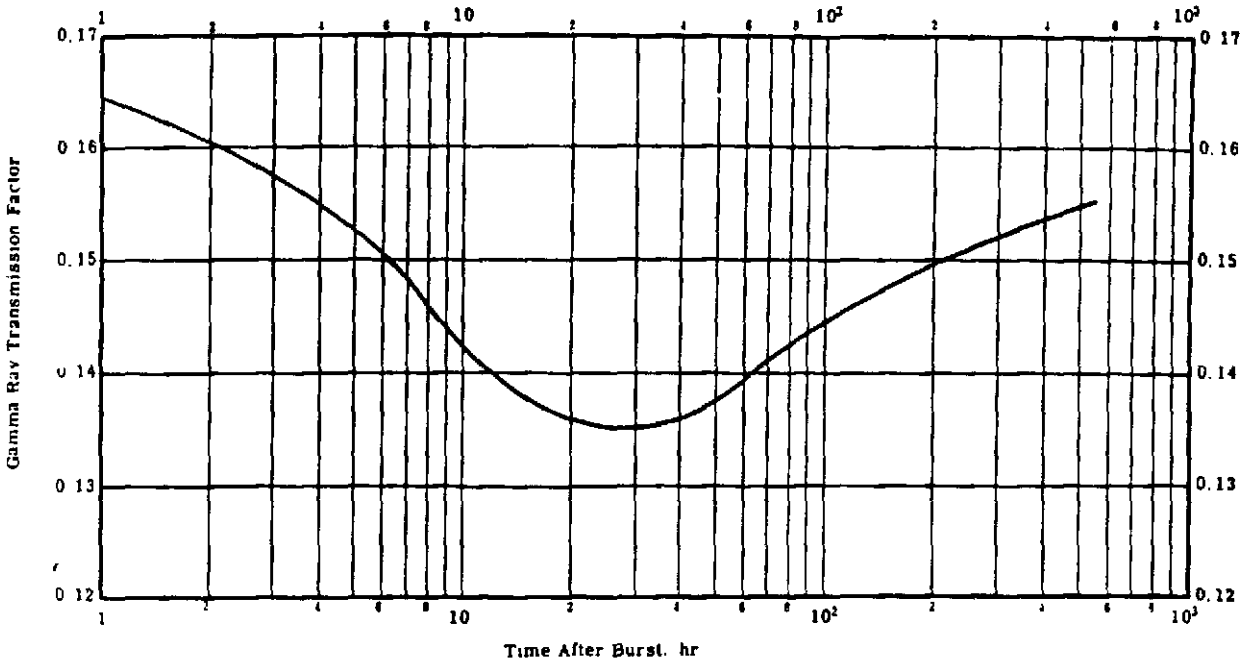

Fig. 5.11:1 Gamma Ray Transmission Factor for Soil (specific gravity = 2) as a Function of Time after Burst

TABLE 5.11:1

Nominal Gamma Ray Transmission Factors for Common Materials

Material	Specific Gravity	Transmission Factors			
		1 in.	4 in.	8 in.	12 in.
Water	1.0	-	0.7	0.6	0.4
Soil	2.0	-	0.6	0.3	0.16
Concrete	2.5	-	0.5	0.2	0.08
Cinder block	1.6	-	0.7	0.3	0.15
Wood	0.6	-	0.9	0.8	0.6
Lead	11.3	0.25	0.004	-	-
Iron	7.0	0.58	0.1	-	-

The middle stories of high buildings in cities make fairly good radiation shelters. They provide a distance factor, and because of the intervening structure, a shielding factor.

Rearrangement of furniture and of anything movable, to come between the receiver and the principal apparent source of dose can be helpful. Any structure or inclosure, whether or not it is high or has a basement, is better than nothing; if the shelter equivalent of at least a basement is not available, however, evacuation should probably be considered.

A very adequate shelter can be prepared in a subground level basement by piling sandbags on a steel or wooden frame to a thickness of 2 or 3 ft, top and sides. If the bags can also be wetted down before the water supply is contaminated, such a shelter would afford almost complete isolation from the external gamma radiation.

Should outside air bearing contaminated particles penetrate a shelter of any sort, a hazard might arise from beta activity deposited in the lungs or on the skin. Some effort should be made, therefore, to exclude large masses of outside air from the shelter.

Figs. 5.11:2 and 5.11:3 reproduce the results of some simple calculations of the shielding effectiveness, predominantly geometrical, or structures with and without basements.[21] In each case the superstructure begins at grade and is circular in shape. In the former case the dose rate is computed for a receiver 3 ft above the ground level; in the latter, for a receiver on the basement floor at the center of the circular cross section of the building. The calculated dose rate includes both unscattered and scattered gamma radiation, contributed by uniformly distributed fallout contamination on an infinite plane surrounding the structure and on the roof of the structure. Dose rates are presented as percentages of the dose rate outside the structure and 3 ft above the ground.

Figure 5.11:2 presents the results for the "no-basement" case, plotted against the structure radius x_s for four different values of structure height y. The lowest curve shows that portion of the radiation which comes from the ground source, independent of the height of the structure ($y = \infty$). The curves are computed for the case of infinitely thin structural materials, i.e., no structural attenuation. No allowance is made for the effect of intervening floors in multistoried buildings. Table 5.11:1 may be used for approximate evaluation of the effect of finite structural thicknesses (roof, walls, floors, etc.) on the results of Fig. 5.11:2

Fig. 5.11:3 presents equivalent results for the case of a structure with basement. An additional parameter y_b is required for the depth of the basement. The same general descriptive remarks apply to this figure as to Fig. 5.11:2. The two lowest curves give the portion of the dose which comes from the ground source, independent of roof height ($y = \infty$) for the two basement depths chosen.

The assumptions on which Figures 5.11:2 and 3 are based are sufficiently crude so that use of these figures should be restricted to qualitative estimates.

5.12 VARIATIONS DUE TO ENVIRONMENT

There are two environments which can greatly alter the fallout dose received by a detector at some point in the fallout region: the environment of the burst point, and the environment of the detector.

The principal environmental factor of interest at the burst point is the nature of the surface over which the bomb was detonated. Present experience for which detailed data are available is limited to the soils of Nevada and the Marshall Islands. Particle size distribution work has been done by USNRDL on the Nevada soil, but little information is available on the Marshall Islands particle size distribution. The prevailing impression is that the Nevada distribution is probably fairly representative of most soils and concrete constructions that might be encountered in the United States and Europe. Experimental work on the fractionation of different soils is, however, vitally needed.

It is not at all clear what sort of fallout pattern will result from water surface and underwater bursts. Although such bursts occurred in the Crossroads, Castle, and Wigwam series, they were not adequately documented for fallout. If a burst occurs in or over deep water, there is a fine aerosol of water created. Whether this aerosol penetrates far downwind, as would light particles, or forms

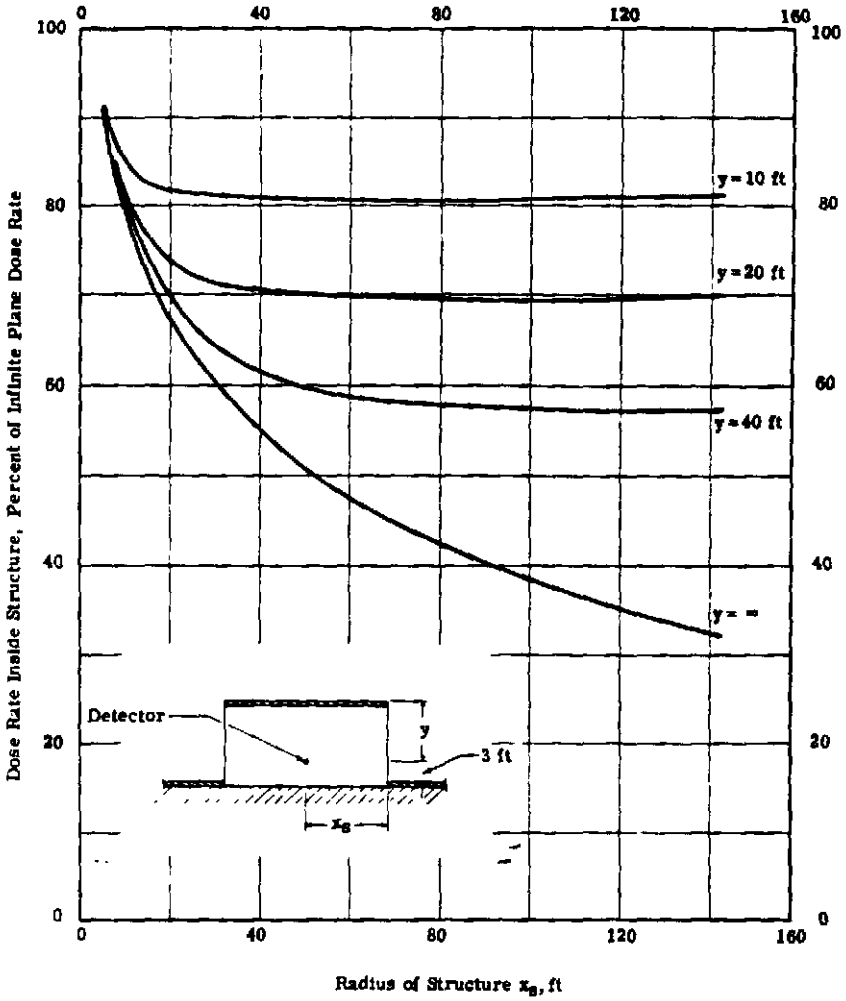

Fig. 5.11:2 Dose Rates Inside Structures without Basements

larger particles and precipitates early, is not established. In addition, a huge column of water is hurled up into the air and it collapses into the water not too far from ground zero. Preliminary information from the Castle tests indicate that the low dose rate contours would be larger and that the high dose rate contours would be smaller for a burst over or under water than for a corresponding burst over a land surface.

Another burst point environmental factor which may sometimes be important is the presence of an isotope subject to neutron activation which can contribute significantly to the gamma radiation source. This has not yet been a serious problem. Activated calcium was found in some quantity after Castle Bravo, but in amounts small compared to the fission product source. The total dose measured after undersea bursts has not shown important amounts of radiation resulting from sodium activation.

Environmental factors in the neighborhood of the receiver can affect the dose in many ways. Heavy foliage can keep a portion of the source suspended. Rough terrain can shield out some effects of the active material shadowed by it. Drifting and blowing of the dust (like snow) by the ground level winds can cause local space and time variations which might increase or decrease the dose. (A receiver in a structure on an essentially plane site would probably record a larger dose on account of drifting on the windward side of the structure.) A well-drained site would probably be subjected to a smaller dose if rain occurred during or after fallout and a poorly drained site would probably receive a larger dose.

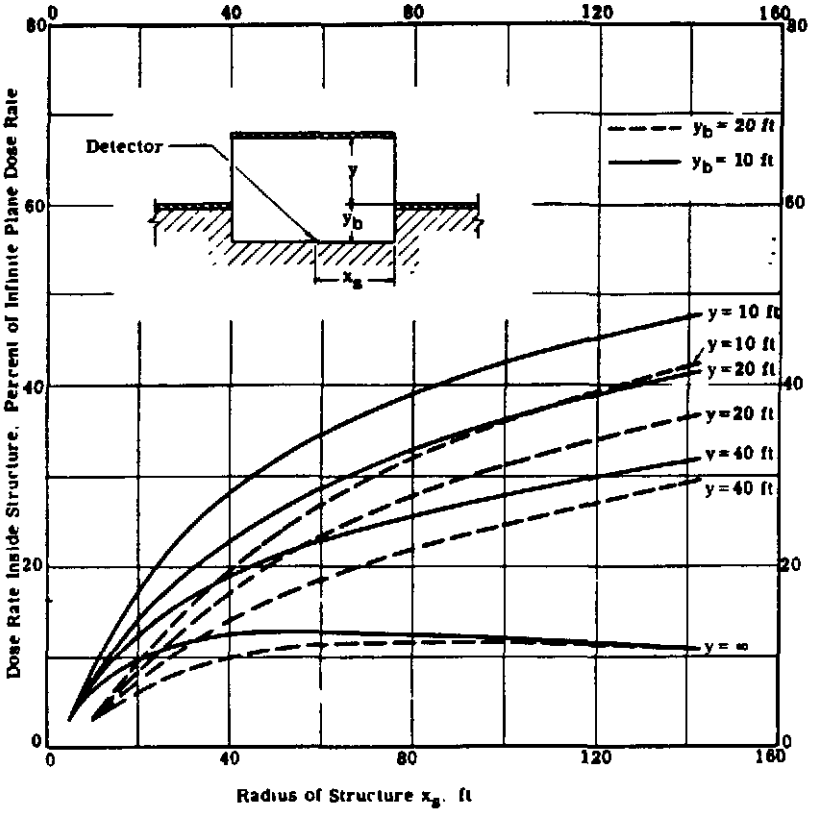

Fig. 5.11:3 Dose Rates Inside Structures with Basements

It is clear that environmental factors, both at burst and receiver point, can substantially influence the dose. Further, while environmental factors at the receiver should influence operational decisions, they are not intrinsically of a nature to lend themselves well to a priori quantitative description.

5.13 *NEUTRON-INDUCED ACTIVITIES*

A second possible source of radioactive fallout material, in addition to the active fission products, is material activated by bomb neutrons. These neutrons can be captured in nearby materials, leading to the formation of new isotopes which are sometimes radioactive. There are three kinds of neutron-induced activities to be considered in weapons effects, namely:

1. activities induced in materials normally present in the bomb,
2. activities induced in materials deliberately added to the bomb to increase its radiological hazard, and
3. activities induced in materials in the environment in which the bomb is exploded.

By far the most important induced activities observed to date are those resulting from the capture of neutrons in the U^{238} and U^{235} normally present in the thermonuclear weapon. According to the observations made in the Castle series,[18] these activities comprise a significant part of the fallout radiation source at times of the order of 30 min, and the major part at times of the order of 3 days. (These contributions came from the U^{239} - Np^{239} chain formed from the capture of a neutron by U^{238}.) Other standard weapon materials do not appear to contribute importantly to the residual gamma radiation source. It is possible, however, that some portion of the initial gamma radiation source may come from (n, γ) reactions in weapon materials.

There has as yet been no experience with activities induced in materials placed in the bomb deliberately for that purpose. The possibility that a material exists which is practical for that purpose cannot now be dismissed.

In both the Marshall Islands and Nevada, activated earth materials have been detected.[18, 19] The quantity of this kind of activity has been only a few percent of the total activity produced by the bombs. Even in the base surges and in the craters of underground bursts, where one would expect such activity to be most concentrated, it has not appeared in very significant amounts in comparison with the fission product contribution (at least in those surface regions where observations were made). It has been found, however, that for air bursts, where there is no fission product fallout, the neutron-induced activity at ground zero may be important. The area around ground zero affected by this neutron-induced activity, resulting from either ground or air bursts of a given weapon, is small compared to the area affected by ground-burst fallout radiation from the given weapon. It is rather difficult to conceive of other situations where the capture of neutrons in environmental materials would contribute importantly to the residual radiation.

5.14 REFERENCES

1. S.M. Greenfield et al. R-265. July 1954. (Secret)
2. C.E. Adams et al. USNRDL-374. Nov. 1952. (Secret)
3. M.G. Schorr. Technical Operations, Inc. Private Communication. April 1955.
4. R.W. Paine, Jr. AFSWP-895. Jan. 1955. (Secret)
5. N.M. Lulejian. ARDC. Private Communication. Aug. 1955.
6. R.R. Rapp. AFSWP-895. Jan. 1955. (Secret)
7. R.R. Rapp. Rand Corp. Private Communication. May 1955.
8. W.W. Kellogg. RM-1378-AEC. Nov. 1954. (Secret)
9. F.H. Clark. NDA 39-25. April 1956. (Unclassified)
10. N.E. Ballou. AFSWP-895. Jan. 1955. (Secret)
11. S.M. Greenfield et al. RM-1676-AEC. April 1956. (Unclassified)
12. D.C. Borg et al. AFSWP-507. May 1954. (Secret)
13. E.R. Schuert. AFSWP-895. Jan. 1955. (Secret)
14. C.F. Kaanda et al. USNRDL-TR-1. Sept. 1953. (Secret)
15. P.I. Richards. Technical Operations Inc. Private Communication. Aug. 1955.
16. R.W. Paine, Jr. AFSWP. Private Communication. Oct. 1955.
17. E.B. Doll and H.K. Gilbert. ITR-1153. June 1955. (Secret)
18. C.S. Cook. AFSWP-895. Jan. 1955. (Secret)
19. C.S. Cook. ITR-1117. May 1955. (Confidential)
20. F.H. Clark. NDA 27-39. Feb. 1955. (Unclassified)
21. A.J. Breslin. NYO-4682-A. Dec. 1955. (Unclassified)

GENERAL REFERENCES

a. E.P. Blizard et al. ORNL-1575. July 1954. (Secret)

b. H. Goldstein and J.E. Wilkins, Jr. NYO-3075. June 1954. (Unclassified)

Chapter 6

RESIDUAL BETA RADIATION

6.1 INTRODUCTION

Detonation tests of about 100 nuclear weapons ranging in yield from 1 KT to 15 MT have established the fact that the larger weapons, of the order of 0.5 MT or more, can contaminate a large area downwind by fallout of radioactive debris. In those cases where fallout becomes a serious problem, the ionization produced by beta particles emitted by the radioactive debris may, under certain circumstances, create a more serious biological hazard than the accompanying gamma radiation. The beta hazard can only occur when personnel are in close proximity to or are substantially unshielded from fallout material; distances from the source of the order of 10 ft in air or shielding thickness of the order of 0.5 gm-cm^{-2} are usually sufficient to render the beta radiation a lesser hazard than the gamma radiation. Some typical situations which may occur (listed in order of probable decreasing importance) are:

1. Irradiation of personnel as a result of fallout adhering to skin or clothing.
2. Irradiation of personnel standing or lying on contaminated ground surfaces.
3. Irradiation of personnel in proximity to heavily contaminated massive objects (airplanes, ships) which have been exposed to the radioactive cloud.

Since a beta hazard will be considered to exist only when it exceeds the gamma hazard, it is clear that the gamma radiation for various situations of interest must also come under scrutiny.

As a first approximation, the disintegration energy of early time fallout is shared equally by the beta and gamma emissions. For example, the average gamma energy of fallout 4 hours after the bomb burst is about 1 Mev, the average beta energy is about 1 Mev, and there are about 1.5 betas emitted per gamma. Because of the vastly different absorption characteristics of betas and gammas, the relative doses are not at all the same. In materials of low atomic number such as air or tissue, the linear energy transfer of a 1-Mev beta is about 70 times that of a 1-Mev gamma. Thus, in the vicinity of a source of equal beta and gamma strengths, the beta dose may be 70 times as great as the gamma dose. On the other hand, because of the rapid dissipation of beta energy with distance in an absorbing medium, the beta flux and dose decrease much more rapidly than the gamma flux and dose.

If humans were equally vulnerable to equal beta and gamma doses, the beta radiation hazard in the vicinity of sources would indeed be formidable. The disability dose for betas is still subject to disagreement; but a figure of 3000 to 5000 rep has won a certain degree of acceptance.[1] The disability gamma dose is commonly taken as 150 to 200 r.[1] Neglecting the small difference between rep and roentgen units, the range of situations for which the beta radiation is a hazard is then roughly limited to those for which the beta-gamma dose ratio is greater than about 20. It should be emphasized that the evaluation of a relative hazard cannot possibly be determined by the beta-gamma dose ratio alone. The intrinsically different depth dose behavior of the two radiations, the difference in biological effect for a given exposure, and the difference in the effect with degree of exposure are decisive factors which must be considered in the determination of the relative hazard in each given situation. For example,

the gamma dose of interest is the total body dose. Though it may be desirable to correct the surface gamma dose by a small factor to account for gamma attenuation in the body, the correction is not sensitive to source geometry and orientation of the body because of the high transparency of tissue to gamma rays. (Low energy gammas are not considered.) On the other hand, the beta dose can always be regarded as a surface dose. The shielding effects of various parts of the body are in this case complete and the resultant dose is quite sensitive to the orientation and distance of the body surface with respect to the source. Consequently, a subject exposed to a ground source of betas will experience an exposure analogous to a sunburn received by a man standing on his head on a hazy day at noon. Although we can make predictions about the effects of a local beta exposure, it is somewhat difficult to define the gross, over-all effect of a varying body exposure to betas.

Because the biological effects of betas and gammas are so different, the use of the concept "relative hazard" may be somewhat questionable. The incapacitating effects of betas can be compared to burns of various degrees: reddening, blistering, and permanent destruction to the skin and sub-tissues. The incapacitating effects of gammas may be roughly indicated according to degree as fatigue, nausea, general disability, and death. The time required for the incidence of these effects is much greater than in the case of beta radiation, perhaps 5 to 10 times as long. The resultant weighting of such effects with their associated time delays in order to formulate a judgment about a set "relative hazard" in the form of one of these radiations is a complex business. Furthermore, even if a relative hazard should be considered to exist for one of the radiations, the hazard may shift if the doses are increased in equal proportion. A 3000-rep beta dose over the lower half of the body might well be considered a greater hazard than a 100-r gamma dose. If both doses are scaled upward by a factor of four, however, it is unlikely that a 12000-rep beta dose would have the lethal effects of a 400-r gamma dose. In general, an increase of the radiation level will tend to shift the hazard to gammas. Situations for which a relative beta hazard can occur would require a gamma dose less than the order of 200 r.

The existence of situations where an independent beta radiation hazard existed was first pointed out in 1949 by Condit, Dyson and Lamb.[2] Such situations have subsequently occurred. Probably the most significant one[3] is the contamination of the populated atolls of Rongerik, Rongelap, Ailinginae, and Utirik by fallout from the Castle Bravo shot in March 1954. The major biological disabilities experienced by the natives were all produced by beta radiation, the beta exposure being a consequence of direct contamination of the skin and clothing.

One should not conclude from the above event that contact exposure to fallout is necessarily a beta hazard. A total exposure slightly greater than that which occurred would have resulted in the incidence of lethality by gammas. In addition, the medical complications from the total body gamma dose were potentially serious. Furthermore, taking protection indoors or prompt bathing would have eliminated or greatly mitigated the beta hazard. The effects of the Marshall Islands fallout clearly indicate, however, that contact exposure of individuals to fallout which does not produce too high a gamma level can result in situations which are primarily a beta hazard. (There exists a possibility that some of the dose is due to very low energy (less than 50-kev) gammas rather than betas but the evidence presently available indicates that this is probably not the case. Thus calculation[4] of the fission product gamma spectrum has shown that there are very few low energy gammas; experiments have shown that the attenuation of the "soft" component of the dose appears to resemble beta particles in the Mev range rather than very low energy gammas.[5])

There is some experimental information available on fallout situations where the importance of betas relative to gammas is marginal rather than clear-cut. The interpretation of these data is not decisive, however. One of the objectives of the succeeding paragraphs is to sketch in greater detail the beta dose and relative hazard in these marginal situations where both beta and gamma radiation may be important.

The beta and gamma fallout doses are dependent on the activity and energy spectra of the source, on the geometry, and on the nature and thickness of the intervening absorbing medium. Although a great deal of information does now exist, the results required to fill in the detailed picture are not complete. Furthermore, much of the information on hand is not consistent. One can only attempt to arrive at "best" or most consistent values of the beta dose, and the absolute accuracy of such values must be considered tentative. In view of the conditional nature of the conclusions, a policy of simplification has

[redacted]

been pursued. As an example, geometrical considerations have been confined to the case of infinitesimally thin, plane isotropic sources shielded by plane absorbers. For this geometry, there exist sufficient calculations and measurements to make detailed statements about the beta dose and the beta-gamma ratio. Furthermore, in view of the limited range of beta particles and the intrinsically large extent of the fallout, this geometry appears to be a reasonable approximation for most operational situations. There are factors which may invalidate this approximation, such as the roughness and finite extent of the real source surface. More important may be the finite and even large size of the fallout source particles. Large particles tend to decrease the beta relative to the gamma source strength due to self-absorption, and to change the source angular distribution from isotropic, particularly for the betas. The importance of these factors is presently unknown.

Point geometrical sources in spherical geometry are of much lesser significance than infinite plane isotropic sources and have been considered to a limited extent only. The extensive calculations required to handle intermediate geometries, such as finite plane sources, are not available at this time.

The determination of the beta dose and the accompanying gamma dose under various situations is conveniently presented in the following sections:

6.2 Radiation Source Characteristics

6.3 Beta-Gamma Dose Ratio at the Source

6.4 Beta Depth Dose Behavior

6.5 Beta-Gamma Biological Hazard

6.6 Miscellaneous Internal Effects.

Section 6.2 considers the beta and gamma energies and activity ratios of the source. These are sufficiently time-dependent to require a time-dependent description. In view of the range of measured and calculated beta-gamma dose ratio values for various situations, Section 6.3 presents a standardized set of values for a clear-cut geometrical situation without the effects of absorbers. The effects of absorbers, such as air and clothing, are considered in Section 6.4. Biological effects and estimates of disability doses are briefly discussed in Section 6.5, and situations where internal beta radiation might be considered a hazard are covered in Section 6.6.

6.2 RADIATION SOURCE CHARACTERISTICS

The relative beta and gamma doses are dependent on the beta and gamma energy spectra and beta-gamma activity ratios of the radioactive fallout source. The activity ratio is defined as the ratio of the number of beta particles to gamma rays produced by the source. An accurate description of the energy spectra and activity ratios over the time interval of interest (1 hour to 30 days) would be comprised of a formidable amount of data but much of this information is not available at the present time. Much effort has been expended in field measurements of the spectra, but the measurements have been handicapped by instrumental limitations. The use of improved techniques such as scintillation spectrometry[6] are encouraging and give promise that accurate spectral distributions for the complete time interval will ultimately be available.

The picture is also rendered difficult by the phenomenon knows as fractionation. The concentration of the condensed nuclides is largely determined by the history of diffusion of their ancestors and their physical and chemical properties at the time of condensation. These are selective properties. As an extreme example, nuclides such as krypton and xenon, which are noble gases, cannot condense until they have decayed into rubidium and iodine, respectively. Thus, the concept of a standard composition source (at a particular reference time) is somewhat tentative. Though the significance of fractionation must be conceded, the incorporation of this somewhat random variable as a modifying parameter of the source energy distribution is not feasible at this time.

To circumvent the lack of detailed knowledge of the energy spectra, it has been customary to speak of "effective" average gamma ray energies and "effective" maximum beta ray energies as functions of time. These effective energies are those single values of the beta and gamma energies

which characterize the entire beta and gamma spectra. Once such effective energies are established it is possible to treat both the beta and gamma sources as monoenergetic. This is the approach followed in the present treatment. Thus Fig. 6.2:1 is a graph of the effective maximum beta energy, effective average gamma energy, and the average beta-gamma activity ratio as a function of time after fission. The figure is taken bodily from a report of Sondhaus[7] and will be used as a standard. The Sondhaus curves are neither exact nor up-to-date but they do present the information which is most useful for estimating the beta-gamma dose ratio and the beta depth dose attenuation. For times greater than one hour, the curves are based on activity calculations of Hunter and Ballou[8] for standard fission products; the shorter time values are based on measurements of fission products.

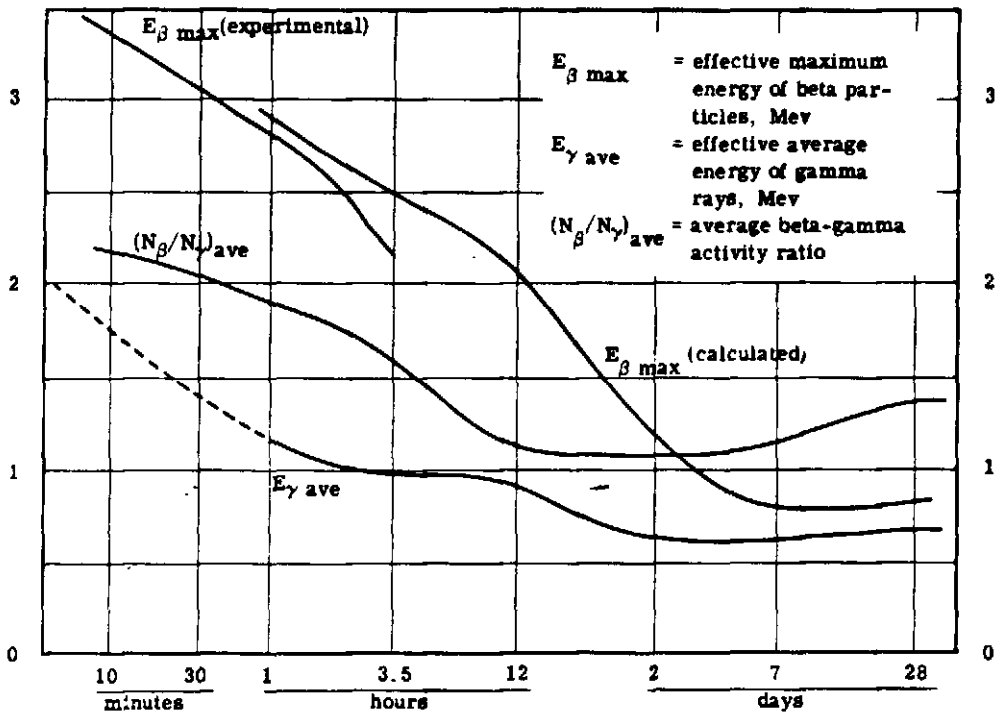

Figure 6.2:1 Beta-Gamma Activity Ratio, and Beta and Gamma Effective Energies at the Source as a Function of Time after Fission. Dashed line is estimated.

In order to determine the effective average beta energy from the effective maximum or endpoint values it is necessary to know the shape of the beta energy spectrum and therefore the type of decay transition which occurs. For present purposes the decay transition known as "allowed" will be assumed together with the resulting relationship between maximum and average beta energy. While this relationship varies with the atomic number as well as with the maximum beta energy, a reasonable value for present purposes is

$$E_{\beta\ ave} = 0.36\ E_{\beta\ max} \qquad (6.2:1)$$

Calculations by Condit et al[2] indicate that the composite spectra do have some resemblance to allowed beta spectra for times less than 30 days.

6.3 BETA-GAMMA DOSE RATIO AT THE SOURCE

The most practical limiting geometrical situation for which the beta-gamma ratio is of interest is the infinite plane isotropic source; this simulates fairly well situations which involve a contaminated ground surface or contamination adhering to the skin. In many practical situations the beta dose may be significantly reduced by the distance of the body tissue from the source and by shielding by clothing and by the body itself. These effects are considered in Section 6.4. In the following paragraphs the object is to determine the beta-gamma dose ratio at the source.

Previous values of the beta-gamma dose ratio range from 40:1 to 157:1. Tochilin and Howland[9] obtained the 157:1 value from a fallout sample using a calibrated thin walled, parallel plate ionization chamber. Tochilin et al[10] obtained an average value of 100:1 using film stacks set below fallout samples in the field. Goulding and Cowper,[11] using a combination of measurements and calculations, obtained a value of 150:1. The early estimates of Condit et al[2] gave a ratio of 150:1 but the calculations were more in the nature of estimates. Later calculations of Teresi and Broido[12] gave a value of 40:1, based on a beta-gamma activity ratio of 1.

Brennan[13] obtained the ratio 10:1 for the quantity

$$\frac{D_{\beta p} + D_{\gamma p}}{D_{\gamma f}}$$

where $D_{\beta p}$ and $D_{\gamma p}$ are the beta and gamma doses to the papillary layer of the human skin, and $D_{\gamma f}$ is the dose measured by a film badge in the shoulder position. This has led to some confusion, since it is not a beta-gamma ratio per se. It is not necessarily inconsistent with other measurements or with the calculations in the present document.

Imrie and Sharp[5] measured the beta-gamma dose ratio using miniature thin walled ionization chambers at the surface of or within simulated human phantoms. Close to the source plane the beta-gamma dose ratio for the first day after the burst was reported as 50:1.

One would expect a range of values for the beta-gamma dose ratio because of varying energies and compositions of the source, but it seems unlikely that these variables should account for more than a 2:1 spread. Differences in source-detector geometry may also be a factor responsible for part of the spread. Further investigation seems to be indicated.

Accurate physical data and rigorous calculations now exist for computing the beta and gamma doses for both point and plane isotropic sources imbedded in a uniform absorbing medium when the source strengths and energy distributions are known or can be estimated. Back-scattering due to medium discontinuities and thick sample effects for the beta sources are perturbations which will be encountered in the field and which will, in general, tend to decrease the beta dose from the values calculated for the geometries described above. These factors not withstanding, for estimating the beta hazard at the present time the calculations are more reliable than the measurements.

It is instructive to indicate first how the beta-gamma dose ratio can be estimated close to a monoenergetic point isotropic source in air. If a 20-hr time after the bomb burst is chosen, Fig. 6.2:1 gives an effective maximum beta energy of 1.7 Mev, an effective average gamma energy of 0.75 Mev, and an average beta-gamma activity ratio of 1.1. With an effective maximum beta energy of 1.7 Mev and assuming the allowed spectrum, the effective average beta energy is 0.6 Mev.

Close to a point isotropic source of 0.6-Mev beta particles in air the beta dose rate in units of erg-sec^{-1}-gm^{-1} is

$$\dot{D}_\beta = \frac{P_{\beta_0} S_\beta}{4\pi R^2 k_{12}} = \frac{(1.71)\, S_\beta}{4\pi R^2 (6.24 \times 10^5)} = \frac{0.28 \times 10^{-5} S_\beta}{4\pi R^2} \quad \frac{\text{erg}}{\text{sec-gm}} \qquad (6.3{:}1)$$

where

k_{12} = 6.24 x 10^5 Mev-erg^{-1}

P_{β_0} = stopping power for betas in standard density air, Mev-cm^2-gm^{-1}

S_β = source strength, betas produced-sec^{-1}

R = distance from point source, cm

For 0.6-Mev betas[14] P_{β_0} is 1.71 Mev-cm^2-gm^{-1}.

The unscattered gamma dose rate close to an isotropic point source of 0.75 Mev gammas in air is

$$\dot{D}_{u\gamma} = \frac{\mu_{a_0} E S_\gamma}{4\pi R^2 k_{12} d_0} = \frac{(3.7 \times 10^{-5})(0.75) S_\gamma}{4\pi R^2 (6.24 \times 10^{-5})(1.29 \times 10^{-3})} = \frac{0.35 \times 10^{-7} S_\gamma}{4\pi R^2} \quad \frac{erg}{sec\text{-}gm} \qquad (6.3:2)$$

where

μ_{a_0} = linear energy-absorption coefficient for gammas in standard density air, cm^{-1}

d_0 = density of air at standard conditions, gm-cm^{-3}

E = gamma energy, Mev

S_γ = source strength, gammas produced-sec^{-1}

For 0.75-Mev gammas[15] μ_{a_0} is 3.7 x 10^{-5} cm^{-1}.

Close to the source the scattered contribution to the gamma dose is small (i.e., the buildup factor is close to 1) and the value derived above for the unscattered gamma dose rate may be taken as the total dose rate $\dot{D}_\gamma$. Thus the ratio of total beta to total gamma dose close to the isotropic source point in air and taking into account the beta-gamma activity ratio of 1.1 is approximately

$$\frac{\dot{D}_\beta}{\dot{D}_\gamma} = \frac{0.28 \times 10^{-5} S_\beta}{0.35 \times 10^{-7} S_\gamma} = (80)(1.1) = 88 \qquad (6.3:3)$$

The dose ratio given above is expressed as the ratio of ergs per gm of air (due to betas) to ergs per gm of air (due to gammas). This is identical to a ratio expressed in terms of rep of betas per r of gammas in air. The same numerical values may, however, also be taken to represent the ratio in terms of rep of betas per r of gammas in tissue, as only a small error is introduced by this assumption.

These estimates are naturally limited in accuracy by the accuracy of Fig. 6.2:1. A rigorous calculation which properly takes into account electron energy degradation and details of the beta spectrum is given by Spencer.[14] He obtains a beta dose rate $\dot{D}_\beta$ in the vicinity of the source which is about 20 percent larger than the result obtained above for monoenergetic betas. Thus

$$\dot{D}_\beta = \frac{0.34 \times 10^{-5} S_\beta}{4\pi R^2} \quad \frac{erg}{sec\text{-}gm} \qquad (6.3:4)$$

The dose computed for monoenergetic betas is low primarily because the low-energy beta component of the spectrum has a greater energy loss per unit path length.

Using Spencer's value, the beta-gamma ratio for 20-hour point source isotropic fallout is

$$\frac{\dot{D}_\beta}{\dot{D}_\gamma} = 105 \qquad (6.3:5)$$

Calculation of the beta-gamma dose ratio for an infinite plane source is complicated by certain practical and theoretical difficulties and no adequate analytical treatment for this ratio is presently available. Under these circumstances only an approximate, admittedly incomplete, treatment is possible. This method is naturally not unique but it is believed to be the most appropriate for simple calculations at this time.

What is done is to take the gamma dose calculated at a distance of 3 ft for an infinite isotropic plane source of zero thickness and to define this as the gamma surface dose. This assumes that the gamma dose does not increase appreciably between 3 ft and the source surface, a reasonable assumption for real surface sources, although incorrect for ideal surfaces. Since 3 ft of air can appreciably reduce the dose from a low energy beta source, this dose is taken at a much closer distance. The analytical beta dose determined by Spencer[14] for finite distances from the source surface is extrapolated to yield a finite result at zero distance; this procedure will define the surface beta dose.

For an isotropic infinite plane source of zero thickness the unscattered gamma dose rate in air is given by[16]

$$\dot{D}_{\mu\gamma} = \frac{\mu_{a_0} E (S_\gamma/A)}{2 k_{12} d_0} \int_{\mu_{t_0} y}^{\infty} \frac{e^{-\mu_{t_0} r} d(\mu_{t_0} r)}{\mu_{t_0} r} \qquad (6.3:6)$$

$$= \frac{\mu_{a_0} E (S\gamma/A)}{2 k_{12} d_0} [E_1(\mu_{t_0} y)]$$

where

S_γ/A = source strength, gammas produced-sec^{-1}-cm^{-1}

$E_1(\mu_{t_0} y)$ = exponential integral

μ_{t_0} = total linear attenuation coefficient for gammas in standard density air, cm^{-1}

y = height of receiver above source plane, cm

r = slant distance from the receiver to a point in the source plane.

Using values appropriate to the 20-hr point, $\mu_{t_0} = 0.87 \times 10^{-4}$ cm^{-1} and the unscattered gamma dose rate 3 ft from the source surface is

$$\dot{D}_{u\gamma} = \frac{(3.7 \times 10^{-5})(0.75)(S\gamma/A)}{(2)(6.24 \times 10^{3})(1.29 \times 10^{-3})} (4.25) = 0.74 \times 10^{-7} (S\gamma/A) \quad \frac{\text{erg}}{\text{sec-gm}} \qquad (6.3:7)$$

The dose buildup factor which corrects for the contribution of the scattered radiation has the value 1.31 at 3 ft[17]. The total gamma dose rate is therefore

$$\dot{D}_\gamma = (1.31)(0.74 \times 10^{-7})(S_\gamma/A) = 0.97 \times 10^{-7} (S\gamma/A) \quad \frac{\text{erg}}{\text{sec-gm}} \qquad (6.3:8)$$

The beta dose rate for an isotropic infinite plane P^{32} source (corresponding to a maximum beta energy of 1.7 Mev) is given by Spencer for finite distances from the source. Extrapolating the dose to zero distance yields a beta dose rate of

$$\frac{\dot{D}_\beta}{S_\beta/A} = 2.0 \times 10^5 \quad \frac{\text{erg-cm}^2}{\text{curie-sec-gm}} \qquad (6.3{:}9)$$

where S_β/A = source strength, betas produced-$\text{sec}^{-1}\text{cm}^{-2}$. The value of 2.0×10^5 was obtained by linear extrapolation on a plot of differential energy dissipation as a function of distance from the source plane. The extrapolation was carried out from a distance corresponding to 50 mg-cm^{-2}

Converting this to the same units as the gamma dose rate yields

$$\dot{D}_\beta = \frac{(2.0 \times 10^5)\ (S_\beta/A)}{3.7 \times 10^{10}} = 0.54 \times 10^{-5}\ (S_\beta/A) \quad \frac{\text{erg}}{\text{sec-gm}} \qquad (6.3{:}10)$$

The beta-gamma dose ratio close to the source plane is then

$$\frac{\dot{D}_\beta}{\dot{D}_\gamma} = \frac{0.54 \times 10^{-5}\ (S_\beta/A)}{0.97 \times 10^{-7}\ (S_\gamma/A)} = \frac{0.54 \times 10^{-5}}{0.97 \times 10^{-7}}\ (1.1) = 61. \qquad (6.3{:}11)$$

These values, strictly speaking, hold only for the 20-hour time point. This time was chosen for the specific example because of the explicit Spencer beta dose calculation for an endpoint energy of 1.7 Mev.

It is interesting to note that the beta-gamma dose ratio, as calculated above, is not extremely sensitive to source geometry. The point isotropic source value is less than twice the plane isotropic source value. Since almost all field situations will be effectively more analogous to the plane isotropic source, the plane isotropic value can be used with reasonable accuracy for all situations.

Although one would a priori expect the beta-gamma dose ratio to be time-dependent because of the time dependence of the energies and the activity ratios, it so happens that the dose ratio, to a fairly good approximation, is independent of time. The beta dose at the source should be fairly independent of energy with regard to the energies actually encounterd. This is because the only factor determining the beta dose which is energy dependent is the energy loss term (stopping power $P_{\beta\theta}$) and this term is quite constant from 10 Mev down to 0.4 Mev. At lower energies it does increase, reaching roughly twice the minimum value at 100 kev. The range at this energy is, however, only 16 mg-cm^{-2}. Betas with this energy or less are not biologically significant, since they can barely penetrate the skin; furthermore, they will be heavily absorbed by the source. Since most of the betas are emitted within the energy interval of constant energy loss, the beta dose at the source surface (and particularly the significant non-low energy component) can be taken as independent of beta energy.

The gamma dose does vary with gamma energy and thus with time. The beta-gamma activity ratio, however, which also enters into the dose ratio and is time-dependent, varies nearly as the gamma dose and effectively eliminates the variation of the dose ratio.

For idealized infinitely thin plane isotropic sources, the beta-gamma dose ratio can therefore be considered to be substantially constant (from 1 hour to 30 days after the time of burst). The values of the dose ratio for plane sources obtained by several investigators from both experimental measurements and theoretical calculations vary from about 40 to about 160. As noted previously, the calculational results appear to be more reliable and are weighted accordingly. Thus, the best all-around compromise value of the beta-gamma dose ratio seems to be of the order of 70 and this value will be used throughout.

6.4 BETA DEPTH DOSE BEHAVIOR

For many situations it is important to determine the attenuation of the beta dose produced by intervening material such as air or clothing. More massive materials, such as building walls or even

a 1/4-in. slab of plywood, will effectively shield out all the betas. Thicknesses of absorbers capable of attenuating the beta dose by a factor of 100 do not appreciably attenuate the gammas.

Fig. 6.4:1 is based upon an allowed beta energy spectrum and gives the attenuation of the beta dose as a function of absorber thickness and maximum beta energy[10]. The curves are the results of measurements on stacks of film exposed to beta emitters Ta^{182}, RaD + RaE, P^{32}, Y^{90}, and Rn^{198} with endpoint energies of 0.5, 1.0, 1.7, 2.3, and 3.4 Mev, respectively. The geometry is that of the infinite plane isotropic source with slab absorbers. The P^{32} depth dose film measurement curve is in excellent agreement with the P^{32} calculations of Spencer[14] and independent P^{32} measurements of Loevinger[14]

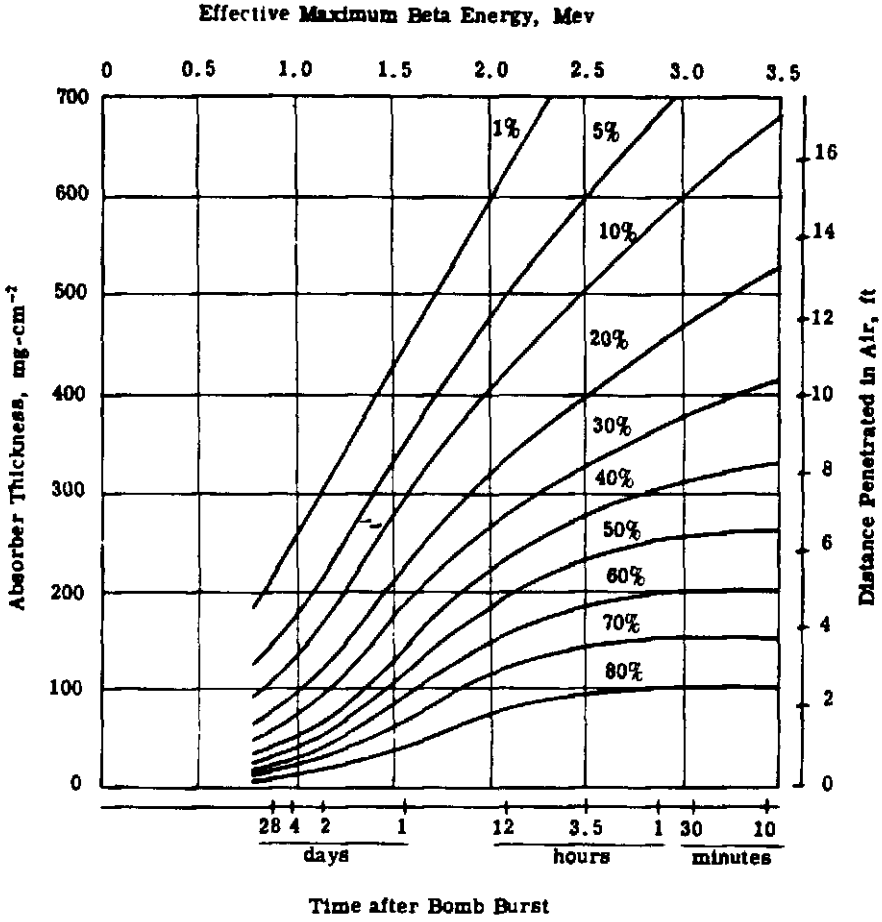

Figure 6.4:1 Beta Depth Dose Curves for an Infinite Plane Isotropic Source Given as a Percentage of the Dose at the Surface.

when the beta dose rate at zero distance from the surface source is taken as 1×10^5 ergs-cm^{-2}-curie^{-1}-sec^{-1}-gm^{-1}. It is noted that the experimental setup used to obtain Fig. 6.4:1 is not necessarily a completely valid model for the actual operational situation since problems like self-absorption by contaminated particles remain unevaluated. The precise value of the dose in the vicinity of the source will always be somewhat ambiguous because of such varying characteristics of the source; nevertheless, by forcing the curves to agree for large absorber thickness one retains confidence in the value of the dose at finite distances.

Fig. 6.4:1 contains a double abscissa (maximum beta energy and time after detonation) and a double ordinate (mg-cm^{-2} and feet of air). The correlation between maximum beta energy and time

after detonation is taken from Fig. 6.2:1 while the air scale is based on the standard air density of 0.001293 gm-cm^{-3}.

Assuming a beta-gamma dose ratio of 70:1 and the depth dose behavior of Fig. 6.4:1, one can make specific statements about the beta hazard for many situations of interest. What is done is to calculate the attenuation of the beta dose by the materials (air, clothing) between the source and the point of interest and multiply this by the known gamma dose at the point of interest, the beta-gamma dose ratio at the source, and a geometrical correction factor. This procedure assumes that there is no attenuation of gammas between source and the point receiving the dose.

It should be noted that the procedure outlined is applicable to the calculation of the beta dose rate only for relatively simple geometries and where the corresponding gamma dose rate is known. For example, it can be used to predict the beta dose rate to a man standing or lying on a contaminated field or in proximity to a contaminated ship or aircraft. For the important situation where fallout particles have adhered to the skin or clothing this calculational procedure is not useful. Indeed, in view of the wide range of possible source particle distributions and strengths it is difficult to conceive of any calculational procedure that is valid. The most that can be said is that when the skin and clothing have become contaminated as a result of the man lying in the contaminated field or by being exposed to the falling particles, the beta dose rate received due to such contamination is probably less than that received while lying in the field. However, since the time period during which the man's skin and clothing are contaminated may be much longer than the period during which he lies in the field, even this conjecture may not be particularly helpful.

For a clothed man standing on contaminated ground, a vertical cylinder can serve as a rough geometrical model. Since the body absorbs all betas, the vertical body surfaces have a line-of-sight view of only half of the source plane. Gamma rays are much more penetrating and points within or at the surface of the body see essentially the entire source plane. Thus the effective beta-gamma dose ratio should be reduced by a factor of approximately two or to a value of 35:1. Typical clothing weights[13] in mg-cm^{-2} are: undershirt 17, shorts 12, shirt 29, trousers 77, field jacket 186. Assuming the man is clothed with the above items, the dose ratio at various parts of the body is obtained by taking into account the attenuation produced both by air and by clothing.

It is evident that for all times of interest the light articles of clothing offer no significant shielding protection against betas. Furthermore, the epidermal layer of skin (about 10 mg-cm^{-2}) can be ignored as a beta shield.

If one assumes an independent beta hazard to exist for situations for which the beta-gamma ratio is greater than 20 (4000 reps of betas as compared with 200 roentgens of gamma radiation), and if one also assumes the surface beta-gamma ratio to be 70:1, then the area in Fig. 6.4:1 below the 30 percent curve corresponds to such situations. For vertical body surfaces where the 35:1 surface beta-gamma ratio applies, the corresponding area is that below the 60 percent curve.

PROBLEM 1

A man stands erect on an infinite plane surface completely contaminated by fission products. The following facts are known: weight of clothing per square centimeter, height of various parts of his body, time elapsed since bomb burst, and average gamma dose rate that he is receiving.

Compute the beta dose rate at the surface of various parts of his body.

Solution

1. Take the surface source beta-gamma ratio to be 70 rep-r^{-1}.
2. From the average height of each body area of interest, compute the equivalent air absorption weight in mg-cm^{-2}.
3. Compute the clothing weight at each body area in mg-cm^{-2}.
4. Find the total absorber weight by adding the results of steps 2 and 3 above.

5. In Fig. 6.4:1, read the abscissa at time after bomb burst and the left ordinate at total absorption weight for each body area. The intersection of these two coordinates gives the beta-gamma dose ratio for an isolated shielded point as a percentage of the infinite plane isotropic source surface dose ratio.

6. It is necessary to apply a geometric correction factor since the affected areas are not isolated points for beta radiation. Any point on the upright man's body surface is shielded from the beta radiation of one-half the plane by the body itself. This is not, however, true of the gammas. The correction factor is therefore one-half.

7. The beta dose rate to an affected area is therefore given by: average gamma dose rate ($r\text{-}hr^{-1}$) x infinite plane isotropic surface source beta-gamma dose ratio ($rep\text{-}r^{-1}$) x absorption correction (expressed in percent of surface dose ratio) x geometric correction.

These factors come respectively from the given data and steps 1, 5, and 6 of the solution.

Example

A man stands erect in an infinite plane field contaminated by fallout. His clothes with typical specific weights are:

Article	Weight, $mg\text{-}cm^{-2}$
undershirt	17
shirt	29
field jacket	186
shorts	12
trousers	77

The affected areas of interest with nominal heights are:

Area	Height, ft
calf	1
thigh	3
chest	4
face	5

The time elapsed since burst is (a) one hour and (b) two days and the average gamma dose he is receiving is for each case 100 $r\text{-}hr^{-1}$.

Compute the beta dose rate at the surface of the given body areas.

1. The source surface beta-gamma ratio is taken as always being 70 $rep\text{-}r^{-1}$.

2. The equivalent air absorption weights computed for each of the areas at 40 $mg\text{-}cm^{-2}\text{-}ft^{-1}$ above ground are:

Area	Air Weight, $mg\text{-}cm^{-2}$
calf	40
thigh	120
chest	160
face	200

3. The clothing absorption weights are:

Area	Clothing Weight, mg-cm^{-2}
calf	77 (trousers)
thigh	89 (trousers, shorts)
chest	232 (jacket, shirt, undershirt)
face	0

4. The total absorption weight for each area is:

Area	Total Weight, mg-cm^{-2}
calf	117
thigh	209
chest	392
face	200

5. The absorption corrections on the beta-gamma dose ratio of the two times selected are from Fig. 6.4:1:

Area	Absorption Correction	
	1 hour	2 days
calf	0.78	0.22
thigh	0.56	0.045
chest	0.27	0.00
face	0.58	0.05

6. Since the body shields out half the field, the geometric correction factor is one-half. (The inner surfaces of the calf and thigh would receive more shielding and have a smaller factor, but this effect will be ignored.)

7. The beta dose rates by body areas for one hour and two days respectively, are:

Time After Burst	Area	Gamma Dose Rate, r-hr^{-1}	Surface Dose Ratio, rep-r^{-1}	Absorption Correction	Geometric Correction	Beta Dose Rate, rep-hr^{-1}
1 hour	calf	100	70	0.78	0.5	2730
	thigh	100	70	0.56	0.5	1960
	chest	100	70	0.27	0.5	945
	face	100	70	0.58	0.5	2030
2 days	calf	100	70	0.22	0.5	770
	thigh	100	70	0.045	0.5	158
	chest	100	70	0.00	0.5	0
	face	100	70	0.05	0.5	175

PROBLEM 2

A man lies prone in a field contaminated by fallout. The following facts are known: weight of clothing per square centimeter, time elapsed since bomb burst, and average gamma dose rate that he is receiving.

Compute the body surface beta dose rate.

Solution

1. Take the source surface beta-gamma ratio as 70 rep-r^{-1}.
2. Compute the clothing weight in mg-cm^{-2} at each body area.
3. Read from Fig. 6.4:1 the absorption correction to the beta-gamma dose ratio at the time given and at the clothing absorption weights computed in step 2.
4. Geometric factor is assumed to be 1 for those parts of the body facing the ground, 0 for the other parts.
5. The beta dose rate is then given by: average gamma dose rate (r-hr^{-1}) x infinite plane isotropic surface source beta-gamma dose ratio (rep-r^{-1}) x absorption correction x geometric correction. These factors come respectively from the given data and steps 1, 2, and 4 of the solution.

Example

A man lies prone in a field contaminated by fallout. The clothing on the covered areas of his body is uniformly 200 mg-cm^{-2}. Five hours have elapsed since bomb burst and the average gamma dose he is receiving is 100 r-hr^{-1}.

Compute the body surface beta dose rate.

1. Take the surface source beta-gamma ratio as 70 rep-r^{-1}.
2. Clothing weight on covered areas is 200 mg-cm^{-2} and on bare areas is 0 mg-cm^{-2}.
3. From Fig. 6.4:1 at 5 hours:

Clothing Weight, mg-cm^{-2}	Absorption Correction
200	0.54
0	1.0

4. The dose to the part of the body facing the ground gets no geometric reduction (factor of 1). Geometry is assumed to reduce dose to other parts to 0.
5. The beta dose rate to parts of the body facing the ground is given by:

Area	Gamma Dose Rate, r-hr^{-1}	Surface Dose Ratio, rep-r^{-1}	Absorption Correction	Geometric Correction	Beta Dose Rate, rep-hr^{-1}
covered	100	70	0.54	1	3780
bare	100	70	1.0	1	7000

[redacted]

PROBLEM 3

A man stands facing a large object contaminated by fallout (ship, tank, airplane). The following facts are given: weight of clothing per square centimeter, distance from contaminated object, time elapsed since bomb burst, and average gamma dose rate he is receiving.

Compute the body surface beta dose rate.

Solution

1. Same as Problem 1.
2. Compute the air absorption weight from the given distance from contaminated object using 40 mg-cm^{-2}-ft^{-1} of air. The absorption weight is the same for all portions of the body.
3. Same as Problem 1.
4. Same as Problem 1.
5. Same as Problem 1.
6. The geometric factor is 1 for portions of the body facing the object, and 0 for portions facing away from the object.
7. Same as Problem 1.

Error

In all the above problems, it is believed that the estimated probable error is a factor of about three. In some rather unimportant cases, the error can be much larger. For instance, where the geometric factor is taken as zero and scattering leads to a negligible but non-zero dose, the error is infinite.

6.5 BETA-GAMMA BIOLOGICAL HAZARD

Although the range 150-200 r has been generally accepted[1,18] as the gamma disability dose, the disability dose for betas has not yet been standardized. The value of 3000 to 5000 rep previously mentioned was taken from the Medical Officers Handbook.[1] The criteria for defining a gamma disability dose are much simpler. Gammas irradiate the entire body with a substantially uniform dose; betas produce a surface dose which cannot be expected to be constant over the body surface. The incidence of the disabling gamma symptoms, nausea, vomiting, and prostration, occur within a few hours. A value of 200 r will produce these symptoms in approximately half the members of a group. The disabling effects of a beta dose (such as the production of severe skin lesions) depend to an extent on the area of the skin affected and do not manifest themselves as rapidly; times of the order of two weeks are required for the production of lesions.

It is quite likely that the concept of beta dose alone is inadequate to predict the biological effects, and more extended information such as the beta depth dose curve in tissue may be necessary. For example, a 4-Mev monoenergetic beta produces the same dose at the outer skin surface as a 0.4-Mev beta, but the total energy deposited in all tissue is 10 times greater. The depth dose curves given in Fig. 6.4:1 can be used to sketch the depth dose curve in tissue as well as in other absorbers.

6.6 MISCELLANEOUS INTERNAL EFFECTS

Effects of internal beta radiation, such as the beta dose received in the lungs due to inhalation of fallout or in the digestive organs due to ingestion of contaminated food and water, are not ordinarily primary hazards as compared with the external beta and gamma dose. One exception lies in the case of insoluble particles inhaled and fixed in one position in the lung. This problem has not yet been successfully evaluated. Calculations of Sondhaus[7] indicate that, with this exception, the beta hazard to the lung is much less than the external total body gamma hazard. Studies[3] of the natives of the Marsh-

[redacted]

Chapter 7

THE ATOMIC CLOUD

7.1 INTRODUCTION

The nature of the atomic cloud enters in the following three ways into considerations of nuclear radiation from a bomb burst.

1. The cloud is the source of most of the initial radiations. (Appreciable portions of the nitrogen capture gamma source, however, originate in absorptions outside the cloud.) Note that for this purpose the cloud is not distinguished from the fireball, which is its luminous predecessor.
2. The active material which deposits on the earth to produce the fallout pattern is generally considered as having its origin in the cloud.
3. The cloud represents a highly radioactive portion of space which may on occasion be approached or penetrated by manned aircraft.

To evaluate the bomb radiation hazards associated with the cloud, it is necessary to have some understanding of the behavior of the cloud, its shape and position in space and time, and its activity content and distribution.

Section 7.2 presents a brief qualitative discussion of the mechanism postulated for cloud dynamics while in Section 7.3 observations and measurements of cloud heights and dimensions are summarized. The last two sections (7.4 and 7.5) discuss the use of these data for calculations of fallout, initial radiation and cloud penetration by aircraft; emphasis is necessarily placed on the last of the three because of the scarcity of adequate information for fallout and initial radiation calculations.

7.2 CLOUD DYNAMICS

There is yet no complete analytical description of cloud dynamics. There exists, however, a considerable body of observational data from which it has been possible to compose empirical relations and to formulate a qualitative description of phenomena. In this description the cloud and the fireball will not be fully distinguished, but will simply be regarded as different stages in the life of the same phenomenon.

The first phase in the life of the fireball is the tremendous expansion occurring at the time of blast. This initial expansion occurs very quickly, being essentially complete in less than one second. During this time motion within the fireball is completely turbulent.

The next phase in the fireball history is a subject of some uncertainty, both as to its actual existence and its basic mechanism.[1,2] This phase is known as the hover time and is a short period in which the top surface of the fireball appears to remain stationary.[3] The hover time may be from 2 to 5 seconds long. The explanation advanced is that there must be an appreciable time for the buoyant

forces to accelerate the fireball upward, these forces being independent of the radial forces associated with the blast. If the hover time actually exists, the buoyant acceleration proceeds very rapidly once it starts, since the rising fireball attains its maximum upward velocity well within the first ten seconds after the blast. After this time, the speed of rise decreases quite rapidly so that in most bursts the cloud attains half its maximum altitude within 1 to 2 minutes after the burst,[3] although the corresponding maximum altitude is not reached for 4 to 10 minutes.[4, 5]

It appears that during the first few seconds of fireball rise the internal motion of the hot gases comprising the fireball begins to evolve, from the initial turbulence into the characteristic toroidal rotation. The resulting general configuration of the fireball is that of a horizontal torus or doughnut. The rotatory motion is caused by the viscous frictional drag of the stationary atmosphere on the outer surfaces of the rising fireball. The rotational movement is downward along the outside surface of the fireball, horizontally inward across the bottom, upward along the surface of the interior hole of the torus, and horizontally outward across the top.

After 10 seconds or a little more, the ascending bubble cools to the point where it is no longer luminous; it is subsequently referred to as the cloud.[6] The rotation, however, continues through this transition and long after. (There is reason to believe that, in some cases at least, it persists until after the cloud has attained its maximum altitude.)

The rapid rise of the fireball/cloud creates a strong updraft below it. This updraft is greatly reinforced near the vertical axis of the torus by the toroidal rotation, which acts like a very powerful pump.

If the burst occurs on the earth surface or sufficiently close to it, surface material is sucked up to form the familiar visible stem, which fans out below the cloud in a cone-shaped skirt with apex at the cloud bottom. From observation it appears that this material is drawn up into the hole in the torus, and falls back to earth in a veil around the stem. It is not believed that this material makes very intimate contact with the highly active bomb materials.[3] In any case, it does not appear to be a very effective scavenger of active materials.

As previously noted, the vertical thrust on the cloud is provided by the buoyant forces of the atmosphere, since the cloud is hotter and is therefore less dense than the surrounding air. There are, however, a number of braking forces which slow and ultimately stop the rise of the cloud. One of these forces is the frictional resistance of the atmosphere to the passage of the cloud. As the cloud rises, its size increases and the frictional resistance opposing the rise likewise increases. The other braking forces all act to increase the average density of the cloud and therefore decrease its buoyancy in the surrounding air. The importance of the individual mechanisms varies with time. Thus, in the fireball stage it is likely that the main mechanism increasing the density is radiative heat loss, which lowers the average temperature. After the cloud stage is reached, there are three processes which operate to increase the cloud density.

1. As the cloud rises it encounters lower atmospheric pressure and expands. In expanding, the cloud temperature decreases and the density increases.
2. During the rise large quantities of air at ambient temperatures are entrained into the cloud; this air cools the cloud by mixing.
3. The density of the ambient air and, thus, its buoyant effect decrease with increasing altitude. The air density is a function of both its pressure and temperature. Air temperature generally tends to decrease with altitude within the troposphere (the inner envelope of the earth's atmosphere) but the air pressure decreases more rapidly, so the net effect is a decrease in density. In the stratosphere temperature increases and the pressure decreases with altitude so that the air density drops much more rapidly.

The effect of variations in atmospheric conditions appears to be limited primarily to only one of the braking mechanisms described above.[7] The atmosphere plays essentially no role during the radiative heat loss period and the decrease of air pressure with altitude is nearly the same for all burst environments. At present it is felt that the characteristics of the cloud rather than the surrounding

atmosphere determine the rate of entrainment of air. The only significant atmospheric variation from shot to shot is the variation of air density with height (which is essentially due to variations of air temperature since the pressure change is, as noted above, fairly uniform). The probable control by the atmospheric temperature lapse rate over the maximum rise of the atomic cloud is demonstrated by the large number of shots which have stopped at the tropopause, by the several low-yield shots which have stopped at temperature inversions in the troposphere, and by the formation of horizontal layers of stem material separated by stable layers of atmosphere.[7]

The cloud finally stops rising when it comes into density (and therefore thermal) equilibrium with its surroundings. This may occur within the troposphere but for high-yield weapons the cloud may penetrate into the stratosphere. If this penetration occurs, the final braking is somewhat expedited by the more rapid decrease of density with altitude in this region. (It should be noted that the equilibrium altitude and dimensions of the cloud at this equilibrium are in reality only temporary quantities. They are the values describing the cloud at the end of the rise period and before the normal dispersing processes of the atmosphere become important.)

It appears that the cloud sometimes overshoots the altitude at which it is in density equilibrium with the surrounding atmosphere by a few thousand feet and then slowly sinks back to its stable level. The reason for this overshoot is not clear but it is believed that it may be attributed to inertia of the cloud mass, which causes a characteristic damped oscillation. The cloud sinks back to its equilibrium position when the gravitational and viscous atmospheric forces overcome these inertial effects.[3,4,5,8]

It has been frequently observed that clouds reaching their equilibrium altitude undergo a rapid and substantial lateral expansion or flattening. This expansion is attributed mostly to the thermodynamic requirement that all parts of the cloud reach approximately the same equilibrium elevation. The toroidal rotation may also have an influence on the effect, but this as yet has not been properly evaluated.

For atmospheres containing appreciable amounts of moisture, another effect may require consideration. The moisture content (in the vapor state) of the lower levels is of the order of 1 to 10 grams per kilogram of air. This moisture condenses at the lower temperature of the upper atmosphere to release about 600 calories of heat for each gram of water vapor. For Nevada shots the total amount of heat released probably does not exceed a value of the order of 0.1 KT of energy but for the Pacific shots, where the moisture content of the air is much higher, the total energy release may be large enough to be important.

7.3 CLOUD HEIGHTS AND DIMENSIONS

In the evolution of an atomic cloud there are many features which are of interest. These include the top of the cloud, the center of gravity of the cloud, the base of the cloud, the bases and tops of layers (if any) of the stem, the diameter and volume of the cloud and stem, and the distribution of the radioactivity within the cloud. Unfortunately, only the top of the cloud has been systematically observed during all of the tests. The other items have been investigated during only a limited number of tests. For this reason, theories have been promulgated and tested only on the maximum height of the cloud.

Three principal theories of cloud rise have been proposed by Taylor[9], Sutton[10], and Machta[11]. While these theories have contributed to the development of understanding of cloud phenomena, they have not yet reached the stage of refinement where predictions made from them should supplement the purely empirical results of the weapons tests.

There is sufficient coherence among the observed experimental results, however, to fit some empirical curves to the data points and to vest considerable confidence in their general validity. A unified theory will probably permit much better fitting to these same data points than our present state of ignorance permits. (In fact, classifying the available data according to season and latitude would permit a more consistent but, at present, less useful set of empirical relations.)

Fig. 7.3:1 is a plot of the equilibrium heights of the tops and bottoms of a great many observed clouds as a function of bomb yield. Data are included from tests at both the Nevada - New Mexico Area and the Marshall Islands Area.

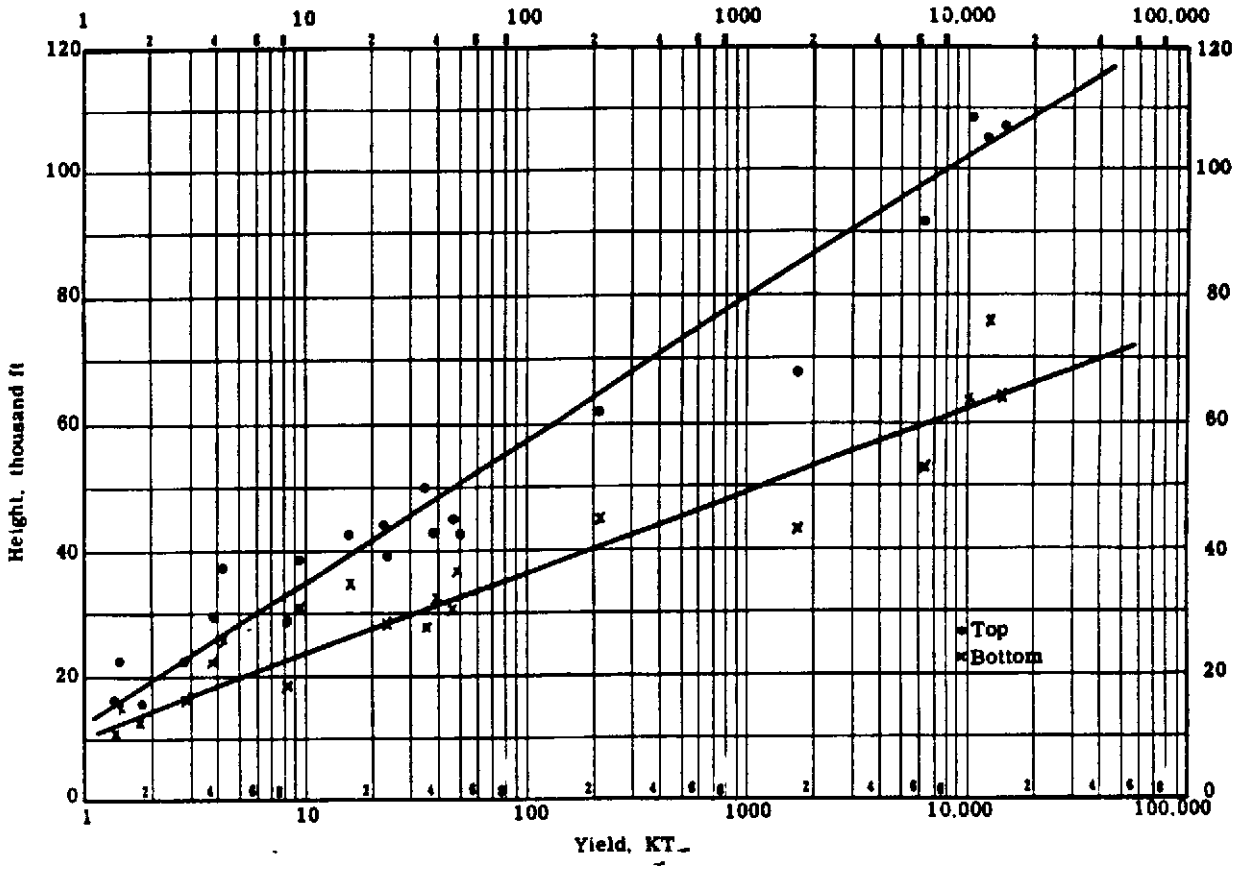

Figure 7.3:1 Experimental Measurements of the Equilibrium Heights of Top and Bottom of Cloud as a Function of Yield for Near-Surface Bursts.

In the construction of this and the other figures in this section, bomb yields were corrected to an equivalent mean sea level value. That is, the actual yield at the burst height was adjusted to an equivalent yield for a sea level burst which produces the same cloud characteristics.

The mean sea level correction[12] used is

$$W_{SL} = \frac{p_{SL}}{p_B} \quad W_B \qquad (7.3:1)$$

where

W_{SL} = equivalent yield at mean sea level

W_B = yield at actual burst height

p_{SL} = pressure at mean sea level

p_B = pressure at actual burst height

There are other parameters besides burst height which affect the cloud characteristics and which vary between shots but no methods are presently available for correcting these variations.

Figs. 7.3:2, 7.3:3, and 7.3:4 are plots of the height of the top, bottom, and center of the cloud as a function of time after burst for various yields. (It should be noted that for high-yield weapons the cloud may not have a clear-cut bottom and Figs. 7.3:3 and 7.3:4 are thus subject to an additional uncertainty in this yield region.) These three figures were obtained by fitting smooth curves to experimental results from about 15 bursts.[3, 5] Adjustments of the smooth curves were made where necessary to obtain reasonable internal consistency.

Fig. 7.3:5 is a plot of the vertical thickness of the cloud as a function of time after burst for various yields. It was constructed by subtracting the values of Fig. 7.3:3 from those of 7.3:2.

Fig. 7.3:6 is a plot of cloud diameter as a function of time after burst for various yields. It was constructed from the same sources and in the same manner as Figs. 7.3:2, 7.3:3, and 7.3:4.

While the cloud heights and dimensions in these figures are given for surface bursts, that is, measured from mean sea level, they may also be applied to near-surface bursts, say below 5,000 ft. In this case the cloud heights presented may be construed as being measured above the burst point. No information is available for the treatment of high altitude bursts.

The maximum error of these figures is believed to be about a factor of two. The test data upon which the curves were based are supposedly good to ± 30 percent but the wide range of tropopause heights, temperature-altitude relations, and wind velocities likely to be encountered under operational conditions greatly increases this expected error.

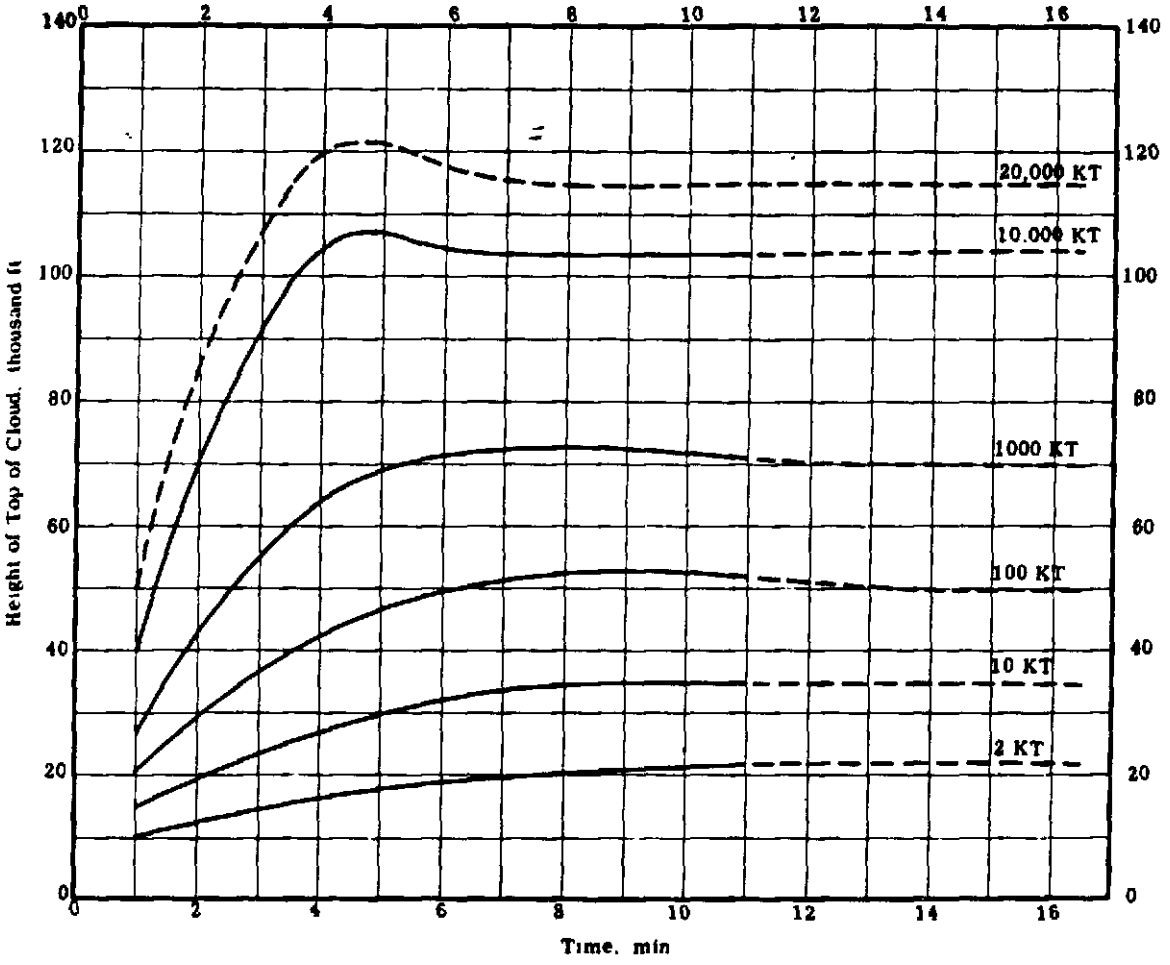

Figure 7.3:2 Height of Top of Cloud as a Function of Yield and Time after Burst for Near-Surface Bursts. Broken curves indicate extrapolated values.

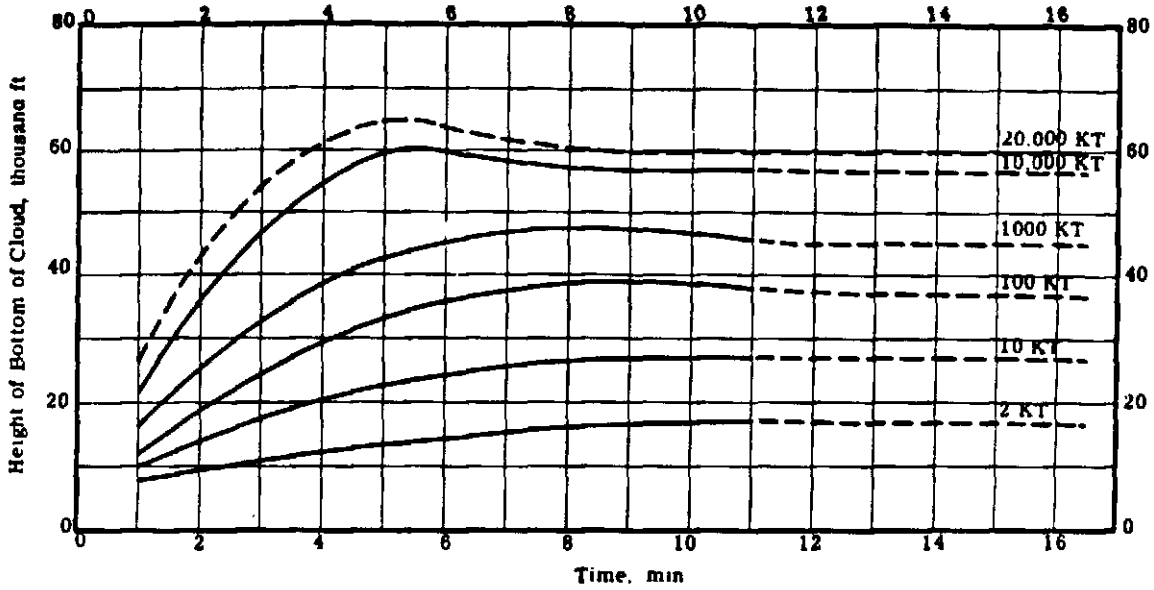

Figure 7.3:3 Height of Bottom of Cloud as a Function of Yield and Time after Burst for Near-Surface Bursts. Broken curves indicate extrapolated values.

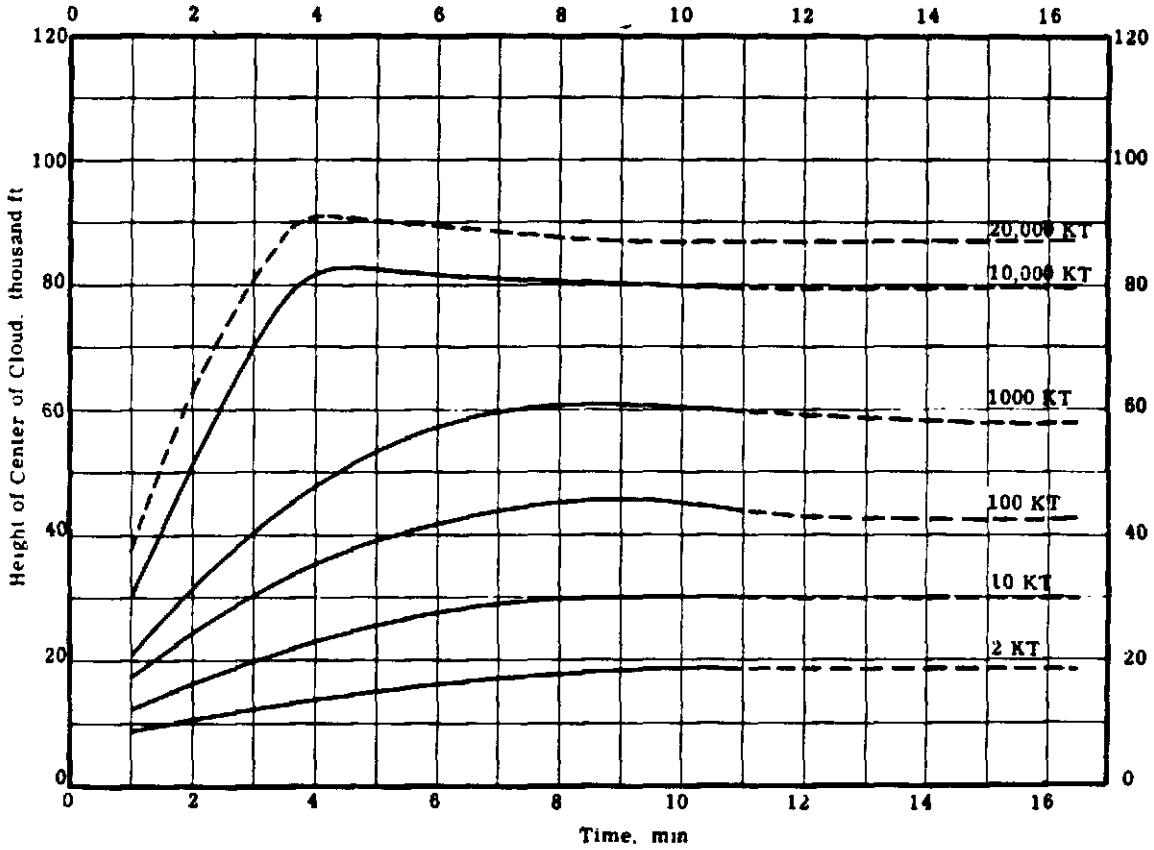

Figure 7.3:4 Height of Center of Cloud as a Function of Yield and Time after Burst for Near-Surface Bursts. Broken curves indicate extrapolated values.

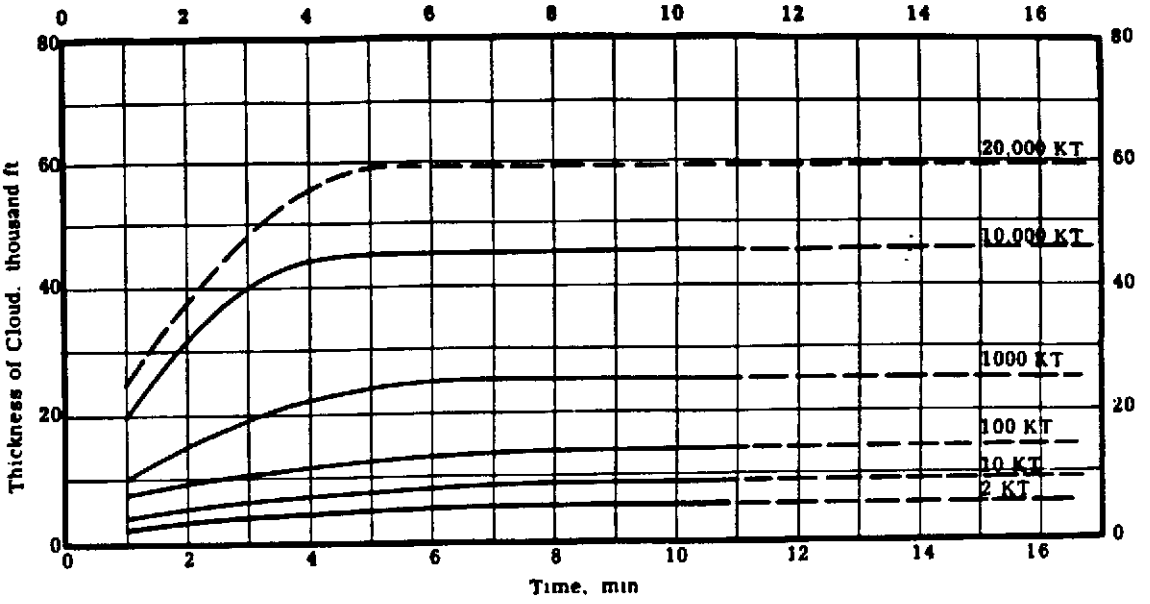

Figure 7.3:5 Thickness of Cloud as a Function of Yield and Time after Burst for Near-Surface Bursts. Broken curves indicate extrapolated values.

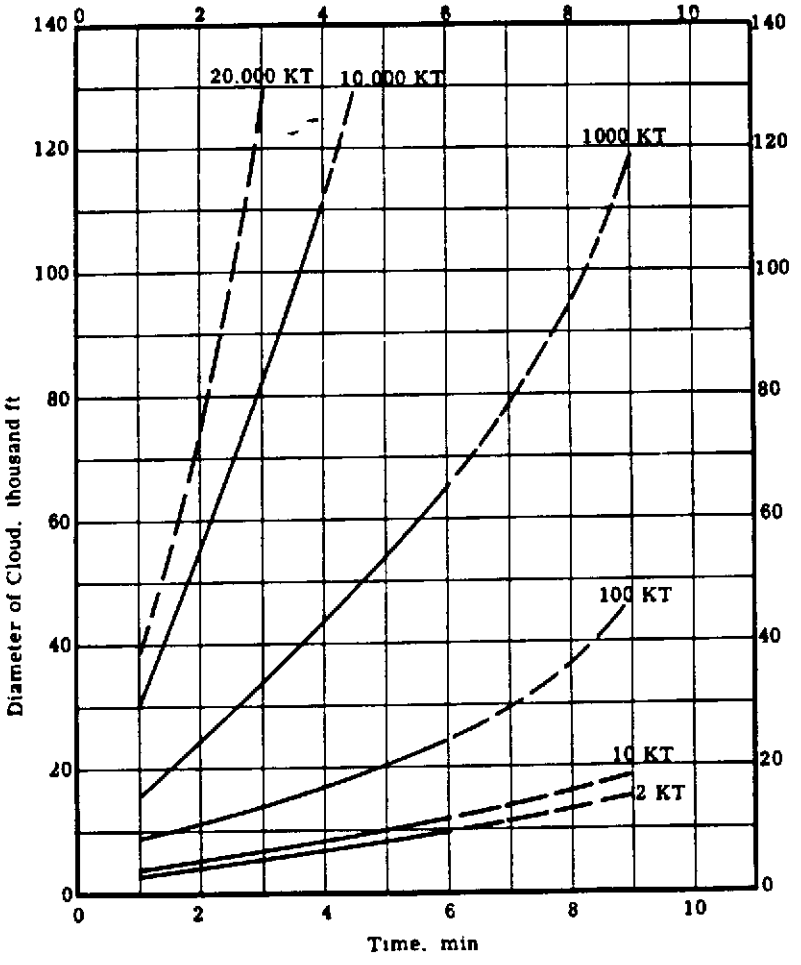

Figure 7.3:6 Diameter of Cloud as a Function of Yield and Time after Burst for Near-Surface Bursts. Broken curves indicate extrapolated values.

PROBLEM 1

For surface or near-surface bursts, find the distance above burst height of the top, bottom, or center of an atomic cloud at any time during the first 15 min after the burst. Yield and burst height of the bomb are known.

Solution

Read height directly from Figs. 7.3:2, 7.3:3, or 7.3:4, (whichever is appropriate) at given time and yield. Add this value to burst height for near-surface bursts.

PROBLEM 2

For surface or near-surface bursts, find the vertical thickness of an atomic cloud at any time during the first 15 min after burst. Yield and burst height of the bomb are known.

Solution

Read thickness directly from Fig. 7.3:5 at the given time and yield.

PROBLEM 3

For surface or near-surface bursts, find the diameter of an atomic cloud at any time during the first 9 min after burst. Yield and burst height of bomb are known.

Solution

Read diameter directly from Fig. 7.3:6 at the given time and yield.

Error

The results of Problems 1, 2, and 3 are estimated to be good to within a factor of two.

7.4 CLOUD CHARACTERISTICS FOR CALCULATION OF FALLOUT AND INITIAL RADIATION

The accuracy of the plots in Section 7.3 or of any other known method for predicting cloud heights is not suitable for input to a fallout computation. Similarly the time dependence is not accurate enough for short times after burst (0 to 30 sec), for use in making cloud rise corrections for initial gamma doses; for this purpose the following empirical relation[13] is recommended for surface and near-surface bursts.

$$y_c = 115\ W^{0.2}\ t^{0.8} \qquad (7.4:1)$$

where

y_c = height of center of cloud above point of burst, ft

W = bomb yield, KT

t = time after burst, sec

This expression may be considered applicable in the range t = 5 to 30 sec. In Fig. 7.4:1 the value of y_c is plotted as a function of time for various values of yield. Extension of these curves agrees as well as can be expected with the data of Fig. 7.3:4.

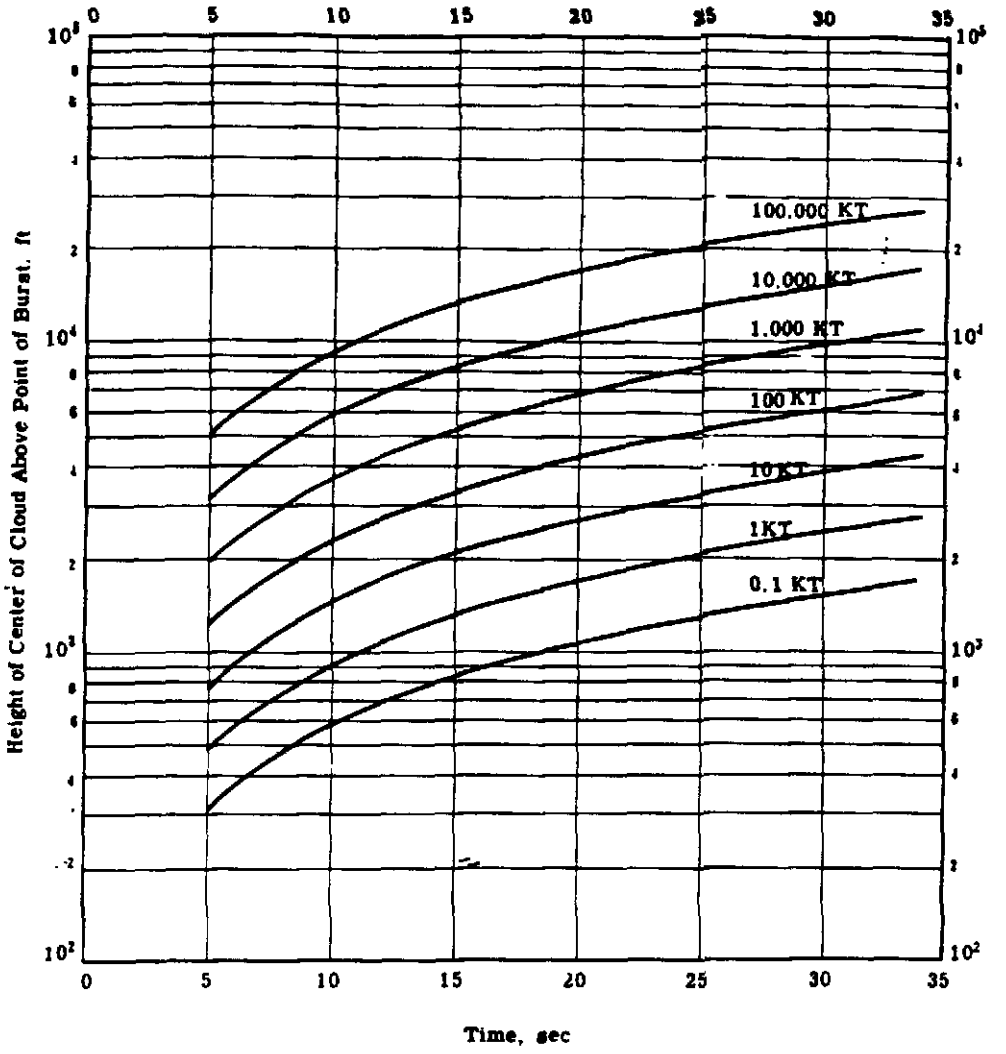

Figure 7.4:1 Height of Center of Cloud for Short Times After Burst as a Function of Yield for Near-Surface Bursts.

7.5 CLOUD CHARACTERISTICS FOR CALCULATION OF AIRCRAFT PENETRATION DOSE

The present principal usefulness of Figs. 7.3:1 through 7.3:6 is the evaluation of radiation hazards for aircraft flying in the vicinity of the atomic cloud. Because both the data in these figures and dose rate information given below are from surface or near-surface bursts, the results presented in this section are similarly restricted.

In addition to cloud heights and dimensions it is necessary to have information regarding the radiation content of the cloud. Qualitatively, it is clear that the dose rate at a given time and place within the cloud is a function of three factors:

1. density of radioactive material,
2. density of entrained inactive material, and
3. density of air.

The dose rate will change with time as determined by the way these three factors change and this in turn depends on:

1. rate of decay of active material,
2. rate of fall of active material,
3. rates of entrainment and fall of inactive material, and
4. rate of expansion of cloud.

Some of these factors are clearly independent of yield. It would appear that the others are also independent of yield, either individually or in combination, at least over some time period. Experimental measurements at Upshot-Knothole[14] supported by less credible measurements at Greenhouse[15], indicate rather strongly that the volume average dose rate encountered within the cloud between 3 and 25 min after the burst is independent of weapon yield.

The most reasonable explanation for this independence of yield is comprised of two factors.

1. The dose received at any given point within the cloud comes predominantly from nearby regions of the cloud, while the dose from remote regions is sufficiently attenuated to be negligible in comparison. The over-all size of the cloud would therefore not be important in determining the dose rate.
2. The volume average density of the active and inactive materials in the cloud is independent of yield. This is a reasonable expectation since the volume of the cloud is known to be roughly proportional to the yield; the amount of debris, both active and inactive, should also be roughly proportional to yield.

It has been determined empirically[14] that the volume average dose rate in the cloud in the period 2 to 25 min after burst is equal to $2.18 \times 10^3\ t^{-2.06}$, rep-min^{-1}, where t is the time after burst, min.

This relation comes to within a factor of two of most measured results. A few Greenhouse measurements fell outside of that range; this may be so because the measurements were made in the stem rather than in the cloud proper or because of errors in the measurements themselves. If one integrates the average dose rate over the time spent in the cloud as in Eq. 7.5:1, the total dose accumulated in the cloud is obtained. This equation for total dose should hold fairly well except for trajectories close to the cloud boundaries.

$$D = \int_{t_e}^{t_e + t_c} 2.18 \times 10^3\ t^{-2.06}\ dt \qquad (7.5:1)$$

where

D = total dose accumulated in cloud, rep

t_e = time of entry into cloud after burst, min

t_c = time spent in cloud, min

Fig. 7.5:1 is a plot of D as a function of t_c for various values of t_e.

The preceding discussion applies only to aircraft flight through the atomic cloud proper. There may be a similar problem involving flight through the stem but the data presently available do not permit evaluation.

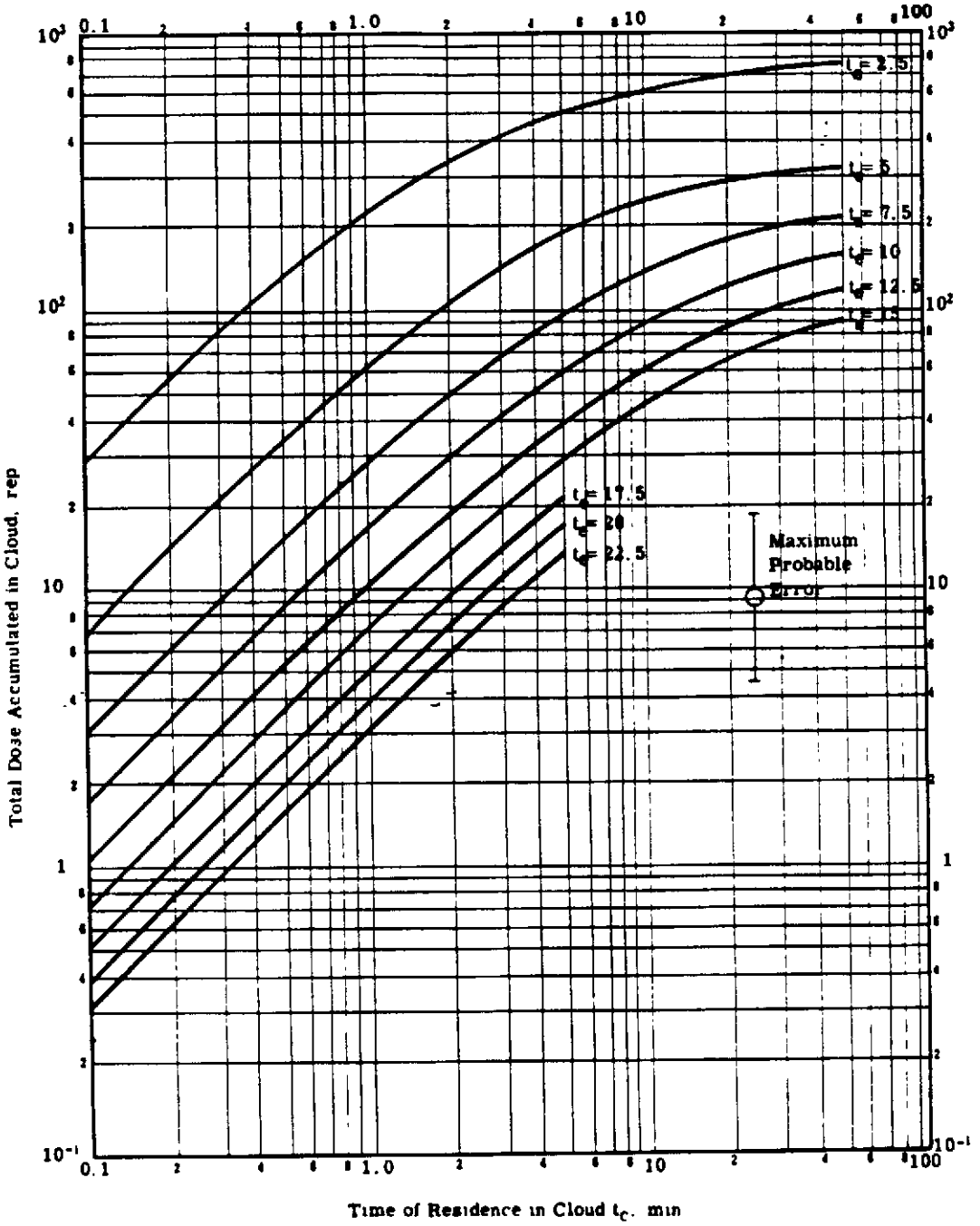

Figure 7.5:1 Total Dose Accumulated in Cloud as a Function of Time of Residence t_c and time of Entry t_e.

PROBLEM 4

It is known that an aircraft penetrates an atomic cloud. Find the time spent in the cloud when the height and speed of the aircraft and the burst height and yield of the bomb are known.

(Note that sufficient information is presented in Figs. 7.3:2 through 7.3:6 to determine in detail how an aircraft flying a given course and speed will penetrate an atomic cloud of known yield, burst time, and height. Thus, one could answer the following questions: Will penetration occur? Exactly where in the cloud will penetration occur? How long will penetration last? The inaccuracies in the data and sensitivity of the results to small variations in operational conditions make such a detailed treatment unwarranted.)

(It is possible to relate rather well the diameter of the cloud to the time after burst and the yield. It is meaningful, therefore, to ask how great a diameter the cloud presents to an aircraft flying in the vicinity at a given time after burst and for a given yield. This is not precisely the problem stated, but it can be loosely so interpreted.)

Solution

To reduce the input conditions to the same units as the working curves, it is desirable to express the aircraft speed in feet per minute. The following conversion factors, while not exact, are well within the accuracy of this treatment.

$$1 \text{ knot} = 1 \text{ nautical mile-hr}^{-1} = 100 \text{ ft-min}^{-1}$$

$$1 \text{ statute mile-hr}^{-1} = 90 \text{ ft-min}^{-1}$$

It will be assumed that the cloud height and dimensions are fixed during the time of the aircraft passage. This is obviously not the true situation since in most circumstances the cloud will still be rising and expanding during the aircraft penetration. For short penetration times, however, the changes in cloud dimensions during penetration will not be large and for longer penetration times average cloud dimensions can be used.

Two separate cases will be demonstrated -- penetration along the cloud diameter and grazing penetration.

A. Assume that the aircraft penetrates along the cloud diameter.

1. Subtract the burst height from the aircraft height to obtain y_c, the height of the center of the cloud above burst at time of penetration.
2. Using Fig. 7.3:4 and the value of y_c and the yield find the time of entry into the cloud t_e.
3. From Fig. 7.3:6 at the given yield and time find the cloud diameter d.
4. Convert the aircraft velocity into feet per minute v.
5. The time spent in the cloud in minutes t_c, is then d/v.

B. Assume that the aircraft makes a grazing penetration -- y feet below (or above) the cloud center and x feet to the side of the vertical axis. (If neither x nor y is greater than 1/4 the cloud diameter, the penetration ought to be considered as being along the diameter. Also, if the cloud growth has reached the phase where considerable flattening has occurred, the penetration should be taken as diametric.) Assume, further, that the cloud is spherical, with diameter given by Fig. 7.3:6.

1. Perform steps 1, 2, 3, and 4 as indicated in A above.
2. Calculate $[4(x^2 + y^2)/d^2]$. This is the square of the fractional radial distance of the aircraft trajectory from the cloud center. Fig. 7.5:2 is a plot of the trigonometric reduction factor

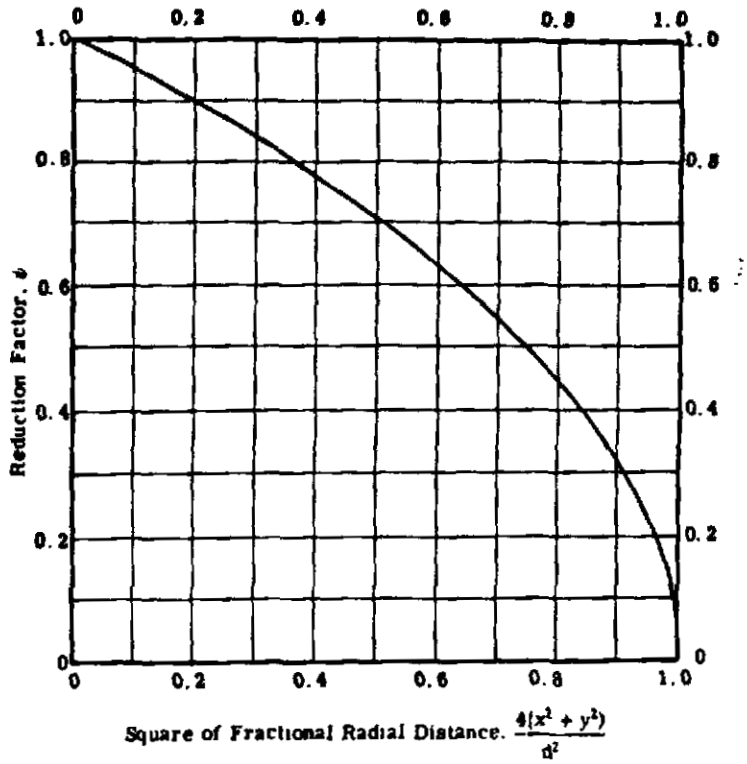

Figure 7.5:2 Diameter Reduction Factor.

ψ in the diameter. Read the value of ψ from Fig. 7.5:2 at the corresponding value of $[4(x^2 + y^2)/d^2]$.

3. The distance traversed by the aircraft is ψd and the time spent in the cloud t_c, is $\psi d/v$.

Error

The error of Problem 4 is estimated to be no more than a factor of two.

PROBLEM 5

It is known that an aircraft penetrates an atomic cloud. Find the dose accumulated in the cloud when the height and speed of the aircraft and the burst height and yield of the bomb are known.

Solution

1. Apply the appropriate methods of Problem 4 to determine the time of entry into the cloud t_e, and the time spent in the cloud t_c.
2. Read the dose accumulated for these values of t_e and t_c from Fig. 7.5:1.

Error

The error in Problem 5 is estimated to be no more than a factor of two.

Example A

An aircraft is flying at 25,000 ft at a speed of 200 knots. A 50-KT bomb is exploded 1000 ft above sea level. If the aircraft penetrates the resulting cloud along its diameter, how long will the aircraft be within the cloud and what dose will the crew experience?

1. The height of the cloud center above burst at the time of penetration will be 25,000 - 1,000 = 24,000 ft.
2. The center of the cloud from a 50-KT bomb rises 24,000 ft from the burst point in 2.8 min, according to Fig. 7.3:4.
3. The cloud diameter of a 50-KT bomb after 2.8 min is 10,000 ft, from Fig. 7.3:6.
4. The aircraft speed is 200 x 100 = 20,000 ft-min^{-1}.
5. The time spent in the cloud is 10,000/20,000 = 0.5 min.
6. From Fig. 7.5:1 the dose accumulated in the cloud for entry time t_e = 2.8 min and time with cloud t_c = 0.5 min is 120 rep.

Example B

Same as Example A except grazing penetration of cloud is made 3,500 ft below and 3,000 ft to the left of the cloud center.

1. Perform steps 1, 2, 3, and 4 as in Example 1 above.
2. $$\frac{4(x^2 + y^2)}{d^2} = \frac{4(3{,}000^2 + 3{,}500^2)}{(10{,}000)^2} = 0.85$$

   From Fig. 7.5:2 a value of $[4(x^2 + y^2)/d^2] = 0.85$ leads to a value of $\psi = 0.39$.
3. The distance traversed by the aircraft is then $\psi d = (0.39)(10,000) = 3{,}900$ ft and the time of traverse t_c = 3,900/20,000 = 0.2 min.
4. From Fig. 7.5:1 the dose accumulated, from entry time t_e = 2.8 min and time within cloud t_c = 0.2 min, is 55 rep.

7.6 REFERENCES

1. J.S. Malik. LASL. Private Communication. Aug. 1955.
2. S.M. Greenfield. Rand Corp. Private Communication. Aug. 1955.
3. S.M. Greenfield et al. R-265. July 1954. (Secret)
4. W.W. Kellogg. RM-1378-AEC. Nov. 1954. (Secret)
5. L. Fussell, Jr. ITR-933. May 1954. (Secret)
6. Effects of Atomic Weapons. USGPO. Sept. 1950. (Unclassified)
7. B.H. Grossman and L. Machta. ITR-1152. May 1955. (Secret)
8. F.A. Berry, Jr. et al. Handbook of Meteorology. McGraw-Hill Book Co. 1945. (Unclassified)
9. G.I. Taylor. MDDC-919. March 1945. (Unclassified)
10. O.G. Sutton. Weather 2. 105-110. 1947. (Unclassified)
11. L. Machta. Bull. Am. Met. Soc. 31. 215-216. June 1950. (Unclassified)
12. P.G. Gallentine. LA-1184. June 1950. (Secret)
13. J.S. Malik. LA-1620. Jan. 1954. (Secret)
14. W.H. Langham et al. WT-743. Dec. 1953. (Secret)
15. G.E. Koch. WT-11. Aug. 1951. (Secret)